

**The effects of extracellular and intracellular Hop on  
cell migration processes**

A thesis submitted in fulfillment of the requirements for  
the degree of

**MASTER OF SCIENCE**

in Biochemistry

of

**Rhodes University**

by

**Lara Contu**

## **DECLARATION**

I declare that this thesis is my own, unaided work. It is being submitted for the degree of Master of Science of Rhodes University. It has not been submitted before for any degree or examination at any other university.

-----

Lara Contu,

February 2014,

Grahamstown

## ABSTRACT

The Hsp70/Hsp90-organising protein (Hop) is a 60 kDa co-chaperone that acts as an adaptor molecule, facilitating the transfer of client proteins between the Hsp70 and Hsp90 chaperone systems. Hop functions both intracellularly and extracellularly and has been implicated in many processes involved in cancer progression, including cell migration and invasion. Little is known about the mechanisms or domains by which extracellular Hop functions. In addition, little is known about the effects of Hop on signalling molecules involved in cell migration and invasion through regulation of actin dynamics. It was hypothesised that both extracellular and intracellular pools of Hop would regulate distinct cell migration processes by activation of cell signalling pathways or direct interactions with signalling intermediates. HS578T cells were treated with recombinant full length and truncated murine Hop proteins (overexpressed and purified in this study) to determine the effects of extracellular Hop and the independent domains on cell migration processes. Additionally, RNA interference (RNAi) techniques were used to determine the effect of Hop knockdown on cell migration related signalling intermediates and cell morphologies. A short hairpin RNA (shRNA) system for the stable knockdown of Hop was developed and used for a number of these studies. Treatment of HS578T cells with the TPR2A2B and TPR1 domains of Hop resulted in a significant decrease in cell migration and caused changes in the actin cytoskeleton and extracellular matrix proteins, gelatin and fibronectin. RhoC immunoprecipitated in a common complex with Hop and Hsp90. Hop knockdown reduced levels of actin and total RhoC, as well as active RhoC. In addition, knockdown of Hop resulted in a reduced migratory phenotype. We interpreted these data to indicate that intracellular Hop played a role in cell migration through regulation of RhoC activity, either through a direct interaction between Hop and RhoC, or an indirect interaction of RhoC with the Hsp90 multichaperone heterocomplex. Taken together, the data suggested that extracellular and intracellular Hop played distinct roles in extracellular and intracellular processes that lead to actin dynamics and cell migration. Understanding the mechanistic role of Hop in these processes is essential as it would aid in assessing the viability of Hop as a potential drug target for the treatment of metastatic cancers.

## TABLE OF CONTENTS

DECLARATION .....	i
ABSTRACT.....	ii
TABLE OF CONTENTS.....	iii
LIST OF FIGURES .....	vii
LIST OF TABLES.....	viii
LIST OF ABBREVIATIONS .....	x
LIST OF SYMBOLS .....	xi
ACKNOWLEDGEMENTS .....	xii
OUTPUTS .....	xiii
Chapter 1.....	1
Literature Review.....	1
1.1 CANCER CELL METASTASIS AND CELL MIGRATION .....	2
1.2 THE EXTRACELLULAR MATRIX AND ROLE OF MMPS IN CANCER CELL BIOLOGY.....	3
1.3 CELL MIGRATION AND THE ACTIN CYTOSKELETON.....	5
1.4 SIGNALLING CASCADES INVOLVED IN ACTIN DYNAMICS .....	8
1.5 ROLE OF ACTIN CYTOSKELETAL REGULATING PROTEINS IN CANCER CELL PROGRESSION .....	13
1.6 MOLECULAR CHAPERONES AND HEAT SHOCK PROTEINS.....	15
1.7 HEAT SHOCK PROTEIN 70 (HSP70) AND HEAT SHOCK PROTEIN 40 (HSP40) .....	17
1.8 HEAT SHOCK PROTEIN 90 (HSP90).....	18
1.9 HSP70/HSP90 ORGANISING PROTEIN (HOP) AND THE HSP90 MULTICHAPERONE HETEROCOMPLEX.....	19
1.10 THE ROLE OF HOP IN CANCER.....	25
1.11 ROLE OF MOLECULAR CHAPERONES IN PROTEINS INVOLVED IN CELL MIGRATION PROCESSES:.....	26
1.12 KNOWLEDGE GAP:.....	28
1.13 HYPOTHESIS:.....	28
1.14 OBJECTIVES:.....	28
Chapter 2.....	29
The effect of exogenous full length and truncated extracellular Hop on cell migration processes .....	29
2.1 INTRODUCTION: .....	30
2.2 MATERIALS:.....	31
2.3 METHODS: .....	31
2.3.1 Sequencing of pGEX3X2000, pGEX3X1400 and pGEX3X700 plasmids.....	31

2.3.2 Confirmation of pGEX-4T1, pGEX3X2000, pGEX3X1400 and pGEX3X700 plasmids by restriction enzyme digestion .....	31
2.3.3 Induction study of GST, GST-mSTI1, GST-TPR2A2B and GST-TPR1 .....	32
2.3.4 SDS-PAGE and Western analysis.....	33
2.3.5 Purification of GST, GST-mSTI1, GST-TPR2A2B and GST-TPR1 .....	33
2.3.6 Glutathione- <i>S</i> -transferase (GST) Pull down Assay.....	35
2.3.7 Endotoxin removal from GST and GST fusion proteins.....	35
2.3.8 Quantitation of Endotoxin in GST and GST fusion proteins .....	36
2.3.9 Cell Proliferation Assay .....	37
2.3.10 Wound Healing Assay .....	37
2.3.11 Gelatin degradation assay .....	37
2.4 RESULTS: .....	38
2.4.1 Conservation of amino acid sequence between human Hop and mSTI1 .....	38
2.4.2 Confirmation of identity of pGEX-4T1, pGEX3X2000, pGEX3X1400 and pGEX3X700 .....	40
2.4.3 Induction study of GST, GST-mSTI1, GST-TPR2A2B and GST-TPR1 .....	44
2.4.4 Purification of GST, GST-mSTI1, GST-TPR2A2B and GST-TPR1 .....	46
2.4.5 GST-mSTI1, GST-TPR2A2B and GST-TPR1 detected by human Hop antibodies.....	49
2.4.6 Confirmation of functionality of the murine GST fusion proteins in a human system by GST pull down assays.....	49
2.4.7 Endotoxin Removal and quantitation of GST and GST fusion proteins.....	51
2.4.8 Analysis of the effect of heterologous mSTI1 proteins on HS578T cell proliferation .....	52
2.4.9 Analysis of the effect of heterologous mSTI1 proteins on HS578T cell migration.....	53
2.4.10 Analysis of the effect of heterologous mSTI1 proteins on the actin cytoskeleton and extracellular matrix of HS578T cells .....	55
2.5 DISCUSSION: .....	59
2.5.1 Treatment of HS578T cells with heterologous mSTI1 proteins had no significant effect on cell proliferation.....	59
2.5.2 Treatment with GST-TPR2A2B and GST-TPR1 significantly decreased migration in HS578T cells.....	61
2.5.3 Treatment with heterologous mSTI1 proteins had differing effects on the actin cytoskeleton and extracellular matrix of HS578T cells .....	62
2.5.4 The TPR2A2B and TPR1 domains of Hop could inhibit cell migration through inducing changes in the extracellular matrix .....	63
2.5.5 Conclusion .....	65
Chapter 3.....	66
The effect of intracellular Hop on cell migration processes using RNA interference .....	66
3.1 INTRODUCTION: .....	67

3.2 MATERIALS:	69
3.3 METHODS:	70
3.3.1 Mammalian cell culture conditions	70
3.3.2 Immunofluorescence staining and confocal microscopy	70
3.3.3 Transfections using siRNA system	70
3.3.4 Immunoprecipitation Assay	71
3.3.5 SDS-PAGE and Western analysis	71
3.3.6 Multiple sequence alignment of TRIPZ shRNA Hop clones with Hop (Human) and mSTI1 ( <i>Mus musculus</i> ) mRNA	72
3.3.7 Plasmid preparation and confirmation of TRIPZ plasmids by restriction enzyme digests	72
3.3.8 Analysis of Hop knockdown and protein expression levels in shRNA treated HEK293T and HS578T cell lines	73
3.3.9 Lentiviral particle production in HEK293T cells	74
3.3.10 Analysis of transduction efficiency of N.T shRNA and shRNA #2 lentiviral particles	75
3.3.11 Selection and propagation of stable cell lines	75
3.3.12 Rho Activation Assay	76
3.3.13 Scanning Electron Microscopy	77
3.3.14 Cell proliferation assay	77
3.4 RESULTS:	78
3.4.1 Association of Hop with Rho family proteins in HS578T cell line	78
3.4.2 Analysis of TRIPZ shRNA clones for development of stable cell lines	82
3.4.3 Development of mammalian cell lines stably transfected with inducible shRNA constructs.	90
3.4.4 Effect of Hop knockdown on RhoC expression and activation	99
3.4.5 The role of Hop in cell proliferation and cell morphology	102
3.5 DISCUSSION:	106
3.5.1 Hop colocalised with RhoA, RhoC and Cdc42, but not RhoB	106
3.5.2 RhoC immunoprecipitated in a common complex with Hop and Hsp90	106
3.5.3 Hop knockdown resulted in a decrease in the levels of actin and RhoC	107
3.5.4 A stable inducible RNAi system for Hop knockdown in HEK293T cells was developed and used for further experiments	107
3.5.5 Hop knockdown resulted in reduced levels of RhoC and interfered with RhoC activation	107
3.5.6 Hop knockdown resulted in non-migratory cell phenotypes and increased cell proliferation	109
3.5.7 Conclusion	110
Chapter 4.	111

Summary, Conclusions and Future Work .....	111
4.1 SUMMARY, CONCLUSIONS AND FUTURE WORK.....	112
REFERENCES .....	114
APPENDICES .....	130
Appendix 1: List of additional materials used .....	130
A1.1 Molecular biology and protein biochemistry reagents .....	130
A1.2 Antibodies and dyes .....	130
A1.3 Tissue culture reagents .....	131
Appendix 2: Steps showing purification procedure of GST, GST-mSTII, GST-TPR2A2B and GST-TPR1 .....	132
Appendix 3: Calculating concentrations of endotoxins using standard curve (EU/mL).....	133
Appendix 4: Quantification of transduction efficiency by automated particle counting using ImageJ .....	134
Appendix 5: Alignment of Hop targeting shRNA clones with Hop mRNA.....	143
Appendix 6: Quantitative analysis of cell morphologies of N.T shRNA and shRNA #2 HEK293T cells .....	148

## LIST OF FIGURES

Figure 1.1: Schematic diagram showing steps required for tumour cell metastasis .....	17
Figure 1.2: Schematic diagram showing GDP/GTP cycling of Ras superfamily .....	23
Figure 1.3: Schematic diagram showing signalling pathways leading to actin polymerisation and the formation of different membrane protrusions. ....	25
Figure 1.4: Schematic diagram showing actin filament nucleation by actin regulating proteins .....	26
Figure 1.5: Schematic Diagram of the TPR Domains of Hop .....	35
Figure 1.6: Schematic diagram showing a model for the functioning of the Hsp90 multichaperone heterocomplex.....	37
Figure 2.1: Conservation of protein sequence between human Hop and mSTI1 .....	53
Figure 2.2: Schematic diagram showing the GST fusion proteins, GST-mSTI1, GST-TPR2A2B and GST-TPR1 expressed from pGEX3X2000, pGEX3X1400 and pGEX3X700 plasmids respectively .....	54
Figure 2.3: Confirmation of identity of pGEX-4T1, pGEX3X2000, pGEX3X1400 and pGEX3X700 plasmids .....	57
Figure 2.4: Induction of recombinant GST-tagged mSTI1 proteins and controls. ....	59
Figure 2.5: Overexpression and purification of GST, GST-mSTI1, GST-TPR2A2B and GST-TPR1.....	61
Figure 2.6: GST-mSTI1, GST-TPR2A2B and GST-TPR1 detectable by human Hop antibodies .....	63
Figure 2.7: GST-mSTI1, GST-TPR2A2B and GST-TPR1 recombinant proteins were able to pull down Hsp90 and/or Hsp70 from human cell lysates .....	64
Figure 2.8: Extracellular mSTI1 proteins had no significant effect on cell proliferation of HS578T cells .....	66
Figure 2.9: Treatment with GST-TPR2A2B and GST-TPR1 significantly decreased migration in HS578T cells.....	68
Figure 2.10: Treatment with heterologous mSTI1 proteins had differing effects on the actin cytoskeleton and extracellular matrix of HS578T cells. ....	70
Figure 3.1: Association of Hop with Rho family proteins in HS578T cell line.....	94
Figure 3.2: Restriction enzyme digests of TRIPZ plasmids with <i>Sa</i> II restriction enzyme. ....	97
Figure 3.3: Transient knockdown of Hop by shRNA reduced levels of actin and RhoC in HEK293T cells .....	101
Figure 3.4: Transient knockdown of Hop by shRNA reduced levels of actin and RhoC in HS578T cells .....	102
Figure 3.5: Lentiviral particle production in HEK293T cells .....	106
Figure 3.6: Confirmation of infectious N.T shRNA and shRNA #2 lentiviral particles and analysis of transduction efficiency in HEK293T cells.....	107
Figure 3.7: Confirmation of infectious N.T shRNA and shRNA #2 lentiviral particles and analysis of transduction efficiency in HS578T cells.....	108
Figure 3.8: Selection and propagation of stably transduced HEK293T and HS578T cell lines .....	110
Figure 3.9: Hop knockdown resulted in reduced levels of RhoC and interfered with RhoC activation. ....	114
Figure 3.10: Hop knockdown results in an increase in proliferation and a change in morphology of HEK293T cells.....	116
Figure 3.11: Hop knockdown reduced membrane ruffles in HEK293T cells.....	118



Supplementary figure 1: Overexpression and purification of GST, GST-mSTI1, GST-TPR2A2B and GST-TPR1. ....	133
Supplementary figure 2: Standard curve for quantification of endotoxin in protein samples (units/mL) .....	134
Supplementary figure 3: Quantification of transduction efficiencies of N.T shRNA and shRNA #2 lentiviral particles in HEK293T cells by automated particle counting using ImageJ .....	141
Supplementary figure 4: Quantification of transduction efficiencies of N.T shRNA and shRNA #2 lentiviral particles in HS578T cells by automated particle counting using ImageJ .....	143
Supplementary figure 5: TRIPZ shRNA Hop clones target different regions of Hop ( <i>Homo sapiens</i> ) and mSTI1 ( <i>Mus musculus</i> ) mRNA.....	148
Supplementary figure 6: Measurement of cell elongation index of N.T shRNA vs shRNA #2 HEK293T cell lines.....	149
Supplementary figure 7: Quantification of membrane ruffles in N.T shRNA and shRNA #2 HEK293T cell lines .....	151

## LIST OF TABLES

Table 2.1: Total protein (mg) and protein yield (mg/L of culture) of purified GST, GST-mSTI1, GST-TPR2A2B and GST-TPR1 .....	62
Table 2.2: Effects of GST, GST-mSTI1, GST-TPR2A2B and GST-TPR1 on proliferation, migration and extracellular matrix proteins of HS578T cells .....	73
Table 3.1: Summary of nucleotide positions and structural motifs / domains at which each shRNA clone targets Hop ( <i>Homo sapiens</i> ) and mSTI1 ( <i>Mus musculus</i> ) mRNA .....	99

## LIST OF ABBREVIATIONS

ADP	Adenosine diphosphate
Ago 2	Argonaute 2
Aha1	Activator of heat shock protein 90
Akt	Protein Kinase B
AmpR	Ampicillin Resistance Gene
ANOVA	Analysis of variance
AR	Androgen receptor
Arf	ADP ribosylation factor
Arp2/3	Actin related protein 2/3
ATP	Adenosine triphosphate
ATPase	Adenosine 5'-triphosphatase
BSA	Bovine serum albumin
cAMP	Cyclic adenosine monophosphate
Cdc37	Cell division cycle 37
Cdc42	Cell division cycle 42
CHIP	Carboxyl terminus of Hsc70-interacting protein
CPD	Critical Point Dryer
cPPT	Central polypurine tract
C-terminal	Carboxy terminal
Cyp40	Cyclophilin 40
DMEM	Dulbecco's modified eagle medium
DMSO	Dimethyl sulfoxide
DNA	Deoxyribonucleic acid
dsRNA	double stranded RNA
DTT	Dithiothreitol
EDTA	Ethylenediaminetetraacetic acid
EEVD	glutamate-glutamate-valine-aspartate motif
ERK	Extracellular signal-regulated kinase
EtBr	Ethidium bromide
F-actin	Filamentous actin
FBS	Foetal bovine serum
FDA	US Food and Drug Administration
Fkbp51/52	FK506 binding protein-51/52
FMNL 2/3	Formin-like protein 2/3
FRET	Fluorescence resonance energy transfer
G-actin	Globular actin
GAPs	GTPase activating proteins
GDI	GDP dissociation inhibitors
GDP	Guanosine diphosphate
GEFs	Guanine nucleotide exchange factors
GFP	Green fluorescent protein
GPCR	G-protein-coupled receptor
GST	Glutathione-S-Transferase
GTP	Guanosine triphosphate
GTPases	Guanosine triphosphatases
Hip	Hsc70-interacting protein
HIV	Human immunodeficiency virus
Hop	Hsp70/Hsp90 organising protein
HRP	Horse radish peroxidase
Hsc70	Heat shock cognate protein 70
Hsps	Heat shock proteins
HUVEC	Human umbilical vein endothelial cells
IPTG	Isopropyl $\beta$ -D-1-thiogalactopyranoside
IRES	Internal ribosomal entry site
LAL	Limulus amebocyte lysate
LB	Luria broth
LPS	Lipopolysaccharide

LSM	Laser scanning microscope
LTR	Long terminal repeat
MAPK	Mitogen activated protein kinase
MEK	Meiosis-specific serine/threonine kinase
mESCs	Mouse embryonic stem cells
miRNAs	microRNAs
MLB	Mg <sup>2+</sup> lysis buffer
MLC	Myosin light chain
MLCK	Myosin light chain kinase
MMPs	Matrix metalloproteinases
mRNA	messenger RNA
NEAA	Non-essential amino acids
NEFs	Nucleotide exchange factors
NFκB	Nuclear Factor Kappa-light-chain-enhancer of activated B cells
NLS	Nuclear localisation signal
N-terminal	Amino terminal
p23	Prostaglandin-E synthase
pAkt	Phosphorylated Akt
Par4	Prostate apoptosis response protein
PBS	Phosphate buffered saline
pERK	Phosphorylated ERK
PI3K	Phosphatidylinositol 3-kinase
PMA	Phorbol 12-myristate 13-acetate
PMSF	Phenylmethanesulfonylfluoride
PPIase	Peptidyl-prolyl-isomerase
PrP <sup>c</sup>	Cellular prion related protein
PSA	Penicillin streptomycin amphotericin
PuroR	Puromycin resistance gene
Rac	Ras-related C3 botulinum
RalBP1	RalA binding protein 1
RBD	Rho binding domain
Rho	Ras homologue
RhoA	Ras homologous A protein
RhoB	Ras homologous B protein
RhoC	Ras homologous C protein
RHOBTB1	Rho-related BTB domain containing 1
RIPA	Radio-immunoprecipitation assay
RISC	RNA-induced silencing complex
RNA	Ribonucleic acid
RNAase	Ribonuclease
RNAi	RNA interference
ROCK	Rho associated protein kinase
rpm	Revolutions per minute
RRE	Rev response element
rtTA3	Reverse tetracycline transactivator
SCAR	Suppressor of cAMP receptor mutation
SDS	Sodium dodecyl sulphate
SDS-PAGE	SDS-polyacrylamide gel electrophoresis
shRNA	short hairpin RNA
SIN LTR	Self-inactivating LTR
siRNA	short interfering RNA
SPR	Surface plasmon resonance
Stat3	Signal transducer and activator of transcription 3
STIP1	Stress-induced phosphoprotein 1
STS	Sequence tagged site
SV40 ori	Simian virus 40 origin of replication
TBE	Tris-Borate-EDTA
TBS	Tris buffered saline
TBS-T	TBS-Tween
TEM	Transmission electron microscopy

TPR	Tetratricopeptide repeat
TRE	Tetracycline response element
tRFP	turbo-Red fluorescent protein
UBC	Human ubiquitin C
VSV-G	Vesicular stomatitis virus G glycoprotein
WASP	Wiscott-Aldrich Syndrome Protein
WAVE	WASP family Verprolin-homologous protein
WPRE	Woodchuck hepatitis posttranscriptional regulatory element
YT	Yeast Tryptone

## LIST OF SYMBOLS

$\alpha$	Alpha
$\beta$	Beta
$\kappa$	Kappa
$\gamma$	Gamma
$^{\circ}\text{C}$	Degree celsius
%	Percent or g/100 mL
U	Units
V	Volts
x g	Relative centrifugal force to gravity
M	Molar
mM	Millimolar
$\mu\text{M}$	Micromolar
nM	Nanomolar
g	Grams
mg	Milligrams
$\mu\text{g}$	Micrograms
ng	Nanograms
L	Litres
mL	Millilitre
$\mu\text{L}$	Microlitres
$\mu\text{m}$	Micrometres
nm	Nanometres
bp	Base pairs
EU/mL	Endotoxin units per millilitre
kDa	Kilodaltons
min	Minutes
mol	Mole
v/v	volume/volume
w/v	weight per volume

## **ACKNOWLEDGEMENTS**

I would like to sincerely thank my supervisor, Dr Adrienne Edkins, for her patience, enthusiasm and encouragement throughout this research project. Without her extensive knowledge, dedication and hard work, this research would not have been possible. I would also like to thank her for giving me the opportunity to present at an international conference, an eye-opening experience where I was once again inspired by the dynamic, fascinating nature of scientific discovery. I would like to extend thanks to my colleagues and friends. Jason, Cindy, Jo, Lorraine, Fortunate, Karim, Dustin, Lance, Morgan, Adam, Claire and all the BioBRU members - I appreciate the support and friendship you have shown me throughout my years at Rhodes more than you know. I am thankful that I was able to share my journey at Rhodes with you all. I will miss you as I continue my journey elsewhere, but I have no doubt that I have made friends for life in this place. I would also like to thank my siblings, Giovanna and Ivano for their love and support during my time away from home. In particular, I would like to thank my parents for giving me the opportunity to attend Rhodes University and continue my postgraduate studies, and for never letting me take my tertiary education for granted. Finally, I would like to thank the DAAD/NRF for funding.

## OUTPUTS

### Publications:

Willmer, T., **Contu, L.**, Blatch, G.L. and Edkins, A.L. (2013) Knockdown of Hop downregulates RhoC expression, and decreases pseudopodia formation and migration in cancer cell lines, *Cancer Letters*, 328(2), pp. 252-260

de la Mare, J., **Contu, L.**, Hunter, M.C., Moyo, B., Sterrenberg, J.N., Mutsvunguma, L.Z., Dhanani, K.C.H. and Edkins, A.L. (2013) Breast cancer: current developments in molecular approaches to diagnosis and treatment, *Recent Patents in Anticancer Drug Discovery*, PMID: 24171821

### Conference outputs (oral presentation):

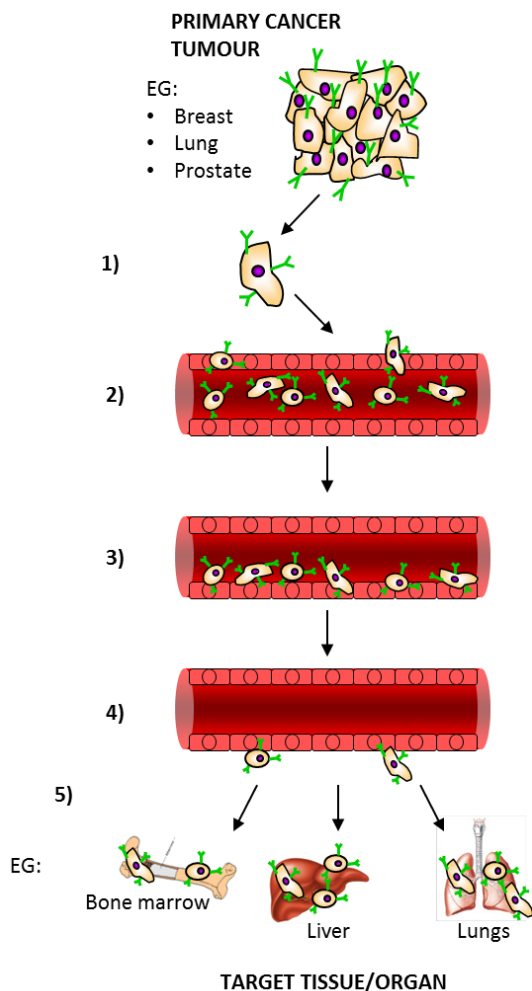
**VI International Congress on Stress Proteins in Biology and Medicine (CSSI 2013). Sheffield, UK (18-22 August, 2013).** The role of Hop in pseudopodia formation in Hs578T metastatic breast cancer cells, **Contu, L.**, Willmer, T., Hunter, M.C., Beckley, S.J., Blatch, G.L. and Edkins, A.L.

# **Chapter 1.**

## **Literature Review**

## 1.1 CANCER CELL METASTASIS AND CELL MIGRATION

Cancer metastasis can be described as the transference of cancerous cells from one part of the body to another by way of the blood or lymphatic systems (Kucia *et al.*, 2005). Cancer cells need to undergo a number of distinct steps in order to form metastases. First, the cancer cells must leave the primary tumour and enter into the peripheral blood or lymph, where they survive in circulation (Kucia *et al.*, 2005; Luker and Luker, 2005) (Figure 1.1). The cells are trafficked to secondary organs (target organs), where they adhere to the endothelium and enter or invade the target tissues by crossing the endothelium; a process that requires the secretion of matrix metalloproteinases (MMPs) (Figure 1.1). It is in the target tissues and organs that the cancer cells proliferate, thereby forming secondary metastatic tumours (Kucia *et al.*, 2005; Luker and Luker, 2005) (Figure 1.1).



**Figure 1.1:** Schematic diagram showing steps required for tumour cell metastasis (Modified from Kucia *et al.*, 2005).



**Figure 1.1: Schematic diagram showing steps required for tumour cell metastasis** (Modified from Kucia *et al.*, 2005).

Step 1: Cancer cells egress from the primary tumour. Step 2: Cells enter into the peripheral blood or lymphatic system, where they are circulated. Step 3) Cells are trafficked to secondary organs or tissues to which they are directed, where they adhere to the endothelium. Step 4: Cells invade the target tissues by crossing through the endothelium, a process that requires the secretion of MMPs. Step 5: Cancer cells proliferate in the secondary organ, thereby forming metastatic tumours.

Cancer cell metastasis is responsible for 90 % of the deaths from cancer (Spano *et al.*, 2012). Cell migration is a fundamental process that is essential for the metastasis of cancer cells and occurs through a dynamic interaction between the intracellular cytoskeleton and the extracellular matrix (Coopman *et al.*, 1998; Egeblad and Werb, 2002).

## **1.2 THE EXTRACELLULAR MATRIX AND ROLE OF MMPS IN CANCER CELL BIOLOGY**

The extracellular matrix itself is a dynamic structure that has an essential role in cell adhesion, cell morphology and cell migration (Streuli, 1999; Egeblad and Werb, 2002). It is made up of collagens, glycoproteins (such as laminin and fibronectin) and proteoglycans (Streuli, 1999; Egeblad and Werb, 2002). These extracellular matrix proteins bind directly to cell surface receptors, thereby triggering and modulating cell signalling cascades involved in a wide variety of cell processes (Streuli, 1999). Remodelling of the extracellular matrix is therefore imperative for essential cell processes such as proliferation, migration, differentiation, vascularisation (angiogenesis) and invasion to occur (Streuli, 1999).

Collagens are triple helical structures, many of which (type I, II, III, V and XI) form fibrils, which interact with integrins thereby regulating cell processes (Egeblad and Werb, 2002). Similarly, fibronectins form networks of fibrils in the extracellular matrix (Vuento *et al.*, 1982; Pickford *et al.*, 2001; Egeblad and Werb, 2002). They have been shown to play a role in cell attachment, morphology, migration and differentiation (Egeblad and Werb, 2002). A 42 kDa proteolytic fragment of fibronectin has been shown to have high affinity for denatured collagen (gelatin) and has therefore been identified as a collagen binding domain (Vuento *et al.*, 1982; Forastieri and Ingham, 1985; Pickford *et al.*, 1997; Pickford *et al.*, 2001). This domain contains type 2 (F2) modules which are responsible for gelatin binding (Collier *et al.*, 1988; Wilhelm *et al.*, 1989; Pickford *et al.*, 1997). It has been demonstrated that fibronectin and collagen are co-distributed in the extracellular matrix of fibroblasts (Vuento *et al.*, 1982; Pickford *et al.*, 1997). Fibronectin has been shown to be distributed in a

regular array along collagen fibrils, together forming fibrillar components of the extracellular matrix (McDonald *et al.*, 1982; Pickford *et al.*, 1997). Fibronectin is required for the deposition and organisation of collagen by fibroblasts and promotes attachment of fibroblasts to the extracellular collagen matrix (McDonald *et al.*, 1982; Vuento *et al.*, 1982; Pickford *et al.*, 1997). Using a quantitative fluorescence-activated cell sorting-phagocytosis assay, Coopman and colleagues (1998) showed that human breast cancer cells were able to phagocytose gelatin, and that a higher phagocytic capacity correlated with a greater invasive capacity. It was demonstrated that gelatin phagocytosis was mediated by the actin cytoskeleton and that phagocytosed gelatin entered the endocytic pathway, suggesting degradation of gelatin by lysosomes (Coopman *et al.*, 1998).

MMPs are enzymes responsible for the degradation and remodelling of the extracellular matrix (Streuli, 1999; Visse and Nagase, 2003). There are 23 identified human MMPs which can be divided into 6 groups based on their structural and functional similarities. One such group is the gelatinases, which is comprised of gelatinase A (MMP-2) and gelatinase B (MMP-9) (Visse and Nagase, 2003). As the name suggests, MMP-2 and MMP-9 are able to digest gelatins, which are denatured collagens (Egeblad and Werb, 2002; Visse and Nagase, 2003).

Many signalling processes that influence cell behaviour are regulated by specific cleavage of extracellular matrix components, including extracellular matrix proteins, cell surface receptors and cell adhesion molecules by MMPs (Streuli, 1999; Egeblad and Werb, 2002; Visse and Nagase, 2003). Specific cleavage of extracellular matrix proteins results in subtle changes in their structures which, in turn, change their interactions with cell surface receptors thereby influencing cell signalling pathways and cell behaviour. Similarly, cleavage results in the release of sequestered growth factors from the extracellular matrix which trigger relevant signalling pathways and influence cell behaviour (Streuli, 1999; Visse and Nagase, 2003). It is therefore evident that MMPs play a large role in regulating the interactions between cells and the extracellular matrix (Egeblad and Werb, 2002).

MMPs have been found to play a role in regulating a number of cancer cell processes, including growth, differentiation, apoptosis, angiogenesis, migration and invasion (Egeblad and Werb, 2002). MMPs have been found to be overexpressed in almost all human cancers compared to normal tissue equivalents (Egeblad and Werb, 2002). Overexpression of MMP-2

and MMP-9 compared to normal ovarian tissue were found in all invasive human ovarian cancers (Kenny *et al.*, 2008). Fibroblasts were found to induce MMP-2 expression in cancer cells (Kenny *et al.*, 2008).

MMP-2 and MMP-9 have been shown to localise in invadopodia (Egeblad and Werb, 2002; Artym *et al.*, 2006). Invasive and metastatic cancer cells use MMP-9 in order to migrate. The cancerous cells may produce MMP-9 or induce the production of MMP-9 in surrounding cells. MMP-9 has been shown to play a role in the formation of blood vessels essential for tumour growth and shown to regulate posttranslational modifications of a variety of cytokines, thereby activating MMPs in a positive feedback loop manner (Van den Steen *et al.*, 2001). Interestingly, Das and colleagues (2008) demonstrated that exposure of MCF-7 breast cancer cells to fibronectin in serum free media resulted in expression and activation of MMP-2 and MMP-9.

### **1.3 CELL MIGRATION AND THE ACTIN CYTOSKELETON**

The downstream signalling pathways, often triggered by changes in the extracellular environment, that lead to cytoskeletal rearrangements, actin polymerisation, cell polarisation, the formation of pseudopodia and cell adhesion (all processes required for cell migration) are of particular interest in metastatic cancer cells (Streuli, 1999; Sun *et al.*, 2010). Cytoskeletal elements play essential roles in the organisation and mechanical support of living cells (Wang and Stamenovic, 2002). A number of essential proteins make up the cytoskeleton of cells. Microtubules, composed of  $\alpha/\beta$ -tubulin heterodimers, are required for spatial organisation of organelles and intracellular transport (Desai and Mitchison, 1997; Nogales *et al.*, 1998). Vinculin, a major cytoskeletal protein, accumulates to form focal adhesions as well as cell-cell adhesions (Gilmore and Burridge, 1996). Vimentin is a major structural protein in intermediate filaments. It plays a role in cell proliferation, migration and contractility (Wang and Stamenovic, 2002). Actin is the main cytoskeletal protein required for cell migration (Taiyab and Rao, 2010).

The actin dynamics within migrating cells involve equilibrium processes between the globular (G-actin) and filamentous (F-actin) forms (Wehrle-Haller and Imhof, 2002; Taiyab and Rao, 2010). Three distinct activities are involved in this process of migration (Condeelis, 1993; Pantaloni *et al.*, 2001). Firstly, protrusion occurs, whereby actin-rich structures

(filopodia, lamellipodia or pseudopodia) are pushed out at the leading edge of the cell. Cell attachment then occurs, whereby the actin cytoskeleton connects across the plasma membrane to the substratum forming focal adhesions. Lastly, traction occurs, whereby the trailing cytoplasm is drawn forward (Condeelis, 1993; Pantaloni *et al.*, 2001). Essentially, dynamic assembly and disassembly of focal adhesions and actin polymerisation occur in order to drive the cell forward (Condeelis, 1993; Pantaloni *et al.*, 2001; Wehrle-Haller and Imhof, 2002; Tsutsumi *et al.*, 2008).

Actin stress fibres are filamentous forms of actin that are often found along lines of tension within cells (Wehrle-Haller and Imhof, 2002). These stress fibres are anchored at focal adhesion sites along the periphery of the cell and their presence is indicative of a stationary cell phenotype (Wehrle-Haller and Imhof, 2002). Microtubules have been demonstrated to play a role in mediating actin cytoskeletal dynamics by regulating the retraction of the trailing cytoplasm. Disruption of microtubule formation resulted in an increase in stress fibre formation and a decrease in lamellipodial activity (Wehrle-Haller and Imhof, 2002). Cross-talk between the actin cytoskeleton and the network of microtubules could be regulated through Rho family GTPases (Wehrle-Haller and Imhof, 2002). It should be noted that activated RhoA has been shown to stimulate the formation of stress fibres, while activated Cdc42 and Rac1 have been shown to induce formation of filopodia and lamellipodia, respectively (Wehrle-Haller and Imhof, 2002).

It is important to distinguish between the different types of membrane protrusions, as their roles in cell motility and adherence differ (Adams, 2001). Filopodia are fine, finger-like projections of the plasma membrane. They have a diameter of approximately 0.2  $\mu\text{m}$  and the length of their extensions can reach several hundred  $\mu\text{m}$  (Adams, 2001). The tips of the projections are rich in bundled, cross-linked actin and are often observed in the initial stages of cell spreading (Faix and Rottner, 2006; Yamaguchi and Condeelis, 2007). Filopodia form attachments, referred to as ‘footpads’ at their tips, where extracellular matrix components, including fibronectin and proteoglycans are deposited (Rosen and Culp, 1977; Culp *et al.*, 1979; Adams, 2001). Although the exact role of filopodia is not well defined, it is proposed that they mediate cell spreading by extension of the membrane at the footpads, as well as through extension of lamellipodia between filopodial attachments (Culp *et al.*, 1979; Adams, 2001; Yamaguchi and Condeelis, 2007). It is also proposed that they play a role in cell

adhesion to the extracellular matrix, and have a sensory guidance role in directing cell polarity and cell motility (Albrecht-Buehler, 1976; Adams, 2001).

Lamellipodia can be described as flat, broad, sheet-like protrusions of the plasma membrane that form at the leading edge of migrating cells (Adams, 2001; Yamaguchi and Condeelis, 2007). Attachment of lamellipodia to the extracellular matrix allows for generation of the force that drives the cell forward (Yamaguchi and Condeelis, 2007). Lamellipodia are rich in bundled F-actin, as well as proteins involved in the regulation of the actin cytoskeleton (Adams, 2001; Yamaguchi and Condeelis, 2007). Dynamic, fan-like structures referred to as membrane ruffles often occur parallel to lamellipodial protrusions. The membrane ruffles can be distinguished by their non-adherent, folded back appearance along the lamellipodial edges (Abercrombie *et al.*, 1970; Adams, 2001). Their presence correlates with lamellipodial protrusion and cell motility. It has also been proposed that membrane ruffles increase the surface area for increased contact to the extracellular matrix (Adams, 2001).

In cancer cells the term ‘pseudopodia’ is adopted for F-actin-rich elongated protrusions of the cell membrane that are functionally equivalent to lamellipodia (Albrecht-Buehler, 1970; Adams, 2001; Yamaguchi and Condeelis, 2007). Cancer cells use these pseudopodial protrusions in order to migrate through the extracellular matrix and establish new tumour sites (Taiyab and Rao, 2010). Highly invasive cancer types such as invasive melanomas and metastatic breast cancers exhibit ventral pseudopodial-like extensions referred to as invadopodia (Yamaguchi and Condeelis, 2007; Schoumacher *et al.*, 2010). A number of essential actin and actin regulating proteins as well as extracellular matrix degradation enzymes are localised in invadopodia (Adams, 2001; Egeblad and Werb, 2002; Artym *et al.*, 2006; Yamaguchi and Condeelis, 2007). Degradation and remodelling of the extracellular matrix are important in order for migration and invasion of cancer cells to occur (Coopman *et al.*, 1998; Yamaguchi and Condeelis, 2007). Invadopodia function by degrading extracellular matrix proteins, thereby migrating through the tumour stroma and invading the blood system. From here these structures can invade target tissues (Kucia *et al.*, 2005; Luker and Luker, 2005; Yamaguchi and Condeelis, 2007). Many integrin receptors, cell adhesion molecules and MMPs are localised in pseudopodia and invadopodia (Adams, 2001; Egeblad and Werb, 2002; Artym *et al.*, 2006). These molecules function to mediate the dynamic interactions between the intracellular cytoskeleton and the extracellular matrix; processes essential for

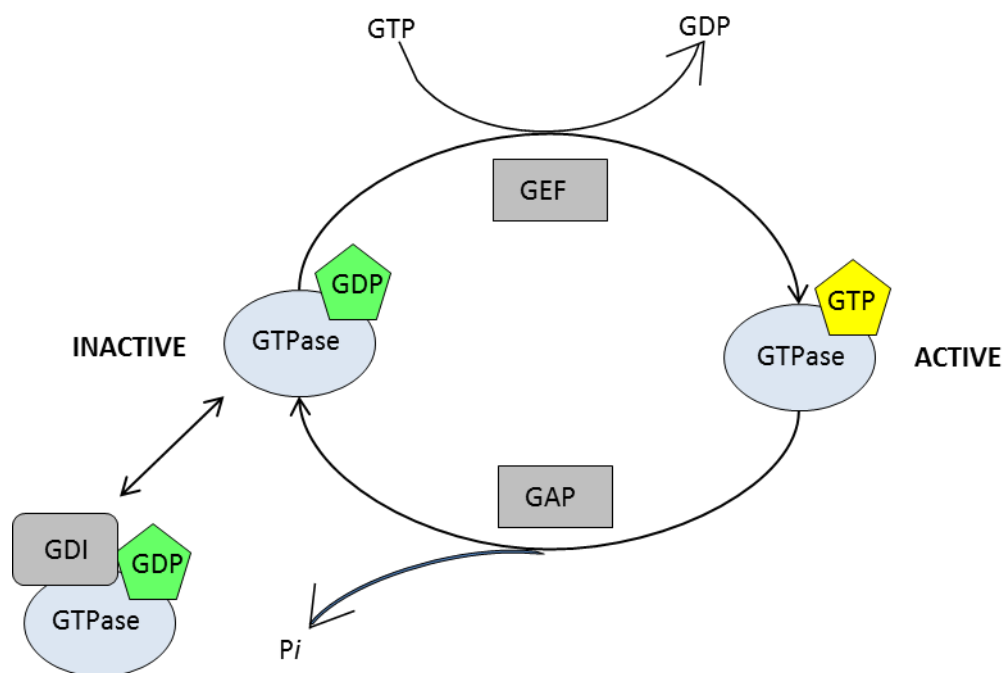
migration and invasion during cancer cell metastasis (Coopman *et al.*, 1998; Yamaguchi and Condeelis, 2007).

#### **1.4 SIGNALLING CASCADES INVOLVED IN ACTIN DYNAMICS**

Directional cell migration occurs when cells sense a directional chemoattractant gradient from the extracellular matrix, which stimulates the reorganisation of the actin cytoskeleton via a cascade of intracellular signals that are locally activated on the cytoplasmic side facing the stimulus (Cho and Klemke, 2002; Brahmabhatt and Klemke, 2003). Essentially, the intracellular signals are spatio-temporally organised within cells such that the activated gradient of signals is thought to facilitate localised actin polymerisation, thereby resulting in polarised cell formations (such as the extension of a dominant leading pseudopodium in the direction of the stimulus) and inducing cell migration (Cho and Klemke, 2002; Brahmabhatt and Klemke, 2003; Tsutsumi *et al.*, 2008; Taiyab and Rao, 2010).

The Ras superfamily of small guanosine triphosphatases (GTPases) are essential molecules in cell signalling cascades, as they function to transfer signals from cell surface receptors through protein kinase cascades, ultimately leading to changes in gene expression and cell morphology or behaviour (Macara *et al.*, 1996; Wennerberg *et al.*, 2005). Ras GTPases regulate these downstream cell biological processes by cycling between their inactive GDP-bound and active GTP-bound states (Figure 1.2). GDP/GTP cycling is regulated by the action of classes of regulatory proteins referred to as guanine nucleotide exchange factors (GEFs) and GTPase activating proteins (GAPs). GEFs function by catalysing the release of bound GDP such that the active GTP-bound state is attained (Macara *et al.*, 1996; DerMardirossian and Bokoch, 2005; Wennerberg, 2005; Karlsson *et al.*, 2009) (Figure 1.2). Activated, GTP-bound GTPases are able to bind and activate a range of downstream effectors (Karlsson *et al.*, 2009). GAPs function to promote the weak, intrinsic GTPase function, enabling the hydrolysis of GTP to GDP, thereby inactivating the GTPase (Macara *et al.*, 1996; DerMardirossian and Bokoch, 2005; Wennerberg, 2005; Karlsson *et al.*, 2009) (Figure 1.2). A further class of regulatory molecules, termed GDP dissociation inhibitors (GDIs) functions by preventing the activation of GDP-bound GTPases, thereby preventing binding and activation of downstream effectors (DerMardirossian and Bokoch, 2005; Karlsson *et al.*, 2009) (Figure 1.2). These processes allow for timed regulation of signalling cascades such that cell functions are correctly performed as required (Macara *et al.*, 1996).

The Ras superfamily is divided into five branches based on their structural and functional similarities. These include Ras, Rho, Rab, Ran and Arf family GTPases. All Ras superfamily proteins contain a structurally conserved ~20 kDa G domain, made up of five GDP/GTP-binding motifs (Wennerberg *et al.*, 2005). The Ras homologous (Rho) family of small GTPases is made up of 20 identified members (Wennerberg *et al.*, 2005). These include the signalling factors Rho, Rac and Cdc42. These signalling factors act downstream of Ras-family GTPases and function to regulate the cytoskeletal response to extracellular stimuli (Macara *et al.*, 1996; Welch, 1999; Mullins, 2000; Wennerberg *et al.*, 2005). Activated Rho has been shown to induce the formation of actin stress fibres and adhesion molecules by reorganisation of existing actin filaments, while activated Rac and Cdc42 have been shown to induce actin polymerisation and lead to the formation of lamellipodia and filopodia, respectively (Macara *et al.*, 1996; Mullins, 2000; Wennerberg *et al.*, 2005). Together, the Rho GTPases have important roles in the regulation of cell morphology, cell migration, cell-cell adhesions and cell-matrix adhesions (Ridley, 2001; Wennerberg *et al.*, 2005).

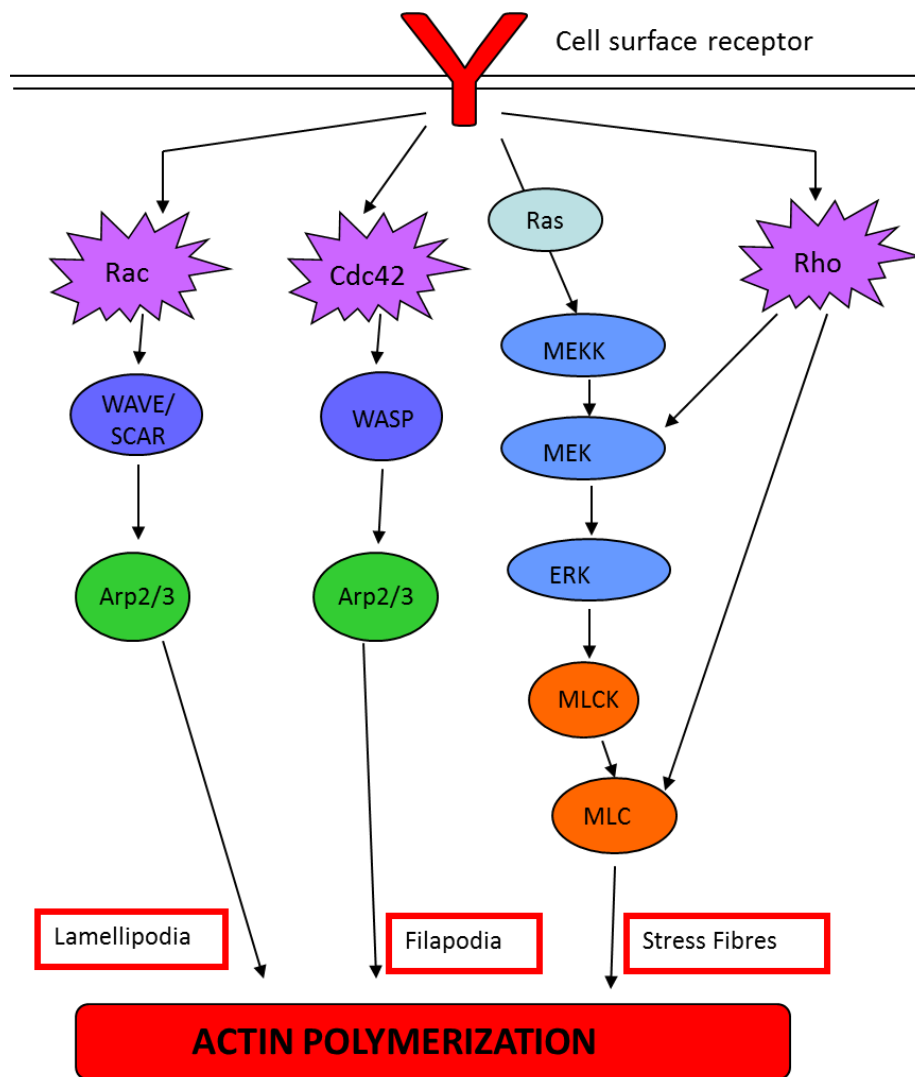


**Figure 1.2: Schematic diagram showing GDP/GTP cycling of Ras superfamily GTPases** (Modified from DerMardirossian and Bokoch, 2005 and Wennerberg *et al.*, 2005). GEFs catalyse the release of GDP from inactive GDP-bound GTPases. This allows for the binding of GTP, resulting in their activation. GAPs hydrolyse GTP to GDP, thereby resulting in their inactivation. GDIs bind GDP-bound GTPases, thereby retaining them in an inactive state.

Rho isoforms have been shown to regulate cell polarity and pseudopodia extension through regulation of myosin light chain kinase (MLCK) and myosin light chain (MLC) phosphorylation (Brahmbhatt and Klemke, 2003) (Figure 1.3). These processes promote assembly of contractile actin-myosin motor units that generate contractile and tension forces that drive the cell forward (Cooper, 2000; Brahmbhatt and Klemke, 2003). The phosphorylation events often occur through activation of MEK/ERK mitogen-activated protein kinase (MAPK) cascades (Brahmbhatt and Klemke, 2003; Taiyab and Rao, 2010; Parri and Chiarugi, 2010) (Figure 1.3). Rac and Cdc42 act through downstream WASP (Wiscott-Aldrich syndrome protein)-family proteins (Mullins, 2000; Cho and Klemke, 2002). The WASP family of proteins is made up of WASP, N-WASP and SCAR (Suppressor of cAMP Receptor mutation), also referred to as WAVE (Welch, 1999; Mullins, 2000). Cdc42 acts through WASP or N-WASP, while Rac acts through SCAR/WAVE (Mullins, 2000) (Figure 1.3).

Activated Rho-family GTPases (Cdc42/Rac) recruit the relevant WASP-family proteins (WASP/SCAR) to the membrane, thereby activating them through protein-protein interactions (Figure 1.3 and Figure 1.4). The WASP-family proteins then recruit and subsequently activate a downstream actin binding complex referred to as the Arp2/3 complex (Welch, 1999; Mullins, 2000) (Figure 1.3 and Figure 1.4). The Arp2/3 complex is made up of seven subunits, two of which are actin-related (Arp2 and Arp3) and the other five of which are novel accessory proteins (p40, p35, p19, p18 and p14) (Mullins, 2000). The Arp2/3 complex catalyses the assembly of F actin filaments from G actin monomers by a process referred to as filament nucleation (Machesky and Gould, 1999; Welch, 1999; Mullins, 2000) (Figure 1.3 and Figure 1.4).

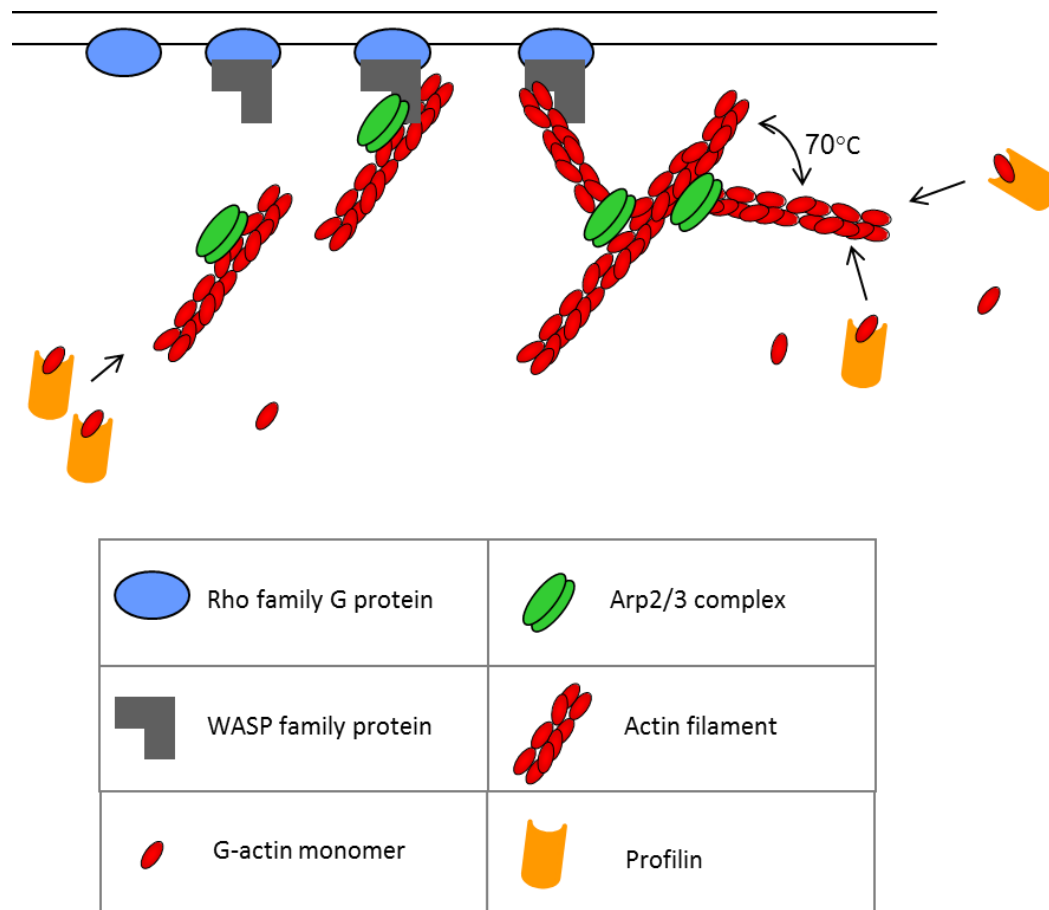




**Figure 1.3: Schematic diagram showing signalling pathways leading to actin polymerisation and the formation of different membrane protrusions.** Rho-family proteins, Rac, Cdc42 and Rho induce changes in the actin cytoskeleton through induction of different intracellular signalling pathways. Rac and Cdc42 act through WASP family proteins (WAVE/SCAR and WASP, respectively), which activate the Arp2/3 complex and catalyse actin filament nucleation. Activation of Rac and Cdc42 lead to formation of lamellipodia and filopodia, respectively. Rho isoforms often act through MEK/ERK MAPK pathways, regulating MLCK and MLC function, which in turn regulate formation of actin stress fibres.

Actin filaments exhibit polarity (Furukawa and Fachheimer, 1997; Mullins, 2000). This allows the Arp2/3 complex to nucleate formation of actin filaments from the minus end, thereby allowing rapid elongation at the plus end. The complex also binds to the sides of pre-existing actin filaments, where actin filament nucleation occurs more efficiently (Machesky and Gould, 1999; Mullins, 2000). The combination of end to side binding allows the Arp2/3 complex to crosslink actin filaments end-to-side at a fixed angle of  $70^\circ$  (Figure 1.4). Repeated rounds of branching nucleation or end-to-side crosslinking result in organised, mechanically rigid actin filament networks (Machesky and Gould, 1999; Welch, 1999;

Mullins, 2000). These actin filament networks ultimately lead to membrane extension and polarity at the leading edges of migrating cells (Welch, 1999; Mullins, 2000; Cho and Klemke, 2002). The Arp2/3 complex has been shown to localise to the actin-rich leading edges of cells, being concentrated in lamellipodia and pseudopodia (Welch, 1999; Mullins, 2000).



**Figure 1.4: Schematic diagram showing actin filament nucleation by actin regulating proteins** (Modified from Alberts *et al.*, 2008; Mullins, 2000 and Witke, 2004). Rho-family proteins recruit WASP-family proteins to the membrane and activate them through protein-protein interactions. WASP-family proteins recruit and activate the Arp2/3 complex which catalyses actin filament nucleation and crosslinking. Profilin binds free actin monomers and shuttles them to the barbed ends of actin filaments, thereby enhancing actin filament elongation.

Other essential actin-binding proteins that function to regulate actin dynamics include profilin, cofilin, gelsolin, thymosin- $\beta$ , capG and capZ (Paunola *et al.*, 2002; Witke, 2004; Ding *et al.*, 2009). Profilin functions by binding G-actin monomers (Figure 1.4). This allows for G-actin monomers present in the cytoplasm to be sequestered such that the pool of free actin monomers available for filament elongation is decreased (Paunola *et al.*, 2002; Witke, 2004; Ding *et al.*, 2009) (Figure 1.4). Profilin activity also catalyses the ADP to ATP

exchange by 1000-fold on G-actin, thereby increasing the pool of ATP-actin monomers in the cell. Profilin then binds ATP-G-actin and shuttles it to the barbed end of the fast growing actin filament, thereby enhancing actin filament elongation/polymerisation (Witke, 2004; Ding *et al.*, 2009) (Figure 1.4). The new regions of the actin filaments are therefore made up of ATP-actin, while the older regions are slowly hydrolysed into ADP-actin and released into the cytoplasm by depolymerisation events (Witke, 2004). The actin binding proteins, cofilin and gelsolin exhibit actin severing activities which sever ADP-actin in filaments, thereby enhancing the rate of actin depolymerisation and playing a role in regulating actin filament turnover in the cell (Moon and Drubin, 1995; Carrier *et al.*, 1997; Witke, 2004). Thymosin- $\beta$ , capG and capZ play roles in inhibiting actin polymerisation (Paunola *et al.*, 2002; Witke, 2004). Thymosin- $\beta$  does this by binding ATP-actin, while capG and capZ function by capping the growing ends of actin filaments, thereby blocking the addition of new ATP-G-actin molecules (Paunola *et al.*, 2002; Witke, 2004).

## **1.5 ROLE OF ACTIN CYTOSKELETAL REGULATING PROTEINS IN CANCER CELL PROGRESSION**

Since cytoskeletal rearrangements are vital for the progression of cancerous cells, it is not surprising that the expression of a number of signalling molecules and downstream effectors related to actin reorganisation and pseudopodia formation have been reported to play important roles in the migration and invasion of tumour cells (Shankar *et al.*, 2010). Such proteins include Rho family GTPases, WASP-family proteins, the Arp2/3 complex, profilin and cofilin (Fritz *et al.*, 1999; Gunnerson *et al.*, 2000; Yanagawa *et al.*, 2001; Otsubo *et al.*, 2004; Wang *et al.*, 2004; Kurisu *et al.*, 2005; Lee *et al.*, 2005; Yamaguchi *et al.*, 2005; Condeelis and Pollard, 2006; Semba *et al.*, 2006; Karlsson *et al.*, 2009).

Overexpression of Cdc42, N-WASP and WAVE1/2/3 (WASP-family proteins), the Arp2/3 complex and cofilin were observed in a range of different cancers including colorectal, melanoma, lung, breast and glioblastoma (Gunnerson *et al.*, 2000; Yanagawa *et al.*, 2001; Otsubo *et al.*, 2004; Wang *et al.*, 2004a; Kurisu *et al.*, 2005; Condeelis and Pollard, 2006; Semba *et al.*, 2006; Yamaguchi and Condeelis, 2007). Similarly, increased expression of Arp2/3 and SCAR/WAVE has been reported to correlate with poor prognosis in breast and liver cancers (Shankar *et al.*, 2010). Reduced levels of N-WASP, the Arp2/3 complex and cofilin resulted in a decrease in the invasive capacity of MTLn3 rat adenocarcinoma cells

(Yamaguchi *et al.*, 2005). Reduced levels of WAVE2 and WAVE3 were shown to correlate with reduced invasive capacity of melanoma and breast cancer cells respectively (Wang *et al.*, 2004a; Kurisu *et al.*, 2005).

Profilin was shown to be highly downregulated in invasive breast cancers compared to their non-cancerous equivalents (Janke *et al.*, 2000; Wang *et al.*, 2002; Roy and Jacobsen, 2004). This correlated with studies demonstrating an overexpression of profilin led to a reduction in cell migration of BT474 invasive breast cancer cells, and suppressed tumour formation in a mouse model (Janke *et al.*, 2000; Roy and Jacobsen, 2004). This also correlated with studies by Bae and colleagues (2009) who demonstrated a reduction in the expression of profilin led to an increase in migration of MDA-MB-231 metastatic breast cancer cells. Mouneimne and colleagues (2012) demonstrated contrasting roles for the profilin isoforms, profilin-1 and the minimally expressed, profilin-2. Interestingly, and perhaps in contrast to the other studies, they demonstrated that knockdown of profilin-1 had an inhibitory effect on cell migration and invasion in SUM159 breast cancer cells, while knockdown of profilin-2 resulted in an increase in cell migration and invasion (Mouneimne *et al.*, 2012; Ding and Roy, 2013).

The Rho-family GTPases have been highly implicated in the regulation of cell migration and invasion of a variety of different cancers (Simpson *et al.*, 2004; Karlsson *et al.*, 2009). An increase in the expression of the Rho GTPase isoforms, RhoA, RhoB and RhoC has been shown to correlate with the progression of tumours in colon, breast, lung and ovarian cancers (Fritz *et al.*, 1999; Fritz *et al.*, 2002; Horiuchi *et al.*, 2003; Simpson *et al.*, 2004). Studies have shown that the different Rho isoforms exhibit distinct functions (Sahai *et al.*, 2002; Simpson *et al.*, 2004; Wu *et al.*, 2010; Vega *et al.*, 2011; Ridley, 2013; Zawistowski *et al.*, 2013). Knockdown of RhoA and RhoC in MDA-MB-231 breast cancer cells showed that RhoC knockdown reduced proliferation and invasion to a much greater extent than RhoA knockdown (Wu *et al.*, 2010). Wu and colleagues (2010) also demonstrated a loss in expression levels of  $\alpha 2\beta 1$  integrin subunits and a subsequent loss in cell-matrix adherence with RhoC knockdown. It was demonstrated that RhoA inhibited, while RhoC stimulated invasion of breast carcinoma cells (Simpson *et al.*, 2004). The interactions of RhoA and RhoC in activating the Rho kinase (ROCK) downstream effector were different, with RhoC having a higher affinity for ROCK (Sahai *et al.*, 2002). RhoC was suggested to play a role in cell morphology, polarised cell migration and invasion through interaction with formin-like-2 (FMNL2) and/or formin-like-3 (FMNL3) effectors, while RhoA was not shown to interact

with FMNL2/3 (Kitzing *et al.*, 2010; Vega *et al.*, 2011). The spatio-temporal activities of RhoA and RhoC during cell migration events were compared (Zawistowski *et al.*, 2013). It was shown that RhoA and RhoC were activated similarly at the cell edges but RhoC was more highly activated at regions more distant from the cell edge. It was also shown that at these more distant regions, RhoC activation occurred before RhoA activation (Zawistowski *et al.*, 2013).

An increase in the expression of RhoC in particular has been shown to correlate with an increased invasion and/or metastatic potential of a number of cancers including pancreatic, colon, breast, melanoma, bladder, hepatocellular, lung and gastric (Suwa *et al.*, 1998; Fritz *et al.*, 1999; van Golen *et al.*, 2000; Clark *et al.*, 2000; Kamai *et al.*, 2003; Wang *et al.*, 2004b; Shikada *et al.*, 2003; Kondo *et al.*, 2004; Simpson *et al.*, 2004; Fingleton, 2007; Karlsson *et al.*, 2009; Ridley, 2013). RhoC knockdown was shown to inhibit cell migration and/or invasion in hepatocellular, prostate and breast carcinoma cell lines (Yao *et al.*, 2006; Wang *et al.*, 2008; Vega *et al.*, 2011). Additionally, RhoC knockdown studies in mouse models demonstrated inhibition of metastasis in lung, hepatocellular and breast carcinomas (Ikoma *et al.*, 2004; Wang *et al.*, 2008; Hakem *et al.*, 2005; Karlsson *et al.*, 2009; Ridley, 2013). A role for RhoC in the regulation of breast cancer stem cell metastasis has also been described (Rosenthal *et al.*, 2012). Interestingly, the microRNAs (miRNAs), miR-138 and miR-493, known to downregulate cancer cell migration have been shown to target RhoC mRNA in tongue and bladder cancer cells (Jiang *et al.*, 2010; Ueno *et al.*, 2012; Ridley, 2013). The activation of RhoC in spatio-temporally distinct zones was shown to regulate the formation of defined invadopodia, through regulation of cofilin phosphorylation (Bravo-Cordero *et al.*, 2011; MacGrath and Koleske, 2011). RhoC activity was shown to be confined to areas surrounding invadopodia, thereby localising cofilin severing activity to invadopodial cores and resulting in the formation of defined invadopodial protrusions (Bravo-Cordero *et al.*, 2011; MacGrath and Koleske, 2011).

## **1.6 MOLECULAR CHAPERONES AND HEAT SHOCK PROTEINS**

The correct folding and functional maturation of many proteins, which include signalling molecules has been shown to be regulated by molecules referred to as molecular chaperones (Gaestel, 2006; Li *et al.*, 2012a). If not regulated, aberrant interactions of nascent or partially folded polypeptides within the intracellular environment could lead to misfolding,

aggregation or misassembly events that would prevent the formation of biologically active native conformations of the proteins (Martin and Hartl, 1997; Fowler *et al.*, 2005; Ellis, 2006; Kampinga and Craig, 2010; Hartl *et al.*, 2011). Molecular chaperones are ubiquitously expressed cellular proteins that function to prevent or reverse these undesirable interactions by mediating the correct folding of the relevant protein substrates (Ellis, 1990; Martin and Hartl, 1997; Ellis, 2005; Ellis, 2006; Koga *et al.*, 2009; Kampinga and Craig, 2010). Molecular chaperones act through non-covalent interactions and do not form part of the final protein structures (Ellis, 1990; Martin and Hartl, 1997; Ellis, 2005; Ellis, 2006). Molecular chaperones are also involved in the translocation of proteins across membranes, as well as the regulation of cell signalling cascades, through mediating conformational changes that allow cell signalling molecules to transform between their active and inactive states (Martin and Hartl, 1997; Gaestel, 2006). Chaperones assist in the presentation of proteins to proteasomes, such that appropriate proteins can be degraded and protein homeostasis within cells can be achieved (Martin and Hartl, 1997; Bagatell and Whitesell, 2004; Hartl *et al.*, 2011). Therefore, molecular chaperones function to maintain protein homeostasis within cells by assisting with the folding, intracellular function and proteolytic turnover of many proteins that act to regulate essential cell processes, including cell growth, migration, differentiation and survival (Bagatell and Whitesell, 2004; Hartl *et al.*, 2011; Kim *et al.*, 2013).

Under stressful environmental conditions (such as high temperatures, hypoxia or acidosis), cellular proteins are more likely to unfold or misassemble (Bagatell and Whitesell, 2004; Ellis, 2005). The requirement for chaperoning activity is therefore increased when cells are exposed to such environmental stresses (Bagatell and Whitesell, 2004; Ellis, 2005). An increase in the expression of heat shock proteins (Hsps), some of which act as molecular chaperones, upon conditions of stress has long been established. This response, termed the heat shock response, has been established as a cellular defense mechanism, and was first discovered by Ferruccio Ritossa (1962), who observed induction of a novel chromosomal puffing pattern in *Drosophila* upon temperature shock (Ritossa, 1962; Welch, 1993). It was Tissières and colleagues (1974) who first identified the protein products, now termed Hsps, that were produced upon induction.

A number of Hsp proteins have been identified and are grouped into families according to their size in kilodaltons (kDa) (Fink, 1999; Kampinga *et al.*, 2009). Some of these include Hsp40, Hsp60, Hsp70, Hsp90, Hsp100 and the small Hsps (Fink, 1999; Mehta *et al.*, 2005;

Kampinga *et al.*, 2009). The molecular chaperones, Hsp70 and Hsp90 are found abundantly in the cytosol of cells and will be described for the purposes of this review (Pratt *et al.*, 2010).

### **1.7 HEAT SHOCK PROTEIN 70 (HSP70) AND HEAT SHOCK PROTEIN 40 (HSP40)**

The chaperone activity of Hsp70 involves recognition of hydrophobic surfaces of unfolded or partially folded proteins and prevention of aggregation by directing misfolded proteins to the ubiquitin-proteasome degradation system of the cell (Pratt *et al.*, 2010; Li *et al.*, 2012a). Hsp70 is also involved in the translocation of proteins across membranes as well as protein stability (Rios *et al.*, 2006; Kampinga and Craig, 2010; Kubota *et al.*, 2010). Hsp70 family proteins are highly conserved and found in almost all organisms (Martin and Hartl, 1997). They are made up of two essential functional domains. The highly conserved N-terminal domain (44 kDa) has a high affinity for ATP and exhibits ATPase activity, which allows for the regulation of substrate binding (Martin and Hartl, 1997; Rüdiger *et al.*, 1997; Bukau and Horwich, 1998). The C-terminal domain (25 kDa) is more variable and is comprised of two functional sub domains, one of which is responsible for peptide binding and the other is responsible for closing the peptide-binding pocket through formation of a lid-like structure (Rüdiger *et al.*, 1997). The C-terminal domain also contains a highly conserved EEVD motif, responsible for interacting with tetratricopeptide repeat (TPR) containing proteins (Odunuga *et al.*, 2003a).

Hsp70 chaperones function closely with members of the Hsp40 chaperone family, which act as co-chaperones, assisting in the maturation of substrate client proteins (Martin and Hartl, 1997). Hsp40 family proteins contain a highly conserved ~70 amino acid N-terminal or C-terminal domain, termed the J-domain (Martin and Hartl, 1997; Kampinga and Craig, 2010). A histidine, proline, aspartate (HPD) motif occurring within a loop between two alpha helices within the J-domain is particularly conserved (Kampinga and Craig, 2010). In addition, Hsp40s contain a peptide binding domain (Kampinga and Craig, 2010). Hsp40s interact with unfolded or partially folded substrate client proteins through their peptide binding domains and bind ATP-bound Hsp70 (“open” conformation) through their J domain (Kampinga and Craig, 2010). This allows for a transient interaction between the client protein and ATP-bound Hsp70 to occur. The interaction of ATP-bound Hsp70 with Hsp40 (through the J-domain) and client protein stimulates the ATPase activity of Hsp70; a process for which the HPD motif is critical (Kampinga and Craig, 2010). Upon ATP hydrolysis, a conformational

change in Hsp70 occurs, resulting in a “closed” conformation. This results in tighter binding and a more stable interaction of ADP-bound Hsp70 with the client protein and promotes the release of Hsp40 from the complex (Martin and Hartl, 1997; Wegele *et al.*, 2006; Kampinga and Craig, 2010).

Stimulation of ATPase activity, also allows for the binding of an Hsp70 interacting protein (Hip) to the ATPase domain, which functions to stabilise Hsp70 in the ADP-bound state (Martin and Hartl, 1997). ADP is dissociated from Hsp70 by binding of nucleotide exchange factors (NEFs) that have a high affinity for ADP-bound Hsp70 (Martin and Hartl, 1997; Kampinga and Craig, 2010). This allows ATP to bind Hsp70, which results in the release of the client protein. If the client protein is not folded into its functional native state, the Hsp40 will rebind to it, and the chaperone cycle will repeat until the native state is achieved (Kampinga and Craig, 2010). Alternatively, the non-functional client protein can be transferred to the degradation machinery of the cell or to another chaperone, such as Hsp90, for complete folding into the native state (Martin and Hartl, 1997).

## **1.8 HEAT SHOCK PROTEIN 90 (HSP90)**

Heat shock protein 90 (Hsp90) is an extremely abundant, ATPase-directed molecular chaperone (Picard, 2002; Koga *et al.*, 2009; Taiyab and Rao, 2010; Li *et al.*, 2012a). Under basal conditions, Hsp90 comprises up to 1 – 2 % of total cellular protein (Bagatell and Whitesell, 2004; Koga *et al.*, 2009). This is increased 2- to 10- fold during environmental stress in order to enhance cell survival (Koga *et al.*, 2009). Many cellular proteins depend on interaction with Hsp90 in order to function correctly. These proteins, known as “client proteins” depend on Hsp90 for their correct folding, functional maturation and trafficking between cellular compartments (Khalil *et al.*, 2011; Koga *et al.*, 2009; Li *et al.*, 2012a).

Hsp90 also functions to stabilise client proteins, thereby preventing Hsp70 dependent degradation by the ubiquitin proteasome system, until required (Pratt *et al.*, 2010). In this way, Hsp90 plays a role in regulating protein degradation, thereby helping to maintain normal protein turnover rates within cells (Koga *et al.*, 2009; Pratt *et al.*, 2010; Li *et al.*, 2012a). Hsp90 can therefore be regarded as having an essential “housekeeping” function within cells (Picard, 2002; Koga *et al.*, 2009). Over 200 Hsp90 client proteins have been described (Li *et al.*, 2012a). The client proteins of Hsp90 include numerous steroid hormone



receptors, kinases and transcription factors, many of which are deregulated or mutated in cancers (Koga *et al.*, 2009; Taipale *et al.*, 2012). Under environmental stress, Hsp90 regulates the repair or degradation of damaged proteins in order to re-establish protein homeostasis (Picard, 2002; Koga *et al.*, 2009; Li *et al.*, 2012a). It should be noted that Hsp90 binds near-native state client proteins, as opposed to nascent client proteins that are bound by Hsp70 (Southworth and Agard, 2011; Li *et al.*, 2012a).

In its native state, Hsp90 occurs as a dimer made up of three regions including the N-terminal region (24-28 kDa), the middle region (38-44 kDa) and the C-terminal region (11-15 kDa) (Csermely *et al.*, 1998; Soti *et al.*, 1998; Meyer *et al.*, 2003; Banerji *et al.*, 2009). The N-terminal domain contains an ATP binding site and ATPase activity of Hsp90 (Banerji, 2009; Li *et al.*, 2012a). This N terminal domain is also the binding domain for the naturally occurring Hsp90 inhibitor, geldanamycin (Koga *et al.*, 2009). By binding this ATP binding site, geldanamycin interferes with Hsp90 function, thereby promoting degradation of key regulatory proteins, many of which are involved in cancer progression (Allan *et al.*, 2006). The middle region forms a highly charged hinge-like structure and is responsible for the binding of client proteins and co-chaperones, while the C-terminal region is responsible for Hsp90 dimerisation (Csermely *et al.*, 1998; Allan *et al.*, 2006; Banerji, 2009). Another known Hsp90 inhibitor, novobiocin, binds at a site within the C-terminal dimerisation domain of Hsp90 (Marcu *et al.*, 2000; Allan *et al.*, 2006). A highly conserved C-terminal MEEVD motif is responsible for binding TPR containing proteins, many of which are cochaperones (Odunuga *et al.*, 2003a; Allan *et al.*, 2006). Novobiocin interferes with binding of cochaperones to Hsp90 at the C-terminus and results in destabilisation of client proteins from Hsp90 (Marcus *et al.*, 2000). Although Hsp90 ATPase activity is weak, it has been considered essential for interactions within the Hsp90 multichaperone heterocomplex (Prodromou *et al.*, 1997; Li *et al.*, 2012a).

## **1.9 HSP70/HSP90 ORGANISING PROTEIN (HOP) AND THE HSP90 MULTICHAPERONE HETEROCOMPLEX**

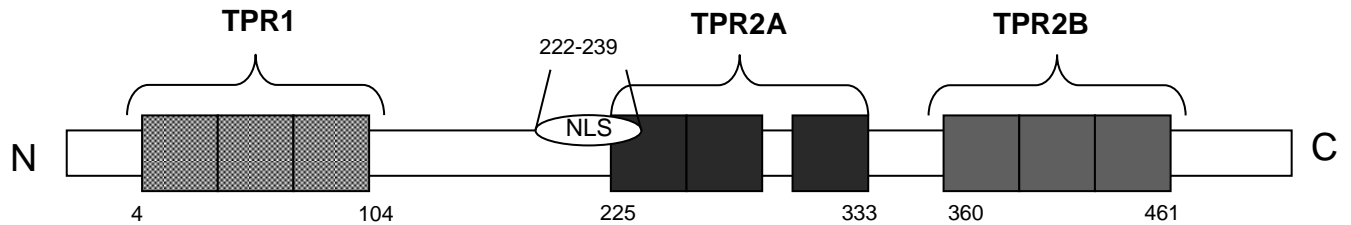
The Hsp70/Hsp90-organising protein (Hop), also known as stress-induced phosphoprotein 1 (STIP1) is a 60 kDa co-chaperone that interacts with the heat shock proteins, Hsp70 and Hsp90, forming part of a dynamic multichaperone heterocomplex (Chen *et al.*, 1996; Van der Spuy *et al.*, 2000; Daniel *et al.*, 2007; Walsh *et al.*, 2011). Hop acts as an adaptor between the

two chaperones and facilitates transfer of protein clients between Hsp70 and Hsp90 (Chang *et al.*, 1997; Wegele *et al.*, 2003; Odunuga *et al.*, 2004; Daniel *et al.*, 2007).

In addition to its intracellular role in the cytoplasm, Hop has also been shown to act extracellularly, and perhaps independently of the Hsp90 heterocomplex, as a cell surface ligand for cellular prion protein (PrP<sup>c</sup>) (Zanata *et al.*, 2002; Lopes *et al.*, 2005; Erlich *et al.*, 2007). The interaction of extracellular Hop and PrP<sup>c</sup> results in the activation of intracellular signalling pathways that promote neuroprotection and neuritogenesis and prevent apoptosis (Zanata *et al.*, 2002; Lopes *et al.*, 2005). The Hop-PrP<sup>c</sup> interaction also induced cell proliferation and enhanced self renewal of neural stem cells (Lopes *et al.*, 2012). In addition, it prevented ischemia-related neuronal death (Beraldo *et al.*, 2013). Extracellular Hop was shown to act independently of PrP<sup>c</sup> to modulate proliferation and cell death in developing retina (Arruda-Carvalho, 2007).

The structure of Hop allows for the interaction with both Hsp70 and Hsp90 and its subsequent function as an adaptor protein (Odunuga *et al.*, 2003a). Hop and homologues of Hop are structurally defined by the presence of nine TPR motifs. The TPR motif is characterised by a degenerate, 34 amino acid consensus sequence that is typically found in varying numbers of tandem repeats (Blatch and Lässle, 1999; Odunuga *et al.*, 2003a; Daniel *et al.*, 2007). Each TPR motif is arranged in a parallel manner such that adjacent  $\alpha$ -helices are antiparallel. The packing of the helices within and between adjacent TPR motifs is identical, thereby resulting in each  $\alpha$ -helix sharing two immediate  $\alpha$ -helical neighbours. The regular repeat of  $\alpha$ -helices creates a right-handed helical conformation (superhelix) that creates an amphipathic channel (Blatch and Lässle, 1999; Van der Spuy *et al.*, 2000). The TPR motifs are characterised as protein-protein interaction modules, with these amphipathic channels serving to accommodate other proteins (Blatch and Lässle, 1999; Daniel *et al.*, 2007). The TPR motifs are grouped into three TPR domains, each comprising three TPR motifs. Hop has three TPR domains, namely TPR1, TPR2A and TPR2B arranged from the amino terminus to the carboxyl terminus of the co-chaperone, as well as a nuclear localisation signal (NLS) that overlaps the TPR2A domain (Odunuga *et al.*, 2003a; Longshaw *et al.*, 2004; Daniel *et al.*, 2007) (Figure 1.5). The N-terminal TPR domain (TPR1) is required to bind to Hsp70, while the central TPR domain (TPR2A) is required for Hsp90 binding (Odunuga *et al.*, 2003a; Daniel *et al.*, 2007; Kubota *et al.*, 2010). Both Hsp70 and Hsp90 bind to their respective TPR

domains on Hop via an EEVD motif on the C terminus of the chaperones (Odunuga *et al.*, 2003a; Daniel *et al.*, 2007).



**Figure 1.5: Schematic Diagram of the TPR Domains of Hop** (Modified from Daniel *et al.*, 2007).

The structure of Hop contains three TPR domains (TPR1 [residues 1-104], TPR2A [residues 225-333] and TPR2B [residues 360-461]) arranged from the N terminus to the C terminus of the protein. Each TPR domain is comprised of three TPR motifs. A NLS (residues 222-239) that overlaps the TPR2A domain is also present. TPR1 is known to bind Hsp70, while TPR2A and TPR2B are required for Hsp90 binding.

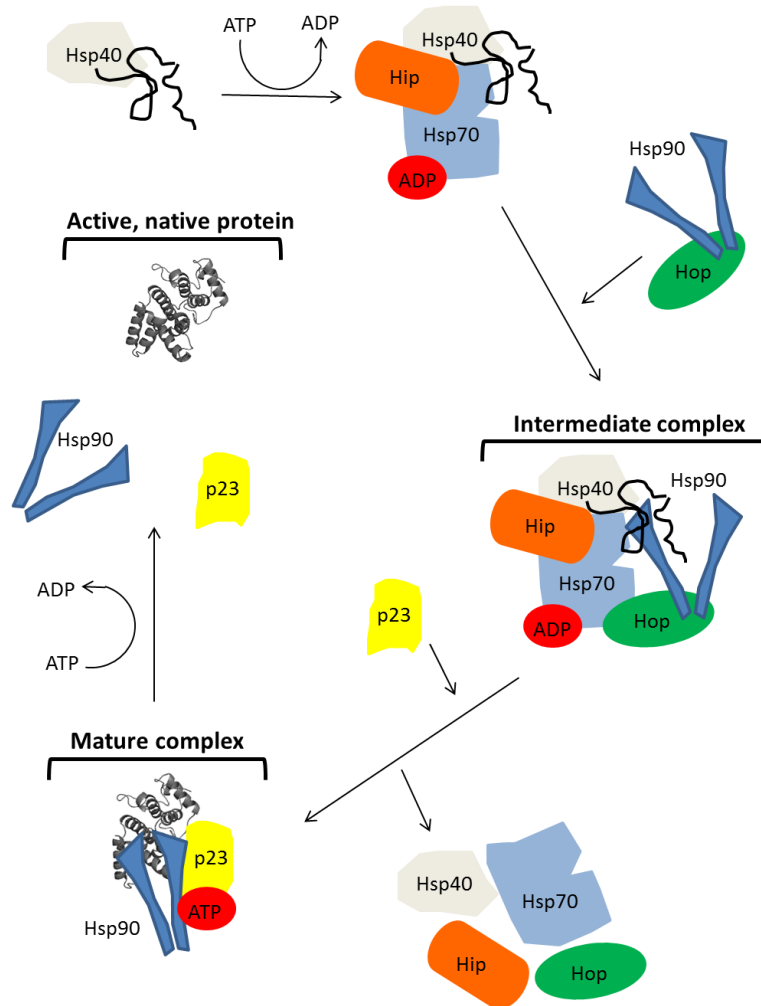
Hop functions by stabilising an open conformation of the Hsp90 dimer, in which the hydrophobic client binding surfaces are accessible for client binding, but the N-terminal domains have undergone a conformational change such that they resemble the closed ATP-bound Hsp90 state (Southworth and Agard, 2011; Lee *et al.*, 2012). This prevents N-terminal dimerisation, which in turn results in inhibition of Hsp90 ATPase activity (Southworth and Agard, 2011; Lee *et al.*, 2012). Hop binds such that the TPR1 domain extends from the Hsp90 dimer cleft, thereby allowing binding of ADP-bound Hsp70 (Southworth and Agard, 2011). Through the use of cross-linking and mass spectrometry techniques, Lee and colleagues (2012) determined that the TPR2A and TPR2B domains of Hop were those responsible for ATPase inhibition of Hsp90. A proposed model in which the TPR2A domain of Hop initially binds the MEEVD motif of Hsp90 has been described (Lee *et al.*, 2012; Schmid *et al.*, 2012). This model proposed that the TPR2A-MEEVD interaction is maintained through a stable interaction between the TPR2B domain of Hop and the middle domain of Hsp90 that occurs, with the aid of the N-terminal domain, after initial TPR2A-MEEVD contact (Lee *et al.*, 2012). It is also possible that Hop forms a network of interactions with Hsp70 and Hsp90 that are not mediated by the TPR domains and contribute to the role of Hop as a scaffolding protein (Odunuga *et al.*, 2003b; Longshaw *et al.*, 2004; Daniel *et al.*, 2007).

One of the initial studies demonstrating the functioning of Hop as an adaptor protein in a multichaperone heterocomplex includes that of Dittmar and colleagues (1997), who showed that Hsp70, Hsp90 and Hop functioned together in a chaperone complex to release a mature, biologically active conformation of the glucocorticoid steroid receptor (an established Hsp90 client protein). Similarly, Chen and Smith (1998) demonstrated that Hop played a role in the maturation of progesterone receptors through functioning as an adaptor protein mediating the associations and chaperoning activities of Hsp70 and Hsp90. Hernández and colleagues (2002) demonstrated that Hop enhanced the functional cooperations of Hsp70 and Hsp90 and suggested that assembly of Hsp70-Hop-Hsp90 complexes influenced the conformational states of client proteins in a selective manner. The role of Hop in the regulation of client proteins by mediating the association between Hsp70 and Hsp90, thereby controlling and enhancing the rate of their chaperoning activities has since been widely established (Longshaw *et al.*, 2009; Kubota *et al.*, 2010; Walsh *et al.*, 2011).

A model for the transfer of proteins from Hsp70 to Hsp90 by Hop in a dynamic multichaperone heterocomplex was shown effectively by Wegele and colleagues (2006). A luciferase substrate was used to analyse the chaperoning activities of individual chaperones compared to the combined chaperoning activities of Hsp70, Hsp40 and Hsp90, in the absence and presence of Hop (Wegele *et al.*, 2006). Hop was shown to stimulate the refolding activity of Hsp70 by several-fold (Wegele *et al.*, 2006). In the presence of an Hsp70-Hsp40 complex, the addition of Hop stimulated an even greater increase in chaperoning activity. When Hsp90 was added to an Hsp40-Hsp70-Hop complex, an even greater increase in the chaperoning activity was observed (Wegele *et al.*, 2006). Chaperoning activity was measured by measuring the percentage of luciferase activity (luminescence), during refolding from a denatured state, over time (Wegele *et al.*, 2006). Hsp90 alone had a low affinity for luciferase substrate and Hop was therefore required for the binding of substrate to Hsp90 (Wegele *et al.*, 2006). The study, along with others, demonstrated that Hop did not possess any chaperoning activity of its own (Chen and Smith, 1998; Hernández *et al.*, 2002; Wegele *et al.*, 2006).

These studies led to the description of a proposed model for the functioning of the Hsp40-Hsp70-Hop-Hsp90 multichaperone complex. It was proposed that initially, Hsp40 binds the non-native, unfolded client protein and subsequently delivers it to Hsp70 through an ATPase directed mechanism, the product of which is stabilised by Hip (as described previously for the chaperoning activity of Hsp70) (Hernández *et al.*, 2002; Wegele *et al.*, 2006) (Figure 1.6).

An intermediate complex is then formed through binding of the Hsp40-Hsp70-client protein complex to a high affinity pre-formed Hop-Hsp90 complex, where transfer of the client protein from Hsp70 to Hsp90 via Hop occurs (Hernández *et al.*, 2002; Wegele *et al.*, 2006) (Figure 1.6). In the complex, Hsp90 binds ATP, which allows for the subsequent binding of p23, an acidic protein that functions to stabilise the activated complex. The binding of p23 results in the dissociation of Hop from the complex and the maturation of the client protein into an active state (Figure 1.6). Subsequent hydrolysis of ATP results in the release of p23 and the mature, biologically active, native protein from Hsp90 (Hernández *et al.*, 2002; Havik and Bramham, 2007; Wegele *et al.*, 2006) (Figure 1.6).



**Figure 1.6: Schematic diagram showing a model for the functioning of the Hsp90 multichaperone heterocomplex.** Hsp40 binds unfolded client protein and transfers it to Hsp70. Hydrolysis of ATP leads to tighter binding of client protein to ADP bound Hsp70. The complex is stabilised by Hip. The complex binds a pre-formed Hop-Hsp90 dimer, forming an intermediate complex in which client protein is transferred from Hsp70 to Hsp90 via Hop. The binding of p23 to ATP-bound Hsp90 results in the dissociation of Hop from Hsp90 and the maturation of the client protein into an active state. The Hsp90-p23-client protein complex is referred to as the mature complex. ATP hydrolysis of Hsp90 in the mature complex allows for the release of active, native protein from Hsp90.

A number of other co-chaperones that have various roles within the Hsp90 multichaperone heterocomplex have also been defined (Li *et al.*, 2012a). Some of these include Fkbp52, Fkbp51, Cyp40, CHIP, Tpr2, Aha1 and Cdc37 (Li *et al.*, 2012a). Fkbp52, Fkbp51 and Cyp40 are peptidyl-prolyl-isomerase (PPIase) domain containing cochaperones involved in client protein maturation (Johnson and Toft, 1994; Pirkel and Buchner, 2001). CHIP is an ubiquitin ligase, functioning to direct client proteins to the ubiquitin proteasome for degradation (Li *et al.*, 2012a). Tpr2 has binding affinity for both Hsp90 and Hsp70 through its TPR domains and is thought to facilitate the reverse transfer of clients from Hsp90 to Hsp70 (Li *et al.*, 2012a). Aha1 stimulates the ATPase activity of Hsp90, thereby inducing conformational changes in Hsp90 (Hessling *et al.*, 2009; Retzlaff *et al.*, 2010). Cdc37 functions specifically in the recruitment of protein kinases to the chaperone complex (Allan *et al.*, 2006; Li *et al.*, 2012a; Taipale *et al.*, 2012). It inhibits Hsp90 ATPase activity by interacting with the N-terminal ATPase binding domain (Allan *et al.*, 2006; Li *et al.*, 2012a; Taipale *et al.*, 2012).

The Hsp70-Hop-Hsp90 multichaperone complex has also been shown to be involved in targeting cytosolic proteins to lysosomes for degradation (Agarraberes and Dice, 2001; Daniel *et al.*, 2007). This occurs as a response to stress conditions such as prolonged starvation or serum withdrawal. In order to be transported to the lysosomal lumen, proteins have to become unfolded. It is thought that Hop may play a role in stabilising the Hsp70-“client protein” complex on the surface of the lysosome, thereby allowing complete unfolding of the client protein before it is imported into the lysosome (Agarraberes and Dice, 2001; Daniel *et al.*, 2007). Longshaw and colleagues (2009) showed that Hop knockdown in mouse embryonic stem cells (mESCs) resulted in a loss of phosphorylated Stat3 levels, which led to a loss in pluripotent ability. This suggested that Hop, within the Hsp90 heterocomplex, could play a role in pluripotent signalling (Longshaw *et al.*, 2009a). A recent study demonstrating the importance of Hop *in vivo*, showed that Hop knockout mice were embryonic lethal and that transgenic expression of the Hop gene could rescue the embryo (Beraldo *et al.*, 2013). This demonstrated a role for Hop in embryonic development (Beraldo *et al.*, 2013).

The studies described, along with further studies have established that the organised action of Hsp70 and Hsp90 under the control of Hop prevents misfolding and aggregation of client proteins, thereby assisting in the correct folding of the proteins and resulting in the formation of functional protein complexes (Longshaw *et al.*, 2009b; Kubota *et al.*, 2010; Walsh *et al.*,

2011). Such client proteins include key regulatory proteins involved in cell survival such as steroid hormone receptors, transcription factors and kinases, many of which are involved in the progression of cancer (Van der Spuy *et al.*, 2000; Kubota *et al.*, 2010; Walsh *et al.*, 2011).

### **1.10 THE ROLE OF HOP IN CANCER**

In cancer cells, Hsp90 is upregulated and its ATPase activity is increased by approximately 50 fold (Taiyab and Rao, 2010). Hsp90 plays an essential role in acquiring and maintaining the capabilities that characterise malignant cancer cells (Koga *et al.*, 2009). These characteristics include sustained angiogenesis, invasion and metastasis, insensitivity to anti-growth signalling, limitless replicative potential, self-sufficiency in growth signalling and the ability to evade apoptosis (Koga *et al.*, 2009). It has been reported that Hsp90 in tumour cells is present almost entirely in a multichaperone complexed state with high ATPase activity, while Hsp90 in normal cells is typically present in a latent, uncomplexed state (Kamal *et al.*, 2003). Overexpression of Hsp70 in tumour cells has also been reported and Hsp70 has been shown to block apoptosis in various cancer cell lines (King *et al.*, 2001; Havik and Bramham, 2007).

Hop has also been shown to be overexpressed in a wide variety of cancers, including pancreatic, hepatocellular, colon and breast cancers (Sun *et al.*, 2007; Kubota *et al.*, 2010; Pimienta *et al.*, 2011; Walsh *et al.*, 2011). Depleted Hop levels were shown to correlate with decreased expression levels of MMPs; enzymes essential for invasion of cancerous cells into the tissue (Walsh *et al.*, 2011). Depleted Hop levels were also shown to correlate with reduced metastatic and invasion potential of several human pancreatic cancers (Walsh *et al.*, 2011). Pimienta *et al.* (2011) were able to cause a dramatic decrease in cell viability of breast cancer cells by blocking the interaction of Hop with Hsp90 through the use of a TPR peptide mimic. Similarly, an anti-TPR peptide that prevented binding of Hsp90 and the TPR2A domain of Hop was shown to induce apoptosis in a variety of cancer cell lines (pancreatic, renal, gastric, lung and prostate) (Horibe *et al.*, 2011).

Hop was shown to interact with tubulin and be involved in tube formation/angiogenesis; processes essential for the maintenance of cancer cells (Li *et al.*, 2012b). Depleted Hop levels resulted in a decrease in cell migration in metastatic MDA-MB-231 and HS578T breast carcinoma cells as well as endothelial HUVEC cells (Li *et al.*, 2012b; Willmer *et al.*, 2013).

Hop was shown to colocalise with the cytoskeletal protein, actin, at the leading edge (lamellipodia and pseudopodia) of metastatic HS578T cells (Willmer *et al.*, 2013). Additionally, Hop was found to be enriched in the pseudopodia compared to the cell body of HS578T cells and depleted levels of Hop were shown to dramatically reduce the formation of pseudopodia in these cells (Willmer *et al.*, 2013).

Roles for extracellular Hop in processes involved in cancer cell progression were revealed. Hop was shown to be secreted by human ovarian cancer cells and subsequently identified as a released biomarker in these cells (Tsai *et al.*, 2012; Chao *et al.*, 2013). Extracellular Hop was shown to increase cell proliferation and migration of ovarian cancer cells by binding ALK2 and activating the SMAD signalling pathway (Tsai *et al.*, 2012). Hop was secreted by A172 human glioblastoma cells and stimulated their proliferation through regulation of MAPK pathways (Erlich *et al.*, 2007). In addition, Hop was shown to function extracellularly as a co-chaperone within the Hsp90 heterocomplex to enhance the activation of MMP-2 in MDA-MB-231 breast cancer cells (Sims *et al.*, 2011).

There is a growing body of data which, together with the findings that Hsp90 is present in complex with Hop in cancer cells compared to its uncomplexed state in normal cells, suggest a role for Hop in the progression of cancer and cancer cell metastases (Kamal *et al.*, 2003).

### **1.11 ROLE OF MOLECULAR CHAPERONES IN PROTEINS INVOLVED IN CELL MIGRATION PROCESSES:**

The role of many molecular chaperones in the regulation of extracellular matrix and cytoskeletal proteins has been studied. Of these, Hsp90 has been the most widely studied. The cytoskeletal proteins, actin, tubulin and vimentin have all been characterised as Hsp90 client proteins (Koyasu *et al.*, 1986; Kellermayer and Csermely, 1995; Williams and Nelsen, 1997; Zhang *et al.*, 2006; Park *et al.*, 2007; Weis *et al.*, 2010). A role for Hsp90 in the chaperoning of the matrix degradation enzymes, MMP2, MMP3 and MMP9 has also been described (Eustace *et al.*, 2004; Yang *et al.*, 2008; Song and Luo, 2010; Stellas *et al.*, 2010; Taiyab and Rao, 2010; Correia *et al.*, 2013). Other actin-regulating Hsp90 client proteins include the Ras-superfamily GTPases, Rac1, RalBP1, RHOBTB1 and the downstream effector, N-WASP (Hu and Mivechi, 2003; Park *et al.*, 2005; Cha *et al.*, 2010; Taipale *et al.*, 2012). Ras superfamily GTPases are monomeric G-proteins that are structurally and



functionally homologous to the  $G\alpha$  subunit of heterotrimeric G-proteins (Wennerberg *et al.*, 2005). The free  $\beta\gamma$  subunit of heterotrimeric G proteins as well as the  $G\alpha$  subunits,  $G\alpha_0$  and  $G\alpha_{12}$  have also been characterised as Hsp90 clients (Inanobe *et al.*, 1994; Busconi *et al.*, 2000; Vaiskunaite *et al.*, 2001). The G-protein subunits, activated by G-protein-coupled receptor- (GPCR) mediated signals, occur upstream of Rho family proteins and function to activate them (Gutkind, 1998; Sun *et al.*, 2010; Teicher and Fricker, 2010). More recently, fibronectin was identified as a putative Hsp90 client protein, and suggested to play a role in extracellular matrix remodelling through stabilisation or assembly of the fibronectin matrix (Hunter *et al.*, 2014).

Other molecular chaperones shown to modulate actin dynamics include Hsp100, which is shown to play a role in the cross-linking of microfilaments and Hsp70, which is speculated to be involved in the stabilisation of actin filaments (Liang and MacRae, 1997). Additionally, colocalisation between Hsp28 and actin has been reported in phorbol ester myristate induced HL-60 human promyelocytic leukemic cell line (Liang and MacRae, 1997). An interaction between Hsp47 and the extracellular matrix protein, collagen IV has been described, with knockdown of Hsp47 resulting in an inability of the collagen matrix to properly form (Nagai *et al.*, 2000; Sauk *et al.*, 2005).

The molecular co-chaperone, Hop, has a role in pseudopodia formation and has been demonstrated to bind F-actin in vitro using co-sedimentation assays (Willmer *et al.*, 2013). Interestingly, Marty and colleagues (2003) demonstrated binding of a TPR1 domain containing protein to several different  $G\alpha$  proteins and demonstrated an interaction between TPR1 and Ras. Li and colleagues (2012) demonstrated that Hop interacted with tubulin and microtubules. It was further demonstrated that Hop lacking a TPR2A domain had the strongest binding affinity to tubulin/microtubules and that TPR2A alone was unable to bind tubulin/microtubules (Li *et al.*, 2012b).

### **1.12 KNOWLEDGE GAP:**

There is increasing evidence demonstrating a role for both extracellular and intracellular Hop in cancer cell progression. Evidence for the role of extracellular Hop in processes essential for cancer cell progression, including proliferation and migration has been described (Tsai *et al.*, 2012; Chao *et al.*, 2013). Little is known about the mechanisms by which extracellular Hop regulates these processes, nor which regions of the Hop protein are required for this activity. This study therefore aimed to determine the effects of independent domains of Hop (TPR2A2B and TPR1) on cell migration processes. This may aid in elucidating mechanistic roles of extracellular Hop in cell behaviour. Knockdown of intracellular Hop was shown to have an inhibitory effect on migration and the metastatic and invasive potential of a variety of cancers (Walsh *et al.*, 2011; Li *et al.*, 2012b; Willmer *et al.*, 2013). Hop was shown to interact directly with the cytoskeletal proteins, tubulin and actin, thereby regulating tube and pseudopodia formation, respectively (Li *et al.*, 2012b; Willmer *et al.*, 2013). Little is known about the effects of Hop on the signalling cascades leading to these changes in cytoskeletal dynamics. This study therefore aimed to investigate the role of intracellular Hop on the signalling pathways that lead to cytoskeletal changes as well as any potential interactions of Hop with these signalling proteins. Interestingly, the Rho-family GTPase, RhoC has emerged quite rapidly as a molecule involved in cancer cell invasion (Ridley, 2013).

### **1.13 HYPOTHESIS:**

Extracellular and intracellular pools of Hop regulate distinct cell migration related processes by activation of cell signalling pathways or direct interactions with signalling intermediates.

### **1.14 OBJECTIVES:**

- 1) To determine the effect of exogenous full length and truncated extracellular Hop on cell migration processes
- 2) To determine the effect of intracellular Hop on cell migration processes using RNA interference

## **Chapter 2.**

# **The effect of exogenous full length and truncated extracellular Hop on cell migration processes**

## 2.1 INTRODUCTION:

A number of studies have demonstrated a role for extracellular Hop in processes required for cancer cell progression, including proliferation and migration. Hop was found extracellularly in the conditioned media of a variety of cancer cell lines, including pancreatic, ovarian, glioblastoma and breast (Erlich *et al.*, 2007; Sims *et al.*, 2011; Walsh *et al.*, 2011; Tsai *et al.*, 2012; Chao *et al.*, 2013). In some cases, Hop was found in the conditioned media along with other members of the Hsp90 multichaperone heterocomplex, including Hsp90, Hsp70, Hsp40 and p23 (Sims *et al.*, 2011; Walsh *et al.*, 2011). Extracellular Hop was shown to stimulate proliferation of ovarian and glioblastoma cells through different transduction pathways (Erlich *et al.*, 2007; Tsai *et al.*, 2012). Extracellular Hop was also shown to have a stimulatory effect on the migration of ovarian cancer cells (Chao *et al.*, 2013). In contrast, Li and colleagues (2012) observed no effect on migration of vascular endothelial cells with treatment with recombinant Hop or a blocking antibody against Hop.

Cell migration processes are regulated by dynamic interactions between the intracellular cytoskeleton and the extracellular matrix (Coopman *et al.*, 1998; Egeblad and Werb, 2002). MMPs are required for the degradation of extracellular matrix proteins such as gelatin and fibronectin to promote such processes, including migration and invasion (Streuli, 1999; Egeblad and Werb, 2002). Interestingly, extracellular Hop co-immunoprecipitated with MMP-2 in the conditioned media of MDA-MB-231 breast and HT-1080 pancreatic cancer cell lines (Sims *et al.*, 2011; Walsh *et al.*, 2011). The presence of extracellular Hop was shown to enhance the activation of MMP-2 compared to extracellular Hsp90 alone in breast cancer cells, while knockdown of Hop in pancreatic cancer cells resulted in a decrease in the expression levels of MMP-2 (Sims *et al.*, 2011; Walsh *et al.*, 2011). Both studies suggested that Hop may act as an extracellular co-chaperone to Hsp90, functioning to enhance activation of MMP-2 (Sims *et al.*, 2011; Walsh *et al.*, 2011).

It is evident that roles for extracellular Hop in cancer cell progression in a variety of cancers are beginning to emerge, but to our knowledge, there are currently no studies demonstrating which domains of the Hop protein are responsible for these observed effects. Recombinant DNA techniques using glutathione-S-transferase affinity tags were therefore used to overexpress and purify full length murine Hop, as well as N-terminal truncated (containing the TPR2A and TPR2B domains) and C-terminal truncated (containing the TPR1 domain)

murine Hop as GST fusion proteins. The purified proteins were used in cell biological assays in order to elucidate the function of extracellular Hop in proliferation, migration and invasion of HS578T metastatic breast cancer cells.

## **2.2 MATERIALS:**

All general reagents and chemicals were purchased from Sigma Aldrich (USA). Specialised reagents are reflected in the method section. Please see Appendix 1 for a list of all additional materials used including molecular weight markers, kits, antibodies and tissue culture reagents.

## **2.3 METHODS:**

### **2.3.1 Sequencing of pGEX3X2000, pGEX3X1400 and pGEX3X700 plasmids**

The pGEX-4T1 (encoding GST), pGEX3X2000 (containing the full length mSTI1 coding sequence [residues 1 -543]), pGEX3X1400 (containing an N-terminal truncated mSTI1 coding sequence containing the TPR2A and TPR2B mSTI1 domains [residues 208-543]) and pGEX3X700 (containing a C-terminal truncated mSTI1 coding sequence containing the TPR1 mSTI1 domain [residues 1-217]) plasmids were produced as part of a previous study (Lässle *et al.*, 1997). The plasmids all contained a glutathione-*S*-transferase (GST) tag as well as an ampicillin resistance gene. The plasmids were sent to Inqaba Biotec (South Africa) for sequencing of the inserts using the pGEX 5' forward primer (5'-GGGCTGGCAAGCCACGTTTGGTG-3') as well as the pGEX 3' reverse primer (5'-CCGGGAGCTGCATGTGTCAGAGG-3'). Sequences were analysed and plasmid maps created using the BioEdit software programme. The proteins expressed from the pGEX-4T1, pGEX3X2000, pGEX3X1400 and pGEX3X700 will henceforth be referred to as GST, GST-mSTI1, GST-TPR2A2B and GST-TPR1, respectively.

### **2.3.2 Confirmation of pGEX-4T1, pGEX3X2000, pGEX3X1400 and pGEX3X700 plasmids by restriction enzyme digestion**

The pGEX-4T1, pGEX3X2000, pGEX3X1400 and pGEX3X700 plasmids were transformed into competent *Escherichia Coli* (*E.coli*) XLI Blue cells obtained from laboratory stocks and plated onto 2 x Yeast Tryptone (2 x YT) (16 g/L tryptone, 10 g/L yeast extract, 5 g/L NaCl) agar plates containing ampicillin (100 µg/mL) and allowed to grow at 37°C overnight.

Transformed colonies were inoculated into 5 mL of 2 x YT broth containing ampicillin (100 µg/mL) and grown at 37°C overnight with shaking (180 rpm). Plasmids were extracted using the Zippy™ Plasmid Miniprep Kit (Cat #: D4019) (Zymo Research, USA) according to manufacturer's protocol and quantified using the Nanodrop 2000. Restriction enzyme digestions of each of the plasmids using the *Pst*I restriction endonuclease were performed in order to confirm the plasmids based on size. Each restriction digestion reaction mixture consisted of 0.2 µg of the relevant plasmid DNA, 5 U of *Pst*I restriction enzyme (Cat #: R611A) (Promega, USA), 2 µL of restriction enzyme 10 x buffer (Buffer H) (Cat #: R008A) (Promega, USA), 0.2 µL of Bovine Serum Albumin (BSA) (10 µg/mL) (Cat #: R396D) (Promega, USA) and was made up to a total reaction volume of 20 µL with nuclease-free H<sub>2</sub>O. Restriction digests were performed for 2 hours at 37°C. Digested and undigested plasmids were loaded with tracking dye into a 1 % (w/v) agarose gel made up in 1 x Tris-Borate-EDTA (TBE) buffer (90 mM Tris, 90 mM Boric Acid, 2 mM ethylenediaminetetraacetic acid [EDTA], 20 µM ethidium bromide [EtBr]) and electrophoresed at 100 V for approximately 45 minutes. Gels were viewed under ultraviolet light and images obtained using the Chemidoc™ (Biorad).

### **2.3.3 Induction study of GST, GST-mSTI1, GST-TPR2A2B and GST-TPR1**

An induction study was performed in order to determine the optimal time period for the expression and purification of recombinant proteins. Single transformed colonies containing the pGEX-4T1, pGEX3X2000, pGEX3X1400 and pGEX3X700 plasmids respectively were inoculated into 5 mL of 2 x YT broth containing ampicillin (100 µg/mL) and incubated at 37°C overnight with shaking (180 rpm). Each of the 5 mL overnight cultures were inoculated into respective flasks containing 50 mL of 2 x YT broth with ampicillin (100 µg/mL) and incubated at 37°C with shaking (180 rpm) until OD<sub>600</sub> readings between 0.6 and 0.8 were obtained. Isopropyl β-D-1-thiogalactopyranoside (IPTG) was added to each culture at a final concentration of 1 mM in order to induce protein expression and cultures were incubated at 37°C with shaking (180 rpm). Samples from each culture were taken before the addition of IPTG (0 hours), as well as 1, 2, 3, 4, 5 and 6 hours post induction with IPTG. An overnight sample for each of the cultures was also taken. Samples were taken by removing 2 mL of culture at each time point and using 1 mL to measure the OD<sub>600</sub> reading and 1 mL for collection of protein samples. Each protein sample was collected by centrifuging the 1 mL culture sample at 13 000 x g for 1 minute and resuspending the pellet in a volume of 1 x phosphate buffered saline (1 x PBS) (137 mM NaCl, 2.7 mM KCl, 10 mM Na<sub>2</sub>HPO<sub>4</sub>, 2 mM

KH<sub>2</sub>PO<sub>4</sub>; pH 7.4). The volume of PBS required was calculated using the following equation ( $x \mu\text{L PBS} = \text{OD}_{600}/[0.5][150]$ ). A lysate stock of non-transformed *E.coli* XLI Blue cells was also made for use as a negative control. A volume of 20  $\mu\text{L}$  of 5 x sodium dodecyl sulphate polyacrylamide gel electrophoresis (SDS-PAGE) sample buffer (60 mM Tris-HCl pH 6.8, 2 % [w/v] SDS, 10 % [v/v] glycerol, 0.01 % [w/v] bromophenol blue, 5 % [v/v]  $\beta$ -mercaptoethanol) was added to 80  $\mu\text{L}$  of each of the resuspended samples. The samples were boiled for 5 minutes and then analysed by SDS-PAGE and western blot analysis.

### **2.3.4 SDS-PAGE and Western analysis**

Samples were separated by SDS-PAGE according to Laemmli (1970). The samples were resolved using a 4 % (v/v) stacking gel and a 12 % (v/v) resolving gel and electrophoresed at 120 V for approximately 1 hour and 15 minutes in 1 x SDS-PAGE running buffer (0.25 mM Tris, 192 mM glycine, 1 % [w/v] SDS). The resolved proteins were transferred from SDS-PAGE gels to nitrocellulose membranes in transfer buffer (13 mM Tris-HCl, 100 mM glycine and 20 % [v/v] methanol) by western blot analysis using the method of Towbin and Gordon (1979) with the Semi Dry blotting system (SD20 Semi Dry Maxi, Lasec, SA) according to manufacturer's protocol. Transfer of proteins was carried out at 20 V, 400 mA for 50 minutes. Ponceau (0.5 % [w/v] Ponceau S, 1 % [v/v] glacial acetic acid) was used as a reversible stain for nitrocellulose membranes for protein in order to confirm whether transfer was successful. The membranes were blocked with Blotto solution (5 % [w/v] milk powder, 0.1 % [v/v] Tween-20 in 1 x Tris-buffered saline [1 x TBS] [50 mM Tris, 150 mM NaCl, pH 7.5]) for 1 hour and incubated with primary antibody (as indicated in figure legends) at 4°C overnight with shaking. The membranes were washed (3 x 10 minute washes) in TBS-T (1 % [v/v] Tween-20 in 1 x TBS) and incubated with species specific horseradish peroxidase-conjugated secondary antibodies in a 5 % (w/v) Blotto solution for 1 hour at room temperature. The membranes were washed (3 x 10 minute washes) in TBS-T and proteins visualised using the SuperSignal<sup>®</sup> West Pico Chemiluminescent Substrate kit (Cat #: 34080) (Thermo Scientific, USA) in either the Chemidoc<sup>™</sup> (Biorad) system or by use of X-Ray film (Agfa HealthCare, Belgium) developed in a dark room using developer, stopper and fixer solutions made up using Agfa reagents (as per manufacturer's protocol).

### **2.3.5 Purification of GST, GST-mSTI1, GST-TPR2A2B and GST-TPR1**

Transformed *E.coli* XLI Blue colonies containing the pGEX-4T1, pGEX3X2000, pGEX3X1400 and pGEX3X700 plasmids respectively were inoculated into 5 mL of 2 x YT

broth with ampicillin (100 µg/mL) and incubated at 37°C overnight with shaking. Each of the 5 mL overnight cultures were inoculated into 50 mL of 2 x YT broth with ampicillin (100 µg/mL) and incubated at 37°C with shaking until an OD<sub>600</sub> reading between 0.6 and 0.8 was obtained. IPTG was added to each of the cultures at a final concentration of 1 mM in order to induce protein expression. Three hours post induction with IPTG, the cells were harvested by centrifugation at 6 000 x g for 15 minutes at 4°C. The supernatant was decanted and the pellet resuspended in 5 mL of 1 x PBS on ice. Lysozyme (1 mg/mL) and phenylmethanesulfonylfluoride (PMSF) (1 mM) were added to the resuspended pellet, kept on ice for 30 minutes and frozen at -20°C overnight. The frozen lysates were thawed on ice, sonicated 6 times, for 30 seconds each time (30 seconds on, 30 seconds off) and centrifuged at 10 000 x g for 30 minutes at 4°C. Samples of pellets resuspended in 1 x PBS (P) and cleared lysates (CL) were kept for SDS-PAGE analysis. The remaining supernatants (*E.coli* lysates) were used for purification of proteins.

Protino<sup>®</sup> Glutathione Agarose 4B beads (Cat #: 745500.10) (Macherey-Nagel, Germany), used for purification of GST-tagged proteins, were prepared by vortexing the bottle and transferring 200 µL of beads per protein to be purified into 15 mL falcon tubes and centrifuging at 500 x g for 5 minutes. The supernatants were discarded and the beads washed once with 1.5 mL of 1 x PBS, centrifuged at 500 x g for 5 minutes and the supernatants discarded. The *E.coli* lysates containing the different GST and GST fusion proteins were added to the prepared glutathione beads, mixed at room temperature on a shaker for 30 minutes and centrifuged at 500 x g for 5 minutes. A sample of the supernatant was taken for SDS-PAGE analysis (Flow-through [FT]) and the remaining supernatant discarded. The pelleted beads with bound protein were washed with 1.5 mL 1 x PBS and centrifuged at 500 x g for 5 minutes. A sample of the supernatant was taken for SDS-PAGE (wash 1 [W1]) and the remainder discarded. The pelleted beads were washed (1.5 mL 1 x PBS) and centrifuged (500 x g) a further two times, collecting samples of the supernatant for SDS-PAGE after each wash (wash 2 [W2] and wash 3 [W3]). The pelleted beads with bound protein were transferred to eppendorf tubes and the proteins eluted by adding 150 µL of elution buffer (50 mM Tris-HCl, 10 mM glutathione, pH 8.0), mixing gently for 10 minutes at room temperature and centrifuging at 500 x g for 5 minutes. The elution process was repeated a total of three times, collecting the supernatants (eluted proteins) each time (elution 1 [E1], elution 2 [E2] and elution 3 [E3]). Samples collected were analysed by SDS-PAGE and



western blot analysis as previously described. Purified proteins from each of the elutions were quantified using a Bradford's assay and stored at -20°C.

### **2.3.6 Glutathione-S-transferase (GST) Pull down Assay**

Protino Glutathione Agarose 4B beads were prepared by vortexing the bottle and transferring 400 µL of beads into an eppendorf tube. The tubes were centrifuged at 500 x g for 5 minutes and the supernatant discarded. The beads were washed three times with 1 mL 1 x PBS, with centrifugation at 500 x g and discarding of the supernatant occurring between each wash. The beads were resuspended in 450 µL 1 x PBS and aliquotted into four 100 µL aliquots. An amount of 20 µg of GST and GST fusion proteins were added to respective tubes containing the beads and a volume of 1 mL 1 x PBS was added to each tube. GST and GST fusion proteins were coupled to the beads by incubation of the reaction mixture at 4°C for 2 hours on a rocker. The reaction mixtures were then centrifuged at 500 x g for 5 minutes and the supernatants discarded.

HS578T cell lysates were prepared in radio-immunoprecipitation assay (RIPA) lysis buffer (50 mM Tris-HCl, 150 mM NaCl, 1 mM EDTA, 1 mM Na<sub>3</sub>VO<sub>4</sub>, 1 % [w/v] NP40, 1 mM sodium deoxycholate, 1 mM PMSF, 2 µg/mL protease inhibitor cocktail) (1 mL per confluent T150 flask) and 300 µL lysate were added to each reaction mixture. A further 1 mL of 1 x PBS was added to each reaction and the mixtures incubated at 4°C for 2 hours on a rocker. The samples were centrifuged at 500 x g for 5 minutes and the supernatants discarded. The pellets were washed three times in 1 x PBS, with centrifugation at 500 x g for 5 minutes and discarding of the supernatant occurring between each wash. The final pellet was resuspended in 50 µL 5 x SDS-PAGE loading buffer and analysed by SDS-PAGE and western blotting as described previously.

### **2.3.7 Endotoxin removal from GST and GST fusion proteins**

The GST and GST fusion proteins were buffer exchanged into endotoxin-free buffer (0.05 M Tris-HCl, 0.4 M NaCl, pH 6.0) using the Zeba Spin Desalting Columns (Cat #: 89882) (Thermo Scientific, USA). Columns were prepared by centrifuging at 1 500 x g for 1 minute to remove the storage solutions. Volumes of 300 µL of endotoxin-free buffer were added to the top of the resin bed and the columns centrifuged at 1 500 x g for 1 minute to remove the buffer. The endotoxin-free buffer was added to the resin bed an additional two times and the solutions discarded after centrifugation. Volumes of 100 µL of the GST and GST fusion

proteins were added to the columns at the centre of the resin beds, centrifuged at 1 500 x g for 2 minutes and the samples collected in eppendorf tubes.

Pierce High Capacity Endotoxin Removal spin columns (Cat #: 88273) (Thermo Scientific, USA) were equilibrated at room temperature and storage solutions discarded after centrifugation. The columns were regenerated by resuspending the resins in 2 mL volumes of 0.2 N NaOH in 95 % (v/v) ethanol and incubating for 2 hours at room temperature. The columns were centrifuged and the solutions discarded. The resins were resuspended in 2 mL volumes of 2 M NaCl, after which the columns were centrifuged and the solutions discarded. The resins were resuspended in 2 mL volumes of endotoxin-free water, after which the columns were centrifuged and the solutions discarded. Resuspension of the resins in endotoxin-free buffer was carried out an additional two times and the solutions discarded. The buffer exchanged GST and GST fusion proteins were diluted in 450 µL of endotoxin-free buffer and added to the resins in the spin columns. The resins were resuspended in the protein solutions by inverting the columns and the columns were incubated with end-over-end mixing at 4°C overnight. The columns were centrifuged and the protein samples collected. Unless otherwise specified, all centrifugation steps were carried out at 500 x g for 1 minute. All buffers were made up in endotoxin-free water.

### **2.3.8 Quantitation of Endotoxin in GST and GST fusion proteins**

The Pierce LAL Chromogenic Endotoxin Quantitation Kit (Cat #: 88282) (Thermo Scientific, USA) was used to detect endotoxin levels in GST and GST fusion proteins before and after removal of endotoxins. The *E.coli* endotoxin standard was reconstituted in endotoxin free water at a concentration of 28 endotoxin units per mL (EU/mL) and used to prepare standard stock solutions of 1, 0.5, 0.25 and 0.1 EU/mL in endotoxin free water. Limulus Amebocyte Lysate (LAL) and the chromogenic substrate were resuspended in endotoxin free water as per manufacturer's instructions. At 37°C, 50 µL of duplicate samples of each standard, each test sample and a blank were dispensed into appropriate wells of a pre-equilibrated 96 well plate and incubated for a further 5 minutes at 37°C. A volume of 50 µL of LAL was added to each well and shaken for 10 seconds. The plate was incubated for a further 10 minutes at 37°C. A volume of 100 µL of chromogenic substrate was added to each well; the plate shaken for 10 seconds and then incubated for 6 minutes at 37°C. A volume of 50 µL of stop reagent (25 % [w/v] acetic acid) was added to each well; the plate shaken for 10 seconds and the absorbance at 405 nm measured. A standard curve of absorbance versus endotoxin concentration

(EU/mL) was created using the absorbance of the endotoxin standard solutions. The endotoxin concentrations of the GST and GST fusion proteins before and after endotoxin removal were calculated using the equation of the standard curve.

### **2.3.9 Cell Proliferation Assay**

HS578T cells were cultured as described in Chapter 3 (Section 3.3.1). Volumes of 100  $\mu$ L of HS578T cells were seeded at a concentration of  $3 \times 10^4$  cells/mL in a 96-well plate and incubated overnight at 37°C. Cells were treated in triplicate with GST, GST-mSTI1, GST-TPR2A2B and GST-TPR1 proteins at a final concentration of 10 nM for 0, 24, 48 and 72 hours. After the appropriate incubation period, cells were incubated for a further 3 hours with 10  $\mu$ L WST-1 cell proliferation reagent (Cat #: 11 644 807 001) (Roche, South Africa) and the absorbance at 440 nm measured. Results were represented as a growth ratio of treated to untreated cells for each of the time periods and results for treatment with each protein was normalised to Day 0, where Day 0 = 100 %.

### **2.3.10 Wound Healing Assay**

HS578T cells were seeded into wound healing culture inserts (Cat #: 80209) (Ibidi, Germany) in a 24-well plate at  $4 \times 10^5$  cells/mL with 70  $\mu$ L volumes per well and incubated overnight at 37°C. Culture inserts were removed and cells were treated in triplicate with GST, GST-mSTI1, GST-TPR2A2B and GST-TPR1 at a final concentration of 10 nM. Images of the wounds generated at 0, 6 and 12 hours post treatment with the relevant proteins were recorded using the Zeiss axiovert fluorescent microscope. The area of the wounds for each treatment at each time period was measured using ImageJ. Wound areas at 6 and 12 hours post treatment were represented as a percentage of the wound area at 0 hours, where the original wound area was represented as 100 %.

### **2.3.11 Gelatin degradation assay**

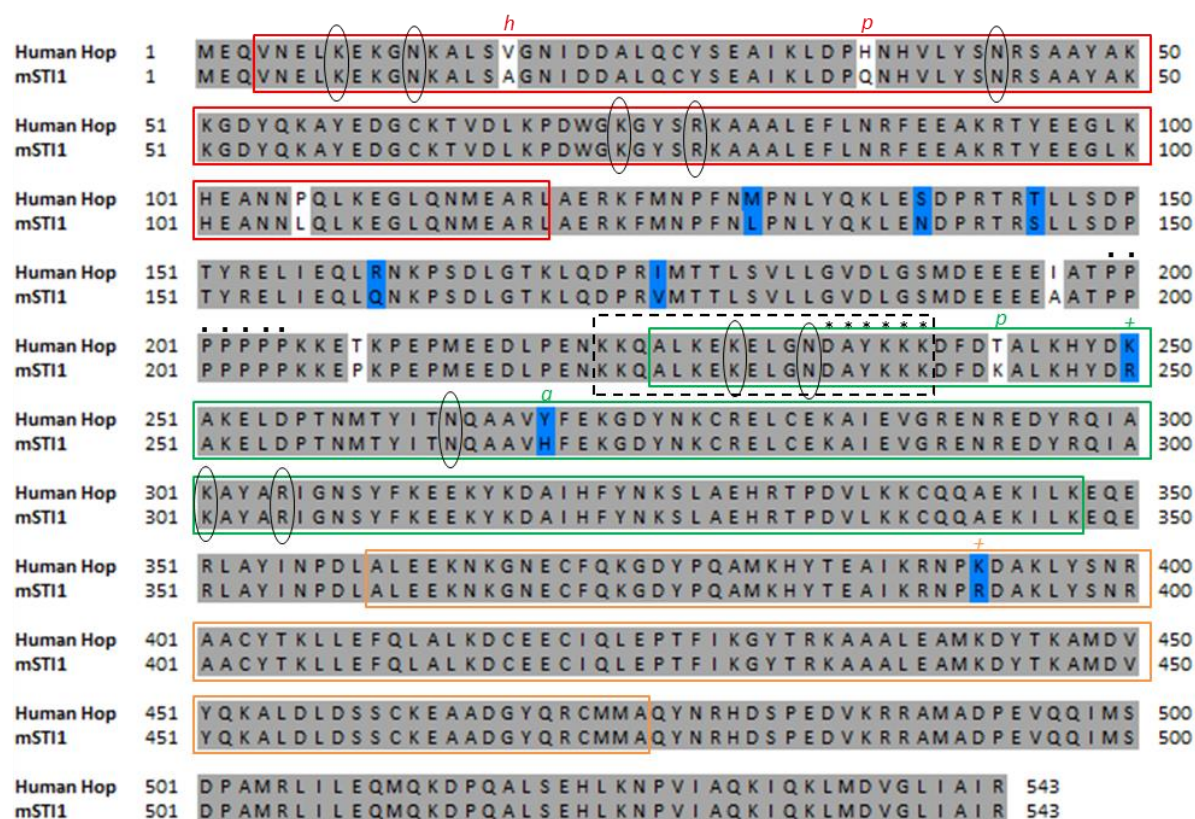
Gelatin-Oregon Green 488 conjugate, henceforth referred to as gelatin-488 (Cat #: G13186) (Life Technologies, USA), was resuspended to 1 mg/mL according to manufacturer's instructions. A 5 % (w/v) unlabelled gelatin, 5 % (w/v) sucrose solution was prepared in distilled water. A 1:8 dilution of the gelatin-488 into the 5 % gelatin/sucrose solution was prepared and 10  $\mu$ L volumes were dispensed into each well of a  $\mu$ -Slide angiogenesis plate (Cat #: 81506) (Ibidi, Germany). The plate was incubated in the dark at 4°C for 1 hour to allow the gelatin to polymerise. Volumes of 50  $\mu$ L of HS578T cells were seeded onto the

gelatin matrices at  $1 \times 10^5$  cells/mL, treated with the relevant GST fusion proteins (10 nM), and incubated overnight at 37°C. Media was subsequently removed and cells were prepared for immunofluorescence staining. Cells were fixed with ice-cold 100 % methanol and blocked with 1 x TBS containing 1 % (w/v) BSA and 0.1 % (v/v) Triton-X for 45 minutes at room temperature. Cells were incubated with rabbit anti-human actin antibody in 0.1 % (w/v) BSA/TBS overnight at 4°C. Cells were washed twice with 0.1 % (w/v) BSA/TBS for 5 minute washes each time and then incubated with anti-rabbit-DyLight 550 fluorescent antibodies for 1 hour at room temperature in the dark. Cells were washed twice with 0.1 % (w/v) BSA/TBS for 5 minutes each time and then rinsed with 1 µg/mL Hoescht-33342 dye to stain the cell nucleus. DAKO mounting media was added to each of the wells and allowed to dry before cells were visualised using the LSM 510 Meta confocal microscope (Zeiss). Images were analysed using ImageJ.

## **2.4 RESULTS:**

### **2.4.1 Conservation of amino acid sequence between human Hop and mSTI1**

The study aimed to use murine Hop proteins (GST-mSTI1, GST-TPR2A2B and GST-TPR1), which would be expressed from readily available plasmids in our laboratory (pGEX3X2000, pGEX3X1400 and pGEX3X700), to determine the effect of extracellular Hop and the relevant domains on cell biological processes in human HS578T breast cancer cells. It was therefore important to first determine whether the murine Hop proteins were likely to be functional in a human system. A pairwise sequence alignment of the amino acid sequences of *Homo sapiens* Hop (human Hop) and *Mus musculus* STI1 (mSTI1) was therefore done in order to determine the protein sequence conservation between the two homologues. The pairwise sequence alignment was performed using ClustalW and Promals3D software programmes (Figure 2.1).



**Figure 2.1: Conservation of protein sequence between human Hop and mSTI1**

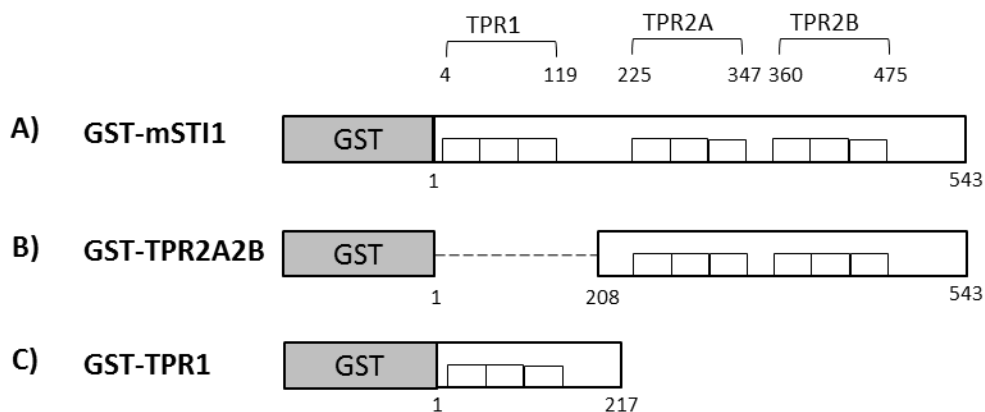
Pairwise sequence alignment of human Hop and mSTI1. Residues highlighted in grey are identical. Residues highlighted in blue are similar. Residues with an 'h' above them are of a similar hydrophobicity. Residues with a 'p' above them are of a similar polarity. Residues with a '+' above them are positively charged. Residues with an 'a' above them are aromatic. The red box (residues 4 – 119) indicated the TPR1 domain. The green box (residues 225 – 347) indicated the TPR2A domain. The orange box (residues 360 – 475) indicated the TPR2B domain. The black ovals indicated residues involved in forming two-carboxylate clamps, essential in binding the chaperones Hsp70 and Hsp90. The black dashed box (residues 222 – 239) indicated the nuclear localisation signal (NLS). The black squares (residues 199 – 205) indicated a polyproline tract. The black asterisks (residues 234 – 239) indicated a DAYKKK motif.

The sequence identity matrix calculated for human Hop and mSTI1 revealed an amino acid sequence identity of 97.4 % between the two sequences with highly conserved sequence identity in TPR1, TPR2A and TPR2B domains (Figure 2.1). Amino acids, Lys<sup>8</sup>, Asn<sup>12</sup>, Asn<sup>43</sup>, Lys<sup>73</sup> and Arg<sup>77</sup> in the TPR1 domain of Hop are predicted to be involved in forming this essential two-carboxylate clamp with the C terminal EEVD of Hsp70 (Odunuga *et al.*, 2003a). These amino acids are conserved in Hop and mSTI1 (Figure 2.1 [black ovals]). Amino acids, Lys<sup>229</sup>, Asn<sup>233</sup>, Asn<sup>264</sup>, Lys<sup>301</sup> and Arg<sup>305</sup> in the TPR2A domain of Hop are predicted to be involved in forming this essential clamp with the C terminal EEVD motif of Hsp90 (Odunuga *et al.*, 2003a) and are also conserved in Hop and mSTI1 (Figure 2.1 [black

ovals]). It can therefore be said that human Hop and mSTI1 at the primary amino acid level are highly similar and expected to have similar functionality. We therefore felt it worthwhile to purify the murine Hop proteins for use in a human system.

#### 2.4.2 Confirmation of identity of pGEX-4T1, pGEX3X2000, pGEX3X1400 and pGEX3X700

The pGEX-4T1, pGEX3X2000, pGEX3X1400 and pGEX3X700 plasmids encoded GST, GST-mSTI1, GST-TPR2A2B and GST-TPR1 respectively. The mSTI1 refers to the full length mSTI1 protein. TPR2A2B refers to a C-terminal mSTI1 fragment containing the TPR2A and TPR2B domains, which binds Hsp90 but not Hsp70; while TPR1 refers to an N-terminal mSTI1 fragment containing the TPR1 domain that binds Hsp70 but not Hsp90 (Figure 2.2) (Odunuga *et al.*, 2003a).



**Figure 2.2: Schematic diagram showing the GST fusion proteins, GST-mSTI1, GST-TPR2A2B and GST-TPR1 expressed from pGEX3X2000, pGEX3X1400 and pGEX3X700 plasmids respectively**

(A) GST-tagged full length mSTI1 protein (aa: 1-543) containing the TPR1, TPR2A and TPR2B domains. (B) N-terminal truncated GST-tagged mSTI1 fusion protein (aa: 208-543) containing the TPR2A and TPR2B domains. (C) C-terminal truncated GST-tagged mSTI1 fusion protein (aa: 1-217) containing the TPR1 domain. (Figure adapted from Odunuga *et al.*, 2003a).

Plasmid maps of pGEX-4T1, pGEX3X2000, pGEX3X1400 and pGEX3X700 plasmids were created using BioEdit software (Figure 2.3, A[i-iv]). The plasmid sequences were analysed for restriction enzyme recognition sites such that an appropriate restriction enzyme could be selected and used to differentiate the specific plasmids based on the molecular weights of the digested linear fragments. The restriction enzyme, *Pst*I, was selected and used for the digestion of pGEX-4T1, pGEX3X2000, pGEX3X1400 and pGEX3X700 plasmids (Figure

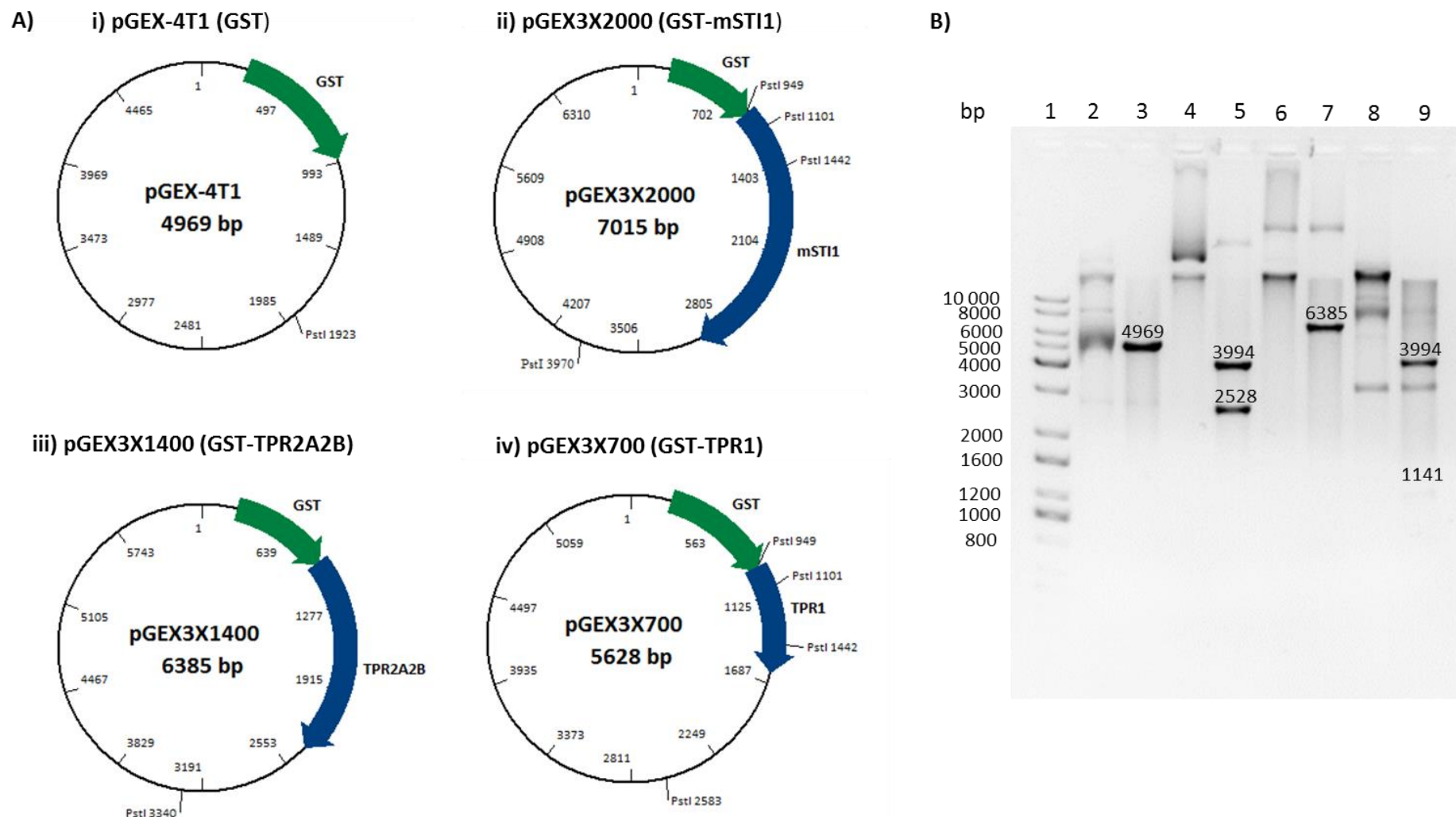
2.3, B). Digested and undigested plasmids were analysed by agarose gel electrophoresis, visualised under UV light and images obtained using the Chemidoc (Figure 2.3, B).

In the undigested plasmid samples (lanes 2, 4, 6, 8), multiple bands occurring at various mobilities were observed (Figure 2.3, B). These bands reflected the presence of different plasmid conformations. The bands that moved furthest in the gel were likely to be supercoiled conformations of plasmid DNA, while the bands observed at lower mobilities were more likely to be nicked circular conformations of plasmid DNA. The pGEX-4T1 plasmid has one *Pst*I recognition site (Figure 2.3, A[i]). Digestion of pGEX-4T1 with *Pst*I would therefore result in a single 4969 bp linear fragment. This corresponded to the band at ~5000 bp observed in lane 2 (Figure 2.3, B). The pGEX3X2000 plasmid has four *Pst*I recognition sites, three of which are contained in the mSTI1 open reading frame (Figure 2.3, A[ii]). Digestion of pGEX3X2000 would therefore result in four linear fragments of sizes 3994 bp, 2528 bp, 341 bp and 152 bp. Bands at ~4000 bp and ~2500 bp were observed in lane 5 (Figure 2.3, B). These bands corresponded to the expected sizes, while the smaller molecular weight fragments that were expected from the *Pst*I digest were too small to visualise on the agarose gel. The pGEX3X1400 plasmid has one *Pst*I recognition site (Figure 2.3, A[iii]). Digestion of pGEX3X1400 with *Pst*I would therefore result in a single 6385 bp linear fragment. This corresponded to the distinct band occurring just above 6000 bp observed in lane 7 (Figure 2.3, B). The pGEX3X700 plasmid has four *Pst*I recognition sites (Figure 2.3, A[iv]). Digestion of pGEX3X700 with *Pst*I would therefore result in four linear fragments of sizes 3994 bp, 1141 bp, 341 bp and 152 bp. In lane 9, bands observed at ~4000 bp and ~1200 bp (Figure 2.3, B) corresponded to the expected sizes, although again, the lower molecular weight fragments were too small to be visualised on the agarose gel. Interestingly, bands resolving just beneath the 3000 bp marker were visible in both the undigested and digested samples of pGEX4T1 (lane 2 and 3) and pGEX3X700 (lane 8 and 9) (Figure 2.3, B). These bands are likely to represent undigested supercoiled fragments of DNA resulting from partial digests of the pGEX4T1 and pGEX3X700 plasmids. Sequencing of the pGEX-4T1, pGEX3X2000, pGEX3X1400 and pGEX3X700 plasmids confirmed the identity of the plasmids and the plasmids were judged to be of sufficient quality for use in subsequent experiments.

The plasmid maps were used to calculate the expected sizes of the GST protein and each of the GST fusion proteins (Figure 2.3, A). GST, encoded from nucleotide position 258 to 960

(Figure 2.3, A[i]) is 720 bp in length which when translated, equates to a protein of ~26 kDa. GST and adjacent full length mSTI1 were encoded from nucleotide position 258 to 3008 (Figure 2.3, A[ii]), together making them 2751 bp in length. This translates to a GST-mSTI1 fusion protein of ~101 kDa. GST and adjacent N-terminal truncated mSTI1 were encoded from nucleotide position 258 to 2378 (Figure 2.3, A[iii]), making them 2120 bp in length. This equates to a GST-TPR2A2B fusion protein of ~78 kDa. GST and adjacent C-terminal truncated mSTI1 were encoded from nucleotide position 258 to 1621 (Figure 2.3, A[iv]), making them 1364 bp in length, equating to a predicted GST-TPR1 fusion protein of ~50 kDa.





**Figure 2.3: Confirmation of identity of pGEX-4T1, pGEX3X2000, pGEX3X1400 and pGEX3X700 plasmids**

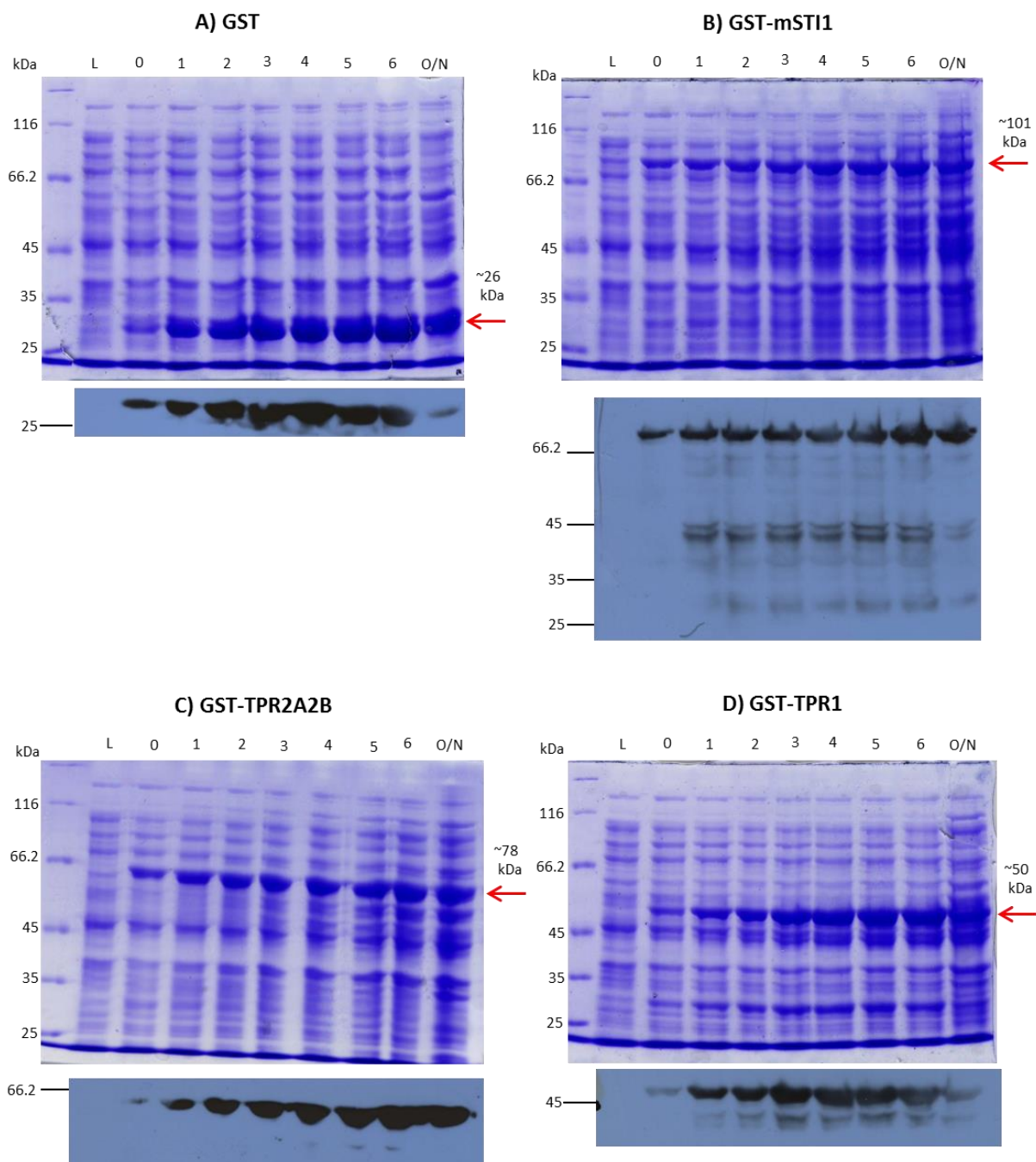
(A) Plasmid maps of (i) pGEX-4T1 (GST), (ii) pGEX3X2000 (GST-mSTI1), (iii) pGEX3X1400 (GST-TPR2A2B) and (iv) pGEX3X700 (GST-TPR1). Plasmid maps were created using BioEdit software. Green arrows represent open reading frame for GST and blue arrows represent open reading frames of mSTI1 and mSTI1 truncations. The position of the *PstI* restriction sites are depicted in each of the plasmids. (B) Restriction enzyme digests of plasmids with *PstI* restriction enzyme. Lane 1 represents the KAPA Universal DNA ladder. Lanes 2, 4, 6 and 8 represent undigested pGEX-4T1, pGEX3X2000, pGEX3X1400 and pGEX3X700 plasmids respectively, while lanes 3, 5, 7 and 9 represent *PstI* digested pGEX-4T1, pGEX3X2000, pGEX3X1400 and pGEX3X700 plasmids respectively. Numbers above bands indicate expected sizes (bp) of linear fragments of plasmid DNA.

### 2.4.3 Induction study of GST, GST-mSTI1, GST-TPR2A2B and GST-TPR1

An induction study was performed to determine the optimal time period for which to induce the expression of GST, GST-mSTI1, GST-TPR2A2B and GST-TPR1 proteins from the pGEX-4T1, pGEX3X2000, pGEX3X1400 and pGEX3X700 plasmids, respectively (Figure 2.4). Protein expression was induced by the addition of 1 mM IPTG and induction samples taken hourly from 0 hours (uninduced) to 6 hours. A sample induced overnight was also taken (O/N). A lysate of non-transformed *E.coli* XLI Blue cells was used as a negative control (L). All samples from the induction study were analysed by SDS-PAGE and western blot analysis (Figure 2.4).

For the GST, GST-mSTI1, GST-TPR2A2B and GST-TPR1 induction studies, bands that increased in intensity from 0 hours to the O/N induction were observed on the relevant SDS-PAGE gels at ~26 kDa, ~100 kDa, ~66 kDa and ~50 kDa, respectively (Figure 2.4, A-D). This corresponded closely to the expected molecular weights of 26 kDa, 101 kDa, 78 kDa and 50 kDa respectively. Western blot analyses with antibodies against GST confirmed the presence of the GST fusion proteins at the corresponding molecular weights (Figure 2.4, A-D). This suggested successful expression of GST and the GST fusion proteins.

For the GST-mSTI1 and GST-TPR1 induction studies, lower molecular weight bands were observed in the western blots in lanes 1-6 and O/N (Figure 2.4, B and D). These bands were likely to be GST-tagged degradation or truncation termination products which could have arisen by cleavage with proteases or incomplete translation, respectively (Terp, 2003). There were no bands observed in the non-transformed lysate (L) samples of each of the induction studies (Figure 2.4, A-D). This indicated that the relevant proteins were only expressed in the presence of the recombinant plasmids. Fainter bands observed in the uninduced samples (0 hours) compared to the induced samples (1 hour - O/N) (Figure 2.4, A-D) were indicative of low levels of protein expression without the addition of IPTG. This was suggestive of leaky expression and can be attributed to the fact that transcription of DNA inserted in the pGEX-4T1 and pGEX3X vector systems is controlled by the constitutively active *taq* promoter (Amann *et al.*, 1983).



**Figure 2.4: Induction of recombinant GST-tagged mSTI1 proteins and controls.**

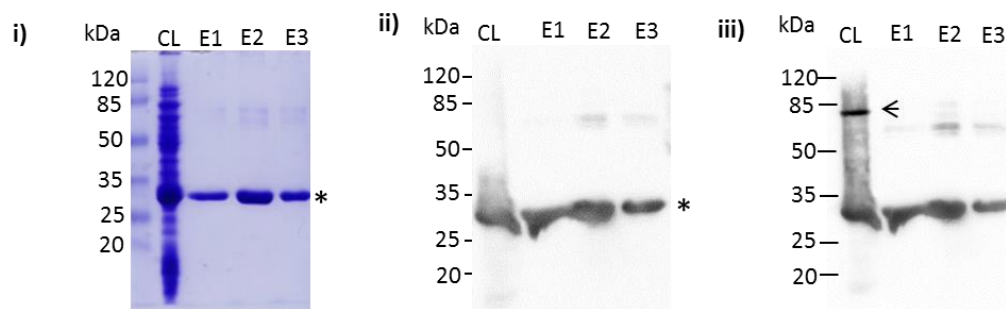
*E. coli* XLI Blue protein induction profiles of (A) GST (pGEX-4T1), (B) GST-mSTI1 (pGEX3X2000), (C) GST-TPR2A2B (pGEX3X1400) and (D) GST-TPR1 (pGEX3X700). For each induction study (A, B, C and D), samples were analysed by SDS-PAGE and western blot analysis using goat anti-GST primary antibody and anti-goat HRP-linked secondary antibodies. The SDS-PAGE gels are presented above the corresponding western blots for each of the induction studies. The first lane contains the unstained molecular weight marker. The lane marked (L) indicates the lysate of non-transformed *E. coli* XLI blue cells used as a negative control. The lane containing uninduced sample is marked (0), the lanes marked (1, 2, 3, 4, 5 and 6) indicate the hours post induction with 1 mM IPTG and the lane marked (O/N) indicates the sample induced overnight. The arrows indicate the induced proteins on the SDS-PAGE gels for each of the induction studies. The estimated sizes of GST and each of the expressed GST fusion proteins are written above the arrows.

The bands corresponding to the GST and GST-fusion proteins observed at each of the time periods for all of the induction studies were prominent (Figure 2.4, A-D), which was indicative of high levels of protein expression for all recombinant proteins. The highest levels of recombinant protein were observed between 3 hours to O/N induction with IPTG for the various recombinant proteins (Figure 2.4, A-D). It was decided that an induction period of 3 hours produced sufficient levels of all recombinant proteins and an induction period of 3 hours was therefore chosen for all subsequent purifications.

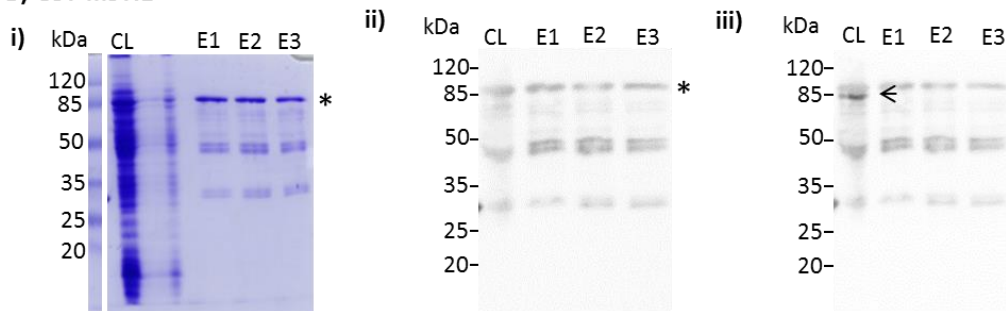
#### **2.4.4 Purification of GST, GST-mSTI1, GST-TPR2A2B and GST-TPR1**

GST, GST-mSTI1, GST-TPR2A2B and GST-TPR1 proteins were purified using Protino<sup>®</sup> Glutathione Agarose 4B beads. Samples were taken at each step of the purification procedure and analysed by SDS-PAGE (Appendix 2, Supplementary figure 1, A-D). For the purification of GST, GST-mSTI1, GST-TPR2A2B and GST-TPR1, bands at approximately 26 kDa, 100 kDa, 80 kDa and 50 kDa respectively, corresponding closely to the expected sizes of 26 kDa, 101 kDa, 78 kDa and 50 kDa respectively, were observed for each of the elution fractions in the SDS-PAGE gels (Figure 2.5, A-D[i]). The concentrations of the elution fractions 1, 2 and 3 for each of the purified proteins were quantified using a Bradford's assay. A quantity of 5 µg of GST protein for elutions 1, 2 and 3 were subsequently loaded in an SDS-PAGE gel, while 2.5 µg of GST-mSTI1, GST-TPR2A2B and GST-TPR1 for elutions 1, 2 and 3 were loaded in SDS-PAGE gels. Elutions 1, 2 and 3 were loaded alongside the cleared lysate (CL) samples of the relevant proteins and analysed by SDS-PAGE and western blot analysis using anti-GST and anti-DnaK antibodies (Figure 2.5, A-D[i, ii and iii]). Western analyses with anti-GST primary antibodies were able to detect the bands at the expected sizes (Figure 2.5, A-D[ii]), suggesting that GST, GST-mSTI1, GST-TPR2A2B and GST-TPR1 were successfully expressed. In the GST-mSTI1, GST-TPR2A2B and GST-TPR1 purifications, lower molecular weight bands were also observed in the SDS-PAGE gels (Figure 2.5, B-D[i]). Western analyses with anti-GST antibodies were able to detect these lower molecular weight bands (Figure 2.5, B-D[ii]). This suggested that the lower molecular weight bands were degradation or truncation products of the GST-fusion proteins. Higher molecular weight bands visible in the GST purification were also detected by western analysis using anti-GST antibodies (Figure 2.5, A[i, ii and iii]). This suggested that there may have been an element of non-specific detection of proteins with the anti-GST antibody.

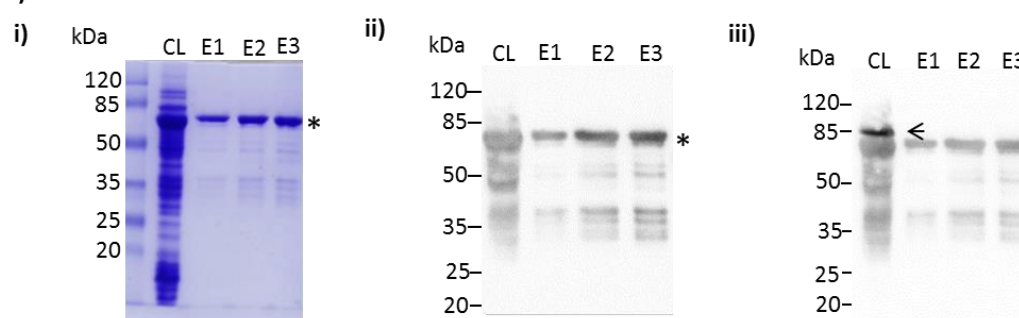
### A) GST



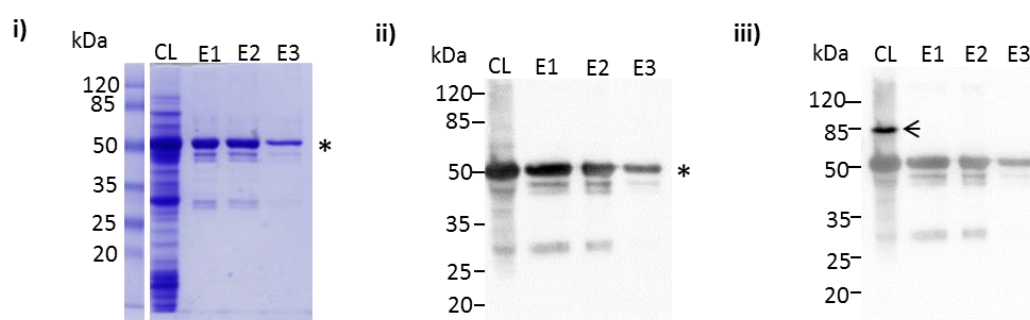
### B) GST-mSTI1



### C) GST-TPR2A2B



### D) GST-TPR1



**Figure 2.5: Overexpression and purification of GST, GST-mSTI1, GST-TPR2A2B and GST-TPR1.**

The letters 'CL' and 'E' represent cleared lysate and elutions respectively. The elution fractions ([A] 5 µg GST, [B] 2.5 µg GST-mSTI1, [C] GST-TPR2A2B and [D] GST-TPR1) were analysed alongside the relevant cleared lysate samples in the SDS-PAGE gels in (i). Western blot analysis of the SDS-PAGE gels shown in (i) using anti-GST primary antibodies and anti-goat HRP-linked secondary antibodies were performed and represented in (ii). The nitrocellulose membranes in (ii) were probed further with anti-DnaK primary antibodies followed by anti-mouse HRP-linked secondary antibodies and shown in (iii). Asterisks indicate the expressed proteins at the expected molecular weights (A-D [i- ii]). Arrows (A-D [iii]) indicate the DnaK proteins from *E.coli* in the cleared lysate fractions only.

Western analysis using the anti-DnaK primary antibody revealed distinct bands at ~85 kDa in the cleared lysate samples only (Figure 2.5, A-D[iii]). This protein related closely to the molecular weight of DnaK (~70 kDa), an Hsp70 chaperone family member protein, expressed in *E.coli* (Shröder *et al.*, 1993). This suggested that although the cleared lysate samples taken during the purification procedure still contained contaminating protein (such as DnaK) from the *E.coli* culture, there were no contaminating DnaK proteins that could be detected by western blot analyses present in any of the protein elutions. This was important because contaminating DnaK in protein purifications could influence the results of subsequent experiments (Rial and Ceccarelli, 2002). It was concluded that since the lower molecular weight bands that were seen were degradation products of the relevant proteins and that there were no contaminating DnaK proteins in the purified protein elutions; the expressed proteins were sufficiently pure for use in subsequent experiments.

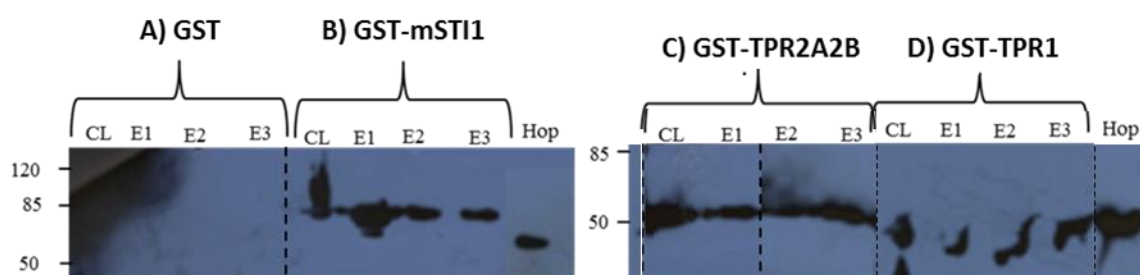
The total protein (in mg) in elutions 1, 2 and 3 and the protein yields from the purifications of GST, GST-mSTI1, GST-TPR2A2B and GST-TPR1 were calculated and reported in Table 2.1.

**Table 2.1: Total protein (mg) and protein yield (mg/L of culture) of purified GST, GST-mSTI1, GST-TPR2A2B and GST-TPR1**

Purified Protein	Elution	Total Protein (mg)	Protein Yield (mg/L)
GST	E1	2.220	94.77
	E2	1.805	
	E3	1.188	
GST-mSTI1	E1	0.893	25.45
	E2	0.329	
	E3	0.179	
GST-TPR2A2B	E1	1.637	48.21
	E2	0.861	
	E3	0.155	
GST-TPR1	E1	1.527	38.53
	E2	0.456	
	E3	0.137	

#### 2.4.5 GST-mSTI1, GST-TPR2A2B and GST-TPR1 detected by human Hop antibodies

Since *in silico* observations revealed high levels of sequence conservation between human Hop and mSTI1 previously (Figure 2.1). We wanted to determine whether human Hop antibodies were able to detect the purified murine Hop fusion proteins (GST-mSTI1, GST-TPR2A2B and GST-TPR1) (Figure 2.6). The purified GST fusion proteins were therefore analysed by SDS-PAGE and western blot analysis using mouse monoclonal anti-human Hop antibodies (Figure 2.6).



**Figure 2.6: GST-mSTI1, GST-TPR2A2B and GST-TPR1 detectable by human Hop antibodies.**

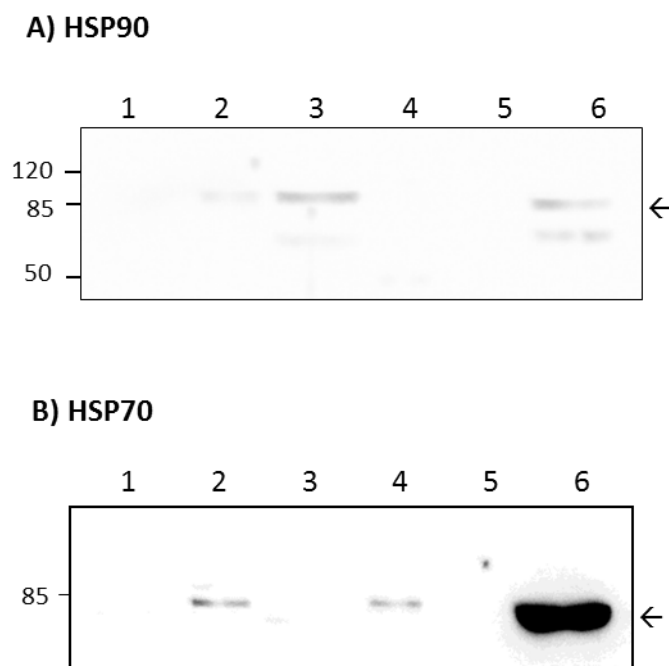
Western blot analysis of (A) GST, (B) GST-mSTI1, (C) GST-TPR2A2B and (D) GST-TPR1, using mouse monoclonal anti-human Hop antibodies. 'CL' – indicated cleared lysate sample. 'E1', 'E2' and 'E3' indicated elutions 1, 2 and 3 of the relevant purified proteins. 'Hop' indicated purified recombinant human Hop protein that was loaded as a positive control for western based detection.

The human Hop antibody was able to detect the full length mSTI1 fusion protein (GST-mSTI1) as well as the truncated mSTI1 proteins (GST-TPR2A2B) and (GST-TPR1) (Figure 2.6, A-D). This species cross-reactivity emphasised the sequence identity between human Hop and mSTI1.

#### 2.4.6 Confirmation of functionality of the murine GST fusion proteins in a human system by GST pull down assays

Further *in vitro* assays were performed to confirm the functionality of the murine Hop proteins in a human system. GST and GST fusion proteins were coupled to glutathione agarose beads and incubated with human breast cancer cell lysates (HS578T) in an attempt to pull down molecular chaperones known to bind the particular TPR domains (Figure 2.7). Pull down samples were analysed for the presence of Hsp90 (Figure 2.7, A) and Hsp70 (Figure 2.7, B) by western blot analysis using anti-Hsp90 and anti-Hsp70 primary antibodies respectively.





**Figure 2.7: GST-mSTI1, GST-TPR2A2B and GST-TPR1 recombinant proteins were able to pull down Hsp90 and/or Hsp70 from human cell lysates**

Pull down assays of GST and GST fusion proteins with HS578T cell lysates were analysed for the presence of Hsp90 (A) and Hsp70 (B) by western blot analyses. Lanes 1, 2, 3, 4, 5 and 6 indicated GST, GST-mSTI1, GST-TPR2A2B, GST-TPR1, beads alone and whole cell lysate input, respectively. Numbers on the left hand side of the western blots indicated molecular weights represented in kDa and arrows indicated the Hsp90 (A) and Hsp70 (B) bands, respectively.

Western analysis to detect the presence of Hsp90, revealed bands occurring at ~90 kDa in lanes 2, 3 and 6 only (Figure 2.7, A), indicating the presence of Hsp90 in these lanes. Western analysis to detect the presence of Hsp70, revealed bands occurring below 85 kDa in lanes 2, 4 and 6 only (Figure 2.7, B), indicating the presence of Hsp70 in these lanes. This indicated that Hsp90 and Hsp70 could be detected in the HS578T whole cell lysate (Figure 2.7, A and B; lane 6). This also indicated that GST-mSTI1 (lane 2) was able to pull down both Hsp90 (Figure 2.7, A) and Hsp70 (Figure 2.7, B) from HS578T cell lysate. GST-TPR2A2B (lane 3) was able to pull down Hsp90 (Figure 2.7, A), but not Hsp70 (Figure 2.7, B) from HS578T cell lysate, and GST-TPR1 (lane 4) was able to pull down Hsp70 (Figure 2.7, B), but not Hsp90 (Figure 2.7, A) from HS578T cell lysate. The absence of bands in lane 1 and lane 5 (Figure 2.7, A and B) indicated that GST or beads alone were not able to pull down Hsp90 or Hsp70, which indicated a lack of non-specific binding of the chaperones. The binding of TPR2A2B to Hsp90 and TPR1 to Hsp70 was in accordance with previous observations using murine cell lysates (Odunuga *et al.*, 2003a), indicating that the murine GST fusion proteins were functional in a human system.



#### **2.4.7 Endotoxin Removal and quantitation of GST and GST fusion proteins**

Since the recombinant proteins were expressed in a bacterial system, they were likely to contain contaminating endotoxins. Endotoxins refer to lipopolysaccharide (LPS) molecules found on the cell membranes of gram negative bacteria (Dawson, 1998; Ryan, 2008; McIntyre and Reinin, 2009). The sensitivity of different cell lines to endotoxins is highly variable and it has even been suggested that some cultured cell lines may have been naturally selected for resistance to endotoxins through long term exposure of high levels of endotoxin. This being said, endotoxins have also been shown to have cytotoxic effects, interfere with cell functions, and cause variability in cell culture experiments (Dawson, 1998; Ryan, 2008; McIntyre and Reinin, 2009). In order to use the recombinant GST fusion proteins to determine the effect of extracellular Hop and its relevant domains on cell processes in cell culture, it was important to limit the endotoxin levels to prevent misinterpretation of results due to endotoxins. This was performed using endotoxin removal spin columns. A chromogenic assay was used to calculate the endotoxin levels of GST and GST fusion proteins compared to a standard curve of known endotoxin standards (EU/mL) (Appendix 3, Supplementary figure 2).

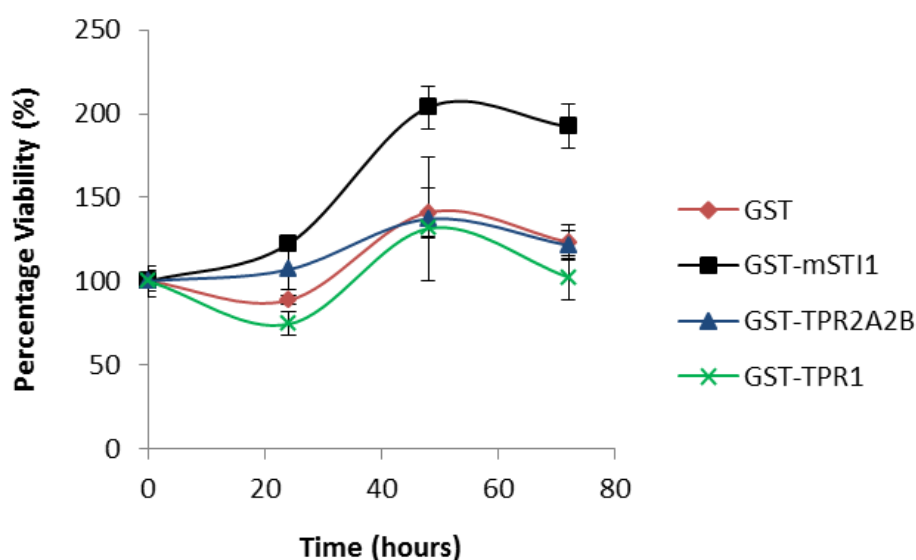
The endotoxin levels in 20 nM concentrations of GST, GST-mSTII, GST-TPR2A2B and GST-TPR1 were tested before and after incubation with the endotoxin removal resin. The levels of endotoxins before removal were 0.06, 2.08, 1.91 and 0.71 EU/mL for GST, GST-mSTII, GST-TPR2A2B and TPR1 respectively. The levels after removal were undetectable, 1.27, 0.38 and 0.01 EU/mL for GST, GST-mSTII, GST-TPR2A2B and GST-TPR1 respectively.

The variability in the cell response to endotoxins makes it difficult to establish critical endotoxin levels (Dawson, 1998). The US Food and Drug Administration (FDA) requires that medical equipment have an endotoxin limit of <0.5 EU/mL (Richter, 2012). Corning cell culture products with an endotoxin level below 0.5 EU/mL are certified as being non-pyrogenic or endotoxin-free, although Corning Inc. certifies that their cell culture products have endotoxin levels below 0.1 EU/mL (Ryan, 2008). BD BioSciences report levels below 0.1 EU/mL to be suitable for *in vivo* studies (McIntyre and Reinin, 2009). Ideally, we wanted to limit the levels of endotoxin in the recombinant proteins to <0.1 EU/mL. For 20 nM recombinant GST and GST-TPR1, we were able to limit the endotoxin levels to below 0.1 EU/mL. For 20 nM GST-TPR2A2B, we were able to limit the endotoxin levels in GST-

TPR2A2B to <0.5 EU/mL. We were unable to limit endotoxin levels of GST-mSTI1 to below 1.27 EU/mL without substantial loss of protein. For treatments of HS578T cells, it was decided to use 10 nM concentrations of recombinant proteins. This diluted endotoxins such that levels were <0.64 EU/mL for all cases.

#### 2.4.8 Analysis of the effect of heterologous mSTI1 proteins on HS578T cell proliferation

A colorimetric WST-1 assay was chosen to measure cell proliferation. WST-1 is a tetrazolium salt that is converted to formazan dye through cleavage by mitochondrial dehydrogenases (Berridge *et al.*, 1996). An increase in the amount of formazan dye (the absorbance of which can be measured spectrophotometrically) therefore correlates with an increase in metabolically active cells. The assay can therefore be used as a measure of cell proliferation. The WST-1 assay was therefore used to compare proliferation of HS578T cells treated with 10 nM of GST, GST-mSTI1, GST-TPR2A2B and GST-TPR1 proteins for 0, 24, 48 and 72 hours (Figure 2.8).



**Figure 2.8: Extracellular mSTI1 proteins had no significant effect on cell proliferation of HS578T cells**

HS578T cells were seeded in 96-well plates and treated with GST, GST-mSTI1, GST-TPR2A2B and GST-TPR1 at a concentration of 10 nM for 0, 24, 48 and 72 hours. Results were represented as ratios of treated to untreated cells at each time period and normalised to treatment at 0 hours, where 0 hours was taken as 100 % viability. Results are representative of three averages. Statistical analysis using a two-way ANOVA with Bonferroni post tests revealed no statistical difference between each of the treatments ( $p > 0.05$ ).

Treatment of HS578T cells with GST-mSTI1 led to an increase in cell proliferation compared to the other treatments. This suggested that the TPR1 and TPR2A2B domains alone were unable to induce cell proliferation. However, the GST-mSTI1 protein had the highest level of

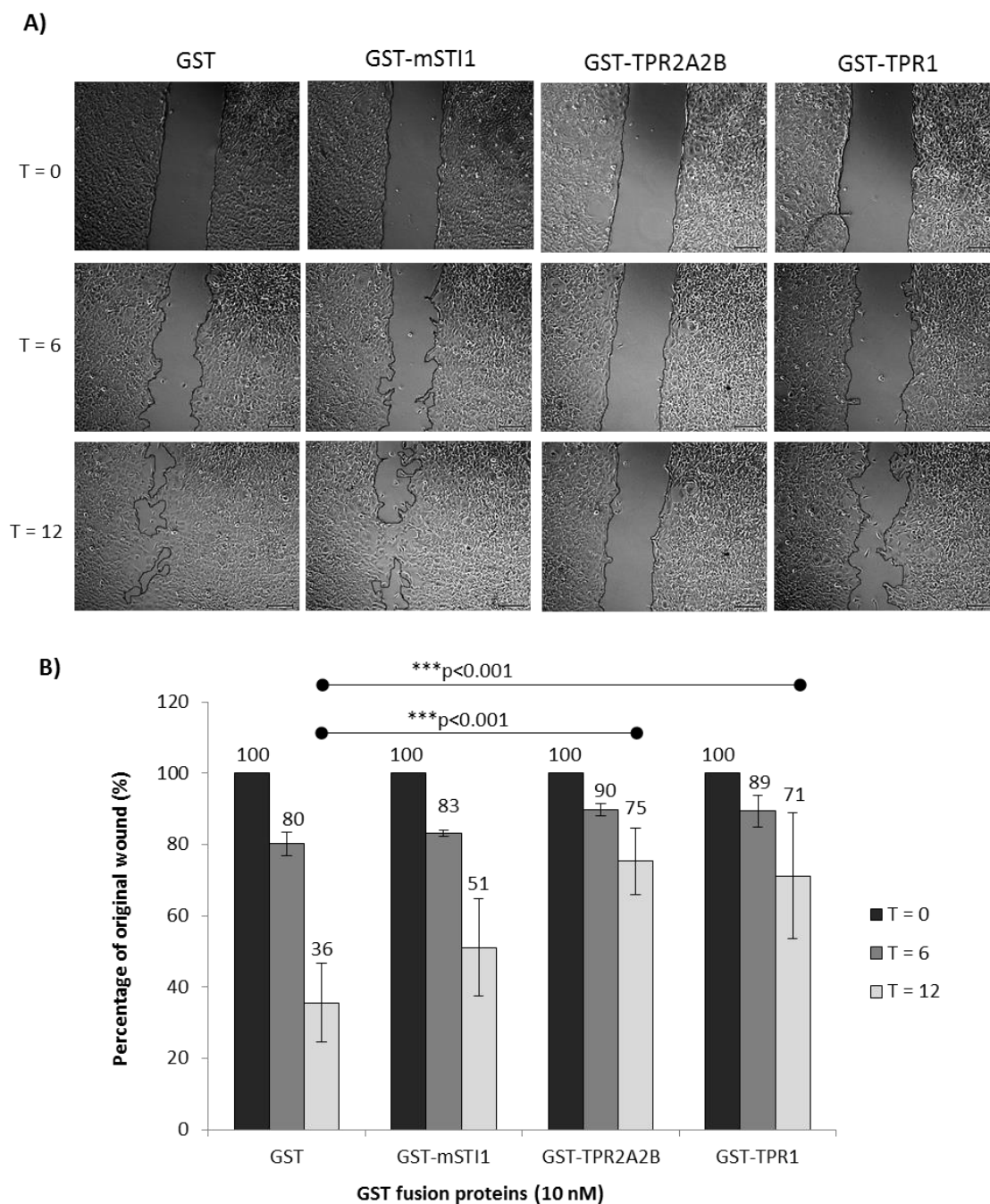
endotoxin and therefore this may have resulted in the increase in cell growth. However, there was no statistical difference between the treatment with GST, GST-mSTI1, GST-TPR2A2B and GST-TPR1 at any of the time periods (Figure 2.8) suggesting that extracellular mSTI1 had no significant effect on proliferation of HS578T cells.

#### **2.4.9 Analysis of the effect of heterologous mSTI1 proteins on HS578T cell migration**

A wound healing assay was performed on cells treated with GST, GST-mSTI1, GST-TPR2A2B and GST-TPR1 at concentrations of 10 nM and cell migration monitored at 6 and 12 hours post treatment (Figure 2.9). These time intervals were selected as we had previously observed that there was no difference in the growth between the different treatments (Figure 2.8).

Images of the wounds recorded at 12 hours post treatment with the relevant treatments revealed a visible difference between migration of cells treated with GST and GST-mSTI1 compared to cells treated with GST-TPR2A2B and GST-TPR1 (Figure 2.9, A). GST and GST-mSTI1 treated cells migrated further towards the centre of the wound, resulting in wound closure in some areas (Figure 2.9, A). In contrast, GST-TPR2A2B and GST-TPR1 treated cells were observed to migrate to a much lesser extent to the centre of the wound (Figure 2.9, A).

At 12 hours post treatment, GST and GST-mSTI1 treated cells had migrated such that their respective wound areas were  $36 \pm 11$  % and  $51 \pm 14$  % of the original wound areas (Figure 2.9, B). GST-TPR2A and GST-TPR1 treated cells had migrated such that their respective wound areas were  $75 \pm 9$  % and  $71 \pm 18$  % of the original wound areas (Figure 2.9, B). Statistical analysis revealed no significant difference in migration between the GST and GST-mSTI1 treated cells, while there was a significant difference in migration between GST and GST-TPR2A2B as well as GST and GST-TPR1 treated cells ( $p < 0.001$ ) (Figure 2.9, B). This suggested that GST-mSTI1 had no effect on migration of HS578T cells, but that GST-TPR2A2B and GST-TPR1 had an inhibitory effect on migration of HS578T cells (Figure 2.9, B).



**Figure 2.9: Treatment with GST-TPR2A2B and GST-TPR1 significantly decreased migration in HS578T cells** (A) HS578T cells were seeded into wound healing culture inserts and allowed to adhere overnight. Cells were treated with 10 nM GST, GST-mSTI1, GST-TPR2A2B and GST-TPR1 respectively and wound sizes monitored at 0, 6 and 12 hours post treatment. Images were recorded using the Zeiss axiovert fluorescent microscope and analysed using ImageJ. Images shown are representatives of three replicate experiments with similar results. (B) The areas of each of the wounds were measured using ImageJ and the wound areas at 6 and 12 hours post treatment were represented as a percentage of the original wound area, where the original wound was represented as 100 %. The average results of three replicates are shown. Statistical analysis using a two-way ANOVA with Bonferroni post tests indicated a significant difference at 12 hours between GST-TPR2A2B and GST-TPR1 treated cells (\*\*\*) compared to cells treated with GST alone. There was no significant difference between cells treated with GST and GST-mSTI1.

#### **2.4.10 Analysis of the effect of heterologous mSTII proteins on the actin cytoskeleton and extracellular matrix of HS578T cells**

Gelatin-488 was dispensed into  $\mu$ -Slide angiogenesis plates and allowed to polymerise at 4°C for 1 hour. HS578T cells were seeded into gelatin matrices and treated with GST, GST-mSTII, GST-TPR2A2B and GST-TPR1 respectively. Immunofluorescent staining was used to stain cells for actin. The cells and gelatin matrix were visualised by confocal microscopy (Figure 2.10, A and B). Z-stacks of equivalent depth for each of the treatments were taken using the Zeiss LSM 510 meta confocal microscope and analysed in ImageJ.

In Z-stack images of HS578T cells seeded into gelatin matrices, red, blue and green channels corresponding to the actin cytoskeleton, cell nuclei and gelatin matrix could be observed throughout the depth of the Z-stack (Figure 2.10, A). This suggested that the HS578T cells were embedded in the gelatin matrix, rather than invading it from above. The gelatin matrix was unevenly dispersed in both the horizontal and vertical planes (Figure 2.10, A). In the merged 3D composite images of the Z-stacks, the gelatin matrix appeared to be fibril-like in morphology, occurring between the actin cytoskeletal junctions (Figure 2.10, B). This suggested that the HS578T cells could be remodelling the gelatin matrix from a soluble gel into fibrils. Differences in the actin staining were observed between the different treatments (Figure 2.10, B, white arrows). For GST and GST-mSTII treated cells, actin-rich borders at lamellipodial edges, indicative of migratory cell phenotypes could be observed (Figure 2.10, B, white arrows). Actin staining revealed that the GST-TPR2A2B treated cells were more spindle-like in morphology, possibly indicating cell tension, indicative of stationary cells (Figure 2.10, B, white arrows). In GST-TPR1 treated cells, actin staining surrounded the periphery of the cell rather than being localised at a leading edge, indicating reduced polarity (Figure 2.10, B, white arrows). Punctate actin staining was also observed which could be indicative of focal adhesions (Figure 2.10, B, white arrows). The presence of focal adhesions with a lack of cell polarity to drive the cell forward could result in stationary cell morphologies. HS578T cells treated with GST, GST-mSTII, GST-TPR2A2B and GST-TPR1 respectively were stained for fibronectin by immunofluorescence staining and images captured by confocal microscopy (Figure 2.10, C). Interestingly, the fibril-like gelatin matrix resembled fibrils similar to those observed in the fibronectin extracellular matrix of HS578T cells (Figure 2.10, B and C).

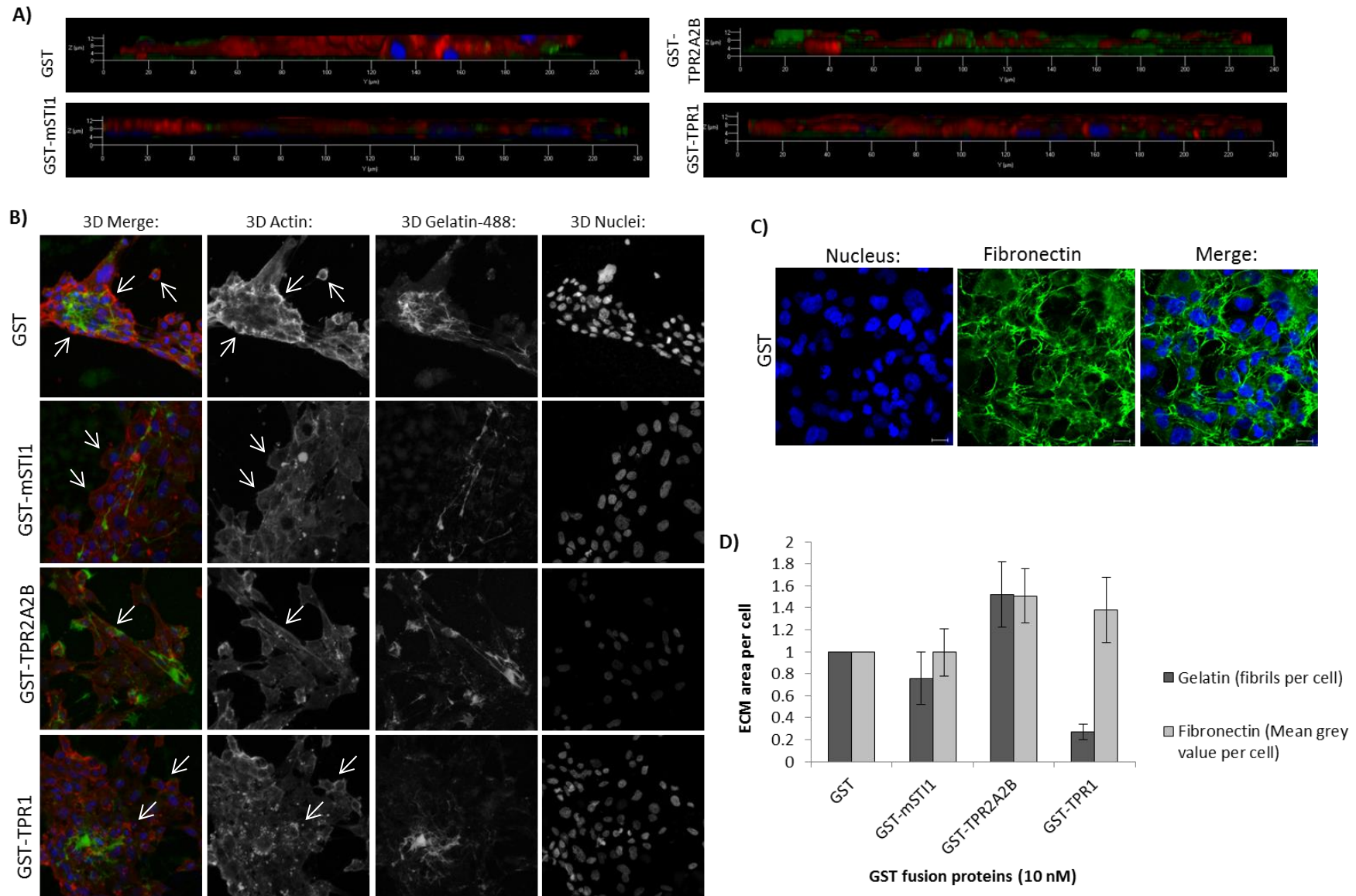
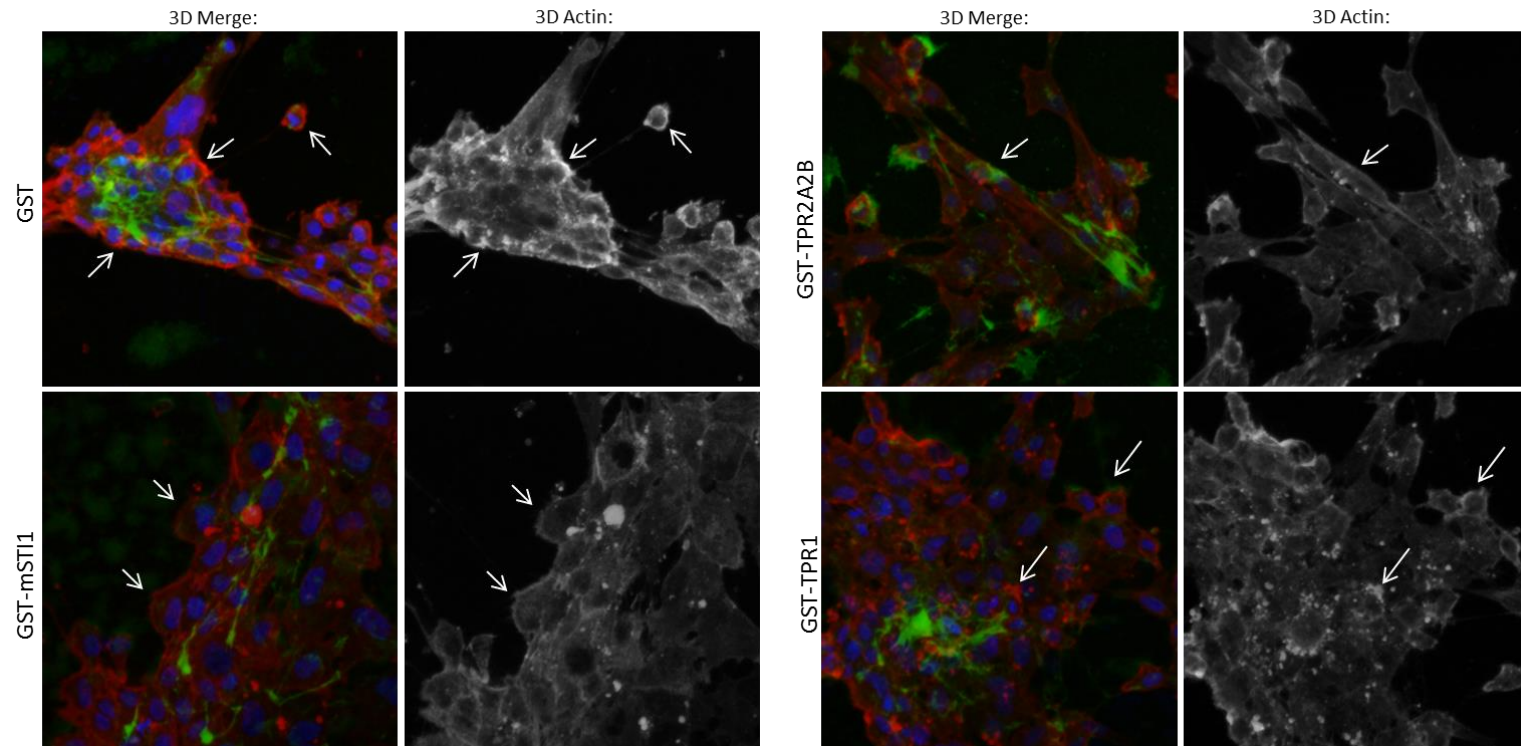


Figure 2.10: Treatment with heterologous mSTI1 proteins had differing effects on the actin cytoskeleton and extracellular matrix of HS578T cells.

## B) LARGER IMAGE



**Figure 2.10: Treatment with heterologous mSTI1 proteins had differing effects on the actin cytoskeleton and extracellular matrix of HS578T cells.** (See Electronic Image 1).

Cells were seeded into gelatin-488 in  $\mu$ -Slide angiogenesis plates and treated with 10 nM GST, GST-mSTI1, GST-TPR2A2B and GST-TPR1 overnight at 37°C, respectively. Z-stacks of each of the treatments encompassing 8 slices (equivalent to 16  $\mu$ m) were taken through the gelatin matrix using the LSM Meta Confocal Microscope (Zeiss) with 40 x objective and represented in (A). Z-stack slices were combined into 3-dimensional (3D) composite images using the 'Stacks - Z-project' function on ImageJ and composite 3D merged, actin, gelatin-488 and nuclei channels represented in (B). Arrows point out differences in actin staining between the different treatments. Cells were seeded onto coverslips in 4-well plates and treated with 10 nM GST, GST-mSTI1, GST-TPR2A2B and GST-TPR1 overnight at 37°C respectively. Cells were stained for fibronectin by immunofluorescence staining and images captured using the LSM Meta Confocal Microscope (Zeiss) with 40 x objective. An example of the fibronectin matrix in HS578T cells treated with GST alone was shown in (C). Threshold analysis by ImageJ on the 3D gelatin-488 channel was used to calculate the area of fibrils in the stacked image. Automated particle counting by ImageJ was used on the 3D nuclei channel to count the number of nuclei in the stacked image. The mean grey value of the fibronectin matrix was measured using ImageJ, as was the number of nuclei per image. The area of gelatin fibrils/number of nuclei for duplicate sets of images and the mean grey value of fibronectin/number of nuclei for triplicate sets of images for each treatment were calculated and represented in (D).



The gelatin fibrils per nucleus as well as the fibronectin matrix fibrils per nucleus for cells treated with GST, GST-mSTII, GST-TPR2A2B and GST-TPR1 were quantified and normalised to the GST control (taken as 1) (Figure 2.10, D). The standard deviations for the gelatin fibrils were calculated from duplicate 3D composite images, while those for the fibronectin matrices were calculated from triplicate single stack images (Figure 2.10, D). It was observed that treatment with GST-mSTII had little or no effect on both the gelatin or fibronectin matrices of HS578T cells compared to the GST control (Figure 2.10, D). Interestingly, treatment with GST-TPR2A2B greatly increased the amount of gelatin fibrils and fibronectin matrix compared to GST treated cells (Figure 2.10, D). Treatment with GST-TPR1 was shown to greatly reduce the number of gelatin fibrils but correlated with an increase in the fibronectin matrix of HS578T cells compared to the GST control (Figure 2.10, D). The data captured for changes observed in gelatin and fibronectin matrices by treatment with recombinant mSTII and mSTII truncated proteins was preliminary and the experimental procedure must be repeated using a range of Hop concentrations in order to determine whether the trends observed were reproducible. A time course study assessing gelatin remodelling at earlier and later time periods should also be conducted.



## 2.5 DISCUSSION:

Recombinant murine Hop GST fusion proteins (GST-mSTI1, GST-TPR2A2B and GST-TPR1) were successfully purified (Figure 2.5 and Table 2.1) and their functionalities in a human system confirmed *in vitro* using HS578T cell lysates (Figure 2.7). The effect of treatment with GST-mSTI1, GST-TPR2A2B and GST-TPR1 compared to the GST control on proliferation, migration and extracellular matrix proteins (gelatin and fibronectin) of HS578T cells was determined and summarised in Table 2.2.

**Table 2.2: Effects of GST, GST-mSTI1, GST-TPR2A2B and GST-TPR1 on proliferation, migration and extracellular matrix proteins of HS578T cells**

	GST	GST-mSTI1	GST-TPR2A2B	GST-TPR1
<b>Proliferation</b>	All results relative to GST treated control samples	Increase	-	-
<b>Migration</b>		-	decrease ***	decrease ***
<b>Gelatin (area of fibrils per cell)</b>		-	increase	decrease
<b>Fibronectin (Mean grey value per cell)</b>		-	increase	increase

A dash ( - ) indicates little or no effect relative to the GST treated sample

Asterisks (\*\*\*) indicate statistically significant ( $p < 0.001$ ) results

### 2.5.1 Treatment of HS578T cells with heterologous mSTI1 proteins had no significant effect on cell proliferation

Treatment with GST-mSTI1 increased proliferation of HS578T cells, although this effect was not statistically significant (Figure 2.8 and Table 2.2). An increase in proliferation by GST-mSTI1 correlated with studies done by Erlich and colleagues (2007) and Tsai and colleagues (2012), who demonstrated that extracellular Hop stimulated proliferation of glioblastoma and ovarian cancer cells, respectively. In studies performed in non-cancerous cell lines, extracellular Hop was shown to have differing effects on cell proliferation. Extracellular Hop was shown to promote proliferation and self-renewal of neural stem cells (Lopes *et al.*, 2012), but reduce proliferation of developing retinal cells (Arruda-Carvalho *et al.*, 2007). Interestingly, Erlich and colleagues (2007) observed no effect on the proliferation of non-cancerous glioma cells. This suggests that the effect of extracellular Hop on cell proliferation is cell line specific. The stimulatory effect on proliferation by extracellular Hop, however, could be common to cancerous cell lines.

The observed increase in proliferation of GST-mSTII treated HS578T cells was not significant (Figure 2.8 and Table 2.2). This could be due to the low concentration (10 nM) of protein used. A range of protein concentrations should be used in order to determine whether the cells exhibited a dose dependent response and whether higher or lower concentrations of extracellular Hop could achieve significant results. The concentrations used were low (10 nM) due to problems encountered with endotoxin removal. Therefore, in order to test a range of concentrations, endotoxin removal must be optimised.

Treatment with GST-TPR2A2B and GST-TPR1 had no effect on proliferation of HS578T cells (Figure 2.8 and Table 2.2). This could suggest that both the TPR2A2B and TPR1 domains of Hop were required for proliferation to occur. This could be tested by treating cells with a combination of GST-TPR2A2B and GST-TPR1 proteins and determining the effects on proliferation. Alternatively, the lack of observed effects could also be due to the low concentration of proteins used. Since GST-mSTII had the highest levels of endotoxins (0.635 EU/mL) compared to GST-TPR2A2B (0.19 EU/mL) and GST-TPR1 (0.005 EU/mL), it is also possible that the stimulatory effect on proliferation could have been due to the presence of contaminating endotoxins. The large and dimeric GST affinity tag may also have interfered with protein function and could be cleaved by thrombin or factor Xa proteases (Terp, 2003). A control in which proliferation of untreated cells was measured could have been included in order to determine whether the GST tag had any effect on proliferation. Although WST-1 assays provide accurate measures of cell viability, alternative cell proliferation assays, such as the BrdU labelling assay which monitors DNA synthesis and cell proliferation, could have been used as a more accurate representation of cell proliferation.

In literature, extracellular Hop was shown to induce proliferation of cancerous cell lines through activation of different signalling cascades, namely the MAPK and phosphatidylinositol 3-kinase (PI3K) pathways for glioblastoma cells and the ALK2/SMAD pathway for ovarian cancer cells (Erlich *et al.*, 2007; Tsai *et al.*, 2012). Interestingly, extracellular Hop was also shown to induce the activation/phosphorylation of ERK in hippocampal neurons, thereby promoting the formation of neurites. It would be interesting to determine whether extracellular Hop (GST-mSTII) or the different domains (GST-TPR2A2B and GST-TPR1) were able to activate any key signalling molecules involved in these signalling cascades. This could be done by determining the expression levels of these key signalling proteins versus their phosphorylated equivalents after treatment with the relevant

proteins. For example, levels of ERK/phosphorylated ERK (pERK), Akt/phosphorylated Akt (pAkt) and SMAD/phosphorylated SMAD proteins could be determined.

### **2.5.2 Treatment with GST-TPR2A2B and GST-TPR1 significantly decreased migration in HS578T cells**

Cell migration for treated cells was observed within a 12 hour period to ensure that any effects observed were not due to proliferation. Treatment with GST-mSTI1 had no statistically significant effect on migration (Figure 2.9 and Table 2.2). This was in contrast with studies done by Chao and colleagues (2013) that showed that extracellular Hop stimulated migration in ovarian cancer cells. Li and colleagues (2012) showed that extracellular Hop had no effect on migration of vascular endothelial cells. This suggests that, similar to the results of the proliferation study, the role of extracellular Hop in cell migration could be cell line specific. As for the proliferation studies, a range of concentrations should be tested to determine whether higher or lower concentrations of extracellular Hop were able to induce cell migration responses. Additionally, endotoxin removal must be optimised to ensure there is no misinterpretation of results due to endotoxins.

Interestingly, treatment with GST-TPR2A2B and GST-TPR1 resulted in a significant decrease in cell migration compared to the GST control (Figure 2.9, Table 2.2). To the best of our knowledge, there are no published reports on the effect of the extracellular Hop domains on cell migration and little is known about the mechanisms by which extracellular Hop regulates cell migration. Chao and colleagues (2013) demonstrated that treatment with anti-Hop antibodies abrogated the stimulatory effect on migration of ovarian cancer cells. The TPR2A2B and TPR1 domains of Hop may act similarly to the anti-Hop antibodies, functioning to abrogate the stimulatory effects of extracellular full length Hop on cell migration. It would therefore be interesting to determine whether HS578T cells release Hop into the extracellular media, and then block endogenous Hop in the experiments before assessing the effects of the GST-fusion proteins.

As for the proliferation studies, a control in which migration of untreated cells was measured could have been included to determine whether the GST tag had any effect on cell migration. A powerful approach for further studies could include the use of live imaging techniques, including tracking of individual cells, in order to monitor cell migration with the relevant treatments.

### **2.5.3 Treatment with heterologous mSTI1 proteins had differing effects on the actin cytoskeleton and extracellular matrix of HS578T cells**

Cancer cell invasion occurs through degradation of the 3D extracellular matrix by downward, MMP-containing, actin-rich membrane protrusions referred to as invadopodia (Egeblad and Werb, 2002; Artym *et al.*, 2006; Schoumacher *et al.*, 2010). In an attempt to observe the effects of the mSTI1 proteins on invasion, a gelatin degradation assay was performed. It was expected that sites of gelatin matrix degradation correlating to sites of invadopodia penetration would be observed by a lack of fluorescence at certain points within an evenly distributed layer of fluorescing gelatin, similar to the phenotype observed by Schoumacher and colleagues (2010). Interestingly, this was not the case, and instead, fibril-like fluorescent gelatin structures were observed for each of the treatments (Figure 2.10, B). It appeared that the HS578T cells could be remodelling the extracellular soluble gelatin into matrix-like fibrils. Gelatin is a form of denatured collagen. Studies have shown that uncleaved gelatin is capable of partial renaturation, resulting in partial recovery of the triple helical collagen structures, thereby leading to the partial recovery of collagen fibrils (Veis *et al.*, 1961; Kühn *et al.*, 1965; Ohyabu *et al.*, 2013). Since the cells were observed to be embedded within the gelatin matrix (Figure 2.10, A), it was possible that the gelatin had re-solubilised at 37°C during the duration of the assay, possibly allowing gelatin matrix remodelling to occur more readily. To the best of our knowledge, this is the first report demonstrating remodelling of soluble gelatin into fibrils in cell culture. This technique could be exploited to elucidate functional interactions between cells and the extracellular environment for a wide range of cell behaviours, including cell proliferation, differentiation, migration and invasion.

In order to deduce whether treatment with extracellular Hop and the different domains may have had an effect on the extent of gelatin matrix remodelling and/or the extracellular fibronectin matrix, the area of gelatin and fibronectin fibrils per cell for each of the treatments was quantified (Figure 2.10, D and Table 2.2). Treatment with full length GST-mSTI1 had little or no effect on the number of gelatin or fibronectin fibrils per cell (Figure 2.10, D and Table 2.2). Treatment with GST-TPR2A2B resulted in an increase in the number of gelatin and fibronectin fibrils per cell (Figure 2.10, D and Table 2.2). Since fibronectin has been shown to be co-distributed with collagen in the extracellular matrix of fibroblasts and has been suggested to be required for the deposition and organisation of collagen by fibroblasts (McDonald *et al.*, 1982; Vuento *et al.*, 1982; Pickford *et al.*, 1997), it was thought that gelatin remodelling might be dependent on the fibronectin matrix. Since fibronectin and collagen

regulate cell processes through interaction with integrins (Hynes, 2002; Olsen and Ninomiya, 1999; Gustafsson and Fassler, 2000), if this was the case, extracellular Hop domains might be having an effect on extracellular matrix remodelling through integrin-mediated processes. Treatment with GST-TPR1, however, resulted in contrasting effects on gelatin (decreased fibrils) compared to fibronectin (increased fibrils) matrices (Figure 2.10, D and Table 2.2) which did not support this assessment.

Differences in the actin cytoskeleton were observed with treatment with the different recombinant Hop proteins (Figure 2.10, B, white arrows). GST-mSTII treated cells had actin staining that could be indicative of a migratory cell phenotype (Figure 2.10, B, white arrows). Although the actin staining for GST-TPR2A2B and GST-TPR1 treated cells differed, both could have been indicative of stationary cell morphologies, which correlated with reduced cell migration in these cells (Figure 2.10, B, white arrows).

#### **2.5.4 The TPR2A2B and TPR1 domains of Hop could inhibit cell migration through inducing changes in the extracellular matrix**

Since MMPs are required for the degradation of the extracellular matrix, thereby promoting migration of invasive and metastatic cancer cells (Streuli, 1999; Egeblad and Werb, 2002; Artym *et al.*, 2006; Van den Steen *et al.*, 2001), degradation of the extracellular matrix may correlate with increased cell migration, while a denser network of extracellular matrix fibrils may correlate with reduced cell migration. This notion is supported by a study done by Coopman and colleagues (1998) which showed that human breast cancer cells were able to phagocytose gelatin, and that a higher phagocytic capacity correlated with a greater invasive capacity of the cells. A loss of fibrils could therefore correlate with increased phagocytic ability and an increased migratory/invasive phenotype, while a denser network of fibrils could correlate with a decrease in phagocytic ability, in turn correlating to a decrease in migration/invasion. The decreased migratory phenotype in HS578T cells treated with GST-TPR2A2B (Figure 2.9 and Table 2.2) correlated with an increased number of gelatin and fibronectin fibrils per cell (Figure 2.10, D and Table 2.2) which is in accordance with this assessment. This was not, however, the case for GST-TPR1 treated cells, which although had a reduced migratory phenotype and an increased fibronectin matrix, resulted in a decreased gelatin matrix (Figure 2.9, Figure 2.10, D and Table 2.2). Either way, treatment with GST-TPR2A2B and GST-TPR1 resulted in observed changes in the gelatin and fibronectin matrices of HS578T cells compared to GST treated cells (Figure 2.10, B-D). This being said,

these data represent a preliminary study and must be repeated to include a range of concentrations and a kinetic study.

Hop has been shown to co-immunoprecipitate with MMP-2 in pancreatic and breast cancer cell lines and suggested to play a role in the activation of MMP-2 within an extracellular Hsp90 multichaperone heterocomplex (Sims *et al.*, 2011; Walsh *et al.*, 2011). Additionally, MMP-2 and fibronectin have been described as client proteins for extracellular Hsp90 (Eustace and Jay, 2004; Hunter *et al.*, 2014). The TPR2A2B and/or TPR1 domains may be interfering with the binding of extracellular full length Hop within the extracellular Hsp90 multichaperone heterocomplex, thereby resulting in reduced chaperoning activity, leading to non-functional extracellular client proteins (MMP-2 and fibronectin), and contributing to a reduced migratory phenotype. It is also possible that the TPR2A2B or TPR1 domains of Hop may be indirectly inhibiting cell migration through remodelling of the extracellular matrix through a regulatory interaction with MMP-2 (Sims *et al.*, 2011; Walsh *et al.*, 2011). Alternatively, treatment with the Hop domains alone could be blocking the interaction of extracellular full length Hop with MMP-2, thereby inhibiting its activation and in turn, leading to an accumulation of extracellular matrix proteins and a reduced migratory phenotype. If this was the case, it would be interesting to test whether treatment with recombinant full length Hop (GST-mSTI1) in combination with the independent Hop domains (GST-TPR2A2B and/or GST-TPR1) would be able to abrogate the inhibitory effects of the independent domains on cell migration. Since a potential interaction between extracellular Hop and MMP-2 has been described (Sims *et al.*, 2011; Walsh *et al.*, 2011) it would be interesting to determine which domain was responsible for binding. This could be readily determined by performing pull down assays using GST-TPR2A2B and GST-TPR1 fusion proteins.

Cell migration processes are regulated by dynamic interactions between the intracellular cytoskeleton and the extracellular matrix (Coopman *et al.*, 1998; Egeblad and Werb, 2002). The changes in the actin cytoskeleton between the different Hop treatments were therefore not surprising (Figure 2.10, B, white arrows). MMPs play a large role in regulating the interactions between the intracellular cytoskeleton and the extracellular matrix of cells (Egeblad and Werb, 2002). It is possible, therefore, that extracellular Hop may be influencing the dynamic changes in the actin cytoskeleton through causing changes in the extracellular environment through regulation of MMP-2.

### **2.5.5 Conclusion**

To the best of our knowledge, there are no published reports on the effect of different domains of extracellular Hop on cell migration, proliferation and the extracellular matrix. Although preliminary, our data suggested that the effects of extracellular Hop on cell proliferation require the full length protein, whereas the TPR1 and TPR2A2B domains inhibited cell migration, possibly by causing changes in the intracellular and extracellular matrix environment, while the full length protein did not. It should not be discounted that the TPR1 and TPR2A2B domains, encompassing different motifs, may mediate their effect through completely independent and unrelated mechanisms. It should also be noted that since the recombinant proteins were expressed in a bacterial system, lack of post-translational modifications (such as glycosylation) could have compromised the stability or quaternary structure of the recombinant proteins (Petsko and Ringe, 2004). It would therefore be interesting to repeat the studies using recombinant proteins expressed in a mammalian system to see whether such modifications had an effect on the results obtained.

## **Chapter 3.**

# **The effect of intracellular Hop on cell migration processes using RNA interference**



### 3.1 INTRODUCTION:

RNA interference (RNAi) is an endogenous cellular mechanism that has been widely exploited and led to a multitude of technologies that have revolutionised the study of gene function, cell biological systems and disease (Fire *et al.*, 1998; McManus and Sharp, 2002; Agrawal *et al.*, 2003; Rao *et al.*, 2009). The RNAi mechanism involves the recognition and binding of large double stranded RNA (dsRNA) molecules by the multicomponent RNAase III family nuclease, DICER (Zamore *et al.*, 2000; Bernstein *et al.*, 2001). The dsRNA is then cleaved by DICER into short dsRNA fragments of approximately 19-23 nucleotides in length, termed short interfering RNA (siRNA) (Zamore *et al.*, 2000; Bernstein *et al.*, 2001; Hammond *et al.*, 2001; McManus and Sharp, 2002; Agrawal *et al.*, 2003). The siRNA is assembled into an RNAi silencing complex (RISC), containing different Argonaute family and argonaute-associated proteins (Zamore *et al.*, 2000; Hammond *et al.*, 2001; Agrawal *et al.*, 2003). Argonaute 2 (Ago 2) functions to cleave and discard one strand of the siRNA. The remaining antisense siRNA strand directs the RISC to the complementary sequence on the target mRNA resulting in cleavage and degradation of the target mRNA, which in turn results in gene silencing (Zamore *et al.*, 2000; Hammond *et al.*, 2001; McManus and Sharp, 2002; Agrawal *et al.*, 2003; Rao *et al.*, 2009). MicroRNAs (miRNAs) are endogenous short, non-coding RNAs that form hairpin structures and are responsible for regulating gene expression through induction of the RNAi pathway (Grishok *et al.*, 2001; Lagos-Quintana *et al.*, 2001; Lau *et al.*, 2001; Lee and Ambros, 2001; McManus and Sharp, 2002; Agrawal *et al.*, 2003; Doench *et al.*, 2003; Zeng *et al.*, 2003; Bartel, 2004). Researchers may silence specific genes of interest by exploiting the endogenous RNAi cell machinery by the use of chemically synthesised siRNAs, as well as synthetic short hairpin RNA (shRNA) constructs that are developed to mimic miRNAs such that they can be used to induce the RNAi pathway (Agrawal *et al.*, 2003; Stegmeier *et al.*, 2005; Silva *et al.*, 2005; Rao *et al.*, 2009).

Hop is upregulated in a wide range of cancers (Sun *et al.*, 2007; Kubota *et al.*, 2010; Pimienta *et al.*, 2011; Walsh *et al.*, 2011). Inhibition of Hop or RNAi mediated depletion of Hop in cancer cells leads to a loss of malignant characteristics (Horibe *et al.*, 2011; Pimienta *et al.*, 2011; Walsh *et al.*, 2011). In particular, Hop knockdown appears to affect cell migration through interaction with cytoskeletal proteins, including actin and tubulin (Li *et al.*, 2012b; Willmer *et al.*, 2013).

Actin polymerisation is a key stage in the formation of pseudopodia (Brahmbhatt and Klemke, 2003; Tsutsumi *et al.*, 2008; Taiyab and Rao, 2010). The study of Rho GTPases, upstream effectors that lead to actin polymerisation and the reorganisation of the actin cytoskeleton, in a wide variety of cancerous cell lines has demonstrated a role for these proteins in the regulation of cell migration, invasion and tumour progression (Fritz *et al.*, 1999; Mullins, 2000; Horiuchi *et al.*, 2003; Simpson *et al.*, 2004; Karlsson *et al.*, 2009).

In particular, RhoC has emerged as a key regulator of invasive cancers (Simpson *et al.*, 2004; Ridley, 2013). Studies done in a wide range of cancer cell lines demonstrated that overexpression of RhoC correlated with malignant characteristics, while RNAi mediated depletion of RhoC levels resulted in a loss of malignant characteristics (Suwa *et al.*, 1998; Fritz *et al.*, 1999; van Golen *et al.*, 2000; Clark *et al.*, 2000; Kamai *et al.*, 2003; Wang *et al.*, 2004b; Shikada *et al.*, 2003; Ikoma *et al.*, 2004; Kondo *et al.*, 2004; Simpson *et al.*, 2004; Hakem *et al.*, 2005; Yao *et al.*, 2006; Fingleton, 2007; Wang *et al.*, 2008; Karlsson *et al.*, 2009; Vega *et al.*, 2011; Rosenthal *et al.*, 2012). In addition, activation of RhoC in spatio-temporally defined areas was shown to regulate the formation of invadopodial protrusions (Bravo-Cordero *et al.*, 2011).

Evidently, Rho GTPases, in particular, RhoC, have been implicated in the regulation of cancer cell invasion and metastasis (Simpson *et al.*, 2004; Ridley, 2013). Additionally, Hop has been shown to promote cancer cell progression and interact with cytoskeletal proteins (Walsh *et al.*, 2011; Li *et al.*, 2012b; Willmer *et al.*, 2013). Little is known, however, about the effects of Hop on the Rho GTPases involved in cancer progression. RNAi (using both siRNA and shRNA via a lentiviral vector delivery system) was therefore used to study the effects of intracellular Hop on cell morphology, RhoC and other Rho family GTPases involved in cell migration processes.

### 3.2 MATERIALS:

The siGENOME non-targeting siRNA negative control, consisting of a scrambled oligonucleotide sequence (5'-AAGCGCGCUUUGUAGGAUUCG-3') (Cat #: D-0012061405) and the siGENOME SMARTpool siRNA targeting Human Hop mRNA (Cat #: M-019802-01-0005), consisting of a pool of four siRNA oligonucleotides:

(5'-GCAAAUAACCCUCAACUGA-3') (Cat #: D-019802-01);

(5'-CCAGAAGGCUUAUGAGGAU-3') (Cat #: D-019802-02);

(5'-GGCAAGGGCUAUUCACGAA-3') (Cat #: D-019802-03) and

(5'-GAGCGUGGGUACAUCGAU-3') (Cat #: D-019802-04), as well as the DharmaFECT transfection reagent (Cat #: T-2004-01) were purchased from Dharmacon Technologies (USA). Henceforth, the siRNA constructs will be referred to as negative siRNA and Hop siRNA respectively.

A set of five short hairpin (sh)RNA clones targeting human Hop in the TRIPZ plasmid backbone, as well as a TRIPZ plasmid containing the non-silencing shRNA control sequence (Cat #: RHS4743) were purchased as glycerol stocks from Open Biosystems (Thermo Scientific) (USA). The clone identities of the five clones were V3THS\_376354 (Cat #: RHS4696-200751377), V3THS\_376355 (Cat #: RHS4696-200749322), V3THS\_376356 (Cat #: RHS4696-200751193), V3THS\_376357 (Cat #: RHS4696-200748588) and V2THS\_78632 (Cat #: RHS4696-200699167). Henceforth, these clones will be referred to as shRNA #1, shRNA #2, shRNA #3, shRNA #4 and shRNA #5 respectively, while the non-targeting shRNA control plasmid will be referred to as N.T shRNA.

The HS578T (ATCC: HTB-126) metastatic breast cancer cell line was from laboratory stocks. The HEK293T cell line was a kind gift from Prof. Sharon Prince (UCT) and the lentiviral packaging plasmids, pMD2.G and psPAX2 were a kind gift from Prof. Marco Weinberg, University of the Witwatersrand.

All general reagents and chemicals were purchased from Sigma Aldrich (USA). Specialised reagents are reflected in the method section. Please see Appendix 1 for a list of all additional materials used including molecular weight markers, kits, antibodies and tissue culture reagents.

### **3.3 METHODS:**

#### **3.3.1 Mammalian cell culture conditions**

The HS578T breast cancer cell line was maintained in Dulbecco's Modified Eagle Medium (DMEM) with 10 % (v/v) Foetal Bovine Serum (FBS), 1 % (v/v) L-Glutamine, 100 U/mL Penicillin Streptomycin Amphotericin (PSA) and 2 mM insulin at 37°C, with 9 % CO<sub>2</sub>. The HEK293T cell line was maintained in DMEM with 10 % (v/v) FBS, 1 % (v/v) L-Glutamine, 0.1 mM non-essential amino acids (NEAA), 1 mM sodium pyruvate, 100 U/ml PSA and 500 µg/mL G418 at 37°C, with 5 % CO<sub>2</sub>.

#### **3.3.2 Immunofluorescence staining and confocal microscopy**

Cells were seeded on sterile glass coverslips in 24-well plates and incubated overnight at 37°C, 9 % CO<sub>2</sub>. Media was removed and cells were washed once with sterile PBS. Cells were fixed by flash-treatment with ice-cold methanol and allowed to air dry completely. Cells were blocked with sterile 1 x TBS containing 1 % (w/v) BSA and 0.1 % (v/v) Triton-X for 45 minutes at room temperature. Cells were incubated with primary antibodies (as described in figure legends) at a dilution of 1:100 in 0.1 % (w/v) BSA/TBS overnight at 4°C. After incubation, cells were washed twice with 0.1 % (w/v) BSA/TBS for 5 minutes each time and then incubated with fluorophore labelled species specific secondary antibodies (as described in figure legends) at a dilution of 1:500 for 1 hour at room temperature in the dark. Cells were washed twice with 0.1 % (w/v) BSA/TBS for 5 minutes each time. Nuclei were stained with 1 µg/mL Hoescht-33342 dye in distilled water and mounted onto slides using DAKO fluorescent mounting medium. The edges of the coverslips were sealed using clear nail varnish and allowed to dry. The cells were visualised using the LSM 510 Meta confocal microscope (Zeiss). Images were recorded using the 63x oil objective and analysed using ZEN 2011 software (Zeiss). Colocalisation analysis of the images was done using the intensity correlation analysis plugin from ImageJ.

#### **3.3.3 Transfections using siRNA system**

HS578T cells were seeded at 90 % confluency in a 6-well plate and incubated overnight at 37°C. Cells were serum starved in non-antibiotic containing, serum-free media for 6 hours prior to transfection. For each transfection reaction, a concentration of 5 µM siRNA was diluted to a total volume of 200 µL in OptiMEM. A volume of 8 µL of DharmaFECT transfection reagent was diluted to a total volume of 200 µL in OptiMEM. The diluted siRNA

and DharmaFECT reagents were incubated for 5 minutes at room temperature, after which the siRNA was added to the DharmaFECT and mixed gently. The siRNA-DharmaFECT complex was incubated at room temperature for 20 minutes and then added to antibiotic-free, complete media to a final volume of 2 mL, such that the final concentration of siRNA was 25 nM. The serum-free media was removed from the cells and replaced with the transfection mixture. Cells were incubated at 37°C and cell lysates of negative siRNA and Hop siRNA transfections were collected at 120 and 144 hours post transfection.

### **3.3.4 Immunoprecipitation Assay**

HS578T cells were grown to confluency in T150 flasks. Cells were washed once with 1 x PBS and lysed on ice for 1 hour with gentle agitation in 1 mL RIPA lysis buffer (50 mM Tris-HCl, 150 mM NaCl, 1 mM EDTA, 1 mM Na<sub>3</sub>VO<sub>4</sub>, 1 % [w/v] NP4O, 1 mM sodium deoxycholate, 1 mM PMSF, 2 µg/mL protease inhibitor cocktail) per flask. Cells were scraped off the surface of the flasks using a cell scraper and lysates collected. Cell debris was removed by centrifugation at 12 000 x g at 4°C for 30 minutes. Volumes of 1 mL of cleared lysates were transferred to new tubes. The test lysate sample was incubated with 5 µg of mouse monoclonal anti-Hop primary antibody for 2 hours at 4°C with gentle agitation. The test and control lysate samples were incubated with 20 µL protein A/G agarose beads overnight at 4°C with gentle agitation. The immunoprecipitated complexes were collected by centrifugation at 1000 x g for 5 minutes at 4°C. The supernatants were discarded and the pellets washed four times with 1 x PBS (pH 7.4). In order to elute the proteins from the beads, the washed pellets were resuspended in 100 µL 100 mM glycine-HCl (pH 3.0) and centrifuged at 1000 x g at 4°C for 5 minutes. The supernatants were collected and 10 µL of 1.5 M Tris-HCl (pH 8.8) were added to each of the supernatants to neutralise the solution. A volume of 24 µL of 5 x SDS-PAGE loading dye was added to each of the samples and the samples were boiled for 5 minutes. Volumes of 20 µL of each of the samples were analysed by SDS-PAGE and western blot analysis.

### **3.3.5 SDS-PAGE and Western analysis**

Cell lysates from each of the transient transfections were made up in 5 x SDS-PAGE sample buffer (60 mM Tris-HCl pH 6.8, 2 % [w/v] SDS, 10 % [v/v] glycerol, 5 % [v/v] β-mercaptoethanol) and quantified using the Nanodrop2000. The lysates were separated by SDS-PAGE according to Laemmli (1970) and the expression levels of various proteins were determined by western blot analysis according to the method of Towbin (Towbin and

Gordon, 1979). The membranes were blocked with a milk solution (1 % [w/v] milk powder, 0.1 % [v/v] Tween-20 in 1 x Tris-buffered saline [TBS]) for 1 hour and incubated with primary antibody (as indicated in figure legends) at 4°C overnight. Anti-Hop, anti-RhoC, anti-actin and anti-Hsp90 primary antibodies were used at a dilution of (1:1000), while anti-Histone H3 was used at a dilution of (1:2500). The membranes were washed (3 x 5 minute washes) in TBS-T (1 % [v/v] Tween-20 in 1 x TBS) and incubated with species specific horseradish peroxidase-conjugated secondary antibodies (1:5000) and Protein-A/G (1:2000) in TBS-T for 1 hour at room temperature. The membranes were washed (3 x 5 minute washes) in TBS-T and proteins visualised using the SuperSignal West Dura extended duration substrate kit by use of X-Ray film (Agfa HealthCare, Belgium) developed in a dark room using developer, stopper and fixer solutions made up using Agfa reagents (as per manufacturer's protocol). Relative expression levels of the various proteins were quantified using densitometry by ImageJ.

### **3.3.6 Multiple sequence alignment of TRIPZ shRNA Hop clones with Hop (Human) and mSTI1 (*Mus musculus*) mRNA**

The sequences of the antisense strands of shRNA #1 (5'-CTGTCGATAGTCTTCTCGG-3'), shRNA #2 (5'-ATAATTTGGCATCTTTCGG-3'), shRNA #3 (5'-AAGTGTTTCGCTGAGTGCCT-3'), shRNA #4 (5'-TTTCTTCTTTGAAGTAGGA-3') and shRNA #5 (5'-AAATATAGAGAGATGAGGC-3') were obtained from Thermo Scientific Open Biosystems using the clone identities of the respective clones. Clustal Omega software programme (<http://www.ebi.ac.uk/Tools/msa/clustalo/>) was used to align the reverse complement of the antisense strands of the respective TRIPZ shRNA Hop clones with the Hop (*Homo sapiens*) mRNA (NM\_006819.2) and mSTI1 (*Mus musculus*) mRNA (NM\_016737.2) in order to determine which region of the Hop and mSTI1 mRNA would be targeted by each of the Hop shRNA clones. A percentage identity matrix comparing the Hop clones with Hop (*Homo sapiens*) and mSTI1 (*Mus musculus*) mRNA was also obtained using Clustal Omega software. Default settings for Clustal Omega were retained for all analyses (<http://www.ebi.ac.uk/Tools/msa/clustalo/>).

### **3.3.7 Plasmid preparation and confirmation of TRIPZ plasmids by restriction enzyme digests**

A volume of 10 µL of pTRIPZ glycerol stocks of the N.T shRNA, shRNA #1, shRNA #2, shRNA #3, shRNA #4 and shRNA #5 plasmids were inoculated into 5 mL of 2 x Luria Broth

(2 x LB) low salt media (20 g/L tryptone, 10 g/L yeast extract, 5 g/L NaCl) with 100 µg/mL ampicillin and incubated at 37°C for 18-19 hours with shaking (180 rpm). The cultures were pelleted by centrifugation for 1 minute at 10 000 x g and the plasmids extracted using the UltraClean Endotoxin-Free Mini Plasmid Prep Kit (Cat #: 12311-100) (MO BIO Laboratories, Inc., USA) according to the manufacturer's instructions. The plasmid DNA was quantified by absorbance at 260 nm using the Nanodrop 2000. Restriction enzyme digests of each of the plasmids using the *Sa*II restriction endonuclease (Cat #: R605A) (Promega, USA) were performed to confirm the plasmids based on size. Each restriction digest reaction mixture consisted of 400 ng of the relevant plasmid DNA, 10 U *Sa*II restriction enzyme, 1 x restriction enzyme buffer (Buffer D) (Cat #: R004A) (Promega, USA) and made up to a total reaction volume of 20 µL with nuclease-free H<sub>2</sub>O. Restriction digests were performed for 2 hours at 37°C. Digested and undigested plasmids were loaded with 6 x tracking dye (0.25 % [w/v] bromophenol blue, 30 % [v/v] glycerol in dH<sub>2</sub>O) into a 1 % (w/v) agarose gel in 1 x TBE buffer (90 mM Tris, 90 mM boric acid, 2 mM EDTA, 20 µM ethidium bromide) and electrophoresed at 100 V for approximately 45 minutes. Gels were viewed under ultraviolet light and images obtained using the Chemidoc imaging system (Biorad).

### **3.3.8 Analysis of Hop knockdown and protein expression levels in shRNA treated HEK293T and HS578T cell lines**

Cells were seeded at 80 % confluency in a 24-well plate in non-antibiotic containing media and incubated overnight at 37°C. Transfection mixtures containing the relevant pTRIPZ shRNA plasmid (500 ng) and X-tremeGENE HP transfection reagent (1.5 µL) (Cat #: 06366236001) (Roche, South Africa) for each of the five shRNA Hop clones were made up to a total volume of 100 µL in OptiMEM, and incubated for 30 minutes at room temperature. A volume of 50 µL of the relevant transfection mixtures was added dropwise to the wells and the cells were incubated at 37°C for 18 hours. The transfection media was removed and replaced with complete media containing doxycycline (1 µg/mL) (Cat #: D9891) (Sigma Aldrich, USA) and incubated at 37°C for 72 hours. The presence of successfully transfected cells was analysed by examining the expression of turboRFP by fluorescence microscopy using the Zeiss axiovert fluorescence microscope. Transient transfections with the five shRNA Hop clones were carried out in both the HEK293T and the HS578T cell lines. Cell lysates were prepared 72 hours post induction with doxycycline (1 µg/mL) and relative expression levels of Hop, actin, RhoC and Histone H3 were determined by western blot analysis and densitometry using ImageJ software.

### 3.3.9 Lentiviral particle production in HEK293T cells

HEK293T cells were seeded into a 6-well plate in non-antibiotic containing media such that they reached a confluency of approximately 80 % after incubation overnight at 37°C, 5 % CO<sub>2</sub>. A transfection mixture containing pTRIPZ N.T shRNA or pTRIPZ shRNA #2 (500 ng/well), pMD2.G (50 ng/well), psPAX2 (450 ng/well) and X-tremeGENE HP transfection reagent (1.5 µL/well) was made up to a volume of 100 µL in OptiMEM (per well) and incubated for 30 minutes at room temperature. A volume of 100 µL of transfection complex was added dropwise to each of four wells containing HEK293T cells. The dish was swirled to ensure even distribution of the complexes throughout the cells and the cells were incubated at 37°C, 5 % CO<sub>2</sub> for 18 hours. After incubation, the media was replaced with complete media and incubated for a further 24 hours at 37°C, 5 % CO<sub>2</sub>. The spent medium (containing virus particles) from the four wells was harvested, pooled, and stored at 4°C overnight. Fresh complete media was added to the cells and the cells were incubated for a further 24 hours at 37°C, 5 % CO<sub>2</sub>. The spent medium (containing virus particles) was harvested and pooled with the media from the previous day. The virus containing medium was filter sterilised through a 0.45 µm filter, aliquotted into 1 mL fractions and stored at -80°C for use in subsequent experiments.

During this stage, two wells were used as positive controls for transfection. The pLVTH plasmid (containing a constitutively expressed GFP marker) and the pTRIPZ N.T shRNA plasmid (containing an inducible turboRFP marker) were used at a concentration of 500 ng/well in their respective transfection mixtures. After incubation at 37°C, 5 % CO<sub>2</sub> overnight, the well containing the pTRIPZ transfection mixture was treated with fresh media containing doxycycline (1 µg/mL) in order to induce expression of turboRFP. The presence of successfully transfected cells was analysed 96 hours post transfection (72 hours post induction with doxycycline) by fluorescence microscopy using the Zeiss axiovert fluorescent microscope.

Transmission Electron microscopy (TEM) was used to analyse the harvested media for the presence of viral particles. The virus particle samples were thawed at 37°C and kept on ice. A volume of 20 µL of sample was pipetted onto a TEM grid and allowed to stand for 30 seconds, after which it was carefully removed using filter paper. A volume of 20 µL of 2 % (v/v) uranyl acetate was pipetted onto the TEM grid and allowed to stand for 30 seconds,



after which it was carefully removed using filter paper. The grid was viewed by transmission electron microscopy using the Zeiss Libra 120 transmission electron microscope (Rhodes University) and images obtained using the Mega View G2 camera.

### **3.3.10 Analysis of transduction efficiency of N.T shRNA and shRNA #2 lentiviral particles**

Cells were seeded at 40 – 50 % confluency in a 6-well plate and incubated overnight at 37°C. N.T shRNA and shRNA #2 virus particle supernatants were thawed at 37°C and kept on ice. Different volumes of virus particle supernatants (200 µL, 400 µL, 600 µL, 800 µL and 1000 µL) were made up to 2 mL in media containing hexadimethrine bromide (polybrene) (Cat #: H9268) (Sigma Aldrich, USA) (8 µg/mL) and incubated for 5 minutes at room temperature. Growth medium was replaced with the medium containing varying volumes of virus particle supernatant and cells incubated overnight at 37°C. The transduction media was removed and the cells washed once with 1 x PBS. Fresh media containing doxycycline (1 µg/mL) was added to each of the wells and the cells were incubated at 37°C for 72 hours. The presence of successfully transduced cells was analysed by examining the expression of turboRFP by fluorescence microscopy using the Zeiss axiovert fluorescence microscope. The number of transduced cells per field of view for each of the virus particle concentrations was quantified using automated counting particle plugin in ImageJ (See Appendix 4). For the HEK293T cell line, the average number of transduced cells per field of view for five fields of view for each virus particle concentration was calculated (Supplementary figure 3). For the HS578T cell line, the average number of transduced cells per field of view, for three fields of view for each virus particle concentration, was calculated (Supplementary figure 4).

### **3.3.11 Selection and propagation of stable cell lines**

A standard curve was constructed by seeding cells at a range of cell numbers (8000, 4000, 2000, 1000, 500, 250, 125) per well in quadruplicate and incubating them overnight at 37°C. Cells were incubated for a further 4 hours with 10 µL of WST-1 cell proliferation reagent and the absorbance at 440 nm measured. The triplicate absorbance measurements were averaged and a standard curve of absorbance versus number of cells was generated. The minimum concentration of puromycin (Cat #: P8833) (Sigma Aldrich, USA) required to kill non-transduced cells was determined by generating a puromycin kill curve. Volumes of 100 µL of cells at a concentration of  $8 \times 10^4$  cells/mL were seeded into wells in each of four 96-well plates and incubated overnight at 37°C. Cells in each plate were treated with a range of

concentrations of puromycin (15 µg/mL, 7.5 µg/mL, 3.75 µg/mL, 1.88 µg/mL and 0.94 µg/mL) in quadruplicate. Plate 1, 2, 3 and 4 were incubated at 37°C for 0, 24, 48 and 72 hours respectively. After the appropriate incubation period, the cells were incubated for a further 4 hours with 10 µL of WST-1 cell proliferation reagent and the absorbance at 440 nm measured. The standard curve and the data generated from each of the time periods were used to generate a puromycin kill curve, reflecting cell death in number of cells with different concentrations of puromycin over a period of 4 days.

Cells were cultured in the presence of puromycin at a chosen concentration of 2 µg/mL to select for stably transduced cells. After 10 days, successfully transduced cells were pooled and the resulting polyclonal cell lines propagated in the presence of fresh puromycin every 3 to 5 days. Glycerol stocks of the polyclonal transduced cell lines were made (10 % [v/v] Dimethyl sulfoxide [DMSO] in complete media) and stored at -80°C and/or liquid nitrogen. The protocol described above was followed for transduction and propagation of HEK293T and HS578T cell lines with N.T shRNA and shRNA #2 virus particles. Henceforth, stable polyclonal HEK293T cell lines transduced with N.T shRNA and shRNA #2 will be referred to as pHEK293T-NT.shRNA and pHEK293T-Hop.shRNA respectively.

### **3.3.12 Rho Activation Assay**

Three T75 flasks each of pHEK293T-NT.shRNA and pHEK293T-Hop.shRNA cells at 50 % confluency were treated with doxycycline (1 µg/mL) for 72 hours at 37°C. A confluent T75 flask of uninduced pHEK293T-NT.shRNA was treated with phorbol 12-myristate 13-acetate (PMA) (20 nM) for 2 hours at 37°C and used as a positive control for the assay. Culture medium was removed and cells were washed twice with ice-cold 1 x PBS. Cells were lysed in 1 mL volumes of ice-cold 1 x Mg<sup>2+</sup> lysis/wash buffer (MLB) (10 % [v/v] glycerol, 10 µg/mL aprotinin and 10 µg/mL leupeptin) and detached from the surface of the flasks using a cell scraper. The cell lysates were incubated for 15 minutes at 4°C with gentle agitation. The lysates were passed through 29-gauge syringe needles three times in order to reduce viscosity and cleared by centrifugation at 14 000 x g for 5 minutes at 4°C. The supernatants were collected, protein concentration quantified using the Nanodrop2000 and stored on ice until use.

Volumes of 500 µL of the PMA treated lysate were aliquotted into two eppendorf tubes and 10 µL of 0.5 M EDTA (pH 8.0) (to a final concentration of 10 mM) were added to each tube.

A volume of 5  $\mu$ L of 100 x GTP $\gamma$ S (to a final concentration of 100  $\mu$ M) was added to one tube and used as a positive control and 5  $\mu$ L of 100 x GDP (to a final concentration of 1 mM) was added to the second tube and used as a negative control. The tubes were incubated for 30 minutes at 30°C with agitation. Volumes of 500  $\mu$ L of triplicate cell lysates of pHEK293T-NT.shRNA and pHEK293T-Hop.shRNA cells were incubated with a volume of 15  $\mu$ L (20  $\mu$ g) of the Rho Assay Reagent slurry for 45 minutes at 4°C with gentle agitation. The agarose beads were collected by centrifugation at 14 000 x g for 10 seconds at 4°C and the supernatant discarded. The beads were washed three times in 0.5 mL 1 x MLB and resuspended in 25  $\mu$ L of 2 x Laemmli reducing sample buffer with 2  $\mu$ L 1 M dithiothreitol (DTT). The samples were boiled for 5 minutes, centrifuged briefly and 20  $\mu$ L samples analysed for the presence of RhoC by SDS-PAGE and western blot analysis.

### **3.3.13 Scanning Electron Microscopy**

The pHEK293T-NT.shRNA and pHEK293T-Hop.shRNA cells were treated with doxycycline (1  $\mu$ g/mL) for 48 hours at 37°C and then seeded at 50 % confluency in the presence of doxycycline (1  $\mu$ g/mL) onto sterile glass coverslips in a 4-well plate and incubated overnight at 37°C. Culture medium was removed and the cells were washed in 1 x PBS. Cells were fixed in ice-cold 2.5 % (v/v) glutaraldehyde phosphate buffer for 6 hours at 4°C. Cells were washed twice with cold phosphate buffer for 10 minutes each time. Cells were dehydrated in increasing concentrations of ethanol (v/v) (30 %, 50 %, 70 %, 80 %, 90 % and 100 %) for 5 minutes at each concentration, with two 5 minute treatments at 100 % ethanol. Coverslips were transferred to Critical Point Dryer (CPD) baskets, filled with ethanol and samples critical point dried for 2 hours in the CPD chamber. Coverslips were mounted onto stubs, coated with gold using the Quorum Q150R S, Advanced Laboratory Solutions, and viewed by scanning electron microscopy (SEM) using the Vega Tescan Scanning Electron Microscope with SEDetector, Rhodes University.

### **3.3.14 Cell proliferation assay**

Volumes of 100  $\mu$ L pHEK293T-NT.shRNA and pHEK293T-Hop.shRNA cells were seeded in a single 96-well plate at a concentration of  $1 \times 10^5$  cells/mL. Triplicate samples of each of the cell lines were induced at 72, 48, 24, 12 hours with doxycycline (1  $\mu$ g/mL) or remained uninduced. The induced cells were seeded alongside uninduced equivalents in order to account for growth over the time period. Cells were incubated with 10  $\mu$ L WST-1 cell proliferation reagent for 3 hours at 37°C and the absorbance at 440 nm measured. The

average percentage of induced:uninduced sample for each of the replicates at each time period for each of the cell lines was calculated and normalised to the 0 hour sample, where T = 0 was made 100 %. Percentage viabilities of induced:uninduced cells were plotted against the induction time periods and the growth profiles of each of the cell lines were compared.

### **3.4 RESULTS:**

#### **3.4.1 Association of Hop with Rho family proteins in HS578T cell line**

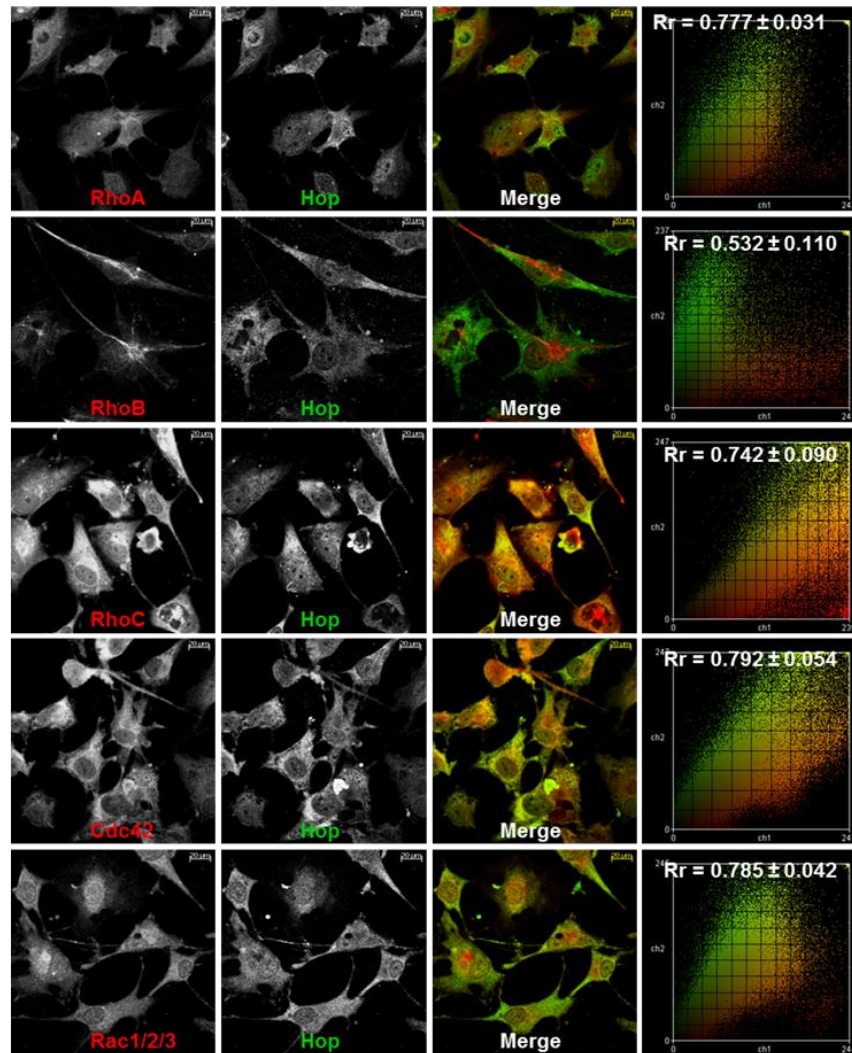
Previous research from our laboratory suggested that Hop may be involved in regulation of actin polymerisation (Willmer *et al.*, 2013). We therefore tested whether Hop colocalised with proteins involved in actin polymerisation. Immunofluorescence staining and confocal microscopy was used to analyse the colocalisation of Hop with the Rho family member signalling molecules, RhoA, RhoB, RhoC, Cdc42 and Rac1/2/3 in HS578T cells (Figure 3.1, A). Colocalisation analysis of confocal microscopy images using Pearson's correlation coefficients (Rr) revealed that there was a strong correlation between the signal intensities of Hop and a number of signalling molecules (RhoA [ $0.777 \pm 0.031$ ], RhoC [ $0.742 \pm 0.090$ ], Cdc42 [ $0.792 \pm 0.054$ ] and Rac1/2/3 [ $0.785 \pm 0.042$ ]) (Figure 3.1, A). This suggested that Hop colocalised strongly with RhoA, RhoC, Cdc42 and Rac1/2/3. The Pearson's correlation coefficient of Hop with RhoB was evidently lower ( $0.532 \pm 0.110$ ), suggesting that Hop colocalised to a lesser extent with RhoB (Figure 3.1, A). Previous immunofluorescence staining using secondary antibodies alone, confirmed that there was no background staining/non-specific binding occurring. Although manufacturers suggest specificity of the primary antibodies, controls to confirm that no cross reactivity between antibodies occurred. Controls whereby rabbit primary antibodies (signalling molecule antibodies) were incubated with anti-mouse secondary antibodies alone, and mouse primary antibodies (anti-Hop) were incubated with anti-rabbit secondary antibodies alone should have been included to eliminate any non-specific signal.

A short interfering RNA (siRNA) system for the knockdown of Hop in HS578T breast cancer cells was optimised previously in our laboratory. This protocol was used for transient Hop knockdown in HS578T cells (Figure 3.1, B). Western blot analysis revealed a clear reduction in the levels of Hop in the Hop siRNA sample compared to the negative control siRNA sample (-ve siRNA) at 120 and 144 hours post transfection with the relevant siRNAs (Figure 3.1, B). This indicated that knockdown of Hop was successfully achieved at 120 and 144

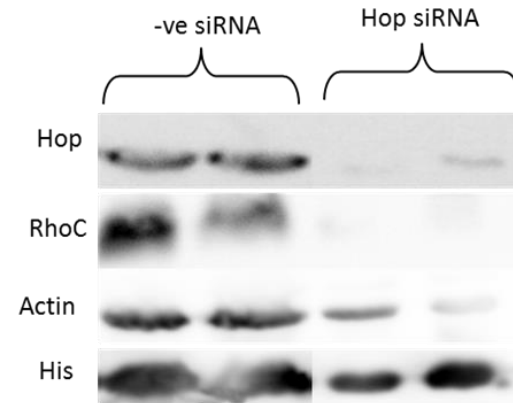
hours post transfection with Hop siRNA (Figure 3.1, B). The effects of Hop knockdown on expression levels of RhoC and actin were determined by western blot analyses (Figure 3.1, B). A clear reduction in the levels of both RhoC and actin were observed in the Hop siRNA samples (120 and 144 hours) compared to the –ve siRNA control samples (Figure 3.1, B). This indicated that knockdown of Hop resulted in reduced levels of both RhoC and actin (Figure 3.1, B).

In order to assess whether there was a direct interaction between Hop and RhoC, Hop was immunoprecipitated from HS578T whole cell lysate (Figure 3.1, C). Confirmation of the Hop immunoprecipitation (IP), as well as the presence of Hsp90 and RhoC in the Hop IP, was determined by western blot analysis (Figure 3.1, C). Western blot analysis of the IP revealed that Hop (~60 kDa) was successfully immunoprecipitated from HS578T whole cell lysate (Figure 3.1, C). In the Hop IP, bands at ~90 kDa and ~25 kDa were detected with anti-Hsp90 and anti-RhoC antibodies respectively. These corresponded to the predicted molecular weights of the proteins (~90 kDa and ~21 kDa) as well as to bands observed in the whole cell lysates (Figure 3.1, C). This suggested that Hsp90 and RhoC were immunoprecipitated with Hop, indicating that RhoC interacted in a common complex with Hop and Hsp90. A number of various sized bands were detected with anti-RhoC antibodies in the whole cell lysate, however (Figure 3.1, C), suggesting non-specific binding of the RhoC antibody could be occurring. The bands occurring at ~50 kDa in each of the IP samples corresponded to the molecular weight of the heavy chain units of the Hop antibody alone (Figure 3.1, C) (Lal *et al.*, 2006).

A)



B)



C)

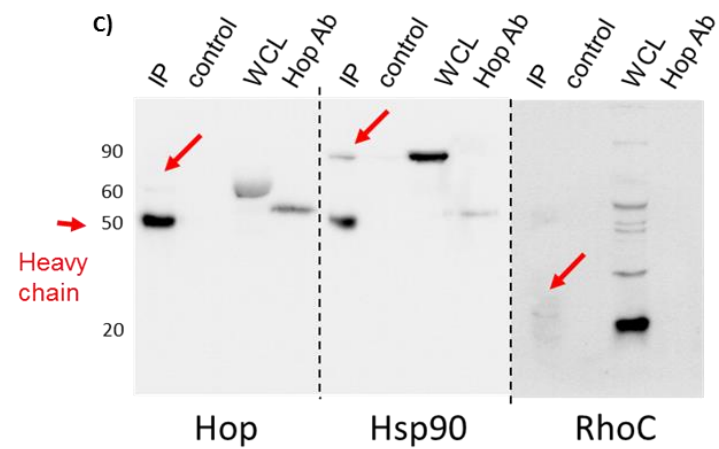


Figure 3.1: Association of Hop with Rho family proteins in HS578T cell line

**Figure 3.1: Association of Hop with Rho family proteins in HS578T cell line.** (See Electronic Image 1)

(A) HS578T cells were seeded onto coverslips and incubated overnight. Cells were fixed with methanol and incubated with primary antibodies raised against the relevant signalling molecule and human Hop followed by donkey anti-rabbit Alexa Fluor 555 (red, first panel) and donkey anti-mouse Alexa Fluor 488 (green, second panel) secondary antibodies. Images were captured using the Zeiss LSM 510 Meta confocal microscope and colocalisation analysis was performed using ImageJ software. Scale bars represent 20  $\mu$ m. The fourth panel indicated fluorescence scattergrams that show the pixel on pixel overlap of the signals between the two channels. The averaged Pearson's correlation coefficient (Rr) values for triplicate images were reflected above each scattergram. (B) HS578T cells were transfected with either negative control siRNA or siRNA targeting Hop. Cell lysates were taken 120 and 144 hours post transfection and expression levels of Hop, RhoC, actin and Histone H3 were analysed by western blot analysis. (C) Hop was immunoprecipitated (IP) from HS578T whole cell lysate (WCL) by incubation with anti-Hop antibodies bound to protein A/G beads. Confirmation of the Hop IP as well as presence of Hsp90 and RhoC in the Hop IP was determined by western blot analysis. Lanes marked 'IP' indicated the Hop IP. Lanes marked 'control' indicated protein A/G beads alone incubated with HS578T lysate. 'Hop Ab' indicated Hop antibody alone. Red arrows depicted the heavy chain Hop antibody as well as the presence of Hop, Hsp90 and RhoC in the Hop IP sample.

### 3.4.2 Analysis of TRIPZ shRNA clones for development of stable cell lines

We elected to use an inducible shRNA system to develop a system for the knockdown of Hop that could be regulated in order to study the role of Hop on Rho activity. Five doxycycline inducible TRIPZ shRNA clones targeting Hop and one control shRNA plasmid were selected for these analyses.

The pTRIPZ plasmid (Thermo Scientific Dharmacon Technical Manual, 2009) contains a number of important features (Figure 3.2, A). The bacterial origin of replication (pUC ori) and ampicillin resistance gene (AmpR) allow propagation and selection of the plasmid in bacterial cells. It contains the relevant shRNA for knockdown of the specific gene of interest (Figure 3.2, A). The tetracycline response element (TRE) acts as a promoter that allows induction of the shRNA in the presence of doxycycline (Das *et al.*, 2004). This initiation process is made possible through the constitutively expressed reverse tetracycline transactivator (rtTA3) that binds the TRE in the presence of doxycycline, thereby activating transcription (Das *et al.*, 2004; Markusic *et al.*, 2005). It has a useful turbo-RFP (tRFP) reporter gene that is co-expressed with the shRNA, allowing for visual tracking of transfection/transduction. The SV40 ori allows for replication of the plasmid in transient mammalian transfections. It contains a *psi* packaging sequence which allows packaging of the plasmid using a lentiviral vector system as well as a Rev response element (RRE) which increases the packaging efficiency (Thermo Scientific Dharmacon Technical Manual, 2009). It contains a 5' long terminal repeat (LTR) and a 3' self-inactivating LTR (SIN LTR) which allow integration of the plasmid into the mammalian cell genome. In addition, the SIN LTR prevents replication of viral particles; an enhanced safety measure of the lentivirus system (Naldini *et al.*, 1996; Zufferey *et al.*, 1998; Trono, 2000; Wu, 2000; Kappes and Wu, 2001; Kappes and Wu, 2003). The central polypurine tract (cPPT) improves transport of the construct into the nucleus and integration into the genome (Van Maele *et al.*, 2003). The presence of a puromycin resistance gene (PuroR) allows for selection and propagation of stable integrants. The human ubiquitin C (UBC) promoter (Figure 3.2, A) allows for constitutive expression of rtTA3 and PuroR and the internal ribosomal entry site (IRES) allows for the expression of rtTA3 and PuroR in a single transcript (Martínez-Salas, 1999). The Woodchuck hepatitis posttranscriptional regulatory element (WPRE) enhances expression (Klein *et al.*, 2006).

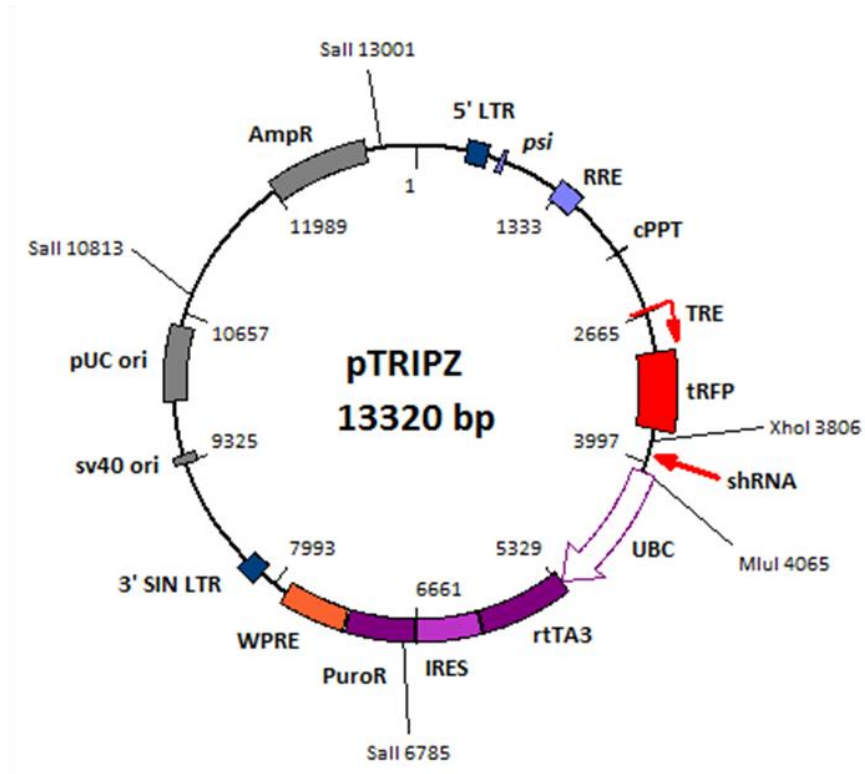


#### 3.4.2.1 Confirmation of TRIPZ plasmids by restriction enzyme digestion

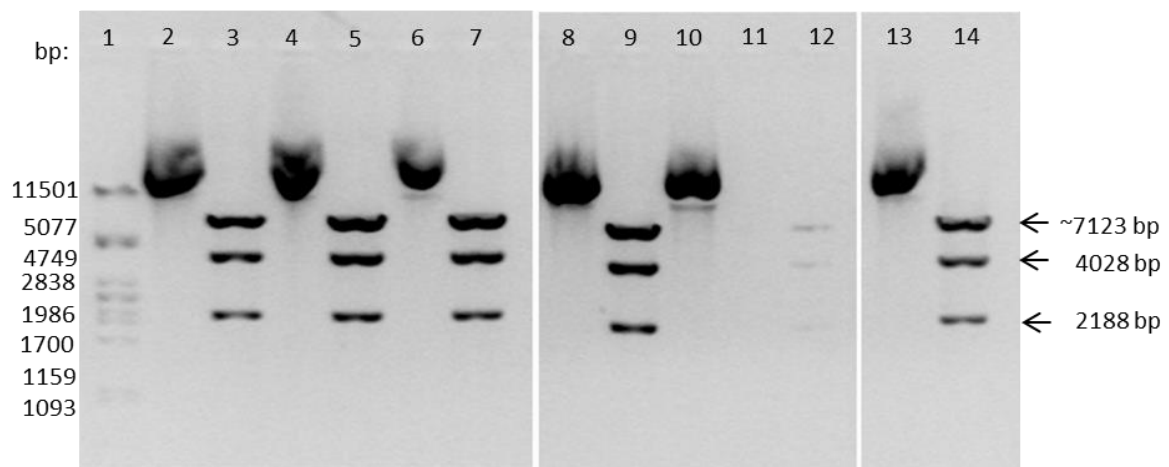
A plasmid map of pTRIPZ was created using BioEdit software (Figure 3.2, A). The sequence of pTRIPZ was downloaded from the Addgene website ([http://www.addgene.org/browse/sequence\\_vdb/5561/](http://www.addgene.org/browse/sequence_vdb/5561/)). The *SalI* restriction enzyme cuts pTRIPZ at 6785 bp, 10813 bp and 13001 bp (Figure 3.2, A). Restriction enzyme digestion with *SalI* would therefore result in three linear fragments of ~7123 bp (including the 19 bp shRNA insert), 4028 bp and 2188 bp.

An endotoxin-free plasmid extraction kit was used to extract the TRIPZ plasmids. The plasmids were digested with the restriction enzyme *SalI* and analysed by agarose gel electrophoresis to confirm the plasmid identity and quality (Figure 3.2, B). For each of the undigested plasmids (Figure 3.2, B: Lanes 2, 3, 6, 8, 10, 13), a predominant bright band, of high mobility, indicative of supercoiled plasmid DNA was visible. For each of the *SalI* digested plasmids (Figure 3.1; Lanes 3, 5, 7, 9, 12, 14), three bright bands corresponding to the expected molecular weights of the digested plasmids (~7123 bp, 4028 bp and 2188 bp) were observed. This confirmed that plasmids with the correct pTRIPZ backbone for each of the shRNA clones were successfully extracted. All gel lanes were clean, with no evidence of degradation or contaminating RNA/chromosomal DNA (Figure 3.2, B). All plasmids were judged to be of sufficient quantity and quality for use in transfection experiments.

A)



B)



**Figure 3.2: Restriction enzyme digests of TRIPZ plasmids with *SalI* restriction enzyme.**

(A) Plasmid map of pTRIPZ vector backbone. (B) Lane 1: Lambda / *PstI* DNA ladder; Lane 2: Undigested N.T shRNA; Lane 3: Digested N.T shRNA; Lane 4: Undigested shRNA #1; Lane 5: Digested shRNA #1; Lane 6: Undigested shRNA #2; Lane 7: Digested shRNA #2; Lane 8: Undigested shRNA #3; Lane 9: Digested shRNA #3; Lane 10: Undigested shRNA #4; Lane 11: Empty; Lane 12: Digested shRNA #4; Lane 13: Undigested shRNA #5; Lane 14: Digested shRNA #5. Numbers beside black arrows indicate expected sizes (bp) of linear fragments of plasmid DNA.

### 3.4.2.2 Alignment of Hop targeting shRNA clones with Hop mRNA

A multiple sequence alignment of the five shRNA Hop clones with the primary nucleotide sequence of Hop (*Homo sapiens*) (NM\_006819.2) and mSTI1 (*Mus musculus*) (NM\_016737.2) was performed using Clustal Omega software (<http://www.ebi.ac.uk/Tools/msa/clustalo/>) (Appendix 5, Supplementary figure 5). The regions of the mRNA at which each shRNA Hop clone targeted, as well as the percentage identities of each of the shRNA clones with Hop and mSTI1 mRNA were summarised and tabulated (Table 3.1). Hop and mSTI1 mRNA have a sequence identity of 87 %.

The shRNA #1 and shRNA #4 clones were shown to target different regions in the TPR6 motif within the TPR2A domain of Hop and mSTI1 mRNA (Table 3.1). The shRNA #2 clone was shown to target the TPR8 and TPR9 motifs within the TPR2B domain (Table 3.1). The shRNA #3 clone was shown to target the mRNA at exon 13 and 14, which occur 3' to the TPR2B domain, but still within the coding sequence (Table 3.1). The shRNA #5 clone was shown to target the Hop and mSTI1 mRNA outside of the protein coding sequence, within a sequence tagged site (STS) region (Table 3.1). All of the shRNA clones had a sequence identity of 100 % with the Hop (*Homo sapiens*) mRNA (Table 3.1). The shRNA #1, shRNA #2, shRNA #3, shRNA #4 and shRNA #5 clones aligned with mSTI1 (*Mus musculus*) mRNA with sequence identities of 84 %, 84 %, 90 %, 95 % and 77 % respectively (Table 3.1). It is evident that each of the clones target different regions of the Hop / mSTI1 mRNA and have different percentage identities to mSTI1 mRNA (Table 3.1).

**Table 3.1: Summary of nucleotide positions and structural motifs / domains at which each shRNA clone targets Hop (*Homo sapiens*) and mSTI1 (*Mus musculus*) mRNA**

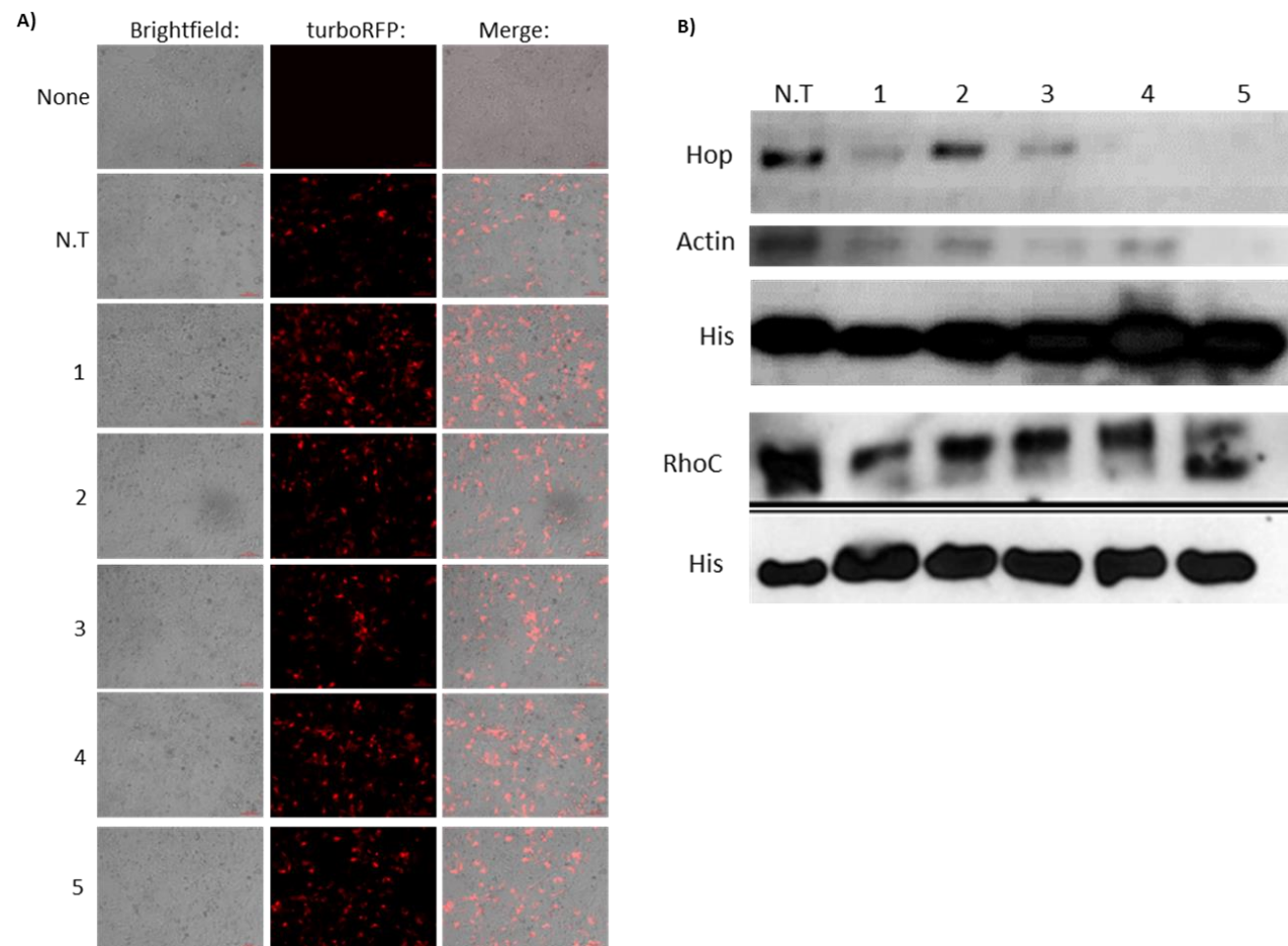
Structural elements:		Nucleotide positions:		Nucleotide positions at which shRNA clones target Hop/mSTI1 mRNA*					
Domains:	Motifs:	Hop mRNA:	mSTI1 mRNA:	shRNA #1:		shRNA #2:		shRNA #3:	
TPR1	TPR1	157...258	148...249						
	TPR2	259...360	253...351						
	TPR3	361...462	355...453						
DP1		568...667	559...658						
TPR2A	TPR4	820...921	811...912						
	TPR5	922...1023	916...1014						
	TPR6	1045...1146	1036...1137	Hop (1123...1141) mSTI1 (1114...1132)		100 84		Hop (1072...1090) mSTI1 (1063...1081)	
TPR2B	TPR7	1225...1326	1216...1317						
	TPR8	1327...1428	1321...1419			Hop (1418...1436) mSTI1 (1409...1427)		100 84	
	TPR9	1429...1530	1420...1521						
DP2		1624...1693	1615...1684						
(within coding sequence – Exon 13 and 14)						Hop (1694...1712) mSTI1 (1685...1703)		100 90	
(outside of coding sequence - STS)								Hop (1878...1896) mSTI1 (1859...1877)	

\*Numbers next to the protein names indicate the percentage identity of shRNA clones with Hop/mSTI1 (%); Full length Hop and mSTI1 mRNA have a sequence identity of 87%.

### **3.4.2.3 Analysis of Hop knockdown efficiencies and expression levels of actin and RhoC for TRIPZ clones in HEK293T and HS578T cell lines**

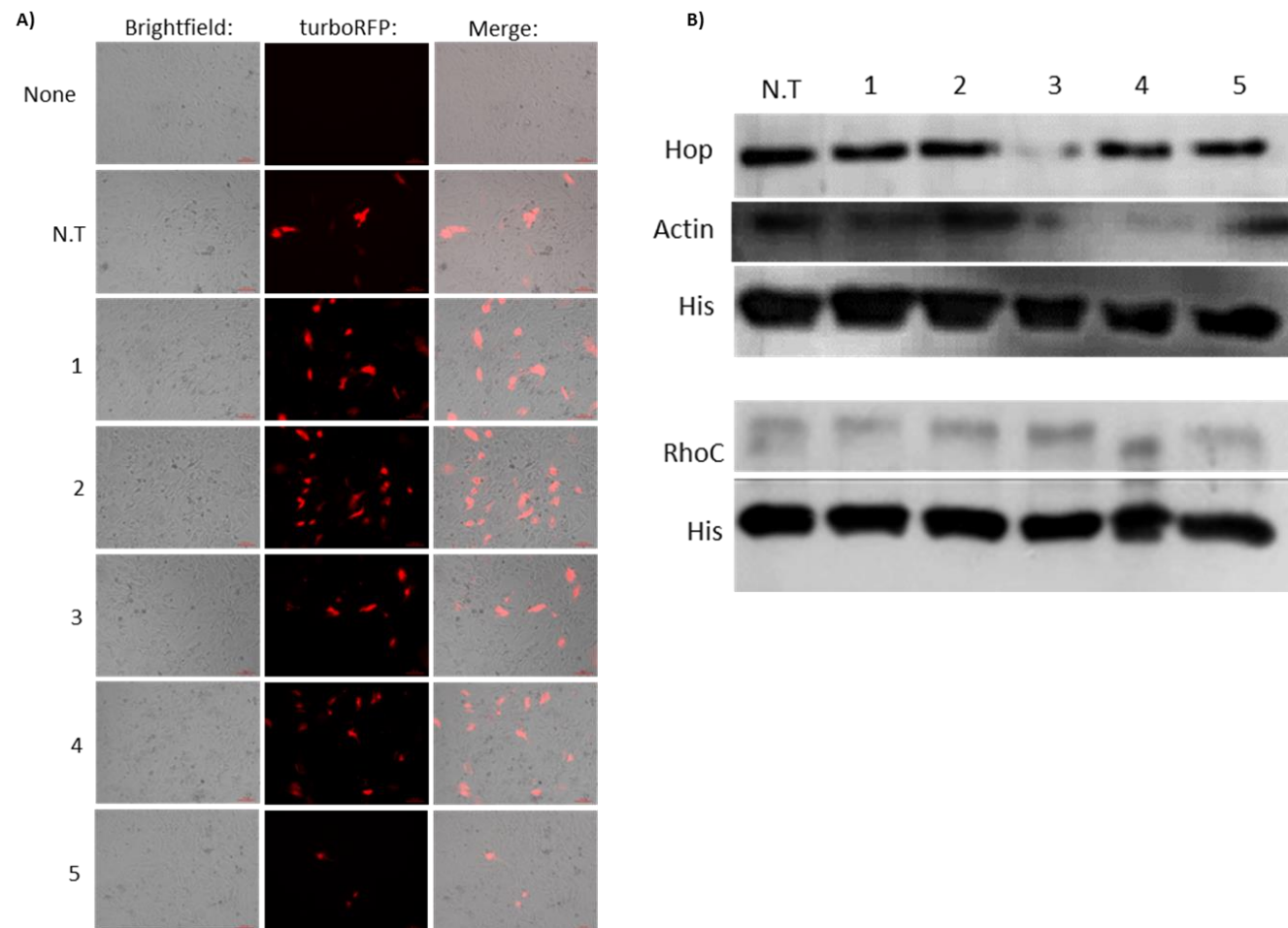
The endotoxin free plasmids were transfected into the cell lines using lipofection. Fluorescence microscopy images of cells transfected with N.T shRNA and Hop shRNA were taken 72 hours post induction with doxycycline. HEK293T and HS578T cell lines are depicted in Figure 3.3 and Figure 3.4, respectively. Successful transfections were identified by the presence of turboRFP (Figure 3.3, A and Figure 3.4, A). The presence of turboRFP was observed in cells transfected with shRNA plasmids, while no turboRFP was observed in the non-transfected control cells (Figure 3.3, A and Figure 3.4, A). This confirmed that transfections of all of the shRNA plasmids into the HEK293T (Figure 3.3, A) and HS578T (Figure 3.4, A) cell lines were successful. A relatively large proportion of cells were positive for turboRFP for most of the TRIPZ clones in both cell lines, which suggested generally high levels of transfection efficiency (Figure 3.3, A and Figure 3.4, A).

Expression levels of Hop, actin and RhoC relative to the Histone H3 loading control for each of the shRNA Hop clones were determined by western blot analysis (Figure 3.3, B and Figure 3.4, B). The expression levels of Hop in cells treated with the five Hop shRNA clones relative to the N.T shRNA control in both the HEK293T and HS578T cell lines 72 hours post induction with doxycycline were observed (Figure 3.3, B and Figure 3.4, B). All Hop shRNA clones exhibited observable levels of Hop knockdown relative to the N.T shRNA control in the HEK293T cell line (Figure 3.3, B). Although less notable, Hop knockdown relative to the N.T shRNA control for all Hop shRNA clones in the HS578T cell line was observed, with shRNA #3 exhibiting the highest levels of Hop knockdown (Figure 3.4, B). Knockdown of Hop resulted in a decrease in the expression levels of actin in both the HEK293T and HS578T cell lines, as observed for each of the shRNA clones (Figure 3.3, B and Figure 3.4, B). RhoC was detected as two bands in the N.T shRNA control samples (Figure 3.3, B and Figure 3.4, B). Interestingly, with the exception of shRNA #5 in HEK293T cells, an apparent loss of the lower RhoC band was observed with knockdown of Hop by shRNA clones compared to the N.T shRNA control (Figure 3.3, B and Figure 3.4, B). It was thought that perhaps the double band indicated active and inactive forms of RhoC and that loss of the lower RhoC band in Hop knockdown cell lysates could be indicative of loss of an activated form of RhoC. A greater decrease in actin and RhoC levels in the HEK293T cell line compared to the HS578T cell line was observed, although this was probably due to higher levels of transfection and Hop knockdown in these cells (Figure 3.3, B and Figure 3.4, B).



**Figure 3.3: Transient knockdown of Hop by shRNA reduced levels of actin and RhoC in HEK293T cells**

For A, B and C, 'N.T' indicates N.T shRNA and numbers 1 – 5 indicate different shRNA clones targeting Hop, namely shRNA #1, shRNA #2, shRNA #3, shRNA #4 and shRNA #5 respectively. (A) Fluorescence microscopy of transient transfections of shRNA plasmids 72 hours post induction with doxycycline (1  $\mu$ g/mL). 'None' indicates non-transfected control. (B) Western blot analyses of cell lysates from transiently transfected HEK293T cells 72 hours post induction with doxycycline. Hop, actin, RhoC and Histone H3 (His) were detected using anti-Hop, anti-actin, anti-RhoC and anti-Histone H3 primary antibodies respectively, followed by anti-mouse HRP-linked secondary antibodies to detect Hop and anti-rabbit HRP-linked antibodies to detect actin, RhoC and Histone H3.



**Figure 3.4: Transient knockdown of Hop by shRNA reduced levels of actin and RhoC in HS578T cells**

For A, B and C, 'N.T.' indicates N.T shRNA and numbers 1 – 5 indicate different shRNA clones targeting Hop, namely shRNA #1, shRNA #2, shRNA #3, shRNA #4 and shRNA #5 respectively. (A) Fluorescence microscopy of transient transfections of shRNA plasmids 72 hours post induction with doxycycline (1  $\mu$ g/mL). 'None' indicates non-transfected control. (B) Western blot analyses of cell lysates from transiently transfected HS578T cells 72 hours post induction with doxycycline. Hop, actin, RhoC and Histone H3 were detected using anti-Hop, anti-actin, anti-RhoC and anti-Histone H3 primary antibodies respectively, followed by anti-mouse HRP-linked secondary antibodies to detect Hop and anti-rabbit HRP-linked antibodies to detect actin, RhoC and Histone H3.

### **3.4.3 Development of mammalian cell lines stably transfected with inducible shRNA constructs.**

The N.T shRNA control as well as the Hop shRNA #2 clone were selected for development of stable, inducible cell lines for the knockdown of Hop. The shRNA #2 clone targeted the TPR8 and TPR9 motifs within the TPR2B domain of Hop/mSTI1 mRNA (Appendix 5, Supplementary figure 5 and Table 3.1). As all Hop shRNA clones were developed to target *Homo sapiens* Hop mRNA, shRNA #2 had 100 % sequence identity to Hop (*Homo sapiens*) mRNA (Table 3.1). The shRNA #2 clone had 84 % sequence identity to mSTI1 (*Mus Musculus*) mRNA, which was the lowest percentage identity with mSTI1 mRNA after the shRNA #5 clone (77 % sequence identity) (Table 3.1). Future studies aim to elucidate the mechanistic role of intracellular Hop and its different domains in cell migration processes by transfection of stable, inducible Hop knockdown cells with plasmids expressing GFP-tagged full length and truncated mSTI1 constructs. It was therefore favourable to select an shRNA clone with a lower percentage identity with mSTI1 mRNA.

The shRNA #2 clone showed moderate levels of Hop knockdown compared to the other Hop shRNA clones, but showed similar levels of Hop knockdown in both HEK293T and HS578T cell lines (Figure 3.3, B and Figure 3.4, B). For shRNA #2, the relative expression levels of actin and RhoC were similar to that of Hop in both the HEK293T and HS578T cell lines (Figure 3.3, B and Figure 3.4, B).

#### **3.4.3.1 Lentiviral particle production in HEK293T cells**

The lentiviral vector system incorporating the packaging plasmids pMD2.G and psPAX2 was used to synthesise lentiviral particles encapsidating the pTRIPZ N.T shRNA control plasmid as well as the pTRIPZ shRNA #2 plasmid (Figure 3.5, A). The lentiviral vector system involved the production of infectious, replication deficient lentiviral particles encapsidating relevant shRNA plasmid sequences by making use of plasmids encoding genes required for the lifecycle of lentiviruses (Naldini *et al.*, 1996; Zufferey *et al.*, 1997). The most widely used lentiviral systems involve the use of a transfer plasmid containing the gene of interest (such as pTRIPZ) and two packaging plasmids. One such plasmid encodes the viral envelope and the other encodes genes required for the encapsidation of the viral genome (Zufferey *et al.*, 1997). Examples of these plasmids are the pMD2.G (<http://www.addgene.org/12259/>) and psPAX2 (<http://www.addgene.org/12260/>) plasmids both deposited in the Addgene database by the laboratory of Didier Trono. The pMD2.G plasmid encodes the vesicular stomatitis



virus G glycoprotein (VSV-G), which allows infection of a broad range of mammalian cells. The psPAX2 plasmid encodes ‘gag’, ‘pol’, ‘rev’ and ‘tat’ HIV proteins, which allow for the encapsidation of the shRNA construct as well as the integration of the construct into the mammalian cell genome (Zufferey *et al.*, 1997). In order to produce the lentiviral particles, the pTRIPZ, pMD2.G and psPAX2 plasmids are cotransfected into a packaging cell line such as HEK293T and the resulting viral particles are collected and used to transduce other cell lines. The HIV envelope proteins have been removed from the system and replaced with the VSV-G protein on the separate plasmid in order to enhance the biosafety of this procedure (Zufferey *et al.*, 1998). The regulatory HIV proteins have also been removed from the system such that viral particles are replication incompetent thereby further enhancing the biosafety (Zufferey *et al.*, 1998). The use of the lentiviral vector delivery system is advantageous as it allows increased entry of the transfer plasmid into a broad range of mammalian cells as well as efficient stable integration of the shRNA into the mammalian cell genome in both dividing and non-dividing cells (Naldini *et al.*, 1996; Zufferey *et al.*, 1997).

Fluorescence microscopy of the pLVTH and pTRIPZ N.T shRNA plasmid transfections in HEK293T cells revealed high transfection efficiencies (Figure 3.5, B). The pLVTH plasmid (containing a constitutively expressed GFP marker) and the pTRIPZ N.T shRNA plasmid (containing an inducible turboRFP marker) were used as positive controls for transfection (Figure 3.5, B). This confirmed that the transfection protocol being used for lentiviral particle production was successful. Transmission Electron microscopy (TEM) was used to analyse the media harvested after transfection for the presence of viral particles (Figure 3.5, C). A lentiviral particle of approximately 80 nm and a number of smaller lentiviral particles were observed by TEM (Figure 3.5, C). Lentiviral particles are known to be 80 – 120 nm in diameter (Tomás *et al.*, 2013). Smaller lentiviral particles that were observed may have been partially formed, non-functional particles.

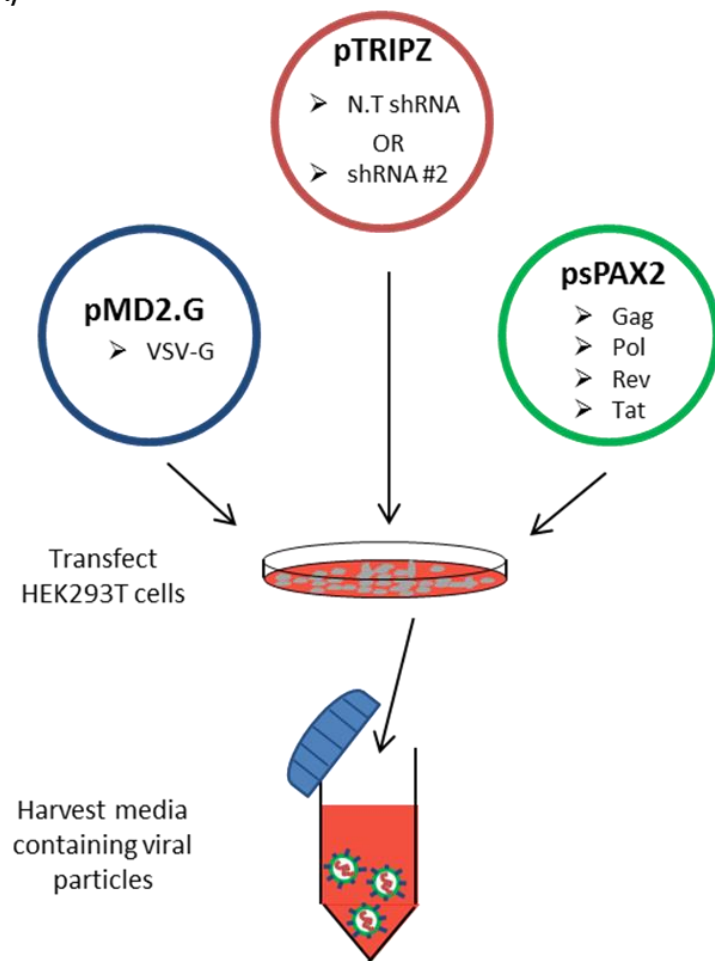
#### **3.4.3.2 Confirmation of infectious N.T shRNA and shRNA #2 lentiviral particles and analysis of transduction efficiency in HEK293T and HS578T cells**

HEK293T and HS578T cells were transduced with increasing volumes of harvested media from N.T shRNA and shRNA #2 lentiviral particle production transfections. Fluorescence microscopy was used to examine the presence of successful transductions 72 hours post treatment with doxycycline (1 µg/mL) (Figure 3.6, A[i] and B[i] and Figure 3.7, A[i] and B[i]). The transduction efficiencies for N.T shRNA and shRNA #2 in HEK293T and HS578T

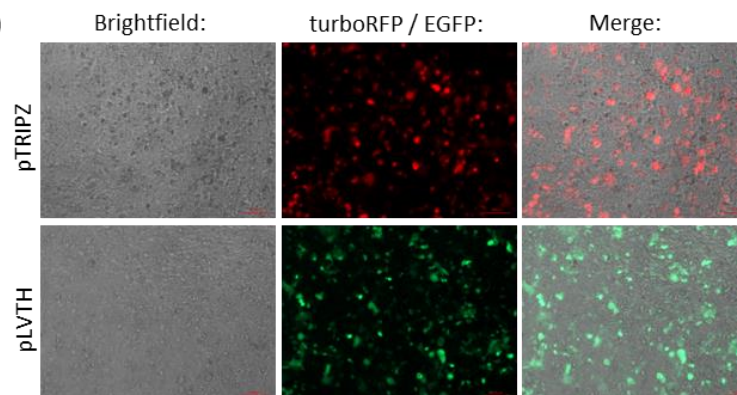
cell lines were quantified using ImageJ and reflected in Figure 3.6, A(ii) and B(ii) and Figure 3.7, A(ii) and B(ii).

Transductions of HEK293T cells with N.T shRNA and shRNA #2 lentiviral particles were successful for all doses of lentiviral particle supernatant used (200  $\mu$ L – 1000  $\mu$ L) (Figure 3.6, A[i and ii] and B[i and ii]). This confirmed the presence of infectious N.T shRNA and shRNA #2 lentiviral particles. A dose dependent increase in the number of successfully transduced cells was observed for both the N.T shRNA and shRNA #2 (Figure 3.6, A[ii] and B[ii]). Transduction efficiencies with N.T shRNA lentiviral particles were notably higher than those with shRNA #2 lentiviral particles (Figure 3.6, A[ii] and B[ii]).

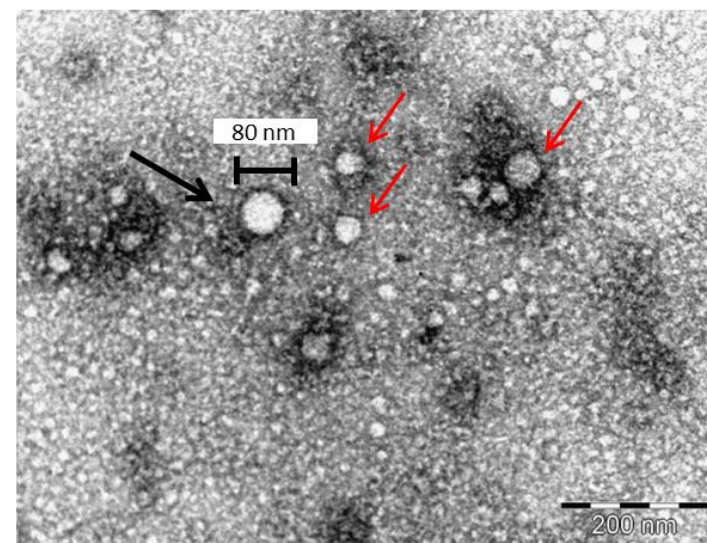
A)



B)

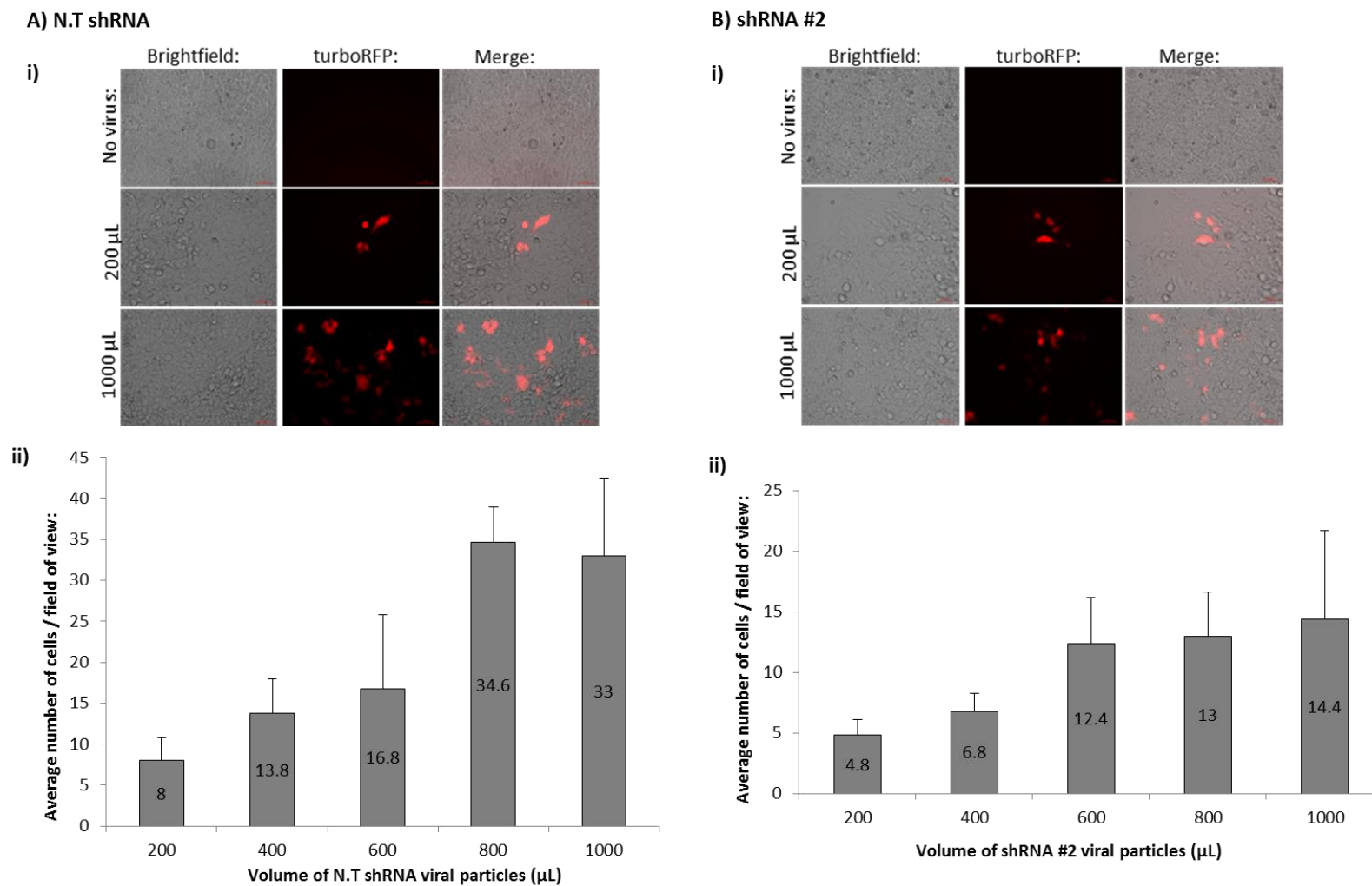


C)



**Figure 3.5: Lentiviral particle production in HEK293T cells**

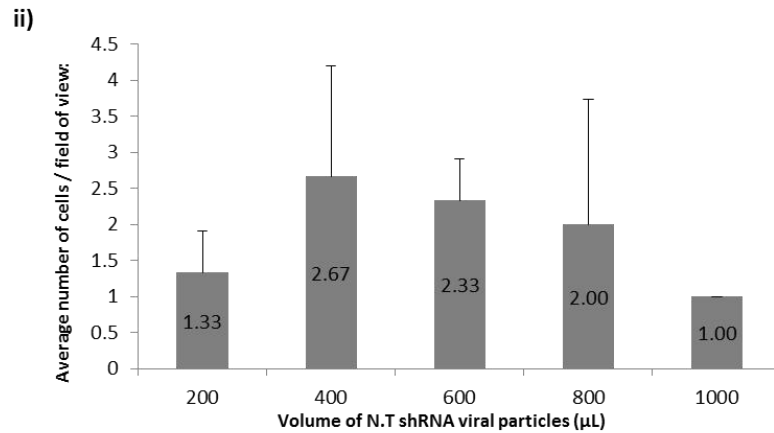
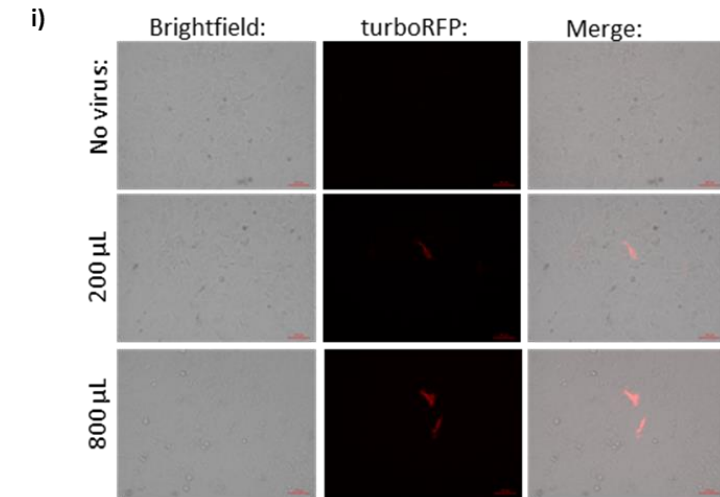
(A) Schematic diagram showing process for lentiviral particle production. (B) Fluorescence microscopy of HEK293T cells 96 hours post transfection with pTRIPZ N.T shRNA and pLVTH plasmids. Images for pTRIPZ N.T shRNA were taken 72 hours post induction with doxycycline (1  $\mu\text{g/mL}$ ). (C) Transmission electron microscopy of N.T shRNA lentiviral particles in cell supernatants. Scale bar (bottom right) reflects 200 nm. Scale bar (within figure) reflects 80 nm. The black arrow depicts a putative lentiviral particle slightly smaller than 80 nm. Red arrows depict putative lentiviral particles smaller than 80 nm.



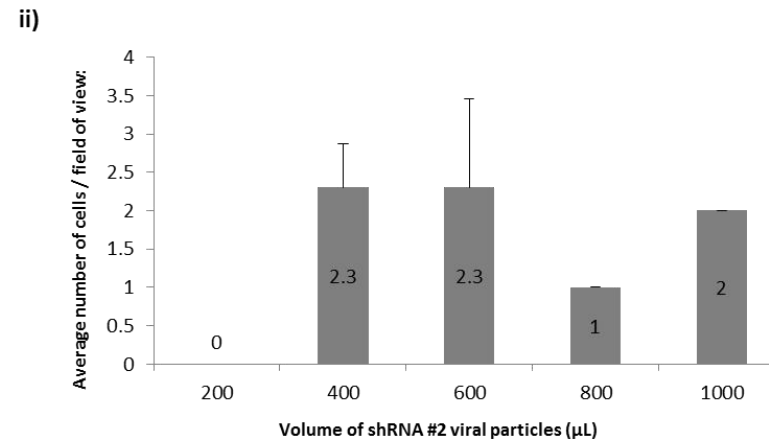
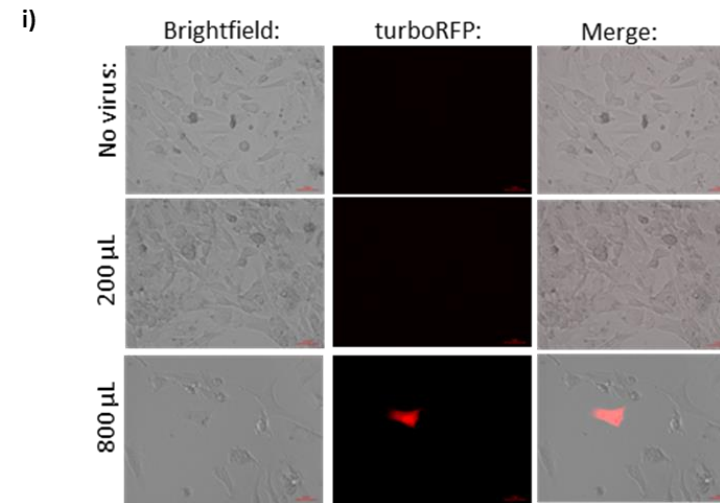
**Figure 3.6: Confirmation of infectious N.T shRNA and shRNA #2 lentiviral particles and analysis of transduction efficiency in HEK293T cells.**

Fluorescence microscopy showing examples of N.T shRNA (A)(i) and shRNA #2 (B)(i) transduced cells (No virus, 200  $\mu$ L and 1000  $\mu$ L) 72 hours post induction with doxycycline (1  $\mu$ g/mL). Successfully transduced cells were reflected by the presence of turboRFP. Transduced cells for five images (five fields of view) for each volume of lentiviral particles were counted using automated particle counting plugin in ImageJ (Appendix 4, Supplementary figure 3). The average number of transduced cells per field of view for N.T shRNA (A)(ii) and shRNA #2 (B)(ii) were calculated and represented as bar graphs.

### A) N.T shRNA



### B) shRNA #2



**Figure 3.7: Confirmation of infectious N.T shRNA and shRNA #2 lentiviral particles and analysis of transduction efficiency in HS578T cells.**

Fluorescence microscopy showing examples of N.T shRNA (A)(i) and shRNA #2 (B)(i) transduced cells (No virus, 200  $\mu$ L and 800  $\mu$ L) 72 hours post induction with doxycycline (1  $\mu$ g/mL). Successfully transduced cells were reflected by the presence of turboRFP. Transduced cells for three images (three fields of view) for each volume of lentiviral particles were counted using automated particle counting by ImageJ (Appendix 4, Supplementary figure 4). The average number of transduced cells per field of view for N.T shRNA (A)(ii) and shRNA #2 (B)(ii) were calculated and represented as bar graphs.

Transduction of HS578T cells with N.T shRNA lentiviral particles were successful for all doses of lentiviral particle supernatant used (200  $\mu$ L - 1000  $\mu$ L) (Figure 3.7, A[i and ii]), while transductions with shRNA #2 lentiviral particles were successful for all doses except the 200  $\mu$ L dose (Figure 3.7, B[i and ii]). This confirmed the presence of infectious N.T shRNA and shRNA #2 lentiviral particles. No correlation between dose of lentiviral particles and the number of successful transductions was observed in this cell line (Figure 3.7, A[ii] and B[ii]). Transduction efficiencies with N.T shRNA (Figure 3.7, A[i and ii]) and shRNA #2 (Figure 3.7, B[i and ii]) lentiviral particles in HS578T cells were very low in comparison with those observed in the HEK293T cells (Figure 3.6, A[i and ii] and B[i and ii]), with an average number of transduced cells per field of view below 3 in all cases.

#### **3.4.3.3 Selection and propagation of stable cell lines**

The minimum concentration of puromycin required to kill non-transduced cells was determined by constructing a puromycin kill curve (Figure 3.8, A). Concentrations of 1.88  $\mu$ g/mL, 3.75  $\mu$ g/mL, 7.5  $\mu$ g/mL and 15  $\mu$ g/mL of puromycin killed the majority of HS578T cells after 1 day of treatment (Figure 3.8, A). Four days after treatment, HS578T cells treated with all tested concentrations of puromycin (0.94  $\mu$ g/mL, 1.88  $\mu$ g/mL, 3.75  $\mu$ g/mL, 7.5  $\mu$ g/mL and 15  $\mu$ g/mL) were non-viable (Figure 3.8, A). A concentration of 2  $\mu$ g/mL of puromycin was chosen for selection of successful transductions. Selection of N.T shRNA stable transductions in HEK293T and HS578T cells by propagation in puromycin (2  $\mu$ g/mL) was successful (Figure 3.8, B and C). After 10 days, successfully transduced colonies/cells were pooled and propagated in fresh puromycin containing medium (2  $\mu$ g/mL) every three to five days. The protocol described was also followed for selection and propagation of shRNA #2 stably transduced HEK293T and HS578T cells (*data not shown*). Stably transduced polyclonal HEK293T cell lines incorporating N.T shRNA and shRNA #2 were successfully created. Stocks of each of the cell lines were made and stored at -80°C and liquid nitrogen and subsequently referred to as pHEK293T-NT.shRNA and pHEK293T-Hop.shRNA. A stably transduced polyclonal HS578T cell line incorporating N.T shRNA was successfully propagated and stocks stored at -80°C and liquid nitrogen. Unfortunately, propagation of a stably transduced HS578T cell line incorporating shRNA #2 was unsuccessful. Due to time constraints, the pHEK293T-NT.shRNA and pHEK293T-Hop.shRNA were used as the model to investigate the role of Hop in cell morphology and Rho activation in subsequent experiments.

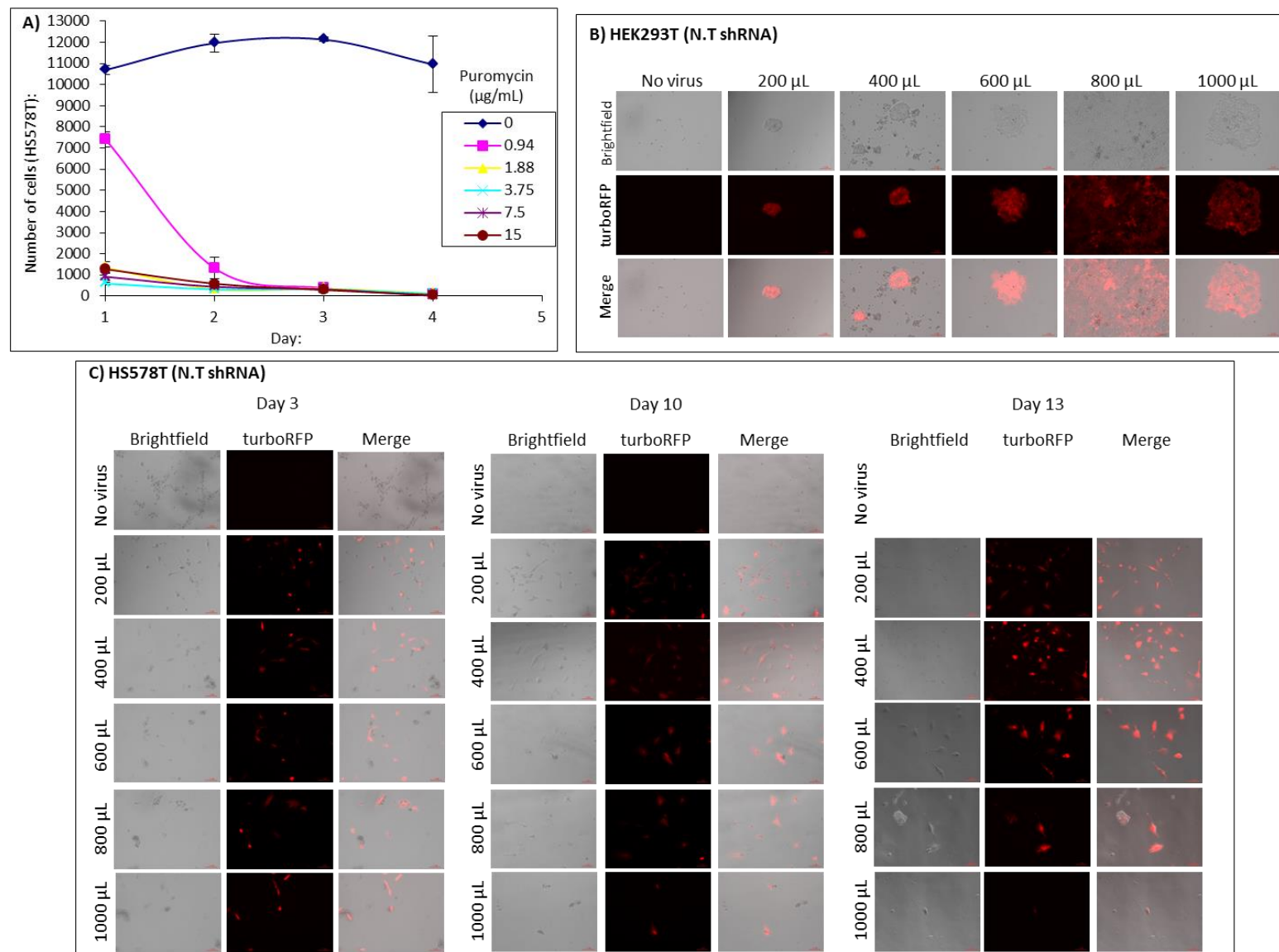


Figure 3.8: Selection and propagation of stably transduced HEK293T and HS578T cell lines

**Figure 3.8: Selection and propagation of stably transduced HEK293T and HS578T cell lines**

(A) Puromycin kill curve showing number of HS578T cells after 1-4 days treatment with 0  $\mu\text{g/mL}$ , 0.94  $\mu\text{g/mL}$ , 1.88  $\mu\text{g/mL}$ , 3.75  $\mu\text{g/mL}$ , 7.5  $\mu\text{g/mL}$  and 15  $\mu\text{g/mL}$  puromycin. Figure shows averages of four replicates. (B) Fluorescence microscopy showing examples of successfully transduced polyclonal HEK293T colonies selected and propagated from varying volumes of N.T shRNA lentiviral particles in the presence of doxycycline (1  $\mu\text{g/mL}$ ) and puromycin (2  $\mu\text{g/mL}$ ). (C) Fluorescence microscopy showing examples of successfully transduced HS578T cells selected and propagated from varying volumes of N.T shRNA lentiviral particles in the presence of doxycycline (1  $\mu\text{g/mL}$ ) and puromycin (2  $\mu\text{g/mL}$ ) at Day 3, Day 10 and Day 13, where Day 1 represents initial treatment with puromycin (2  $\mu\text{g/mL}$ ).



Failure to propagate shRNA #2 transduced HS578T cells could have been due to insertional inactivation of certain genes that affected cell growth or survival. Alternatively, since depleted Hop levels inhibited proliferation of HS578T cells (Willmer, 2011), it is possible that leaky expression of the shRNA #2 clone occurred, thereby resulting in Hop knockdown and in turn affecting cell growth or survival of these cells.

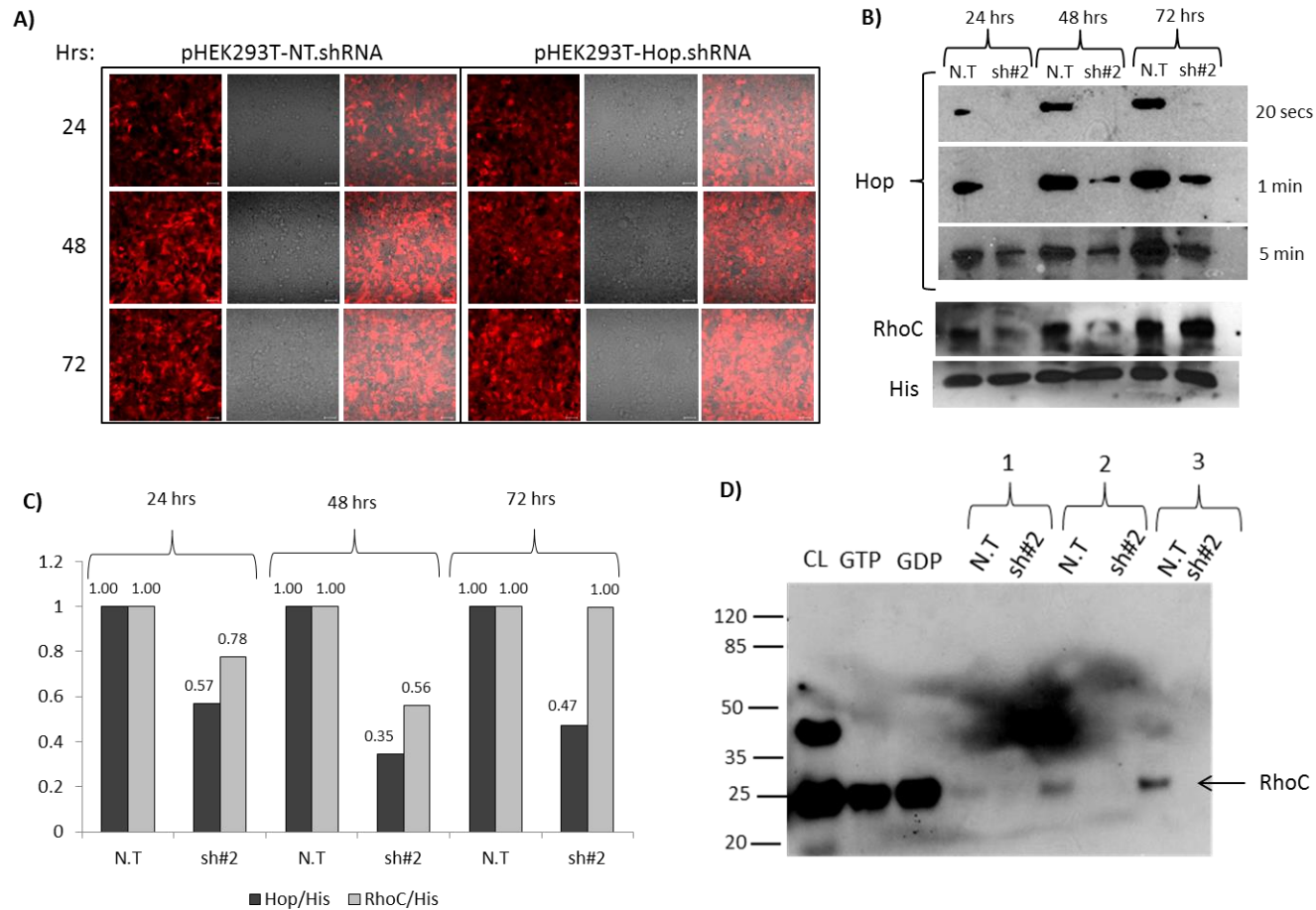
#### **3.4.4 Effect of Hop knockdown on RhoC expression and activation**

The expression of shRNA from pHEK293T-NT.shRNA and pHEK293T-Hop.shRNA stable cell lines was induced with doxycycline (1 µg/mL). Fluorescence images were taken at 24, 48 and 72 hours post induction, after which cell lysates for each of the time periods were made and analysed for the expression of Hop and RhoC by western blot analysis and densitometry (Figure 3.9, A, B and C). For both the pHEK293T-NT.shRNA and pHEK293T-Hop.shRNA cell lines, expression of turboRFP could be seen after 24 hours induction with doxycycline (1 µg/mL), with an increase in expression levels after 48 hours induction (Figure 3.9, A). Most, if not all cells, were positive for turboRFP after 72 hours induction (Figure 3.9, A). A clear decrease in the levels of Hop in pHEK293T-Hop.shRNA cells compared to pHEK293T-NT.shRNA cells was observed after 24, 48 and 72 hours induction (Figure 3.9, B). Hop knockdown was observed to be greatest at 48 hours post induction but increased at 72 hours post induction (Figure 3.9, C). A decrease in the expression levels of RhoC was observed at 24 and 48 hours post induction (Figure 3.9, B and C). Interestingly, at 72 hours post induction, when Hop levels also increased, the levels of RhoC in pHEK293T-Hop.shRNA cells were observed to return to levels similar to those observed in pHEK293T-NT.shRNA cells (Figure 3.9, B and C).

A Rho activation assay was performed on triplicate samples of pHEK293T-NT.shRNA and pHEK293T-Hop.shRNA cell lines and analysed for the presence of RhoC by western blot analysis (Figure 3.9, D). The Rho activation assay makes use of Rhotekin Rho Binding Domain (RBD) agarose known to specifically bind activated (GTP bound) Rho proteins (Reid *et al.*, 1996). Western blot analysis of the Rho activation assay samples revealed distinct bands occurring at ~25 kDa, corresponding to the predicted size of RhoC (21 kDa), in the 'CL', 'GTP', 'GDP', and triplicate (1, 2, 3) 'N.T' samples. No RhoC bands were visible in the triplicate 'sh#2' test samples that correspond to triplicate independent cell lysates in which Hop levels were depleted (Figure 3.9, D). This indicated that Rhotekin RBD agarose was able to pull down RhoC from pHEK293T-NT.shRNA cell lysates, but not from

pHEK293T-Hop.shRNA cell lysates (Figure 3.9, D). This suggested that Hop knockdown interfered with activation of RhoC in HEK293T cells. The unexpected presence of RhoC in the GDP control sample (Figure 3.9, D) however, indicated that Rhotekin RBD may have pulled down both GTP and GDP bound RhoC. This indicated that loss of RhoC in Hop knockdown cell lysates could be indicative of total RhoC and not only GTP bound RhoC. This could be tested by using a fluorescence resonance energy transfer (FRET)-based RhoC biosensor, such as the one created by Zawistowski and colleagues (2013), to determine RhoC activation levels in live cell suspensions. The bands observed in the 'CL', 'GTP' and 'GDP' samples were thick, indicating high levels of RhoC in the samples (Figure 3.9, D). Since PMA treated cells were used for 'CL', 'GTP' and 'GDP' samples, it was suggested that PMA stimulated high levels of RhoC activation. It could therefore be possible that the high levels of activated RhoC might have prevented us from seeing a reduction in activated RhoC between GTP and GDP controls.

RhoC antibodies also detected a band occurring at approximately 40 kDa in the 'CL' sample (Figure 3.9, D). This could have been due to non-specific binding of the antibody. This was not the first time, however, that RhoC was detected at a higher molecular weight in our studies (See Figure 3.1, C). It may, therefore, be worthwhile to attempt to identify the higher molecular weight band observed in the 'CL' sample (Figure 3.9, D) by mass spectrometry.



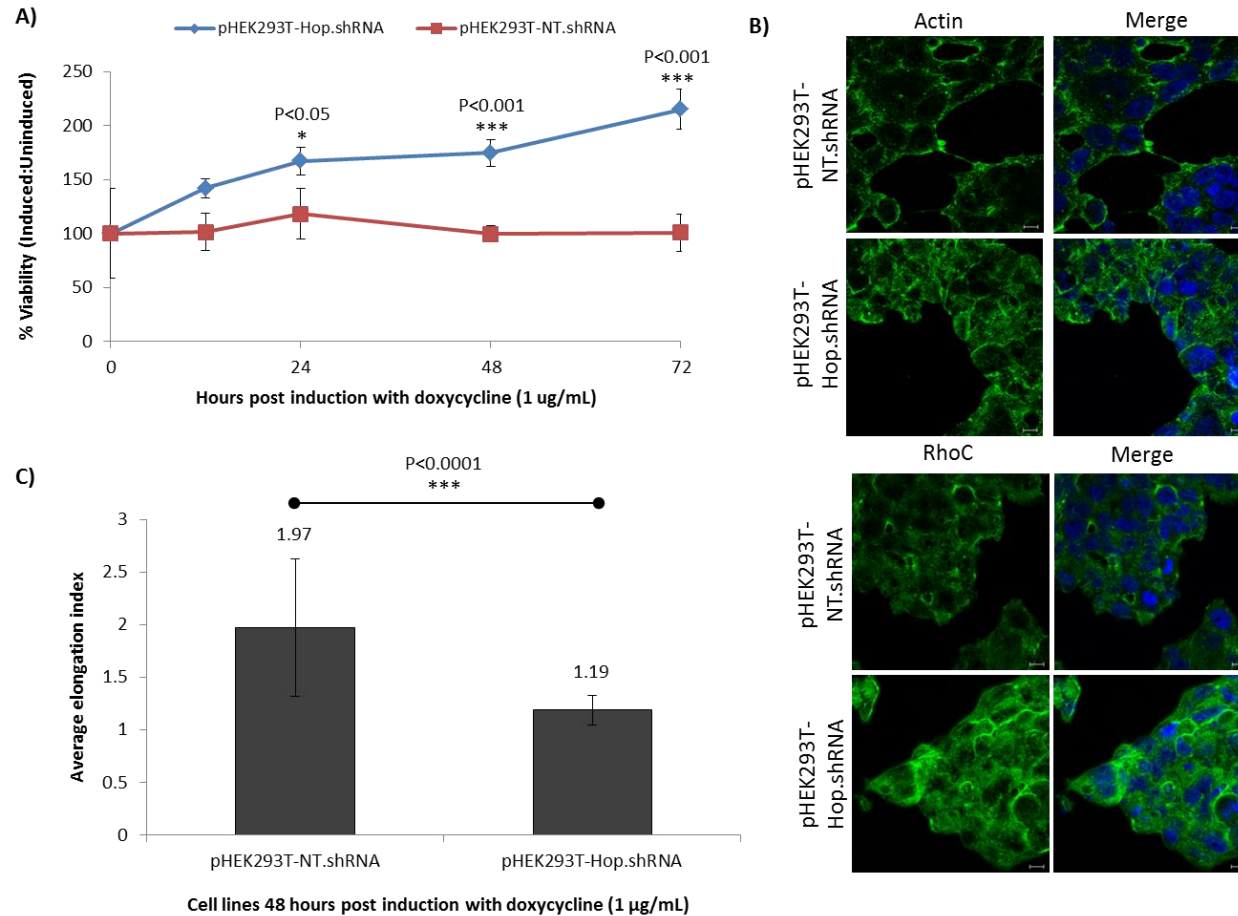
**Figure 3.9: Hop knockdown resulted in reduced levels of RhoC and interfered with RhoC activation.** (A) Fluorescence microscopy of pHEK293T-NT.shRNA and pHEK293T-Hop.shRNA cell lines 24, 48 and 72 hours post induction with doxycycline (1  $\mu$ g/mL). Scale bar represents 50  $\mu$ m. (B) Western blot analyses of cell lysates from pHEK293T-NT.shRNA and pHEK293T-Hop cell lines 24, 48 and 72 hours post induction with doxycycline. Hop, RhoC and Histone H3 (His) were detected using anti-Hop, anti-RhoC and anti-Histone H3 primary antibodies respectively, followed by anti-mouse HRP-linked secondary antibodies to detect Hop and anti-rabbit HRP-linked antibodies to detect RhoC and Histone H3. Multiple exposures (times indicated on the right of the image) are shown for the Hop western blot analysis. (C) Expression levels of Hop and RhoC relative to the His loading control at each time period were determined by densitometry using ImageJ. The 1 minute exposure was used for densitometry analysis of Hop levels. The ratios of Hop to His and RhoC to His were normalised to the pHEK293T-NT.shRNA sample at each of the relative time points. (D) Western blot analysis of Rho activation assay of triplicate samples (1, 2, 3) of pHEK293T-NT.shRNA (N.T) and pHEK293T-Hop.shRNA (sh#2) cell lines analysed for the presence of RhoC. 'CL' indicated cleared lysate. 'GTP' indicated a positive control for the pull down of activated Rho and 'GDP' indicated a negative control. The Rho activation assay for the GTP and GDP controls were done using uninduced pHEK293T-NT.shRNA cell lysates prepared after treatment with PMA (20 nM) for 2 hours.

### 3.4.5 The role of Hop in cell proliferation and cell morphology

A WST-1 assay was used to compare the cell proliferation profiles of pHEK293T-NT.shRNA and pHEK293T-Hop.shRNA cells at 0, 12, 24, 48 and 72 hours post induction with doxycycline (1  $\mu\text{g/mL}$ ) (Figure 3.10, A). An increase in proliferation of pHEK293T-Hop.shRNA cells compared to pHEK293T-NT.shRNA cells was observed at 12, 24, 48 and 72 hours post induction with doxycycline (1  $\mu\text{g/mL}$ ) (Figure 3.10, A). This increase was statistically significant at 24, 48 and 72 hours (Figure 3.10, A).

Confocal microscopy was used to compare the localisation of actin and RhoC in the pHEK293T-NT.shRNA and pHEK293T-Hop.shRNA cell lines (Figure 3.10, B). In pHEK293T-NT.shRNA cells, distinct actin staining at cell borders was observed (Figure 3.10, B). Actin stress fibres at cell-cell junctions as well as actin-rich pseudopodial extensions were also visible (Figure 3.10, B). In pHEK293T-Hop.shRNA cells, actin staining was more diffuse throughout the cytoplasm, although actin-rich cell borders were also visible (Figure 3.10, B). No pseudopodial extensions were observed in the pHEK293T-Hop.shRNA cells (Figure 3.10, B). The pHEK293T-NT.shRNA cells appeared larger and more elongated than the pHEK293T-Hop.shRNA cells (Figure 3.10, B). RhoC staining appeared to localise throughout the cytoplasm in both the pHEK293T-NT.shRNA and pHEK293T-Hop.shRNA cell lines (Figure 3.10, B). Interestingly, increased RhoC staining at cell edges of pHEK293T-Hop.shRNA cells compared to pHEK293T-NT.shRNA cells was observed (Figure 3.10, B).

Using images obtained from confocal microscopy, the average elongation index for each of the cell lines was compared (Figure 3.10, C). The elongation index (calculated as the ratio of the length to the breadth of the cell) was used as an indication of cell morphology (circular versus elongated), where values occurring close to 1 were indicative of rounded cell morphologies and values greater than 1 were indicative of more elongated cell morphologies (Adapted from methods of Kosla *et al.*, 2013 and Tchoghandjian *et al.*, 2013). A statistically significant difference of the average elongation indices between the two cell lines was reported (Figure 3.10, C). The pHEK293T-NT.shRNA cells had an average elongation index of  $1.97 \pm 0.66$ , while the pHEK293T-Hop.shRNA cells had an average elongation index of  $1.19 \pm 0.14$  (Figure 3.10, C). This indicated that the pHEK293T-NT.shRNA cells had more elongated cell morphologies, while the pHEK293T-Hop.shRNA cells were more rounded in shape.

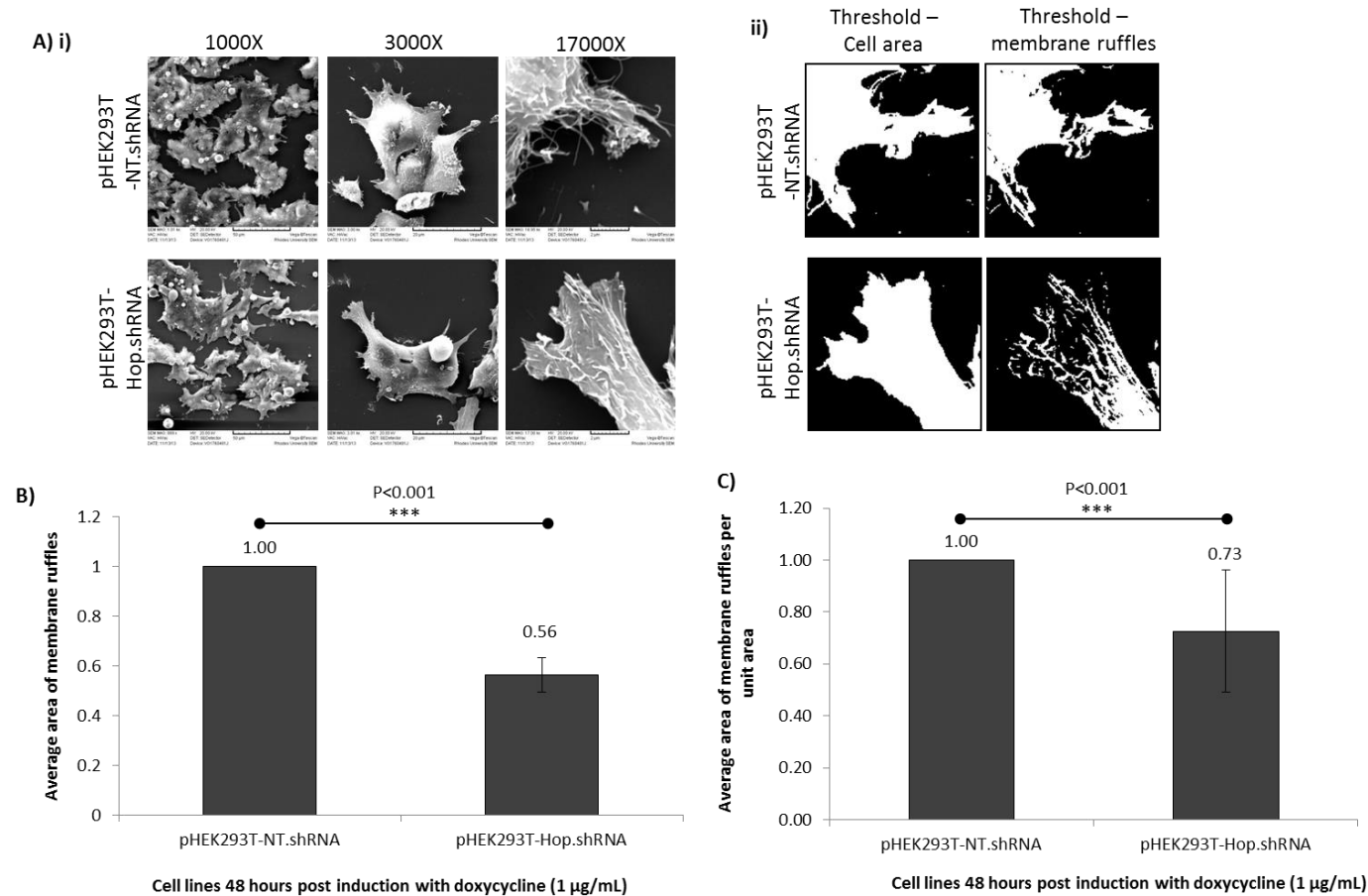


**Figure 3.10: Hop knockdown results in an increase in proliferation and a change in morphology of HEK293T cells**

(A) WST-1 assay showing proliferation of pHEK293T-NT.shRNA and pHEK293T-Hop.shRNA cells 0, 12, 24, 48 and 72 hours post induction with doxycycline (1 µg/mL). Percentage viability was represented as a ratio of induced cells versus uninduced equivalents. A two-way analysis of variance (ANOVA) with Bonferroni post tests revealed a significant difference between the two cell lines at 24 ( $p < 0.05$ )\*, 48 and 72 ( $p < 0.001$ )\*\*\* hours post induction. (B) Confocal microscopy showing actin and RhoC localisation in pHEK293T-NT.shRNA and pHEK293T.Hop.shRNA cells 48 hours post induction with doxycycline (1 µg/mL). Cells were fixed with methanol and incubated with anti-actin and anti-RhoC primary antibodies respectively, followed by donkey anti-rabbit 488 (green) secondary antibodies. The nuclei were stained blue with Hoescht-33342. Images were captured using the Zeiss LSM 510 Meta confocal microscope and analysed by Zeiss 2011 software. Scale bars represent 10 µm. (C) The average elongation index was calculated by obtaining a ratio of the length:breadth for 15 cells for each of the cell lines (See Appendix 6, Supplementary figure 6). Images were analysed using ImageJ. An unpaired, two-tailed t-test ( $n = 15$ ) revealed a significant difference in elongation index between the two cell lines ( $p < 0.0001$ )\*\*\*.

The cell morphologies of each of the cell lines were observed using Scanning Electron Microscopy (SEM) (Figure 3.11, A[i]). SEM images were used to compare the average area of membrane ruffles in each of the cell lines (Figure 3.11, A[ii], B and C). Interestingly, in the SEM images, pseudopodial extensions were observed in both the pHEK293T-NT.shRNA and pHEK293T-Hop.shRNA cell lines (Figure 3.11, A[i]). In the 3000X magnification image, the pseudopodial extensions in the pHEK293T-NT.shRNA cells appeared to have more defined points/edges, whereas the pseudopodial extensions of the pHEK293T-Hop.shRNA cells appeared to be flattened or less pointed (Figure 3.11, A[i]). In the 17000X magnification image, very fine filapodial extensions or membrane ruffles were observed to extend beyond the boundaries of the cell in the pHEK293T-NT.shRNA image (Figure 3.11, A[i]). Although these membrane ruffles were observed in the 17000X magnification image of the pHEK293T.Hop.shRNA cell, the ruffles appeared to be shortened and were not visible beyond the boundaries of the cell (Figure 3.11, A[i]).

The membrane ruffles per area of pHEK293T-Hop.shRNA and pHEK293T-NT.shRNA cells were quantified using threshold analysis by ImageJ as described in Appendix 6, Supplementary figure 7. There was a statistically significant decrease in membrane ruffles in the pHEK293T-Hop.shRNA cell line (0.56) compared to the pHEK293T-NT.shRNA cell line (1) for images captured at 17000X magnification (Figure 3.11, B). Additionally, a statistically significant decrease in membrane ruffles per unit area in the pHEK293T-Hop.shRNA cell line (0.73) compared to the pHEK293T-NT.shRNA cell line (1) for images captured at 3000X magnification was observed (Figure 3.11, C). A measure of the length of filapodial extensions beyond the boundary of the cell for pHEK293T-NT.shRNA versus pHEK293T.Hop.shRNA cells would also be an interesting comparison. A greater number of images at 17000X magnification should be captured such that these filapodial extensions can be measured and compared.



**Figure 3.11: Hop knockdown reduced membrane ruffles in HEK293T cells.** (A)(i) After 48 hours induction with doxycycline, cells were fixed and prepared for scanning electron microscopy. Cells were visualised using the Vega Tescan Scanning Electron Microscope, Rhodes University and images captured using the SEDetector. Terms ‘1000X, 3000X and 17000X’ represent the magnifications at which the images were captured. (ii) An example demonstrating the measurement of total cell area and membrane ruffles using threshold analysis by ImageJ. (B) The average area of membrane ruffles for each of the cell lines was calculated by obtaining a ratio of area of membrane ruffles per total cell area for triplicate images at 17000X magnification and represented in a bar graph. The average area of membrane ruffles was normalised to the pHEK293T-NT.shRNA cell line. An unpaired, two-tailed t-test revealed a significant difference in membrane ruffles ( $p < 0.001$ \*\*\* between the two cell lines. (C) The average area of membrane ruffles per unit area for each of the cell lines was calculated by obtaining a ratio of area of membrane ruffles per area of field of view for 25 selected fields of view from five images at 3000X magnification and represented in a bar graph. The area of membrane ruffles was measured using threshold analysis by ImageJ (See Appendix 6, Supplementary figure 7). The average area of membrane ruffles per unit area was normalised to the pHEK293T-NT.shRNA cell line. An unpaired, two-tailed t-test revealed a significant difference in membrane ruffles per unit area ( $p < 0.0001$ \*\*\* between the two cell lines.

### 3.5 DISCUSSION:

#### 3.5.1 Hop colocalised with RhoA, RhoC and Cdc42, but not RhoB

Hop was shown to colocalise with RhoA, RhoC, Cdc42 and Rac1/2/3, signalling molecules involved in actin cytoskeletal dynamics (Figure 3.1, A). Colocalised staining of Hop with the respective signalling molecules was evident in the pseudopodial protrusions of the HS578T cells (Figure 3.1, A). Interestingly, Hop did not colocalise with RhoB (Figure 3.1, A). Instead, RhoB staining was concentrated at distinct perinuclear regions, indicative of microtubular staining (Figure 3.1, A). Previous studies have demonstrated that colocalisation between two proteins can be indicative of a binding interaction between the two proteins (Wang *et al.*, 2010). This was shown by Wang and colleagues (2010) who demonstrated colocalisation and binding between prostate apoptosis response protein (Par4) and the NFκB transcription factor in human colon cancer cells. Colocalisation of Hop with the actin signalling molecules therefore suggested a possible interaction of Hop with these signalling pathways.

#### 3.5.2 RhoC immunoprecipitated in a common complex with Hop and Hsp90

RhoC has emerged as a key regulator of invasive cancers and activation of RhoC was shown to regulate invadopodia formation (Simpson *et al.*, 2004; Bravo-Cordero *et al.*, 2011; Ridley, 2013). Hop, RhoC and Hsp90 co-immunoprecipitated from HS578T whole cell lysate using Hop antibodies (Figure 3.1, C). This suggested an interaction of RhoC within the Hsp90 multichaperone heterocomplex. Some members of the Ras-superfamily GTPases (Rac1, RalBP1, RHOBTB1), as well as the Gα subunit of heterotrimeric G proteins (functionally homologous to Ras superfamily GTPases), have been characterised as Hsp90 client proteins (Busconi *et al.*, 2000; Vaiskunaite *et al.*, 2001; Hu and Mivechi, 2003; Cha *et al.*, 2010; Taipale *et al.*, 2012).

RhoC could therefore have been binding to Hsp90. Whether a direct interaction between Hop and RhoC exists, remains to be explored. Interestingly, a study by Marty and colleagues (2003) in a *Saccharomyces cerevisiae* system demonstrated binding of a TPR1 domain containing protein to Ras. Additionally, Lapouge and colleagues (2000) demonstrated binding of the small GTPase, Rac.GTP, to the TPR domain of the p67<sup>phox</sup> protein. It is therefore possible that a direct interaction between Hop and RhoC could be occurring at one



of the TPR domains of Hop. This interaction could be readily explored in our laboratory through pull down assays or surface plasmon resonance (SPR) using the GST fusion proteins (GST-mSTI1, GST-TPR2A2B and GST-TPR1) described in Chapter 2.

### **3.5.3 Hop knockdown resulted in a decrease in the levels of actin and RhoC**

Transient knockdown of Hop in both HS578T (Figure 3.1, B and Figure 3.3, B) and HEK293T (Figure 3.4, B) cells resulted in a decrease in expression levels of both actin and RhoC. The effect of Hop knockdown on actin levels could have resulted from a direct interaction between Hop and actin described by Willmer and colleagues (2013) in HS578T cells. Although unexplored, there exists a potential actin binding motif in the TPR2A domain of Hop (DAYKKK). We identified this motif as a putative actin binding domain due to its similarity to the DAIKKK actin binding motif found in cofilin (Yonezawa *et al.*, 1989; Cravchik *et al.*, 1994). The effect of Hop knockdown on RhoC expression may have resulted from an interaction with Hop, either directly or within the Hsp90 chaperone complex. This can be supported by previous studies that have shown that knockdown of Hop results in a substantial reduction of various Hsp90 client proteins (Beraldo *et al.*, 2013). Since Rho family GTPases regulate actin cytoskeletal dynamics (Wehrle-Haller and Imhof, 2002; Shankar *et al.*, 2010), an interaction between Hop and RhoC could also have influenced actin levels.

### **3.5.4 A stable inducible RNAi system for Hop knockdown in HEK293T cells was developed and used for further experiments**

In order to extend our studies on the effects of Hop knockdown on RhoC and cell migration processes, an inducible RNAi system using stable lentiviral incorporation of shRNA was developed. Due to unsuccessful development of this system in the metastatic HS578T breast cancer cell line within time constraints, we were compelled to conduct further studies using the non-cancerous HEK293T cell line. We believed that this cell line would nonetheless act as a valuable model in the study of Hop on RhoC and cell migration processes.

### **3.5.5 Hop knockdown resulted in reduced levels of RhoC and interfered with RhoC activation**

A time course study in pHEK293T-Hop.shRNA cells exhibiting Hop knockdown at 24, 48 and 72 hours post induction, revealed reduced levels of RhoC at 24 and 48 hours (Figure 3.9,

B and C). At 72 hours post induction, however, levels of RhoC returned to those observed in pHEK293T-NT.shRNA control cells (Figure 3.9, B and C). Essentially, RhoC levels were recovered after 72 hours of Hop knockdown. Interestingly, preliminary studies by Willmer (2011) demonstrated that Hop knockdown resulted in an increase in the levels of the cochaperone Cdc37, while Hsp90 and Hsp70 levels remained unchanged. Taken together, this could suggest that Hop knockdown may have led to the compensatory upregulation of an alternative cochaperone, such as Cdc37, that may be able to support RhoC expression. Mass spectrometry on whole cell lysates from Hop knockdown versus control cells could be performed to conduct a proteomic study to identify proteins/cochaperones that are upregulated as a result of Hop knockdown. In addition, immunoprecipitation of the Hsp90 complex from Hop knockdown cells at varying time points post induction could be analysed for Cdc37 and the identified upregulated cochaperones by western blot analysis. The Hsp90 IP could additionally be resolved on an SDS-PAGE gel and analysed by mass spectrometry to identify all components acting within the complex.

This result also prompted us to wonder whether Hop was perhaps playing a role in the activation of RhoC. GTP-bound RhoC could not be pulled down from pHEK293T-Hop.shRNA cells, while it could be pulled down from pHEK293T-NT.shRNA cells (Figure 3.9, D). This suggested that Hop knockdown interfered with RhoC activation and may play a role in modulating RhoC activation. Molecular chaperones have been shown to play a role in regulating RhoGEF activity (Kamynina *et al.*, 2007; Wu *et al.*, 2013). Human RhoGEFs include Dbp, Vav and Bcr proteins (Boguski and McCormick, 1993). Dbp ubiquitination has been shown to be regulated by the molecular chaperones Hsc70 (constitutive Hsp70 isoform) and Hsp90 (Kamynina *et al.*, 2007). Additionally, binding of the Hsp90 co-chaperone, cell division cycle 37 homologue (Cdc37), to the RhoGEF, Vav3, was shown to enhance activation of the androgen receptor (AR) activity in prostate cancer cells (Wu *et al.*, 2013). Perhaps Hop played a role in modulating RhoC activation through interacting with RhoGEFs, thereby catalysing the release of GDP from inactive RhoC and allowing for GTP binding and activation of RhoC to occur. In order to test whether Hop interacted with RhoGEFs, Hop IP assays could be performed and probed for the presence of the RhoGEFs, Dbp, Vav and Bcr using anti-Dbp, anti-Vav and anti-Bcr antibodies respectively.

### **3.5.6 Hop knockdown resulted in non-migratory cell phenotypes and increased cell proliferation**

RhoC has been suggested to play a role in cell morphology, polarised cell migration, invasion, and the formation of invadopodia (Kitzing *et al.*, 2010; Bravo-Cordero *et al.*, 2011; Vega *et al.*, 2011). Since Hop knockdown had an effect on RhoC and actin, both of which have vital roles in migratory cell phenotypes, we felt it would be interesting to determine the effects of Hop knockdown on cell morphologies. RhoC was observed to be localised more at the cell edges/cell-to-cell adhesions of pHEK293T-Hop.shRNA cells compared to pHEK293T-NT.shRNA cells (Figure 3.10, B). Additionally, the effects on cell morphology of pHEK293T-Hop.shRNA cells compared to pHEK293T-NT.shRNA cells included: a disorganised actin cytoskeleton; a reduction in actin-rich pseudopodial extensions; more rounded cell morphologies; flattened pseudopodial extensions; shortened membrane ruffles and a decrease in membrane ruffles (Figure 3.10, B and Figure 3.11, A, B and C). These cell morphologies were indicative of a non-migratory phenotype and correlated with studies done by Willmer and colleagues (2013) that showed that Hop knockdown inhibited the formation of pseudopodia in HS578T cells (Willmer *et al.*, 2013). Taken together, these results suggested that Hop knockdown could be having an effect on cell migration of HEK293T cells. Wound healing assays could be performed in order to test this assessment.

Hop knockdown resulted in an increase in cell proliferation of HEK293T cells (Figure 3.10, A). This correlated with data by Willmer (2011) that showed an observed increase in proliferation of MDA-MB-231 breast cancer cells with Hop knockdown. Interestingly, Willmer (2011) also showed a decrease in cell proliferation of HS578T breast cancer cells with Hop knockdown. This suggested that the effects of Hop knockdown on proliferation were cell line specific. The Rho GTPases are also known to regulate cell proliferation (Debidda *et al.*, 2005). Perhaps inhibitory effects on the migratory pathways in HEK293T cells, caused by depletion in the levels of Hop, were as a result of enhanced activation of proliferation pathways. In order to determine the effects of Hop knockdown on different signalling pathways, expression levels of a range of Rho GTPases and their downstream effectors including RhoA, RhoB, Cdc42, Rac1/2/3, MEK, ERK, Arp2/3 and WASP on Hop knockdown versus non Hop knockdown cell lysates at different time points should be determined by western blot analyses.

### **3.5.7 Conclusion**

Taken together, the effect of Hop knockdown on expression levels of RhoC, cell morphology and the actin cytoskeleton, along with the immunoprecipitation of RhoC with Hop and Hsp90, suggested that Hop may play a role in regulation of actin cytoskeletal dynamics through regulating RhoC activity by a number of proposed mechanisms. In order to further study the role of Hop on cell behaviour (in particular, cell migration and invasion) clonal HEK293T and HS578T stable cell lines for the knockdown of Hop will be developed for use in future studies.

## **Chapter 4.**

# **Summary, Conclusions and Future Work**

## 4.1 SUMMARY, CONCLUSIONS AND FUTURE WORK

A number of roles for both extracellular and intracellular Hop in cancer cell progression have been described (Kamal *et al.*, 2003; Sun *et al.*, 2007; Kubota *et al.*, 2010; Pimienta *et al.*, 2011; Walsh *et al.*, 2011; Tsai *et al.*, 2012; Chao *et al.*, 2013; Willmer *et al.*, 2013). It was shown that treatment with anti-TPR peptides that inhibited binding of Hsp90 and Hop could reduce cell viability and induce apoptosis in various cancers (Horibe *et al.*, 2011; Pimienta *et al.*, 2011). Targeting Hop for the treatment of metastatic cancers is therefore a current therapeutic avenue that is being explored.

The extracellular TPR2A2B and TPR1 domains of Hop significantly decreased cell migration in HS578T cells (Figure 2.9 and Table 2.2). Treatment also resulted in changes in the actin cytoskeleton as well as the extracellular matrix proteins, gelatin and fibronectin (Figure 2.10 and Table 2.2). MMP-2 and fibronectin have been described as client proteins of Hsp90 (Eustace and Jay, 2004; Hunter *et al.*, 2014). Additionally, Hop was shown to interact with MMP-2 and act within the extracellular Hsp90 multichaperone complex to activate MMP-2 (Sims *et al.*, 2011; Walsh *et al.*, 2011). It was therefore suggested that endogenous extracellular Hop may interact with MMP-2, inducing changes in the extracellular matrix environment. This would in turn stimulate intracellular signalling pathways resulting in dynamic changes in the actin cytoskeleton that would promote migration. It was proposed that treatment with the TPR2A2B or TPR1 domains of Hop could prevent binding of extracellular endogenous Hop to MMP-2, thereby preventing the extracellular signals from stimulating an intracellular migratory response. The TPR2A2B and TPR1 domains could be further explored as potential drugs targeting Hop for the inhibition of cancer cell migration.

Knockdown of Hop resulted in reduced levels of actin and RhoC (Figure 3.1, B; Figure 3.3, B and C; Figure 3.4, B and C; Figure 3.9, B and C) and appeared to interfere with the activation of RhoC (Figure 3.9, D). RhoC levels were recovered after 72 hours of Hop knockdown (Figure 3.9, B and C). In addition, knockdown of Hop resulted in a reduced migratory phenotype (Figure 3.10, B and C and Figure 3.11, A, B and C) and RhoC was immunoprecipitated in a common complex with Hop and Hsp90 (Figure 3.1, C). It was suggested that intracellular Hop played a role in cell migration through regulation of RhoC. It was proposed that this occurred through a direct interaction with RhoC. It was also proposed

that recovery of RhoC levels could have occurred due to compensatory upregulation of another cochaperone, such as Cdc37. Furthermore, it was suggested that Hop may play a role in RhoC activation by interacting with RhoGEFs, a study which should be further explored. Targeting intracellular Hop, therefore, could reduce the migratory or invasive phenotypes of metastatic cancers through downregulation of RhoC expression and/or activity and should be further explored.

Whether extracellular or intracellular Hop was acting solely as a co-chaperone within the Hsp90 multichaperone complex, or whether it could act independently from the complex should also be further explored. Roles for extracellular Hop, independent of the Hsp90 multichaperone complex, have been described in studies in neural cell biology where extracellular Hop has been shown to interact with cellular prion related protein (PrP<sup>c</sup>) (Zanata *et al.*, 2002; Lopes *et al.*, 2005; Erlich *et al.*, 2007). Studies could be performed in the presence and absence of Hsp90 inhibitors, geldanamycin (N-terminal inhibitor) and novobiocin (C-terminal inhibitor) in order to test this assessment (Neckers, 2002; Goetz *et al.*, 2003).

Interestingly, knockdown of Hop increased proliferation of HEK293T cells (Figure 3.10, A), while previous studies showed that Hop knockdown increased proliferation in MDA-MB-231 cells, but decreased proliferation in HS578T cells (Willmer, 2011). It appears that the effect of Hop knockdown varies with different cell lines. Future studies should therefore aim to characterise the role of Hop/effect of Hop knockdown in a wide range of cell types.

Taken together, these data suggest that Hop may play a role in regulating both extracellular proteins (involved in the remodelling of the extracellular environment) and intracellular signalling pathways, both of which are known to lead to actin dynamics and cell migration/invasion. Future studies would also aim to elucidate whether the role of extracellular and/or intracellular Hop in these processes was independent or dependent on the Hsp90 multichaperone complex. A better understanding of the mechanistic role of Hop in pathways involved in cancer cell progression would aid in assessing the viability of Hop as a potential drug target for the treatment of metastatic cancers.

## REFERENCES

- Abercrombie, M., Heaysman, J.E.M. and Pegrum, S. (1970) The locomotion of fibroblasts in culture: II. "Ruffling", *Experimental Cell Research*, **60**(3), pp. 437–444.
- Adams, J.C. (2001) Cell-matrix contact structures, *Cellular and Molecular Life Sciences*, **58**, pp. 371–392.
- Agarraberes, F.A. and Dice, J.F. (2001) A molecular chaperone complex at the lysosomal membrane is required for protein translocation, *The Journal of Cell Science*, **114**(13), pp. 2491–2499.
- Agrawal, N., Dasaradhi, P.V.N., Mohmmmed, A., Malhotra, P., Bhatnagar, R.K. and Mukherjee, S.K. (2003) RNA Interference: Biology, Mechanism, and Applications, *Microbiology and Molecular Biology Reviews*, **67**(4), pp. 657–685.
- Alberts, B., Johnson, A., Lewis, J., Raff, M., Roberts, K. and Walter, P. (2008) Molecular Biology of the cell, 5<sup>th</sup> Edition, Chapter 16, The Cytoskeleton, pp. 966–998, Garland Science, New York.
- Albrecht-Buehler, G. (1976) Filopodia of spreading 3T3 cells: do they have a substrate-exploring function? *The Journal of Cell Biology*, **69**(2), pp. 275–286.
- Allan, R.K., Mok, D., Ward, B.K. and Ratajczak, T. (2006) Modulation of Chaperone Function and Cochaperone Interaction by Novobiocin in the C-terminal Domain of Hsp90, *The Journal of Biological Chemistry*, **281**(11), pp. 7161–7171.
- Amann, E., Brosius, J. and Ptashne, M. (1983) Vectors bearing a hybrid *trp-lac* promoter useful for regulated expression of cloned genes in *Escherichia coli*, *Gene*, **25**, pp. 167–178.
- Arruda-Carvalho, M., Njaine, B., Silveira, M.S., Linden, R. and Chiarini, L.B. (2007) Hop/STI1 modulates retinal proliferation and cell death independent of PrP<sup>C</sup>, *Biochemical and biophysical research communications*, **361**(2), pp. 474–480.
- Artym, V.V., Zhang, Y., Seillier-Moiseiwitsch, F., Yamada, K.M. and Mueller, S.C. (2006) Dynamic interactions of cortactin and membrane type 1 matrix metalloproteinase at invadopodia: defining the stages of invadopodia formation and function, *Cancer research*, **66**(6), pp. 3034–3043.
- Bae, Y.H.O., Ding, Z., Zou, L.I., Wells, A., Gertler, F. and Roy, P. (2010) Loss of Profilin-1 Expression Enhances Breast Cancer Cell Motility by Ena/VASP Proteins, *Journal of Cell Physiology*, **219**(2), pp. 354–364.
- Bagatell, R. and Whitesell, L. (2004) Altered Hsp90 function in cancer: A unique therapeutic opportunity, *Molecular Cancer Therapeutics*, **3**(8), pp. 1021–1030.
- Banerji, U. (2009) Heat shock protein 90 as a drug target: some like it hot, *Clinical cancer research*, **15**(1), pp. 9–14.
- Bartel, D.P. (2004) MicroRNAs: Genomics, Biogenesis, Mechanism, and Function, *Cell*, **116**, pp. 281–297.
- Beraldo, F.H., Soares, I.N., Goncalves, D.F., Fan, J., Thomas, A.A., Santos, T.G., Mohammad, A.H., Roffé, M., Calder, M.D., Nikolova, S., Haij, G.N., Guimaraes, A.L., Massensini, A.R., Welch, I., Betts, D.H., Gros, R., Drangova, M., Watson, A.J., Bartha, R., Prado, V.F., Martins, V.R. and Prado, M.A. (2013) Stress-inducible phosphoprotein 1 has unique cochaperone activity during development and regulates cellular response to ischemia via the prion protein, *The FASEB journal*, **27**(9), pp. 3594–3607.
- Bernstein, E., Caudy, A.A., Hammond, S.M. and Hannon, G.J. (2000) Role for a bidentate ribonuclease in the initiation step of RNA interference, *Nature*, **409**, pp. 363–366.
- Berridge, M.V., Tan, A.S., McCoy, K.D. and Wang, R. (1996) The biochemical and cellular basis of cell proliferation assays that use tetrazolium salts, *Biochemica*, **4**, pp. 15–20.



- Blatch, G.L. and Lässle, M. (1999) The tetratricopeptide repeat: a structural motif mediating protein-protein interactions, *BioEssays*, **21**, pp. 932-939.
- Boguski, M.S. and McCormick, F. (1993) Proteins regulating Ras and its relatives, *Nature*, **366**(6456), pp. 643-654.
- Brahmbhatt, A.A. and Klemke, R.L. (2003) ERK and RhoA Differentially Regulate Pseudopodia Growth and Retraction during Chemotaxis, *The Journal of Biological Chemistry*, **278** (15), pp. 13016-13025.
- Bravo-Cordero, J. J., Oser, M., Chen, X., Eddy, R., Hodgson, L. and Condeelis, J. (2011) A novel spatiotemporal RhoC activation pathway locally regulates cofilin activity at invadopodia, *Current biology*, **21**(8), pp. 635–644.
- Bukau, B. and Horwich, A.L. (1998) The Hsp70 and Hsp60 chaperone machines. *Cell*, **92**(3), pp. 351–366.
- Busconi L., Guan, J. and Denker, B.M. (2000) Degradation of heterotrimeric Galpha(o) subunits via the proteasome pathway is induced by the hsp90-specific compound geldanamycin, *The Journal of Biological Chemistry*, **275**(3), pp. 1565-1569.
- Carrier, M. F., Laurent, V., Santolini, J., Melki, R., Didry, D., Xia, G.X., Hong, Y., Chua, N.H. and Pantaloni, D. (1997) Actin depolymerizing factor (ADF/cofilin) enhances the rate of filament turnover: implication in actin-based motility, *The Journal of cell biology*, **136**(6), pp. 1307–1322.
- Cha, B., Lim, J.W., Kim, K.H. and Kim, H. (2010) HSP90beta interacts with Rac1 to activate NADPH oxidase in *Helicobacter pylori*-infected gastric epithelial cells, *The International Journal of Biochemistry and Cell Biology*, **42**(9), pp. 1455-1461.
- Chang, H.C., Nathan, D.F. and Lindquist, S. (1997) In vivo analysis of the Hsp90 cochaperone Sti1 (p60), *Molecular and Cellular Biology*, **17**(1), pp. 318-325.
- Chao, A., Lai, C.H., Tsai, C.L., Hsueh, S., Lin, C.Y., Chou, H.H., Lin, Y.J., Chen, H.W., Chang, T.C. and Wang, T.H. (2013) Tumor stress-induced phosphoprotein1 (STIP1) as a prognostic biomarker in ovarian cancer, *PLoS one*, **8**(2), e57084
- Chen, S., Prapapanich, R., Rimerman, A., Honoré, B. and Smith, D.F. (1996) Interactions of p60, a mediator of progesterone receptor assembly, with heat shock proteins hsp90 and hsp70, *Molecular Endocrinology*, **10**(6), pp. 682-693.
- Chen, S. and Smith, D. (1998) Hop as an Adaptor in the Heat Shock Protein 70 (Hsp70) and Hsp90 Chaperone Machinery, *Journal of Biological Chemistry*, **273**(52), pp. 35194–35200.
- Cho, S.Y. and Klemke, R.L. (2002) Purification of pseudopodia from polarized cells reveals redistribution and activation of Rac through assembly of a CAS/Crk scaffold, *The Journal of Cell Biology*, **156**(4), pp. 725-736.
- Clark, E.A., Golub, T.R., Lander, E.S. and Hynes, R.O. (2000) Genomic analysis of metastasis reveals an essential role for RhoC, *Nature*, **406**(6795), pp. 532-535.
- Collier I.E., Wilhelm, S.M., Eisen, A.Z., Marmer, B.L., Grant, G.A., Seltzer, J.L., Kronberger, A., He, C.S., Bauer, E.A. and Goldberg, G.I. (1988) H-ras oncogene-transformed human bronchial epithelial cells (TBE-1) secrete a single metalloproteinase capable of degrading basement membrane collagen. *The Journal of Biological Chemistry*, **263**(14), 6579–6587.
- Condeelis, J. (1993) Life at the leading edge: the formation of cell protrusions, *Annual Review of Cell Biology*, **9**, pp. 411-444.
- Condeelis, J. and Pollard, J.W. (2006) Macrophages: obligate partners for tumor cell migration, invasion, and metastasis, *Cell*, **124**(2), pp. 263-266.

- Cooper, G.M. (2000) *The Cell: A Molecular Approach*, 2<sup>nd</sup> Edition, Chapter 11, Actin, Myosin, and Cell Movement, Sinauer Associates, Sunderland.
- Coopman, P.J., Do, M.T., Thompson, E.W. and Mueller, S.C. (1998) Phagocytosis of cross-linked gelatin matrix by human breast carcinoma cells correlates with their invasive capacity, *Clinical cancer research*, **4**(2), pp. 507–515.
- Correia, A.L., Mori, H., Chen, E.I., Schmitt, F.C. and Bissell, M.J. (2013) The hemopexin domain of MMP3 is responsible for mammary epithelial invasion and morphogenesis through extracellular interaction with HSP90 $\beta$ , *Genes and Development*, **27**(7), pp. 805-817.
- Cravchik, A., Reddy, D. and Matus, A. (1994) Identification of a novel microtubule-binding domain in microtubule-associated protein 1A (MAP1A), *Journal of cell science*, **107**, pp. 661–672.
- Culp, L.A., Murray, B.A. and Rollins, B.J. (1979) Fibronectin and proteoglycans as determinants of cell-substratum adhesion, *Journal of Supramolecular Structure*, **11**(3), pp. 401–427.
- Daniel, S., Söti, C., Csermely, P., Bradley, G. and Blatch, G.L. (2007) Networking of chaperones by co-chaperones, Chapter 3, *An Hsp70/Hsp90 Co-Chaperone That Functions Within and Beyond Hsp70/Hsp90 Protein Folding Pathways*, pp. 26-37, Landes Bioscience, South Africa.
- Das, A.T., Zhou, X., Vink, M., Klaver, B., Verhoef, K., Marzio, G. and Berkhout, B. (2004) Viral evolution as a tool to improve the tetracycline-regulated gene expression system, *The Journal of biological chemistry*, **279**(18), pp. 18776–18782.
- Das, S., Banerji, A., Frei, E. and Chatterjee, A. (2008) Rapid expression and activation of MMP-2 and MMP-9 upon exposure of human breast cancer cells (MCF-7) to fibronectin in serum free medium, *Life Sciences*, **82**, pp. 467-476.
- De Los Rios, P., Ben-Zvi, A., Slutsky, O., Azem, A. and Goloubinoff, P. (2006) Hsp70 chaperones accelerate protein translocation and the unfolding of stable protein aggregates by entropic pulling, *Proceedings of the National Academy of Sciences (PNAS)*, **103**(16), pp. 6166–6171.
- Debidda, M., Wang, L., Zang, H., Poli, V. and Zheng, Y. (2005) A role of STAT3 in Rho GTPase-regulated cell migration and proliferation, *The Journal of biological chemistry*, **280**(17), pp. 17275–17285.
- DerMardirossian, C. and Bokoch, G.M. (2005) GDIs: central regulatory molecules in Rho GTPase activation, *Trends in Cell Biology*, **15**(7), pp. 356-363.
- Desai, A. and Mitchison, T.J. (1997) Microtubule polymerization dynamics, *Annual Review of Cell and Development Biology*, **13**, pp. 83-117.
- Ding, Z., Gau, D., Deasy, B., Wells, A. and Roy, P. (2009) Both actin and polyproline interactions of Profilin-1 are required for migration, invasion and capillary morphogenesis of vascular endothelial cells, *Experimental cell research*, **315**(17), pp. 2963–2973.
- Ding, Z. and Roy, P. (2013) Profilin-1 versus profilin-2: two faces of the same coin? *Breast cancer research*, **15**(3), pp. 311.
- Dittmar, K. D. (1997) Folding of the Glucocorticoid Receptor by the Reconstituted hsp90-based Chaperone Machinery, *Journal of Biological Chemistry*, **272**(20), pp. 13047–13054.
- Doench, J.G., Petersen, C.P. and Sharp, P.A. (2003) siRNAs can function as miRNAs, *Genes and Development*, **17**(4), pp. 438-442.
- Egeblad, M. and Werb, Z. (2002) New functions for the matrix metalloproteinases in cancer progression, *Nature reviews. Cancer*, **2**(3), pp. 161–174.

- Ellis, R.J. and Hemmingsen, S.M. (1990) Molecular chaperones: proteins essential for the biogenesis of some macromolecular structures, *Trends in biochemical sciences*, **14**(8), pp. 339–342.
- Ellis, R.J. (2005) Molecular Chaperones and Cell Signalling, Chaperone function: The orthodox view, pp. 3–41, Cambridge University Press, Cambridge.
- Ellis, R.J. (2006) Molecular chaperones: assisting assembly in addition to folding, *Trends in biochemical sciences*, **31**(7), pp. 395–401.
- Erlich, R.B., Kahn, S.A., Lima, F.R.S., Muras, A.G., Martins, R.A.P., Linden, R., Chiarini, L.B., Martins, V.R. and Neto, V.M. (2007) STI1 promotes glioma proliferation through MAPK and PI3K pathways, *GLIA*, **55**, pp. 1690–1698.
- Eustace, B.K., Sakurai, T., Stewart, J.K., Yimlamai, D., Unger, C., Zehetmeier, C., Lain, B., Torella, C., Henning, S.W., Beste, G., Scroggins, B.T., Neckers, L., Ilag, L.L. and Jay, D.G. (2004) Functional proteomic screens reveal an essential extracellular role for hsp90 alpha in cancer cell invasiveness, *Nature cell biology*, **6**(6), pp. 507–514.
- Eustace, B.K. and Jay, D.G. (2010) Extracellular roles for the molecular chaperone, hsp90, *Cell Cycle*, **9**(23), pp. 4769.
- Faix, J. and Rottner, K. (2006) The making of filopodia, *Current Opinion in Cell Biology*, **18**(1), pp. 18–25.
- Fingleton, B. (2007) Molecular targets in metastasis: lessons from genomic approaches, *Cancer genomics & proteomics*, **4**(3), pp. 211–222.
- Fink, A.L. (1999) Chaperone-mediated protein folding, *Physiological Reviews*, **79**(2), pp. 425–449.
- Fire, A., Xu, S., Montgomery, M.K., Kostas, S.A., Driver, S.E. and Mello, C.C. (1998) Potent and specific genetic interference by double-stranded RNA in *Caenorhabditis elegans*, *Letters to Nature*, **391**, pp. 806–811.
- Forastieri, H. and Ingham, K.C. (1985) Interaction of Gelatin with a Fluorescein-labeled 42-kDa Chymotryptic Fragment of Fibronectin, *Journal of Biological Chemistry*, **260**(19), pp. 10546–10550.
- Fowler, D.M., Koulov, A.V., Alory-Jost, C., Marks, M.S., Balch, W.E. and Kelly, J.W. (2005) Functional amyloid formation within mammalian tissue, *PLoS Biology*, **4**(1), e6.
- Fritz, G., Just, I. and Kaina, B. (1999) Rho GTPases are over-expressed in human tumors, *International journal of cancer. Journal international du cancer*, **81**(5), pp. 682–687.
- Fritz, G., Brachetti, C., Bahlmann, F., Schmidt, M. and Kaina, B. (2002) Rho GTPases in human breast tumours: expression and mutation analyses and correlation with clinical parameters, *British journal of cancer*, **87**(6), pp. 635–644.
- Furukawa, R. and Fechheimer, M. (1997) The structure, function, and assembly of actin filament bundles, *International Review of Cytology*, **175**, pp. 29–90.
- Gaestel, M. (2006) Molecular Chaperones in Signal Transduction, *Molecular Chaperones in Health and Disease; Handbook of Experimental Pharmacology*, **172**, pp. 93–109.
- Gilmore, A.P. and Burridge, K. (1996) Regulation of vinculin binding to talin and actin by phosphatidylinositol-4-5-bisphosphate, *Nature*, **381**, pp. 531–535.
- Goetz, M.P., Toft, D.O., Ames, M.M. and Erlichman, C. (2003) The Hsp90 chaperone complex as a novel target for cancer therapy, *Annals of Oncology*, **14**, pp. 1169–1176.
- Grishok, A., Pasquinelli, A.E., Conte, D., Li, N., Parrish, S., Ha, I., Baillie, D.L., Fire, A., Ruvkun, G. and Mello, C.C. (2001) Genes and mechanisms related to RNA interference regulate expression of the small temporal RNAs that control *C. elegans* developmental timing, *Cell*, **106**(1), pp. 23–34.

- Gunnensen, J.M., Spirkoska, V., Smith, P.E., Danks, R.A. and Tan, S.S. (2000) Growth and migration markers of rat C6 glioma cells identified by serial analysis of gene expression, *Glia*, **32**(2), pp. 146–154.
- Gustafsson, E. and Fassler, R. (2000) Insights into extracellular matrix functions from mutant mouse models, *Experimental Cell Research*, **261**(1), pp. 52–68.
- Gutkind, J.S. (1998) The pathways connecting G protein-coupled receptors to the nucleus through divergent mitogen-activated protein kinase cascades, *Journal of Biological Chemistry*, **273**(4), pp. 1839–1842.
- Hakem, A., Sanchez-Sweetman, O., You-Ten, A., Duncan, G., Wakeham, A., Khokha, R. and Mak, T.W. (2005) RhoC is dispensable for embryogenesis and tumor initiation but essential for metastasis, *Genes & development*, **19**(17), pp. 1974–1979.
- Hammond, S.M., Boettcher, S., Caudy, A.A., Kobayashi, R. and Hannon, G.J. (2001) Argonaute2, a link between genetic and biochemical analyses of RNAi, *Science*, **293**(5532), pp. 1146–1150.
- Hartl, F.U., Bracher, A. and Hayer-Hartl, M. (2011) Molecular chaperones in protein folding and proteostasis, *Nature*, **475**(7356), pp. 324–332.
- Havik, B. and Bramham, C.R. (2007) Additive viability-loss following hsp70/hsc70 double interference and Hsp90 inhibition in two breast cancer cell lines, *Oncology reports*, **17**(6), pp. 1501–1510.
- Hernández, M.P., Sullivan, W.P. and Toft, D.O. (2002) The assembly and intermolecular properties of the hsp70-Hop-hsp90 molecular chaperone complex, *The Journal of biological chemistry*, **277**(41), pp. 38294–38304.
- Hessling, M., Richter, K. and Buchner, J. (2009) Dissection of the ATP-induced conformational cycle of the molecular chaperone Hsp90, *Nature Structural and Molecular Biology*, **16**, pp. 287–293.
- Horibe, T., Kohno, M., Haramoto, M., Ohara, K. and Kawakami, K. (2011) Designed hybrid TPR peptide targeting Hsp90 as a novel anticancer agent, *Journal of Translational Medicine*, **9**(8), pp. 1–12.
- Horiuchi, A., Imai, T., Wang, C., Ohira, S., Feng, Y., Nikaido, T. and Konishi, I. (2003) Up-regulation of small GTPases, RhoA and RhoC, is associated with tumor progression in ovarian carcinoma, *Laboratory Investigation; a journal of technical methods and pathology*, **83**(6), pp. 861–870.
- Hu, Y. and Mivechi, N.F. (2003) HSF-1 interacts with Ral-binding protein 1 in a stress-responsive, multiprotein complex with HSP90 in vivo, *The Journal of Biological Chemistry*, **278**(19), pp. 17299–17306.
- Hunter, M.C., O'Hagan, K.L., Kenyon, A., Dhanani, K.C., Prinsloo, E. and Edkins, A.L. (2014) Hsp90 Binds Directly to Fibronectin (FN) and Inhibition Reduces the Extracellular Fibronectin Matrix in Breast Cancer Cells, *PLoS One*, **9**(1), e86842.
- Hynes, R. (1999) Guidebook to the Extracellular Matrix, Anchor and Adhesion Proteins, pp. 380–408, Oxford University Press, Oxford, UK.
- Hynes, R.O. (2002) Integrins: Bidirectional, allosteric signaling machines, *Cell*, **110**, pp. 673–687.
- Ikoma, T., Takahashi, T. and Nagano, S. (2004) A Definitive Role of RhoC in Metastasis of Orthotopic Lung Cancer in Mice A Definitive Role of RhoC in Metastasis of Orthotopic Lung Cancer in Mice, *Clinical cancer research*, **10**(3), pp. 1192–1200.
- Inanobe, A., Takahashi, K. and Katada, T. (1994) Association of the beta gamma subunits of trimeric GTP-binding proteins with 90-kDa heat shock protein, hsp90, *Journal of Biochemistry*, **115**(3), pp. 486–492.
- Janke, J., Schluter, K., Jandrig, B., Theile, M., Kolble, K., Arnold, W., Grinstein, E., Schwartz, A., Estevez-Schwarz, L., Schlag, P.M., Jockusch, B.M. and Scherneck, S. (2000) Suppression of tumorigenicity in breast

cancer cells by the microfilament protein profilin 1, *The Journal of Experimental Medicine*, **191**(10), pp. 1675–1686.

Jiang, L., Liu, X., Kolokythas, A., Yu, J., Wang, A., Heidbreder, C. E., Shi, F. and Zhou, X. (2010) Downregulation of the Rho GTPase signaling pathway is involved in the microRNA-138-mediated inhibition of cell migration and invasion in tongue squamous cell carcinoma, *International journal of cancer*, **127**(3), pp. 505–512.

Johnson, J.L. and Toft, D.O. (1994) A novel chaperone complex for steroid receptors involving heat shock proteins, immunophilins, and p23, *The Journal of Biological Chemistry*, **269**(40), pp. 24989–24993.

Kamai, T., Tsujii, T., Arai, K., Takagi, K., Asami, H., Ito, Y. and Oshima, H. (2003) Significant association of Rho/ROCK pathway with invasion and metastasis of bladder cancer, *Clinical Cancer Research: an official journal of the American Association for Cancer Research*, **9**(7), pp. 2632–2641.

Kamal, A., Thao, L., Sensintaffer, J., Zhang, L., Boehm, M.F., Fritz, L.C. and Burrows, F.G. (2003) A high-affinity conformation of Hsp90 confers tumour selectivity on Hsp90 inhibitors, *Nature*, **425**, pp. 407–410.

Kampinga, H.H., Hageman, J., Vos, M.J., Kubota, H., Tanguay, R.M., Bruford, E.A., Cheetham, M.E., Chen, B. and Hightower, L.E. (2009) Guidelines for the nomenclature of the human heat shock proteins, *Cell Stress and Chaperones*, **14**(1), pp. 105–111.

Kampinga, H.H. and Craig, E.A. (2010) The HSP70 chaperone machinery: J proteins as drivers of functional specificity, *Nature reviews Molecular cell biology*, **11**(8), pp. 579–592.

Kamynina, E., Kauppinen, K., Duan, F., Muakkassa, N. and Manor, D. (2007) Regulation of proto-oncogenic Dbl by chaperone-controlled, ubiquitin-mediated degradation, *Molecular and cellular biology*, **27**(5), pp. 1809–1822.

Kappes, J.C. and Wu, X. (2001) Safety considerations in vector development, *Somatic Cell and Molecular Genetics*, **26**, pp. 147–158.

Kappes, J.C. and Wu, X. (2003) Production of trans-lentiviral vector with predictable safety, *Methods Molecular Medicine*, **76**, pp. 449–465.

Karlsson, R., Pedersen, E.D., Wang, Z. and Brakebusch, C. (2009) Rho GTPase function in tumorigenesis, *Biochimica et biophysica acta*, **1796**(2), pp. 91–98.

Kellermayer, M.S.Z. and Csermely, P. (1995) ATP induces dissociation of the 90 kDa heat shock protein (HSP90) from F-actin: Interference with the binding of heavy meromyosin, *Biochemical and Biophysical Research Communications*, **211**(1), pp. 166–174.

Kenny, H.A., Kaur, S., Coussens, L.M. and Lengyel, E. (2008) The initial steps of ovarian cancer cell metastasis are mediated by MMP-2 cleavage of vitronectin and fibronectin, *The Journal for clinical investigation*, **118**(4), pp. 1–29.

Khalil, A.A., Kabapy, N.F., Deraz, S.F. and Smith, C. (2011) Heat shock proteins in oncology: Diagnostic biomarkers or therapeutic targets? *Biochimica et Biophysica Acta (BBA) - Reviews on Cancer*, **1816**(2), pp. 89–104.

Kim, Y.E., Hipp, M.S., Bracher, A., Hayer-Hartl, M. and Hartl, F.U. (2013) Molecular chaperone functions in protein folding and proteostasis, *Annual Review of Biochemistry*, **82**, pp. 323–355.

King, F., Wawrzynow, A., Höhfeld, J. and Zylicz, M. (2001) Co-chaperones Bag-1, Hop and Hsp40 regulate Hsc70 and Hsp90 interactions with wild-type or mutant p53, *The EMBO Journal*, **20**(22) pp. 6297–6305.

Kitzing, T.M., Wang, Y., Pertz, O., Copeland, J.W. and Grosse, R. (2010) Formin-like 2 drives amoeboid invasive cell motility downstream of RhoC, *Oncogene*, **29**, pp. 2441–2448.

- Klein, R., Ruttkowski, B., Knapp, E., Salmons, B., Günzburg, W.H. and Hohenadl, C. (2006) WPRE-mediated enhancement of gene expression is promoter and cell line specific, *Gene*, **372**, pp. 153–161.
- Koga, F., Kihara, K. and Len, N. (2009) Inhibition of cancer invasion and metastasis by targeting the molecular chaperone heat-shock protein 90, *Anticancer Research*, **29**(3), pp. 797–808.
- Kondo, T., Sentani, K., Oue, N., Yoshida, K., Nakayama, H. and Yasui, W. (2004) Expression of RHOC is associated with metastasis of gastric carcinomas, *Pathobiology*, **71**(1), pp. 19–25.
- Kosla, J., Paňková, D., Plachý, J., Tolde, O., Bicanová, K., Dvořák, M., Rösel, D. and Brábek, J. (2013) Metastasis of aggressive amoeboid sarcoma cells is dependent on Rho/ROCK/MLC signaling, *Cell communication and signaling*, **11**(51), pp. 1–13.
- Koyasu, S., Nishida, E., Kadowaki, T., Matsuzaki, F., Iida, K., Harada, F., Kasuga, M., Sakai, H. and Yahara, I. (1986) Two mammalian heat shock proteins, HSP90 and HSP100 are actin binding proteins, *Proceedings of the National Academy of Science of the United States of America*, **83**(21), pp. 8054–8058.
- Kubota, H., Yamamoto, S., Itoh, E., Abe, Y., Nakamura, A., Izumi, Y., Okada, H., Iida, M., Nanjo, H., Itoh, H. and Yamamoto, Y. (2010) Increased expression of co-chaperone HOP with HSP90 and HSC70 and complex formation in human colonic carcinoma, *Cell stress chaperones*, **15**(6), pp. 1003–1011.
- Kucia, M., Reca, R., Miekus, K., Wanzeck, J., Wojakowski, W., Janowska-Wieczorek, A., Ratajczak, J. and Ratajczak, M.Z. (2005) Trafficking of Normal Stem Cells and Metastasis of Cancer Stem Cells Involve Similar Mechanisms: Pivotal Role of the SDF-1–CXCR4 Axis, *Stem Cells*, **23**, pp. 879–894.
- Kühn, K., Engel, J., Zimmermann, B. and Grassmann, W. (1965) Renaturation of soluble collagen. 3. Reorganization of native collagen molecules from completely separated units, *Archives of Biochemistry and Biophysics*, **105**(1965) 387–403.
- Kurusu, S., Suetsugu, S., Yamazaki, D., Yamaguchi, H. and Takenawa, T. (2005) Rac-WAVE2 signaling is involved in the invasive and metastatic phenotypes of murine melanoma cells, *Oncogene*, **24**(8), pp. 1309–1319.
- Laemmli, U.K. (1970) Cleavage of structural proteins during the assembly of the head of bacteriophage T4, *Nature*, **227**, pp. 680–685.
- Lagos-Quintana, M., Rauhut, R., Lendeckel, W. and Tuschl, T. (2001) Identification of novel genes coding for small expressed RNAs, *Science*, **294**(5543), pp. 853–858.
- Lapouge, K., Smith, S.J.M., Walker, P.A., Gamblin, S.J., Smerdon, S.J. and Rittinger, K. (2000) Structure of the TPR Domain of p67<sup>phox</sup> in Complex with Rac-GTP, *Molecular cell*, **6**, pp. 899–907.
- Lässle, M., Blatch, G.L., Kundra, V., Takatori, T. and Zetter, B.R. (1997) Stress-inducible, murine protein mSTI1: characterization of binding domains for heat shock proteins and in vitro phosphorylation by different kinases. *The Journal of Biological Chemistry*, **272**, pp. 1876–1884.
- Lau, N.C., Lim, L.P., Weinstein, E.G., Bartel, D.P. (2001) An abundant class of tiny RNAs with probable regulatory roles in *Caenorhabditis elegans*, *Science*, **294**(5543), pp. 858–862.
- Lee, R.C. and Ambros, V. (2001) An extensive class of small RNAs in *Caenorhabditis elegans*, *Science*, **294**(5543), pp. 862–864.
- Lee, Y.J., Mazzatti, D.J., Yun, Z. and Keng, P.C. (2005) Inhibition of invasiveness of human lung cancer cell line H1299 by over-expression of cofilin, *Cell biology international*, **29**(11), pp. 877–883.
- Lee, C.T., Graf, C., Mayer, F.J., Richter, S.M. and Mayer, M.P. (2012) Dynamics of the regulation of Hsp90 by the co-chaperone Sti1, *The EMBO journal*, **31**(6), pp. 1518–1528.
- Li, J., Soroka, J. and Buchner, J. (2012a) The Hsp90 chaperone machinery: conformational dynamics and regulation by co-chaperones, *Biochimica et biophysica acta*, **1823**(3), pp. 624–635.

- Li, J., Sun, X., Wang, Z., Chen, L., Li, D., Zhou, J. and Liu, M. (2012b) Regulation of vascular endothelial cell polarization and migration by Hsp70/Hsp90-organizing protein, *PLoS one*, **7**(4), pp. 1-9.
- Liang, P. and MacRae, T.H. (1997) Molecular chaperones and the cytoskeleton, *Journal of Cell Science*, **110**, pp. 1431-1440.
- Longshaw, V.M., Chapple, J.P., Balda, M.S., Cheetham, M.E. and Blatch, G.L. (2004) Nuclear translocation of the Hsp70/Hsp90 organizing protein mSTI1 is regulated by cell cycle kinases. *Journal of Cell Science*, **117**( 5), pp. 701-710.
- Longshaw, V.M., Baxter, M., Prewitz, M. and Blatch, G.L. (2009a) Knockdown of the co-chaperone Hop promotes extranuclear accumulation of Stat3 in mouse embryonic stem cells, *European Journal of Cell Biology*, **88**(3), pp. 153–166.
- Longshaw, V.M., Stephens, L.L., Daniel, S. and Blatch, G.L. (2009b) The TPR2B domain of the Hsp70/Hsp90 organizing protein (Hop) may contribute towards its dimerization. *Protein and Peptide Letters*, **16**(4), pp. 402-407.
- Lopes, M.H., Hajj, G.N.M., Muras, A.G., Mancini, G.L., Castro, R.M.P.S., Ribeiro, K.C.B., Brentani, R.R., Linden, R. and Martins, V.R. (2005) Interaction of cellular prion and stress-inducible protein 1 promotes neuritogenesis and neuroprotection by distinct signaling pathways, *The Journal of neuroscience*, **25**(49), pp. 11330–11339.
- Lopes, M.H. and Santos, T.G. (2012) Prion potency in stem cells biology, *Prion*, **6**(2), pp. 142–146.
- Luker, K.E. and Luker, .D. (2005) Functions of CXCL12 and CXCR4 in breast cancer, *Cancer Letters*, **238**, pp. 30-41.
- Macara, I.G., Lounsbury, K.M., Richards, S.A., McKiernan, C. and Bar-Sagi, D. (1996) The Ras superfamily of GTPases, *FASEB journal : official publication of the Federation of American Societies for Experimental Biology*, **10**(5), pp. 625–630.
- MacGrath, S.M. and Koleske, A.J. (2011) Invadopodia: RhoC runs rings around cofilin, *Current biology*, **21**(8), pp. R280–R282.
- Machesky, L.M. and Gould, K.L. (1999) The Arp2/3 complex: a multifunctional actin organizer, *Current Opinion in Cell Biology*, **11**(1), pp. 117-121.
- Marcu, M.G., Chadli, A., Bouhouche, I., Catelli, M. and Neckers, L.M. (2000) The heat shock protein 90 antagonist novobiocin interacts with a previously unrecognized ATP-binding domain in the carboxyl terminus of the chaperone, *The Journal of biological chemistry*, **275**(47), pp. 37181–37186.
- Markusic, D., Oude-Elferink, R., Das, A.T., Berkhout, B. and Seppen, J. (2005) Comparison of single regulated lentiviral vectors with rtTA expression driven by an autoregulatory loop or a constitutive promoter, *Nucleic acids research*, **33**(6), e63.
- Martin, J. and Hartl, F.U. (1997) Chaperone-assisted protein folding, *Current opinion in structural biology*, **7**(1), pp. 41–52.
- Martínez-Salas, E. (1999) Internal ribosome entry site biology and its use in expression vectors, *Current opinion in biotechnology*, **10**(5), pp. 458–464.
- Marty, C., Browning, D.D. and Ye, R.D. (2003) Identification of Tetratricopeptide Repeat 1 as an Adaptor Protein That Interacts with Heterotrimeric G Proteins and the Small GTPase Ras, *Molecular and Cellular Biology*, **23**(11), pp. 3847–3858.

- McDonald, J.A., Kelley, D.G. and Broekelmann, T.J. (1982) Role of Fibronectin in Collagen Deposition: Fab' to the Gelatin-binding Domain of Fibronectin Inhibits Both Fibronectin and Collagen Organization in Fibroblast Extracellular Matrix, *Journal of Cell Biology*, **92**, pp. 485–492.
- McManus, M.T. and Sharp, P.A. (2002) Gene silencing in mammals by small interfering RNAs, *Nature reviews Genetics*, **3**(10), pp. 737–747.
- Mehta, T.A., Greenman, J., Ettelaie, C., Venkatasubramanian, A., Chetter, I.C. and McCollum, P.T. (2005) Heat shock proteins in vascular disease--a review, *European Journal of Vascular and Endovascular Surgery: the official journal of the European Society for Vascular Surgery*, **29**(4), pp. 395-402.
- Meyer, P., Prodromou, C., Hu, B., Vaughan, C., Roe, S.M., Panaretou, B., Piper, P.W. and Pearl, L.H. (2003) Structural and functional analysis of the middle segment of hsp90: implications for ATP hydrolysis and client protein and cochaperone interactions, *Molecular cell*, **11**(3), pp. 647–658.
- Moon, A. and Drubin, D.G. (1995) The ADF/Cofilin Proteins: Stimulus-responsive Modulators of Actin Dynamics, *Molecular Biology of the Cell*, **6**(11), pp. 1423–1431.
- Mouneimne, G., Hansen, S.D., Selfors, L.M., Petrak, L., Hickey, M.M., Gallegos, L.L., Simpson, K.J., Lim, J., Gertler, F.B., Hartwig, J.H., Mullins, R.D. and Brugge, J.S. (2012) Differential remodeling of actin cytoskeleton architecture by profilin isoforms leads to distinct effects on cell migration and invasion, *Cancer Cell*, **22**(5), pp. 615-630.
- Mullins, R.D. (2000) How WASP-family proteins and the Arp2/3 complex convert intracellular signals into cytoskeletal structures, *Current Opinion in Cell Biology*, **12**, pp. 91-96.
- Nagai, N., Hosokawa, M., Itohara, S., Adachi, E., Matsushita, T., Hosokawa, N., and Nagata, K. (2000) Embryonic Lethality of Molecular Chaperone Hsp47 Knockout Mice Is Associated with Defects in Collagen Biosynthesis, *The Journal of Cell Biology*, **150**(6), pp. 1499-1506.
- Naldini, L., Blömer, U., Gallay, P., Ory, D., Mulligan, R., Gage, F.H., Verma, I.M. and Trono, D. (1996) In vivo gene delivery and stable transduction of nondividing cells by a lentiviral vector, *Science*, **272**(5259), pp. 263-267.
- Neckers, L. (2002) Hsp90 inhibitors as novel cancer chemotherapeutic agents, *Trends in Molecular Medicine*, **8**(4), pp. 55-6.
- Nogales, E., Wolf, S.G. and Downing, K.H. (1998) Structure of the  $\alpha\beta$ -tubulin dimer by electron crystallography, *Nature*, **391**(6663), 199-203.
- Odunuga, O.O., Hornby, J.A., Bies, C., Zimmermann, R., Pugh, D.J.R. and Blatch, G.L. (2003a) Tetratricopeptide repeat motif-mediated Hsc70-mSTI1 interaction: molecular characterization of the critical contacts for successful binding and specificity, *The Journal of Biological Chemistry*, **278**(9), pp. 6896-6904.
- Odunuga, O.O., Hornby, J.A. and Blatch, G.L. (2003b) Structural analyses suggest the existence of functionally important inter-domain interactions in the co-chaperone murine stress-inducible protein I, *Molecular and cellular proteomics*, **2**(9), pp. 588.
- Odunuga, O.O., Longshaw, V.M. and Blatch, G.L. (2004) Hop: more than an Hsp70/Hsp90 adaptor protein, *BioEssays: news and reviews in molecular, cellular and developmental biology*, **26**(10), pp. 1058-1068.
- Ohyabu, Y., Yunoki, S., Hatayama, H. and Teranishi, Y. (2013) Fabrication of high-density collagen fibril matrix gels by renaturation of triple-helix collagen from gelatin, *International journal of biological macromolecules*, **62**, pp. 296–303.
- Olsen, B.R. and Ninomiya, Y. (1999) Guidebook to the Extracellular Matrix, Anchor and Adhesion Proteins, pp. 380-408, Oxford University Press, Oxford, UK.



- Otsubo, T., Iwaya, K., Mukai, Y., Mizokami, Y., Serizawa, H., Matsuoka, T. and Mukai, K. (2004) Involvement of Arp2/3 complex in the process of colorectal carcinogenesis, *Modern pathology*, **17**(4), pp. 461–467.
- Pantaloni, D., Le Clainche, C. and Carlier, M.F. (2001) Mechanism of actin based motility, *Science*, **292**(5524), pp. 1502-1506.
- Park, S.J., Suetsugu, S. and Takenawa, T. (2005) Interaction of HSP90 to N-WASP leads to activation and protection from proteasome-dependent degradation, *The EMBO Journal*, **24**(8), pp. 1557-1570.
- Park, S.J., Suetsugu, S., Sagara, H. and Takenawa, T. (2007) HSP90 cross-links branched actin filaments induced by N-WASP and the Arp2/3 complex, *Genes to Cells: devoted to molecular and cellular mechanisms*, **12**(5), pp. 611-622.
- Parri, M. and Chiarugi, P. (2010) Rac and Rho GTPases in cancer cell motility control, *Cell Communication and Signaling*, **8**, pp. 23.
- Paunola, E., Mattila, P.K. and Lappalainen, P. (2002) WH2 domain: a small, versatile adapter for actin monomers. *FEBS letters*, **513**(1), pp. 92–97.
- Petsko, G.A. and Ringe, D. (2004) Protein Structure and Function, Chapter 1, From Sequence to Structure, pp. 28-29, New Science Press Ltd., USA.
- Picard, D. (2002) Heat-shock protein 90, a chaperone for folding and regulation, *Cellular and Molecular Life Sciences (CMLS)*, **59**(10), pp 1640-1648.
- Pickford, A.R., Potts, J.R., Bright, J.R., Phan, I. and Campbell, I.D. (1997) Solution structure of a type 2 module from fibronectin: implications for the structure and function of the gelatin-binding domain, *Structure*, **5**(3), pp. 359–370.
- Pickford, A.R., Smith, S.P., Staunton, D., Boyd, J. and Campbell, I.D. (2001) The hairpin structure of the (6)F1(1)F2(2)F2 fragment from human fibronectin enhances gelatin binding, *The EMBO journal*, **20**(7), pp. 1519–1529.
- Pimienta, G., Herbert, K.M. and Regan, L. (2011) A compound that inhibits the HOP-Hsp90 complex formation and has unique killing effects in breast cancer cell lines, *Molecular Pharmaceutics*, **8**(6), pp. 2252-2261.
- Pirkkl, F. and Buchner, J. (2001) Functional analysis of the Hsp90-associated human peptidyl prolyl cis/trans isomerases FKBP51, FKBP52 and Cyp40, *Journal of Molecular Biology*, **308**(4), pp. 795–806.
- Pratt, W.B., Morishima, Y., Peng, H.M. and Osawa, Y. (2011) Role of the Hsp90/Hsp70-Based Chaperone machinery in making triage decisions when proteins undergo oxidative and toxic damage, *Experimental Biology and Medicine*, **235**(3), pp. 278–289.
- Prodromou, C., Roe, S.M., O'Brien, R., Ladbury, J.E., Piper, P.W. and Pearl, L.H. (1997) Identification and Structural Characterization of the ATP/ADP-Binding Site in the Hsp90 Molecular Chaperone, *Cell*, **90**(1), pp. 65-75.
- Prohászka, Z., Csermely, P., Schnaider, T., Csaba, S. and Nardai, G. (1998) The 90-kDa Molecular Chaperone Family: Structure , Function, and Clinical Applications. A Comprehensive Review. *Pharmacology and Therapeutics*, **79**(2), pp. 129–168.
- Rao, D.D., Vorhies, J.S., Senzer, N. and Nemunaitis, J. (2009) siRNA vs. shRNA: similarities and differences, *Advanced drug delivery reviews*, **61**(9), pp. 746–759.
- Retzlaff, M., Hagn, F., Mitschke, L., Hessling, M., Gugel, F., Kessler, H., Richter, K. and Buchner, J. (2010) Asymmetric activation of the hsp90 dimer by its cochaperone aha1, *Molecular Cell*, **37**(3), pp. 344-354.
- Rial, D.V. and Ceccarelli, E.A. (2002) Removal of DnaK contamination during fusion protein purifications, *Protein expression and purification*, **25**(3), pp. 503–507.

- Ridley, A.J. (2001) Rho GTPases and cell migration, *Journal of Cell Science*, **114**(Pt 15), pp. 2713-2722.
- Ridley, A.J. (2013) RhoA, RhoB and RhoC have different roles in cancer cell migration, *Journal of microscopy*, **251**(3), pp. 242–249.
- Ritossa, F. (1962) A new puffing pattern induced by temperature shock and DNP in *Drosophila*, *Experientia*, **18**(12), pp. 571–573.
- Rosen, J.J. and Culp, L.A. (1977) Morphology and cellular origins of substrate-attached material from mouse fibroblasts, *Experimental Cell Research*, **107**(1), pp. 139–149.
- Rosenthal, D.T., Zhang, J., Bao, L., Zhu, L., Wu, Z., Toy, K., Kleer, C.G. and Merajver, S.D. (2012) RhoC impacts the metastatic potential and abundance of breast cancer stem cells, *PLoS one*, **7**(7), pp. 1-9.
- Roy, P. and Jacobsen, K. (2004) Overexpression of profilin reduces the migration of invasive breast cancer cells, *Cell Motility and the Cytoskeleton*, **57**, pp. 84-95.
- Rudiger, S., Buchberger, A. and Bukau, B. (1997) Interaction of Hsp70 chaperone with substrates, *Nature Structural Biology*, **4**, pp. 342-349.
- Sahai, E. and Marshall, C.J. (2002) RHO-GTPases and cancer, *Nature Reviews. Cancer*, **2**(2), pp. 133-142.
- Sauk, J.J., Nikitakis, N. and Siavash, H. (2005) Hsp47 a novel collagen binding serpin chaperone, autoantigen and therapeutic target, *Frontiers in Bioscience: a journal and virtual library*, **10**, pp. 107-118.
- Schmid, A.B., Lagleder, S., Gräwert, M.A., Röhl, A., Hagn, F., Wandinger, S.K., Cox, M.B., Demmer, O., Richter, K., Groll, M., Kessler, H. and Buchner, J. (2012) The architecture of functional modules in the Hsp90 co-chaperone Sti1/Hop, *The EMBO Journal*, **31**(6), pp. 1506-1517.
- Schoumacher, M., Goldman, R.D., Louvard, D. and Vignjevich, D.M. (2010) Actin, microtubules, and vimentin intermediate filaments cooperate for elongation of invadopodia, *The Journal of Cell Biology*, **189**(3), pp. 541-556.
- Schröder, H., Langer, T., Hartl, F. and Bukaul, B. (1993) DnaK, DnaJ and GrpE form a cellular chaperone machinery capable of repairing heat-induced protein damage, *The EMBO journal*, **12**(11), pp. 4137–4144.
- Semba, S., Iwaya, K., Matsubayashi, J., Serizawa, H., Kataba, H., Hirano, T., Kato, H., Matsuoka, T. and Mukai, K. (2006) Coexpression of actin-related protein 2 and Wiskott-Aldrich syndrome family verproline-homologous protein 2 in adenocarcinoma of the lung, *Clinical cancer research*, **12**(8), pp. 2449–2454.
- Shankar, j., Messenberg, A., Chan, J., Underhill, M., Foster, L.J. and Nabi, I.R. (2010) Pseudopodial Actin Dynamics Control Epithelial-Mesenchymal Transition in Metastatic Cancer Cells, *Cancer Research*, **70**(9), pp. 3780-3790.
- Shikada, Y., Yoshino, I., Okamoto, T., Fukuyama, S., Kameyama, T. and Maehara, Y. (2003) Higher expression of RhoC is related to invasiveness in non-small cell lung carcinoma, *Clinical Cancer Research: an official journal of the American Association for Cancer Research*, **9**(14), pp. 5282-5286.
- Silva, J.M., Li, M.Z., Chang, K., Ge, W., Golding, M.C., Rickles, R.J., Siolas, D., Hu, G., Paddison, P.J., Schlabach, M.R., Sheth, N., Bradshaw, J., Burchard, J., Kulkarni, A., Cavet, G., Sachidanandam, R., McCombie, W.R., Cleary, M.A., Elledge, S.J. and Hannon, G.J. (2005) Second-generation shRNA libraries covering the mouse and human genomes, *Nature Genetics*, **37**(11), pp. 1281-1288.
- Simpson, K.J., Dugan, A.S. and Mercurio, A.M. (2004) Functional analysis of the contribution of RhoA and RhoC GTPases to invasive breast carcinoma, *Cancer Research*, **64**(23), pp. 8694–8701.
- Sims, J.D., McCready, J. and Jay, D.G. (2011) Extracellular Heat Shock Protein (Hsp)70 and Hsp90 $\alpha$  Assist in Matrix Metalloproteinase-2 Activation and Breast Cancer Cell Migration and Invasion, *PLoS One*, **6**(4), e18848.

- Snoek-van Beurden, P.A.M. and Von den Hoff, J.W. (2005) Zymographic techniques for the analysis of matrix metalloproteinases and their inhibitors, *BioTechniques*, **38**(1), pp. 73–83.
- Song, X. and Luo, Y. (2010) The regulatory mechanism of Hsp90 $\alpha$  secretion from endothelial cells and its role in angiogenesis during wound healing, *Biochemical and biophysical research communications*, **398**(1), pp. 111–117.
- Soti, C., Radics, L., Yahara, I. and Csermely, P. (1998) Interaction of vandate oligomers and permolybdate with the 90-kDa heat-shock protein, Hsp90, *European Journal of Biochemistry/ FEBS*, **255**(3), pp. 611–617.
- Southworth, D.R. and Agard, D.A. (2011). Client-loading conformation of the Hsp90 molecular chaperone revealed in the cryo-EM structure of the human Hsp90:Hop complex, *Molecular cell*, **42**(6), pp. 771–781.
- Spano, D., Heck, C., De Antonellis, P., Christofori, G. and Zollo, M. (2012) Molecular networks that regulate cancer metastasis, *Seminars in cancer biology*, **22**(3), pp. 234–249.
- Stegmeier, F., Hu, G., Rickles, R.J., Hannon, G.J. and Elledge, S.J. (2005) A lentiviral microRNA-based system for single-copy polymerase II-regulated RNA interference in mammalian cells, *Proceedings of the National Academy of Sciences*, **102**(37), pp. 13212–13217.
- Stellas, D., Hamidieh, A.E. and Patsavoudi, E. (2010) Monoclonal antibody 4C5 prevents activation of MMP2 and MMP9 by disrupting their interaction with extracellular HSP90 and inhibits formation of metastatic breast cancer cell deposits, *BioMed Central Cell Biology*, **11**(51), pp. 1–9.
- Streuli, C. (1999) Extracellular matrix remodelling and cellular differentiation, *Current opinion in cell biology*, **11**(5), pp. 634–640.
- Sun, W., Xing, B., Sun, Y., Du, X., Lu, M., Hao, C., Lu, Z., Mi, W., Wu, S., Wei, H., Gao, X., Zhu, Y., Jiang, Y., Qian, X. and He, F. (2007) Proteome analysis of hepatocellular carcinoma by two-dimensional difference gel electrophoresis: novel protein markers in hepatocellular carcinoma tissues, *Molecular and cellular proteomics*, **6**(10), pp. 1798–1808.
- Sun, X., Cheng, G., Hao, M., Zheng, J., Zhou, X., Zhang, J., Taichman, R.S., Pienta, K.J. and Wang, J. (2010) CXCL12 / CXCR4 / CXCR7 chemokine axis and cancer progression, *Cancer and Metastasis Reviews*, **29**(4), pp. 709–722.
- Suwa, H., Ohshio, G., Imamura, T., Watanabe, G., Arai, S., Imamura, M., Narumiya, S., Hiai, H. and Fukumoto, M. (1998) Overexpression of the rhoC gene correlates with progression of ductal adenocarcinoma of the pancreas, *British Journal of Cancer*, **77**(1), pp. 147–152.
- Taipale, M., Krykbaeva, I., Koeva, M., Kayatekin, C., Westover, K.D., Karras, G.I. and Lindquist, S. (2012) Quantitative analysis of HSP90-client interactions reveals principles of substrate recognition. *Cell*, **150**(5), pp. 987–1001.
- Taiyab, A. and Rao, C.M. (2010) HSP90 modulates actin dynamics: Inhibition of HSP90 leads to decreased cell motility and impairs invasion, *Biochimica et Biophysica Acta - Molecular Cell Research*, **1813**(1), pp. 213–221.
- Tchoghandjian, A., Jennewein, C., Eckhardt, I., Rajalingam, K. and Fulda, S. (2013) Identification of non-canonical NF- $\kappa$ B signaling as a critical mediator of Smac mimetic-stimulated migration and invasion of glioblastoma cells, *Cell death & disease*, **4**(3), e564.
- Teicher, B.A. and Fricker, S.P. (2010) CXCL12 (SDF-1)/CXCR4 Pathway in Cancer, *Clinical Cancer Research*, **26**, pp. 2927–2931.
- Terpe, K. (2003) Overview of tag protein fusions: from molecular and biochemical fundamentals to commercial systems, *Applied microbiology and biotechnology*, **60**(5), pp. 523–533.
- Tissières, A., Mitchell, H.K. and Tracy, U.M. (1974) Protein synthesis in salivary glands of *Drosophila melanogaster*: relation to chromosome puffs, *Journal of Molecular Biology*, **84**(3), pp. 389–398.

- Tomás, H.A., Rodrigues, A.F., Alves, P.M. and Coroadinha, A.S. (2013) Gene Therapy – Tools and Potential Applications, Chapter 12, Lentiviral Gene Therapy Vectors: Challenges and Future Directions, pp. 287-317, Intech
- Towbin, H., Staehelin, T. and Gordon, J. (1979) Electrophoretic transfer of proteins from polyacrylamide gels to nitrocellulose sheets: procedure and some applications. *Proceedings of the National Academy of Sciences of the United States of America*, **76**(9), pp. 4350-4354.
- Trono, D. (2000) Lentiviral vectors: turning a deadly foe into a therapeutic agent, *Gene therapy*, **7**(1), pp. 20–23.
- Tsai, C.L., Tsai, C.N., Lin, C.Y., Chen, H.W., Lee, Y.S., Chao, A., Wang, T.H., Wang, H.S. and Lai, C.H. (2012) Secreted stress-induced phosphoprotein 1 activates the ALK2-SMAD signaling pathways and promotes cell proliferation of ovarian cancer cells, *Cell Reports*, **2**, pp. 283-293.
- Tsutsumi, S., Scroggins, B., Koga, F., Lee, M., Trepel, J., Felts, S., Carreras, C. and Neckers, L. (2008) A small molecule cell-impermeant Hsp90 antagonist inhibits tumor cell motility and invasion, *Oncogene*, **27**(17), pp. 2478-2487.
- Ueno, K., Hirata, H., Majid, S., Yamamura, S., Shahryari, V., Tabatabai, Z. L., Hinoda, Y. and Dahiya, R. (2012) Tumor suppressor microRNA-493 decreases cell motility and migration ability in human bladder cancer cells by downregulating RhoC and FZD4, *Molecular cancer therapeutics*, **11**(1), pp. 244–253.
- Vaiskunaite, R., Kozasa, T. and Voyno-Yasenetskaya, T.A. (2001) Interaction between the G alpha subunit of heterotrimeric G12 protein and Hsp90 is required for Gα12 signaling, *The Journal of Biological Chemistry*, **276**, 46088-46093.
- Van den Steen, P.E., Opdenakker, G., Wormald, M.R., Dwek, R.A. and Rudd, P.M. (2001) Matrix remodelling enzymes, the protease cascade and glycosylation, *Biochimica et biophysica acta*, **1528**(2-3), pp. 61–73.
- Van der Spuy, J., Kana, B.D., Dirr, H.W. and Blatch, G.L. (2000) Heat shock cognate protein 70 chaperone-binding site in the co-chaperone murine stress-inducible protein 1 maps to within three consecutive tetratricopeptide repeat motifs, *The Biochem Journal*, **345**, pp. 645-651.
- Van Golen, K.L., Wu, Z.F., Qiao, X.T., Bao, L.W. and Merajver, S.D. (2000) RhoC GTPase, a novel transforming oncogene for human mammary epithelial cells that partially recapitulates the inflammatory breast cancer phenotype, *Cancer Research*, **60**(20), pp. 5832-5838.
- Van Maele, B., De Rijck, J., De Clercq, E. and Debyser, Z. (2003) Impact of the Central Polypurine Tract on the Kinetics of Human Immunodeficiency Virus Type 1 Vector Transduction, *Journal of virology*, **77**(8), pp. 4685–4694.
- Vega, F.M., Fruhwirth, G., Ng, T. and Ridley, A.J. (2011) RhoA and RhoC have distinct roles in migration and invasion by acting through different targets, *The Journal of cell biology*, **193**(4), pp. 655–665.
- Veis, A., Anesey, J. and Cohen, J. (1961) The long range reorganization of gelatin to the collagen structure, *Archives of Biochemistry and Biophysics*, **94**, pp. 20-31.
- Visse, R. and Nagase, H. (2003) Matrix metalloproteinases and tissue inhibitors of metalloproteinases: structure, function, and biochemistry, *Circulation research*, **92**(8), pp. 827–39.
- Vuento, M., Salonen, E., Osterlund, K. and Stenman, U.H. (1982) Essential charged amino acids in the binding of fibronectin to gelatin, *The Biochemical journal*, **201**(1), pp. 1–8.
- Walsh, N., Larkin, A., Swan, N., Conlon, K., Dowling, P., McDermott, R. and Clynes, M. (2011) RNAi knockdown of Hop (Hsp70/Hsp90 organising protein) decreases invasion via MMP-2 down regulation, *Cancer Letters*, **306**, pp. 180-189.

- Wang, N. and Stamenovic, D. (2002) Mechanics of vimentin and intermediate filaments, *Journal of Muscle Research and Cell Motility*, **23**, pp. 535-540.
- Wang, W., Wyckoff, J.B., Frohlich, V.C., Oleynikov, Y., Huttelmaier, S., Zavadil, J., Cermak, L., Bottinger, E.P., Singer, R.H., White, J.G., Segall, J.E. and Condeelis, J.S. (2002) Single cell behavior in metastatic primary tumors correlated with gene expression patterns revealed by molecular profiling. *Cancer Research*, **62**(21), pp. 6278 – 6288.
- Wang, W., Goswami, S., Lapidus, K., Wells, A.L., Wyckoff, J.B., Sahai, E., Singer, R.H., Segall, J.E. and Condeelis, J. S. (2004a) Identification and testing of a gene expression signature of invasive carcinoma cells within primary mammary tumors. *Cancer Research*, **64**(23), pp. 8585-8594.
- Wang, W., Yang, L.Y., Huang, G.W., Lu, W.Q., Yang, Z.L., Yang, J.Q. and Liu, H.L. (2004b) Genomic analysis reveals RhoC as a potential marker in hepatocellular carcinoma with poor prognosis, *British Journal of Cancer*, **90**(12), pp. 2349-2355.
- Wang, W., Wu, F., Fang, F., Tao, Y. and Yang, L. (2008) Inhibition of invasion and metastasis of hepatocellular carcinoma cells via targeting RhoC in vitro and in vivo, *Clinical cancer research*, **14**(21), pp. 6804–6812.
- Wang, B.D., Kline, C.L.B., Pastor, D.M., Olson, T.L., Frank, B., Luu, T., Sharma, A.K., Robertson, G., Weirauch, M.T., Patierno, S.R., Stuart, J.M., Irby, R.B. and Lee, N.H. (2010) Prostate apoptosis response protein 4 sensitizes human colon cancer cells to chemotherapeutic 5-FU through mediation of an NFκB and microRNA network, *Molecular Cancer*, **9**, pp. 98.
- Wegele, H., Haslbeck, M., Reinstein, J. and Buchner, J. (2003) Sti1 is a novel activator of the Ssa proteins, *The Journal of Biological Chemistry*, **278**(28), pp. 25970-25976.
- Wegele, H., Wandinger, S.K., Schmid, A.B., Reinstein, J. and Buchner, J. (2006) Substrate transfer from the chaperone Hsp70 to Hsp90, *Journal of molecular biology*, **356**(3), pp. 802–811.
- Wehrle-Haller, B. and Imhof, B.A. (2003) Actin, microtubules and focal adhesion dynamics during cell migration, *The international journal of biochemistry and cell biology*, **35**(1), pp. 39–50.
- Weis, F., Moullintraffort, L., Heichette, C., Chrétien, D. and Garnier, C. (2010) The 90-kDa heat shock protein Hsp90 protects tubulin against thermal denaturation, *The Journal of Biological Chemistry*, **285**(13), pp. 9525-9534.
- Welch, N.J. (1993) Heat shock proteins functioning as molecular chaperones: their roles in normal and stressed cells, *Molecular Chaperones*, **339**(1289), pp. 71-77.
- Welch, M.D. (1999) The world according to Arp: regulation of actin nucleation by the Arp2/3 complex, *trends in Cell Biology*, **9**(11), pp. 423-427.
- Wennerberg, K., Rossman, K.L. and Der, C.J. (2005) The Ras superfamily at a glance, *Journal of cell science*, **118**(5), pp. 843–846.
- Wilhelm S.M., Collier, I.E., Marmer, B.L., Eisen, A.Z., Grant, G.A. and Goldberg, G.I. (1989) SV40-transformed human lung fibroblasts secrete a 92 kDa type IV collagenase which is identical to that secreted by normal human macrophages. *The Journal of Biological Chemistry*, **264**, 17213–17221.
- Williams, N.E. and Nelsen, E.M. (1997) HSP70 and HSP90 homologs are associated with tubulin in hetero-oligomeric complexes, cilia and the cortex of Tetrahymena, *Journal of Cell Science*, **110**(14), pp. 1665-1672.
- Willmer, T (2011) MSc Thesis: The role of Hsp90/Hsp70 organising protein (Hop) in the Proliferation, Survival, and Migration of Breast Cancer Cells.
- Willmer, T., Contu, L., Blatch, G.L. and Edkins, A.L. (2013) Knockdown of Hop downregulates RhoC expression, and decreases pseudopodia formation and migration in cancer cell lines, *Cancer Letters*, **328**(2), pp. 252-260.

- Witke, W. (2004) The role of profilin complexes in cell motility and other cellular processes, *Trends in cell biology*, **14**(8), pp. 461–469.
- Wu, X., Wakefield, J.K., Liu, H., Xiao, H., Kralovics, R., Prchal, J.T. and Kappes, J.C. (2000) Development of a novel trans-lentiviral vector that affords predictable safety, *Molecular therapy: the journal of the American Society of Gene Therapy*, **2**(1), pp. 47–55.
- Wu, M., Wu, Z.F., Rosenthal, D.T., Rhee, E.M. and Merajver, S.D. (2010) Characterization of the roles of RHOC and RHOA GTPases in invasion, motility, and matrix adhesion in inflammatory and aggressive breast cancers, *Cancer*, **116**(11), pp. 2768–2782.
- Wu, F., Peacock, S.O., Rao, S., Lemmon, S.K. and Burnstein, K.L. (2013) Novel interaction between the co-chaperone Cdc37 and Rho GTPase exchange factor Vav3 promotes androgen receptor activity and prostate cancer growth, *The Journal of biological chemistry*, **288**(8), pp. 5463–5474.
- Yamaguchi, H., Lorenz, M., Kempiak, S., Sarmiento, C., Coniglio, S., Symons, M., Segall, J., Eddy, R., Miki, H., Takenawa, T. and Condeelis, J. (2005) Molecular mechanisms of invadopodium formation: the role of the N-WASP-Arp2/3 complex pathway and cofilin, *The Journal of cell biology*, **168**(3), pp. 441–452.
- Yamaguchi, H. and Condeelis, J. (2007) Regulation of the actin cytoskeleton in cancer cell migration and invasion. *Biochimica et biophysica acta*, **1773**(5), pp. 642–652.
- Yanagawa, R., Furukawa, Y., Tsunoda, T., Kitahara, O., Kameyama, M., Murata, K., Ishikawa, O. and Nakamura, Y. (2001) Genome-wide screening of genes showing altered expression in liver metastases of human colorectal cancers by cDNA microarray. *Neoplasia*, **3**(5), pp. 395–401.
- Yang, Y., Rao, R., Shen, J., Tang, Y., Fiskus, W., Nechtman, J., Atadja, P. and Bhalla, K. (2008) Role of acetylation and extra-cellular location of heat shock protein 90 $\alpha$  in tumor cell invasion, *Cancer Research*, **68**(12), pp. 4833–4842.
- Yao, H., Dashner, E.J., van Golen, C.M. and van Golen, K.L. (2006) RhoC GTPase is required for PC-3 prostate cancer cell invasion but not motility, *Oncogene*, **25**(16), pp. 2285–2296.
- Yonezawa, N., Nishida, E., Ohba, M., Seki, M., Kumagai, H. and Sakai, H. (1989) An actin-interacting heptapeptide in the cofilin sequence. *European Journal of Biochemistry/FEBS*, **183**(1), pp. 235–238.
- Zamore, P.D., Tuschl, T., Sharp, P.A. and Bartel, D.P. (2000) RNAi: double-stranded RNA directs the ATP-dependent cleavage of mRNA at 21 to 23 nucleotide intervals, *Cell*, **101**(1), pp. 25–33.
- Zanata, S.M., Lopes, M.H., Mercadante, A.F., Hajj, G.N., Chiarini, L.B., Nomizo, R., Freitas, A.R., Cabral, A.L., Lee, K.S., Juliano, M.A., de Oliveira, E., Jachieri, S.G., Burlingame, A., Huang, L., Linden, R., Brentani, R.R., Martins, V.R. (2002) Stress-inducible protein 1 is a cell surface ligand for cellular prion that triggers neuroprotection, *The EMBO Journal*, **21**(13), pp. 3307–3316.
- Zawistowski, J.S., Sabouri-Ghomi, M., Danuser, G., Hahn, K.M. and Hodgson, L. (2013) A RhoC biosensor reveals differences in the activation kinetics of RhoA and RhoC in migrating cells, *PloS one*, **8**(11), e79877.
- Zeng, Y. and Cullen, B.R. (2003) Sequence requirements for microRNA processing and function in human cells, *Rna*, **9**(1), pp. 112–123.
- Zhang, D.H., Marconi, A., Xu, L.M., Yang, C.X., Sun, G.W., Feng, X.L., Ling, C.Q., Qin, W.Z., Uzan, G. and d'Alessio, P. (2006) Tripterine inhibits the expression of adhesion molecules in activated endothelial cells, *Journal of Leukocyte Biology*, **80**(2), pp. 309–319.
- Zufferey, R., Nagy, D., Mandel, R.J., Naldini, L. and Trono, D. (1997) Multiply attenuated lentiviral vector achieves efficient gene delivery in vivo, *Nature Biotechnology*, **15**(9), pp. 871–875.

Zufferey, R., Dull, T., Mandel, R.J., Bukovsky, A., Quiroz, D., Naldini, L. and Trono, D. (1998) Self-inactivating lentivirus vector for safe and efficient in vivo gene delivery, *Journal of virology*, **72**(12), pp. 9873–9880.

### **Technical Manuals:**

Dawson, M.E. (1998). *The Significance of Endotoxin to Cell Culture and Biotechnology*, Associates of Cape Cod Incorporated, LAL Update, **16**(1).

McIntyre, C.A. and Reinin, G. (2009). *Reduction in endotoxin levels after performing the prepare for aseptic sort procedure on the BD FACS Aria II Flow Cytometer*, San Jose: BD Biosciences

Richter, S. (2012). *FDA updates medical device endotoxin testing program (new guidance)*, USA: Microtest Laboratories Incorporated.

Ryan, J. (2008). *Endotoxins and Cell Culture: Technical Bulletin*, USA: Corning Incorporated Life Sciences.

Thermo Scientific. (2009). *Thermo Scientific Inducible TRIPZ LentiViral shRNA*, USA: Thermo Scientific.

## APPENDICES

### Appendix 1: List of additional materials used

#### A1.1 Molecular biology and protein biochemistry reagents

The EndoFree Plasmid Maxi Kit (Cat #: 12362) was from Qiagen (Netherlands). The Lambda bacteriophage DNA digested with *Pst*I (Cat #: LSM-VI-NM2427) was purchased from Life Sciences Advanced Technologies Inc. (USA). The KAPA Universal DNA ladder (Cat #: KL6302) was purchased from KAPA Biosystems (South Africa). The Unstained Protein Molecular Weight Marker (Cat #: 26610) and the Prestained Protein Molecular Weight Marker (Cat #: 26612) were purchased from Thermo Scientific (USA). Western Blotting apparatus, Hybond Support Nitrocellulose membranes were purchased from Bio-Rad (USA). The Supersignal West Dura extended duration substrate (Cat #: 34075) and the Protein A/G Peroxidase (Cat #: 32490) were purchased from ThermoScientific (USA). Protein A/G agarose beads (Cat #: sc-2003) were from Santa Cruz Biotechnology (USA). The Rho activation assay kit (Cat #: 17-294) was from Millipore (Germany).

#### A1.2 Antibodies and dyes

Goat polyclonal anti-GST antibody (Cat #: 27457701) was purchased from GE Healthcare (UK) and used at a dilution of 1:2000. Mouse monoclonal anti-DnaK (*E.coli*) antibody (Cat #: ADI-SPA-880) and mouse monoclonal anti-Hop antibody (Cat #: SRA-1500) were purchased from Enzo Life Sciences (UK) and both used at a dilution of 1:1000 for western analysis. Anti-Hop antibody was used at a dilution of 1:100 for immunofluorescence staining. The RhoGTPase antibody sampler kit (Cat #: 9968S) containing rabbit IgG monoclonal anti-RhoA, anti-RhoC and anti-Cdc42 and rabbit polyclonal anti-RhoB and anti-Rac1/2/3 primary antibodies was purchased from Cell Signaling Technologies (USA) and antibodies used at a dilution of 1:1000 for western analysis and 1:100 for immunofluorescence staining. Rabbit, N-terminal anti-actin (Cat #: A2103) was purchased from Sigma Aldrich (USA) and used at a dilution of 1:1000 for western analysis and 1:100 for immunofluorescence staining. Goat polyclonal IgG anti-Hsp90 $\alpha/\beta$  (Cat #: sc-1055) was purchased from Santa Cruz Biotechnology (USA) and used at a dilution of 1:1000 for western analysis. Rabbit polyclonal anti-Histone H3 (Cat #: 9715L) was purchased from Cell Signaling Technologies (USA) and used at a dilution of 1:2500 for western analysis. Donkey anti-goat IgG-HRP secondary

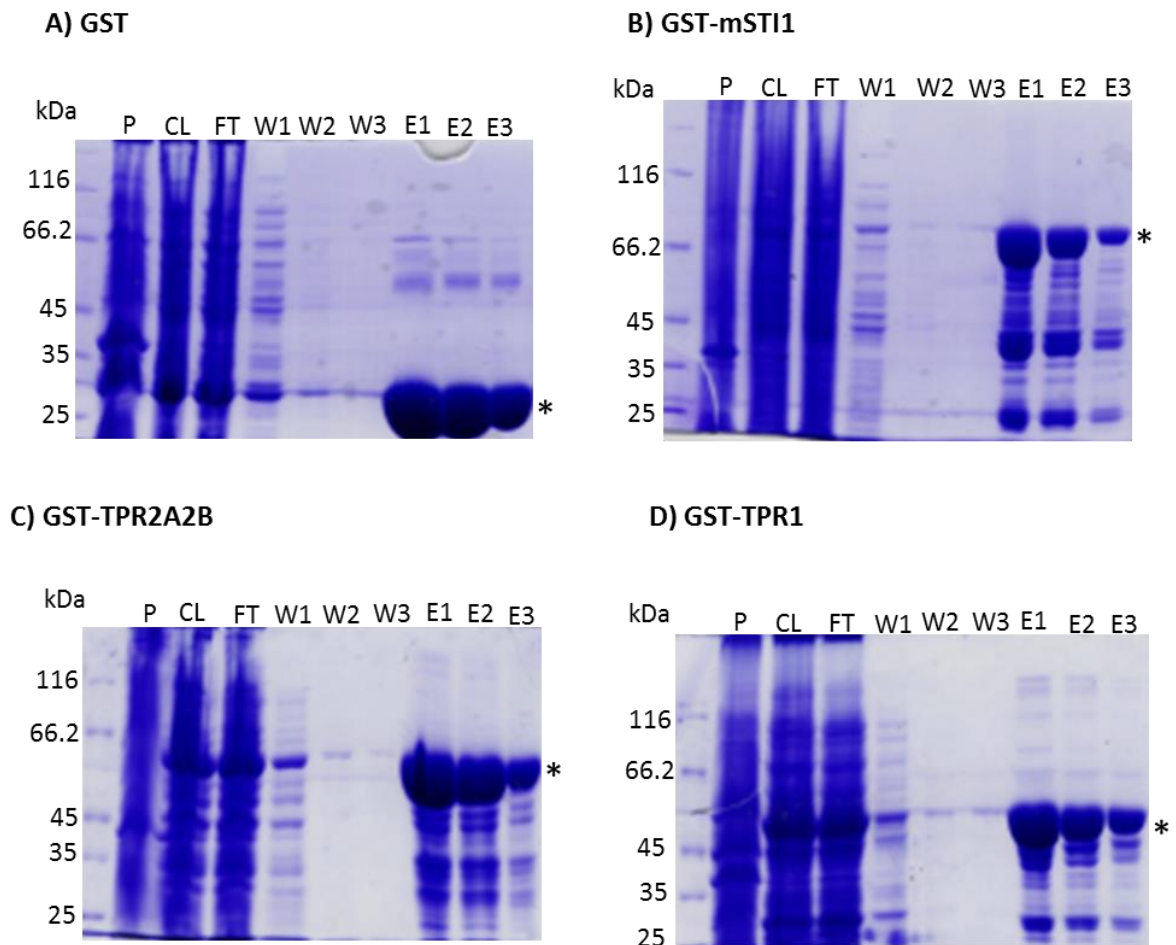


antibody (Cat #: sc-2020) was purchased from Santa Cruz Biotechnology (USA) and goat anti-mouse IgG-HRP secondary antibody (Cat #: 474-1806) was purchased from Kirkegaard and Perry Laboratories (USA). Donkey anti-rabbit IgG-HRP secondary antibody (Cat #: ab6802) was from Abcam (UK) and goat anti-mouse IgG-HRP secondary antibody (Cat #: A2304) was from Sigma Aldrich (USA). All HRP-linked secondary antibodies were used at a dilution of 1:5000. Donkey anti-rabbit IgG DyLight 550 (Cat #: ab96892), donkey anti-rabbit IgG DyLight 488 (Cat #: ab96891) and donkey anti-mouse IgG DyLight 488 (Cat #: ab96875) fluorescent antibodies were purchased from Abcam (UK) and used at a dilution of 1:500. Hoescht-33342 (Cat #: 14533) was from Sigma Aldrich (USA).

### **A1.3 Tissue culture reagents**

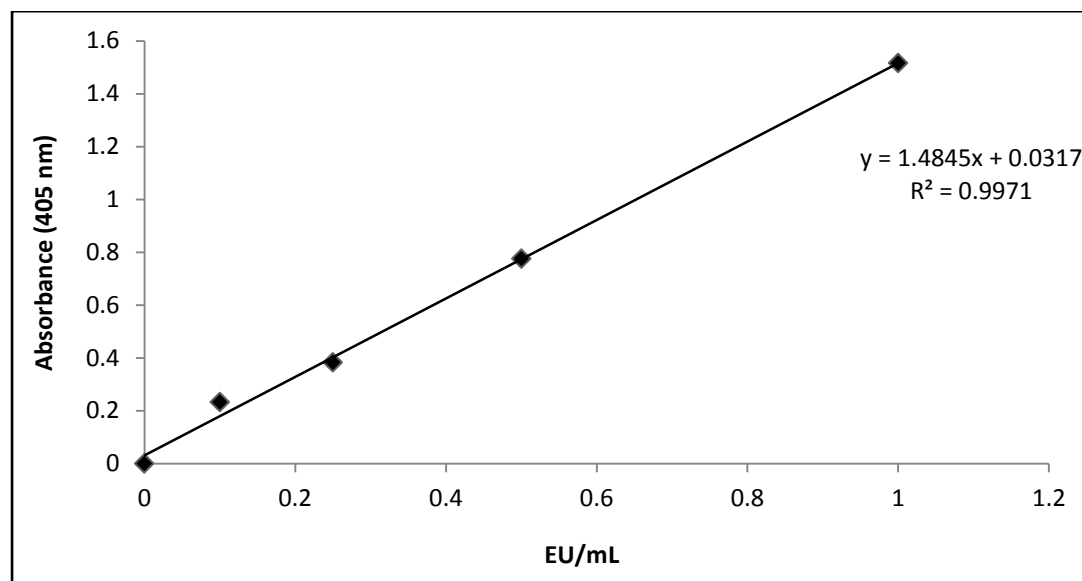
Trypsin-EDTA, Dulbecco's Modified Eagle Medium (DMEM), and penicillin streptomycin amphotericin (PSA) were purchased from Gibco Life technologies (USA). L-Glutamine (Cat #: G7513), MEM sodium pyruvate (Cat #: S8636) and MEM non-essential amino acids (NEAA) (Cat #: M7145) were purchased from Sigma Aldrich (USA). Foetal bovine serum (FBS) (Cat #: S181H) was purchased from BioWest (USA). NovoRapid recombinant human insulin was from Nordisk pharmaceuticals (Denmark). Tissue culture plasticware was purchased from NEST Biotechnology Co (Lasec) (China).

## Appendix 2: Steps showing purification procedure of GST, GST-mSTI1, GST-TPR2A2B and GST-TPR1



**Supplementary figure 1: Overexpression and purification of GST, GST-mSTI1, GST-TPR2A2B and GST-TPR1.** Samples collected from each stage of the purification process for (A) GST, (B) GST-mSTI1, (C) GST-TPR2A2B and (D) GST-TPR1 are represented in the SDS-PAGE gels. The letters above each lane of the SDS-PAGE gels and western blots represent the samples taken at each stage of the purification process (P = pellet; CL = cleared lysate; FT = flow through; W = washes; E = elutions). Asterisks indicate the expressed proteins at the expected molecular weights of approximately 26 kDa, 101 kDa, 78 kDa and 50 kDa for GST, GST-mSTI1, GST-TPR2A2B and GST-TPR1 respectively.

### Appendix 3: Calculating concentrations of endotoxins using standard curve (EU/mL)






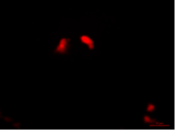


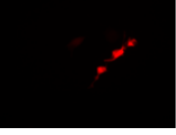

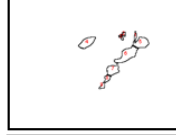
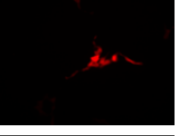

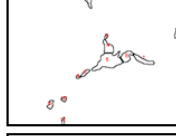


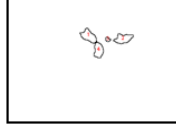


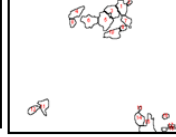
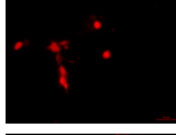

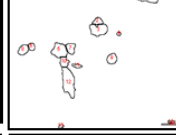
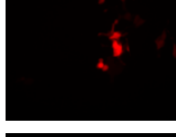

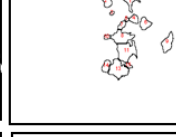
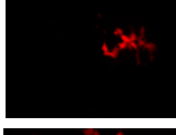

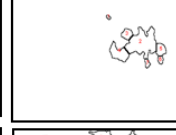
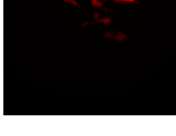


**Supplementary figure 2: Standard curve for quantification of endotoxin in protein samples (units/mL)**  
A chromogenic assay was used to plot standard solutions of endotoxins (1.0, 0.50, 0.25, 0.1 EU/mL)

#### **Appendix 4: Quantification of transduction efficiency by automated particle counting using ImageJ**

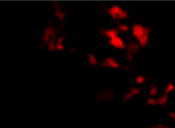

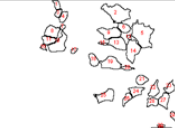
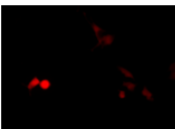

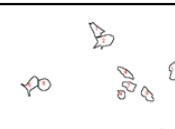
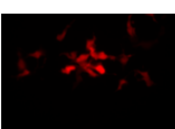


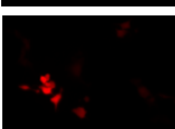
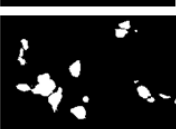
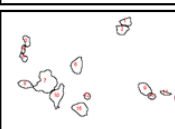
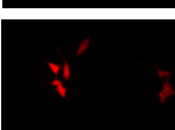

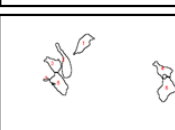
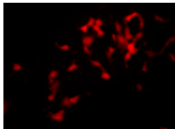
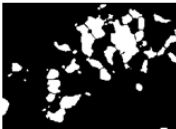
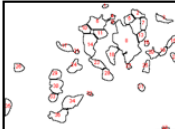
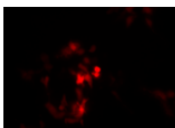

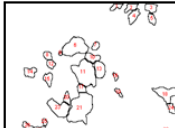
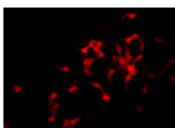

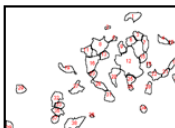
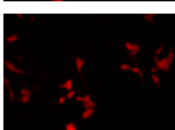

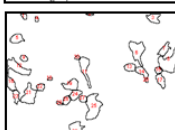
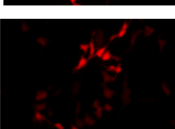

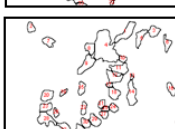
Successfully transduced cells were reflected by the presence of turboRFP. Cells positive for turboRFP were therefore counted using automated particle counting by ImageJ. Images were changed to 16-bit images by selecting “Image → Type → 16-bit”. The “Image → Adjust → Threshold” function was used to apply a threshold of 14 with a ‘dark background’ to each of the images. The “Process → Binary → Watershed” function was used to separate/cut apart particles that had merged together. Automated particle counting was then performed using the “Analyse → Analyse particles” function. Pixels smaller than 30 were excluded from the count to account for small ‘noise’ pixels. “Show outlines” was selected in order to visualise the particles that were counted. Images showing cells positive for turboRFP (from which the automated counting was performed), threshold images, and outlines were shown (Supplementary figure 3 and Supplementary figure 4).

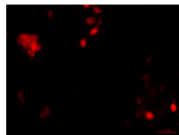

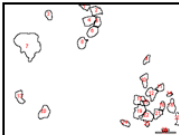
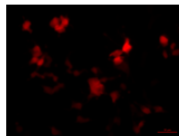

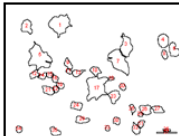
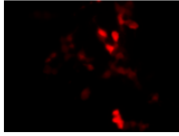


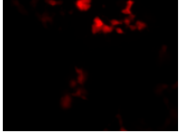

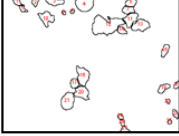
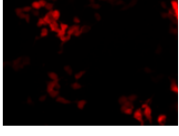

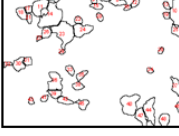
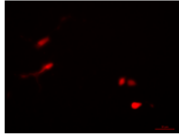

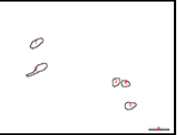
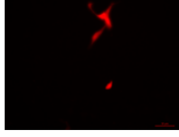

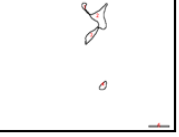
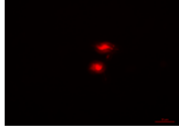

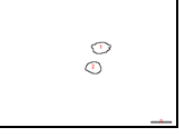






For the HEK293T cell line, automated cell counting was performed for five images (five fields of view) for five different volumes (200  $\mu$ L, 400  $\mu$ L, 600  $\mu$ L, 800  $\mu$ L and 1000  $\mu$ L) of N.T shRNA and shRNA #2 lentiviral particles (Supplementary figure 3). For the HS578T cell line, automated cell counting was performed for three images (three fields of view) for five different volumes (200  $\mu$ L, 400  $\mu$ L, 600  $\mu$ L, 800  $\mu$ L and 1000  $\mu$ L) of N.T shRNA and shRNA #2 lentiviral particles (Supplementary figure 4). It should be noted that no successful transductions were observed for the 200  $\mu$ L volume of shRNA #2 lentiviral particles, accounting for the absence of a cell count for that result. Transduction efficiencies for each volume of N.T shRNA and shRNA #2 lentiviral particles in HEK293T and HS578T cell lines were therefore quantified by calculating the average number of transduced particles per field of view (Supplementary figure 3 and Supplementary figure 4).

A)	N.T shRNA (HEK293T cells)
----	---------------------------

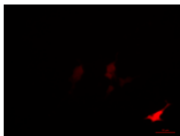

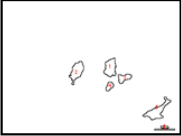
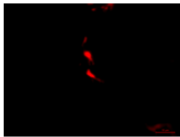

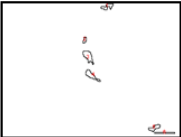
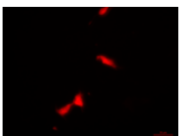

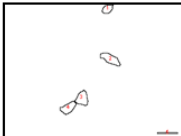
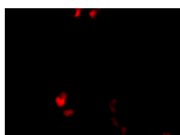

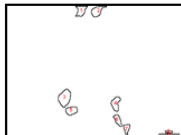
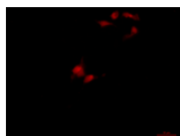


i)		turboRFP	Threshold	Outlines	No. of cells	Average No. of cells/ field of view	Standard deviation
200 $\mu$ L	1)				6	8	2.74
	2)				8		
	3)				9		
	4)				12		
	5)				5		
ii)		turboRFP	Threshold	Outlines	No. of cells	Average No. of cells/ field of view	Standard deviation
400 $\mu$ L	1)				18	13.8	4.21
	2)				15		
	3)				16		
	4)				7		
	5)				13		

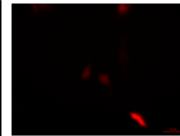

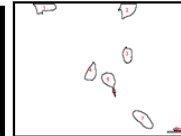
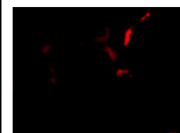

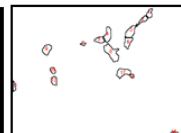
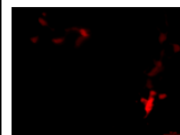

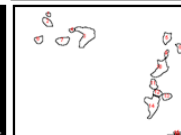
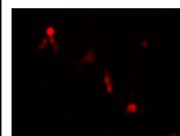

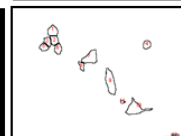
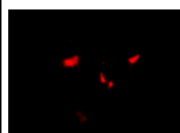


A)	N.T shRNA (HEK293T cells)
----	---------------------------

iii)		turboRFP	Threshold	Outlines	No. of cells	Average No. of cells/ field of view	Standard deviation
600 $\mu$ L	1)				31	16.8	8.96
	2)				11		
	3)				19		
	4)				15		
	5)				8		
iv)		turboRFP	Threshold	Outlines	No. of cells	Average No. of cells/ field of view	Standard deviation
800 $\mu$ L	1)				38	34.6	4.39
	2)				29		
	3)				40		
	4)				33		
	5)				33		

A) N.T shRNA (HEK293T cells)							
v)					No. of cells	Average No. of cells/ field of view	Standard deviation
		turboRFP	Threshold	Outlines			
1000 $\mu$ L	1)				27	33	9.51
	2)				37		
	3)				26		
	4)				27		
	5)				28		
B) shRNA #2 (HEK293T cells)							
i)					No. of cells	Average No. of cells/ field of view	Standard deviation
		turboRFP	Threshold	Outlines			
200 $\mu$ L	1)				6	4.8	1.30
	2)				5		
	3)				3		
	4)				6		
	5)				4		

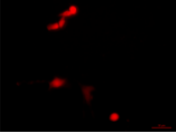


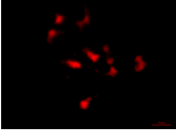


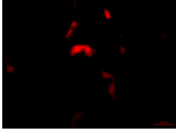


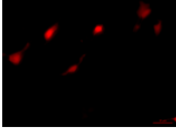

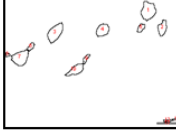
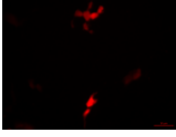

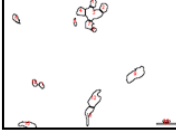
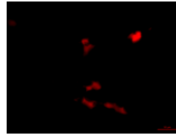


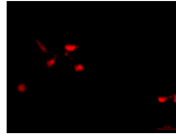

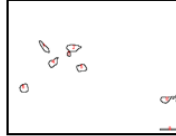


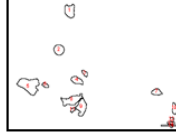



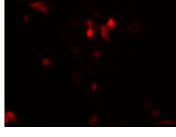

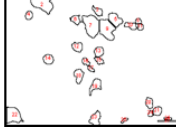
B) shRNA #2 (HEK293T cells)

ii)					No. of cells	Average No. of cells/ field of view	Standard deviation
		turboRFP	Threshold	Outlines			
400 $\mu$ L	1)				7	6.8	1.48
	2)				6		
	3)				5		
	4)				9		
	5)				7		

iii)					No. of cells	Average No. of cells/ field of view	Standard deviation
		turboRFP	Threshold	Outlines			
600 $\mu$ L	1)				9	12.4	3.78
	2)				16		
	3)				16		
	4)				13		
	5)				8		



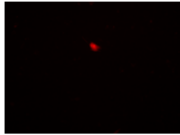


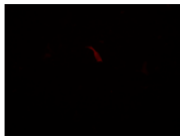
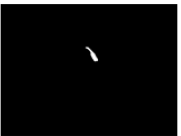

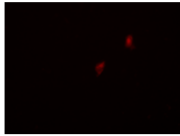


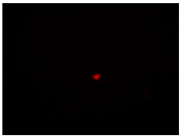





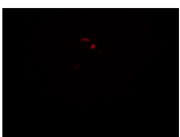

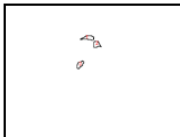
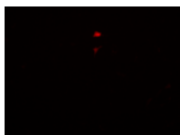



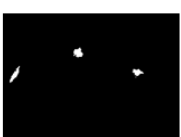
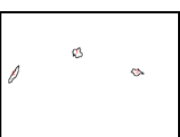
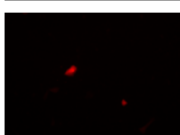


B)	shRNA #2 (HEK293T cells)
----	--------------------------



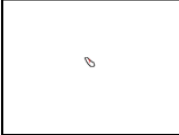



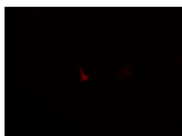
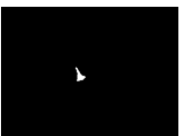
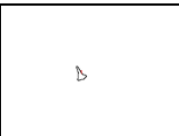
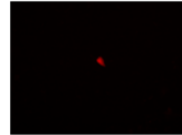


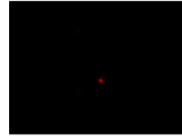


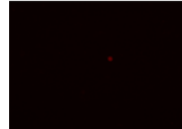
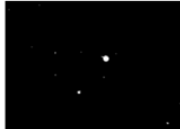
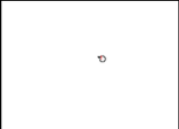
iv)		turboRFP	Threshold	Outlines	No. of cells	Average No. of cells/ field of view	Standard deviation
800 $\mu$ L	1)				7	13	3.67
	2)				13		
	3)				16		
	4)				13		
	5)				16		
v)		turboRFP	Threshold	Outlines	No. of cells	Average No. of cells/ field of view	Standard deviation
1000 $\mu$ L	1)				10	14.4	7.3
	2)				9		
	3)				14		
	4)				12		
	5)				27		

**Supplementary figure 3: Quantification of transduction efficiencies of N.T shRNA and shRNA #2 lentiviral particles in HEK293T cells by automated particle counting using ImageJ**

HEK293T cells were transduced with increasing volumes ([i] 200  $\mu$ L, [ii] 400  $\mu$ L, [iii] 600  $\mu$ L, [iv] 800  $\mu$ L and [v] 1000  $\mu$ L) of (A) N.T shRNA and (B) shRNA #2 lentiviral particles. Fluorescence microscopy was used to examine the presence of successful transductions 72 hours post treatment with doxycycline (1  $\mu$ g/mL). Successfully transduced cells were reflected by the presence of turboRFP. Successfully transduced cells for five images (five fields of view) for each volume of lentiviral particles were counted using automated particle counting by ImageJ. Thresholds and outlines during particle counting analysis for each of the images were shown. The average number of transduced cells per field of view and the relevant standard deviations for each volume of (A) N.T shRNA and (B) shRNA #2 lentiviral particles were calculated.

A)	<b>N.T shRNA (HS578T cells)</b>
----	---------------------------------

i)		turboRFP	Threshold	Outlines	No. of cells	Average No. of cells/ field of view	Standard deviation
200 $\mu$ L	1)				1	1.33	0.58
	2)				1		
	3)				2		
ii)		turboRFP	Threshold	Outlines	No. of cells	Average No. of cells/ field of view	Standard deviation
400 $\mu$ L	1)				1	2.67	1.53
	2)				4		
	3)				3		
iii)		turboRFP	Threshold	Outlines	No. of cells	Average No. of cells/ field of view	Standard deviation
600 $\mu$ L	1)				2	2.33	0.58
	2)				3		
	3)				2		

A) N.T shRNA (HS578T cells)							
					No. of cells	Average No. of cells/ field of view	Standard deviation
iv)							
		turboRFP	Threshold	Outlines			
800 $\mu$ L	1)				1	2	1.73
	2)				4		
	3)				1		
v)					No. of cells	Average No. of cells/ field of view	Standard deviation
		turboRFP	Threshold	Outlines			
1000 $\mu$ L	1)				1	1	0
	2)				1		
	3)				1		

**Supplementary figure 4: Quantification of transduction efficiencies of N.T shRNA and shRNA #2 lentiviral particles in HS578T cells by automated particle counting using ImageJ**

HS578T cells were transduced with increasing volumes ([i] 200  $\mu$ L, [ii] 400  $\mu$ L, [iii] 600  $\mu$ L, [iv] 800  $\mu$ L and [v] 1000  $\mu$ L) of (A) N.T shRNA and (B) shRNA #2 lentiviral particles. Fluorescence microscopy was used to examine the presence of successful transductions 72 hours post treatment with doxycycline (1  $\mu$ g/mL). Successfully transduced cells were reflected by the presence of turboRFP. Successfully transduced cells for three images (three fields of view) for each volume of lentiviral particles were counted using automated particle counting by ImageJ. Thresholds and outlines during particle counting analysis for each of the images were shown. The average number of transduced cells per field of view and the relevant standard deviations for each volume of (A) N.T shRNA and (B) shRNA #2 lentiviral particles were calculated.

## Appendix 5: Alignment of Hop targeting shRNA clones with Hop mRNA

Hop mRNA	1	CTAGAAGAACTCGACCAGTGAGCAGGCGAGGAAGGGGCGGGAGCC--GGGGTCCCGGTAGCTTCTAGTAGGTTCCAGAAGGCGGCGCGTGC	98
mSTI1 mRNA	1	-----GTGTTCAACCAGTGAGCAGGCGAGGAAGGGGCGGTAACCTGGGGTCCCGGCAGCTTCTAGTAGGTTCCAGAAGGCGGCGCGTGC	94
shRNA#1	1	-----	1
shRNA#2	1	-----	1
shRNA#3	1	-----	1
shRNA#4	1	-----	1
shRNA#5	1	-----	1
Hop mRNA	99	CGCGGAGCGGACGGATTTCGATTCAACGGGGTTCCGGACCGCGCTGCGCTATGAGCAGGTCAATGAGCTGAAGGAGAAAGGCAACAAGGCCCTGAGCGTG	198
mSTI1 mRNA	95	CGCGGAGCGGACGAATTTCGATTCAACGGGGTTCCGGGCCA----GGCTATGAGCAGGTGAATGAGCTAAAGGAGAAGGGCAATAAGGCCCTGAGTGCT	189
shRNA#1	1	-----	1
shRNA#2	1	-----	1
shRNA#3	1	-----	1
shRNA#4	1	-----	1
shRNA#5	1	-----	1
Hop mRNA	199	GGTAACATCGATGATGCCTTACAGTGCTACTCCGAAGCTATTAAGCTGGATCCCCACAACCACGTGCTGTACAGCAACCGTTCTGCTGCCTATGCCAAGA	298
mSTI1 mRNA	190	GGGAACATTGATGATGCCTTACAGTGCTACTCTGAGGCAATTAACTAGATCCCCAGAACCATGTGCTCTACAGCAATCGCTCTGCAGCCTACGCCAAGA	289
shRNA#1	1	-----	1
shRNA#2	1	-----	1
shRNA#3	1	-----	1
shRNA#4	1	-----	1
shRNA#5	1	-----	1
Hop mRNA	299	AAGGAGACTACCAGAAGGCTTATGAGGATGGCTGCAAGACTGTTCGACCTAAAGCCTGACTGGGGCAAGGGCTATTACGAAAAGCAGCAGCTCTAGAGTT	398
mSTI1 mRNA	290	AAGGAGACTACCAGAAGGCCTATGAGGACGGCTGCAAGACTGTTGACCTGAAGCCTGACTGGGGCAAGGGTATTCAAGAAAAGCAGCAGCCCTTGAATT	389
shRNA#1	1	-----	1
shRNA#2	1	-----	1
shRNA#3	1	-----	1
shRNA#4	1	-----	1
shRNA#5	1	-----	1
Hop mRNA	399	CTTAAACCGCTTTGAAGAAGCCAAGCGAACCTATGAGGAGGGCTTAAACACGAGGCAAATAACCTCAACTGAAAGAGGGTTTACAGAATATGGAGGCC	498
mSTI1 mRNA	390	CCTAAACCGGTTTGAGGAAGCCAACGAACCTATGAAGAAGGTTTAAACATGAAGCCAATAATCTCCAGCTTAAGGAGGGCTTGCAGAACATGGAGGCC	489
shRNA#1	1	-----	1
shRNA#2	1	-----	1
shRNA#3	1	-----	1
shRNA#4	1	-----	1
shRNA#5	1	-----	1

Hop mRNA	499	AGGTTGGCAGAGAGAAAAATTCATGAACCCTTTCAACATGCCTAATCTGTATCAGAAGTTGGAGAGTGATCCCAGGACAAGGACACTACTCAGTGATCCTA	598
mSTI1 mRNA	490	AGGTTGGCAGAGAGGAAATTCATGAATCCATTCAACTTGCCTAATCTATACCAAAAGTTGGAAAACGACCCCAGGACAAGGTCGCTGCTCAGTGACCCCA	589
shRNA#1	1	-----	1
shRNA#2	1	-----	1
shRNA#3	1	-----	1
shRNA#4	1	-----	1
shRNA#5	1	-----	1
Hop mRNA	599	CCTACCGGGAGCTGATAGAGCAGCTACGAAACAAGCCTTCTGACCTGGGCACGAAACTACAAGATCCCCGGATCATGACCACTCTCAGCGTCCTCCTTGG	698
mSTI1 mRNA	590	CCTACAGGGAGCTCATAGAACAGCTGCAGAACAGCCGTGACACCTGGGCACGAAACTACAGGATCCCCGGGTGATGACTACTCTGAGTGTCCTCCTTGG	689
shRNA#1	1	-----	1
shRNA#2	1	-----	1
shRNA#3	1	-----	1
shRNA#4	1	-----	1
shRNA#5	1	-----	1
Hop mRNA	699	GGTCGATCTGGGCAGTATGGATGAGGAGGAAGAGATTGCAACACCTCCACCACCACCCCCTCCCAAAAAGGAGACCAAGCCAGAGCCAATGGAAGAAGAT	798
mSTI1 mRNA	690	GGTTGATCTGGGCAGCATGGATGAAGAGGAAGAGGCAGCAACACCCCCACCCCACCTCCTCCCAAAAAGGAGCCCCAAGCCAGAACCAATGGAAGAAGAT	789
shRNA#1	1	-----	1
shRNA#2	1	-----	1
shRNA#3	1	-----	1
shRNA#4	1	-----	1
shRNA#5	1	-----	1
Hop mRNA	799	CTTCCAGAGAATAAGAAGCAGGCACTGAAAGAAAAAGAGCTGGGGAACGATGCCTACAAGAAGAAAGACTTTGACACAGCCTTGAAGCATTACGACAAAG	898
mSTI1 mRNA	790	CTTCCAGAGAATAAGAAACAGGCACTGAAAGAGAAGGAGCTGGGAAATGATGCCTACAAGAAGAAAGATTTTGACAAGGCCCTGAAGCATTATGACAGAG	889
shRNA#1	1	-----	1
shRNA#2	1	-----	1
shRNA#3	1	-----	1
shRNA#4	1	-----	1
shRNA#5	1	-----	1
Hop mRNA	899	CCAAGGAGCTGGACCCCACTAACATGACTTACATTACCAATCAAGCAGCGGTATACTTTGAAAAGGGCGACTACAATAAGTGCCGGGAGCTTTGTGAGAA	998
mSTI1 mRNA	890	CCAAGGAACTGGACCCTACCAACATGACCTACATAACTAATCAAGCAGCTGTGCACCTTTGAGAAGGGCGACTATAACAAATGCCGGGAGCTCTGTGAGAA	989
shRNA#1	1	-----	1
shRNA#2	1	-----	1
shRNA#3	1	-----	1
shRNA#4	1	-----	1
shRNA#5	1	-----	1

Hop mRNA	999	GGCCATTGAAGTGGGGAGAGAGAAAACCGAGAAGACTATCGACAGATTGCCAAAGCATATGCTCGAATTGGCAACTCCTACTTCAAAGAAGAAAAGTACAAG	1098
mSTI1 mRNA	990	GGCCATTGAAGTGGGCAGAGAGAAACCGAGAGGACTACCGGCAGATCGCCAAAGCTTATGCCCGAATTGGCAATTCCTATTTCAAAGAAGAAAAGTACAAG	1089
shRNA#1	1	-----CCGAGAAGACTATCGACAG-----	19
shRNA#2	1	-----	1
shRNA#3	1	-----	1
shRNA#4	1	-----TCCTACTTCAAAGAAGAAA-----	19
shRNA#5	1	-----	1
Hop mRNA	1099	GATGCCATCCATTTCTATAACAAGTCTCTGGCAGAGCACCGAACCCCA	1198
mSTI1 mRNA	1090	GATGCTATACATTTCTACAACAAGTCTCTAGCAGAGCACCGAACCCCA	1189
shRNA#1	19	-----	19
shRNA#2	1	-----	1
shRNA#3	1	-----	1
shRNA#4	19	-----	19
shRNA#5	1	-----	1
Hop mRNA	1199	GGCTGGCCTACATAAACCCCGACCTGGCTTTGGAGGAGAAGAACAAGGCAACGAGTGTTTTTCAGAAAGGGGACTATCCCCAGGCCATGAAGCATTATAC	1298
mSTI1 mRNA	1190	GCTTGGCTTATATCAACCCTGACTTGGCTTTGGAGGAGAAGAACAAGGCAACGAATGCTTCCAGAAAGGGGACTACCCCCAAGCCATGAAGCACTATAC	1289
shRNA#1	19	-----	19
shRNA#2	1	-----	1
shRNA#3	1	-----	1
shRNA#4	19	-----	19
shRNA#5	1	-----	1
Hop mRNA	1299	AGAAGCCATCAAAAGGAACCCGAAAGATGCCAAATTATACAGCAATCGAGCTGCCTGCTACACCAAACCTCCTGGAGTTCCAGCTGGCACTCAAGGACTGT	1398
mSTI1 mRNA	1290	AGAAGCCATTAAAAGGAACCCGAGAGATGCCAAACTGTACAGCAACCGAGCTGCCTGCTACACCAAGCTCCTGGAGTTTCAGCTGGCACTCAAGGACTGT	1389
shRNA#1	19	-----	19
shRNA#2	1	-----CCGAAAGATGCCAAATTAT-----	19
shRNA#3	1	-----	1
shRNA#4	19	-----	19
shRNA#5	1	-----	1
Hop mRNA	1399	GAGGAATGTATCCAGCTGGAGCCGACCTTCATCAAGGGTTATACACGGAAAGCCGCTGCGCTGGAAGCGATGAAGGACTACACCAAAGCCATGGATGTGT	1498
mSTI1 mRNA	1390	GAGGAGTGCATCCAGCTAGAGCCAACCTTCATCAAGGGTTATACACGGAAAGCAGCTGCTCTGGAAGCCATGAAGGACTATACAAAAGCCATGGATGTGT	1489
shRNA#1	19	-----	19
shRNA#2	19	-----	19
shRNA#3	1	-----	1
shRNA#4	19	-----	19
shRNA#5	1	-----	1

Hop mRNA	1499	ACCAGAAGGCGCTAGACCTGGACTCCAGCTGTAAGGAGGCGGCAGACGGCTACCAGCGCTGTATGATGGCGCAGTACAACCGGCACGACAGCCCCGAAGA	1598
mSTI1 mRNA	1490	ACCAAAAAGCGTTAGACCTGGACTCCAGCTGTAAGGAAGCAGCAGATGGTTACCAACGCTGTATGATGGCACAGTACAACAGACATGATAGCCCTGAGGA	1589
shRNA#1	19	-----	19
shRNA#2	19	-----	19
shRNA#3	1	-----	1
shRNA#4	19	-----	19
shRNA#5	1	-----	1
Hop mRNA	1599	TGTGAAGCGACGAGCCATGGCCGACCCTGAGGTGCAGCAGATCATGAGTGACCCAGCCATGCGCCTTATCCTGGAACAGATGCAGAAGGACCCCCAGGCA	1698
mSTI1 mRNA	1590	TGTGAAGCGGCGGGCCATGGCTGACCCTGAGGTGCAGCAGATAATGAGTGACCCAGCCATGAGACTCATCCTGGAGCAGATGCAAAAGGACCCCCAGGCT	1689
shRNA#1	19	-----	19
shRNA#2	19	-----	19
shRNA#3	1	-----AGGCA	5
shRNA#4	19	-----	19
shRNA#5	1	-----	1
Hop mRNA	1699	CTCAGCGAACACTTAAAGAATCCTGTAATAGCACAGAAGATCCAGAAGCTGATGGATGTGGGTCTGATTGCAATTTCGGTGAATGACTTGTTTCATCCC-CCC	1797
mSTI1 mRNA	1690	CTGAGCGAACACTTAAAGAATCCTGTAATAGCGCAGAAGATCCAGAAGCTGATGGATGTGGGTCTCATCGCAATTTCGGTGAATAACTTGCTTTTCCCCCTC	1789
shRNA#1	19	-----	19
shRNA#2	19	-----	19
shRNA#3	6	CTCAGCGAACACTT-----	19
shRNA#4	19	-----	19
shRNA#5	1	-----	1
Hop mRNA	1798	TTCCCTTCGCCCTCATGTGGAAAGAGGAGCTGGGACCGCGGCGAGCAGCACGGAGCGGAAGGGAGAGCAGGGGA-GAGAAGGCCTCATCTCTCTATATTT	1896
mSTI1 mRNA	1790	TTCCCTTCGCCA--ATGAGG-AAGGCGAGCTGGGAAGGTGGCGAGCAGCACTGGGCAGAGGGGG-----GGAGAAGAAAGGCTT--ATCTTTATATTT	1877
shRNA#1	19	-----	19
shRNA#2	19	-----	19
shRNA#3	19	-----	19
shRNA#4	19	-----	19
shRNA#5	1	-----GCCTCATCTCTCTATATTT	19
Hop mRNA	1897	ATACATAACCCCGGGGAAGACACAGAGACTCGTACCTGCGCTGTTTGTGCCGCCGCTGCCTCTGGGCCCTCCCAGCACACGCATGGTCTCTTCACCGCTG	1996
mSTI1 mRNA	1878	ATACATGCCTACAAGGAAGACA---GACTCATCC-----AGCGCCACCT-CGGGCCCTCCCAGCACACGCATGGTCTCTTCACTGCTG	1956
shRNA#1	19	-----	19
shRNA#2	19	-----	19
shRNA#3	19	-----	19
shRNA#4	19	-----	19
shRNA#5	19	-----	19



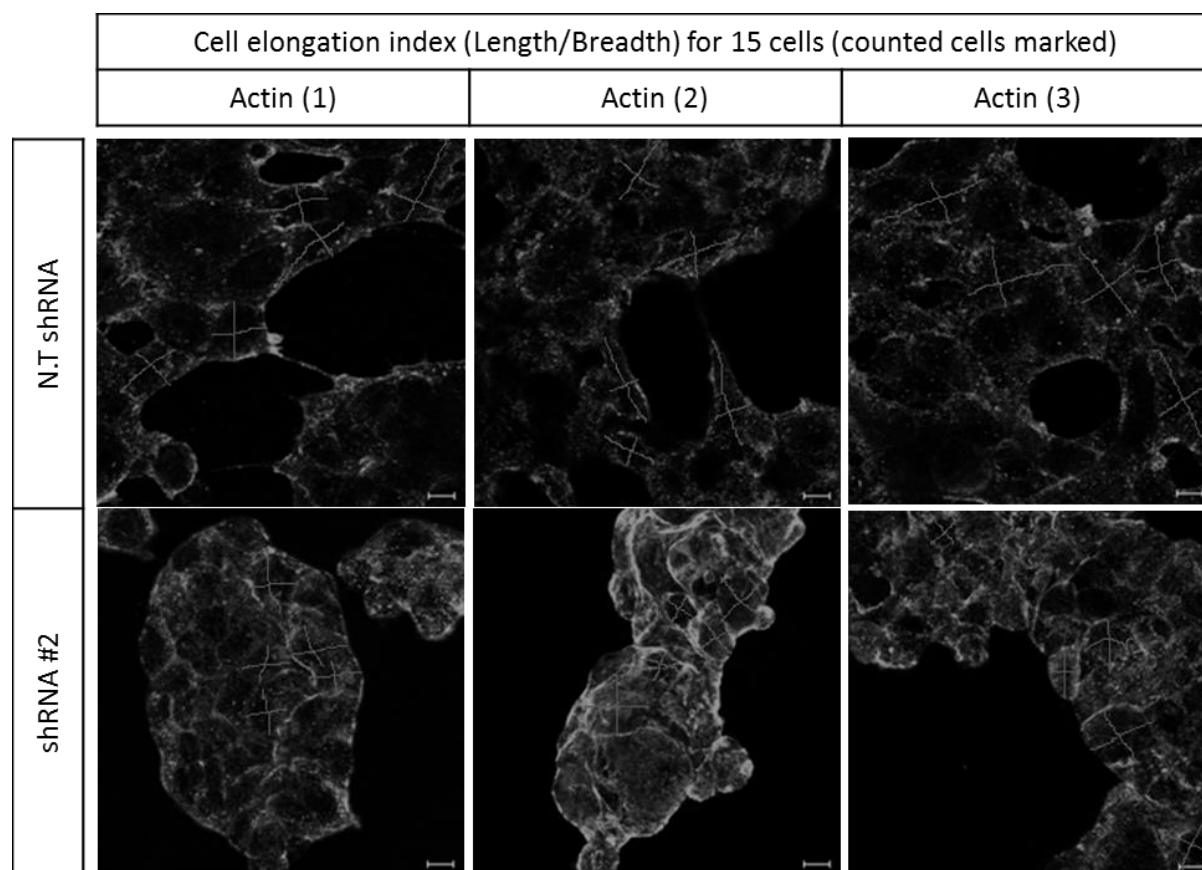
<b>Hop mRNA</b>	1997	CCCTCGAGTTCCATGTCTCTTTCCCCT-----GCCCCTAGTTGCTGTCTCGGCTGCTCTCCCATAGTTGGTTTTTTTTTTATTTGGGGCAGTGG	2085
<b>mSTI1 mRNA</b>	1957	CCCTCAATC--CGAGTGTCTTCCCCTGCCAGTCCTAGCCTCCCCGTCAGTGTCTCGGCTGCTCCCCCATAGTTGGTTAT-TTTTTATTTGGGGCAGTGG	2053
<b>shRNA#1</b>	19	-----	19
<b>shRNA#2</b>	19	-----	19
<b>shRNA#3</b>	19	-----	19
<b>shRNA#4</b>	19	-----	19
<b>shRNA#5</b>	19	-----	19
<b>Hop mRNA</b>	2086	GCATGTTATGGGGAGGGGAGGGGGTTCTTC-CAGCCTCAGGTCCCAGCTGTCTCACGTTGTTTATTCTGCGTCCCCCTTCTCCAATAAAACAAGCCAGTTG	2184
<b>mSTI1 mRNA</b>	2054	GTGC-ATACGGGGAGGGGAGGGTGTTCCTCCCAACCTAGGGTCCCAGCTGTCTTACCTGTTCTTACCCACGTCCC-TCCTCAATA-AAGAAGCCAGTCA	2150
<b>shRNA#1</b>	19	-----	19
<b>shRNA#2</b>	19	-----	19
<b>shRNA#3</b>	19	-----	19
<b>shRNA#4</b>	19	-----	19
<b>shRNA#5</b>	19	-----	19
<b>Hop mRNA</b>	2185	GGCGTGGTTATATGTTGAAAAAAAAAAAAAAAAAAAA 2219	
<b>mSTI1 mRNA</b>	2151	GGCGTGGTTATATGTTGCTACGG----- 2173	
<b>shRNA#1</b>	19	-----	19
<b>shRNA#2</b>	19	-----	19
<b>shRNA#3</b>	19	-----	19
<b>shRNA#4</b>	19	-----	19
<b>shRNA#5</b>	19	-----	19

#### Supplementary figure 5: TRIPZ shRNA Hop clones target different regions of Hop (*Homo sapiens*) and mSTI1 (*Mus musculus*) mRNA

Multiple sequence alignment of shRNA #1, shRNA #2, shRNA #3, shRNA #4 and shRNA #5 with Hop (*Homo sapiens*) and mSTI1 (*Mus musculus*) mRNA. Nucleotides highlighted in grey indicate residues identical to the relevant shRNA clones. The red box indicates the TPR1 domain. The green box indicates the TPR2A domain. The orange box indicates the TPR2B domain. The start codon and stop codon of the coding sequence are highlighted in yellow.

## Appendix 6: Quantitative analysis of cell morphologies of N.T shRNA and shRNA #2 HEK293T cells

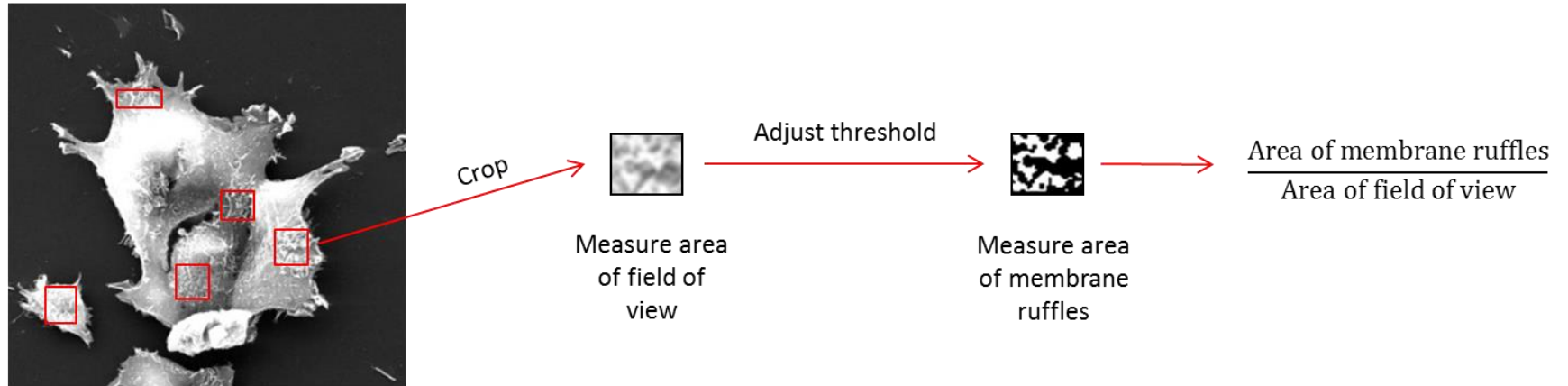
The cell elongation indices (Supplementary figure 6) as well as the area of membrane ruffles per unit area (Supplementary figure 7) for N.T shRNA and shRNA #2 cells were quantified using ImageJ.



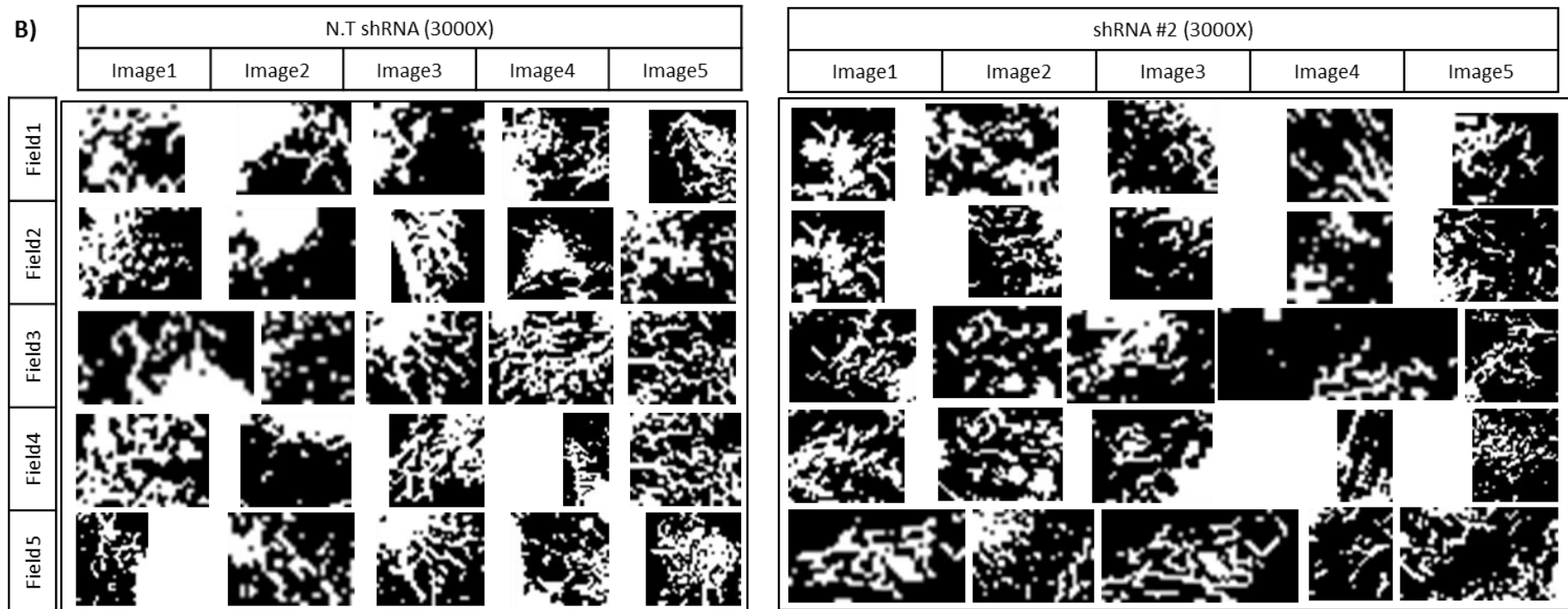
### Supplementary figure 6: Measurement of cell elongation index of N.T shRNA vs shRNA #2 HEK293T cell lines

For each cell line, 15 cells with well-defined actin borders were selected (five cells in each of three images) and the length and breadth of each cell measured using ImageJ. Grey markings indicate the length and breadth of the selected cells. The average cell elongation index was calculated by obtaining a ratio of length:breadth for each cell.

A)



B)



**Supplementary figure 7: Quantification of membrane ruffles in N.T shRNA and shRNA #2 HEK293T cell lines**

(A) Schematic diagram demonstrating the process used to quantify membrane ruffles. Five fields of view containing membrane ruffles were selected from images captured at 3000X magnification. The area of each field of view was measured using ImageJ. The threshold of each field of view was adjusted such that 'dark background' was selected and the majority of the membrane ruffles were coloured. This allowed the area of the membrane ruffles to be measured using ImageJ. The average area of membrane ruffles per unit area was then calculated by obtaining a ratio of area of membrane ruffles:area of field of view for 25 fields of view. (B) Five fields of view for five images for the N.T shRNA and the shRNA #2 cell lines were analysed as in (A).